ANALYSIS OF THE THERMAL RESPONSE OF PROTECTIVE FABRICS

Howard L. Morse, et al

Acurex Corporation
Mountain View, California

January 1973

AFML-TR-73-17

ANALYSIS OF THE THERMAL RESPONSE OF PROTECTIVE FABRICS

H. L. Morse
J. G. Thompson
K. J. Clark
K. A. Green
C. B. Moyer

Aerotherm Division/Acurex Corporation

TECHNICAL REPORT AFML-TR-73-17

January 1973

AIR FORCE MATERIALS LABORATORY
AIR FORCE SYSTEMS COMMAND
WRIGHT-PATTERSON AIR FORCE BASE
OHIO 45433

220

NOTICES

When Government drawings, specifications or other data are used for any purpose other than in connection with a definitely related Government procurement operation, the United States Government thereby incurs no responsibility nor any obligation whatsoever; and the fact that the Government may have formulated, furnished or in any way supplied the said drawings, specifications, or other data is not to be regarded by implication or otherwise as in any manner licensing the holder or any other person or corporation, or conveying any rights or permission to manufacture, use, or sell any potential invention that may in any way be related thereto.

Copies of this report should not be returned unless return is required by security considerations, contractual obligations, or notice on a specific document.

UNCLASSIFED

Security Classification

DOCUMENT CONTROL DATA - R & D

Security classification of title, body of abstract and indexing annotation must be entered when the overall report is classified)

1 ORIGINATING ACTIVITY (Corporate author) Aerotherm Division/Acurex Corporation 485 Clyde Avenue Mountain View, CA 94040	2a. REPORT SECURITY CLASSIFICATION Unclassified 2b. GROUP

3 REPORT TITLE

Analysis of the Thermal Response of Protective Fabrics

4 DESCRIPTIVE NOTES (Type of report and inclusive dates)

June 1971 through June 1972

5 AUTHOR(S) (First name, middle initial, last name)

Howard L. Morse — Kenneth A. Green
James G. Thompson — Carl B. Moyer
Kimble J. Clark

6 REPORT DATE January 1973	7a. TOTAL NO. OF PAGES 219	7b. NO. OF REFS 72
8a. CONTRACT OR GRANT NO. F33615-72-C-1298 b. PROJECT NO 7320 c. 02 d	9a. ORIGINATOR'S REPORT NUMBER(S) AFML-TR-73-17 9b. OTHER REPORT NO(S) (Any other numbers that may be assigned this report)	

10 DISTRIBUTION STATEMENT

Approved for public release; distribution unlimited.

11 SUPPLEMENTARY NOTES	12. SPONSORING MILITARY ACTIVITY AFML (MBC) Wright-Patterson AFB, Ohio 45433

13 ABSTRACT

The objective of this program was to develop a theoretical and empirical mathematical relationship to define the fabric-skin system's response when exposed to a JP-4 fuel fire. Critical fabric parameters, such as optical, thermo-chemical and physical characteristics are defined in a manner which will allow the fabric designer to develop improved thermally protective light weight fabrics. The computer code evaluates the model parameter variation in terms of resultant human skin burns. A comparison of the analytical model results with laboratory and fire pit data demonstrates excellent correlation within the limits of the present study.

In addition to the basic fabric parameter study, three fabrics were specifically defined in terms of their thermal response. Nomex, PBI and stabilized PBI fabrics were modeled analytically by experimental determination of their thermal response characteristics. Stabilized PBI fabrics provided the best protection of the three fabrics because the fabric did not shrink, break apart or ignite. Nomex fabrics provided the least protection because the hot fabric shrank to contact with the skin, broke apart allowing direct exposure of the skin, and continued to burn upon egress from the fire. Unstabilized PBI fabrics did shrink to contact with the underlying skin and allowed a burn to occur. The extent of the burn under the Nomex fabric was more severe than for the unstabilized PBI fabric.

The above results were derived from the mathematical model and then further evidence of the validity of the results was demonstrated by laboratory experiments and by fire pit evaluations conducted by the Air Force. Three second fire pit exposures of mannikins clothed in flight suits made from each fiber type showed the average resultant body area burned in thirty tests to be 49.8% for Nomex, 28.4% for unstabilized PBI, and 11.4% for stabilized PBI.

DD FORM 1 NOV 1473 REPLACES DD FORM 1473, 1 JAN 64, WHICH IS OBSOLETE FOR ARMY USE.

UNCLASSIFIED

Security Classification

14 KEY WORDS	LINK A		LINK B		LINK C	
	ROLE	WT	ROLE	WT	ROLE	WT
Flight Suit Fabrics Thermally Protective Fabrics Aircraft Crash Fires Skin Burn Injury Skin Thermal Model Fabric Thermal Model Fire Modelling						

ia

ANALYSIS OF THE THERMAL RESPONSE OF PROTECTIVE FABRICS

by

Howard L. Morse
James G. Thompson
Kimble J. Clark
Kenneth A. Green
Carl B. Moyer

Aerotherm Division/Acurex Corporation

Technical Report No. AFML-TR-73-17

i.ii

FOREWORD

This report was prepared by Aerotherm Acurex Corporation, Mountain View, California, under U. S. Government Contract No. F33615-72-C-1298. This contract was initiated under Project 7320, "Fibrous Materials for Decelerators and Structures," Task 732002, "Fibrous Structural Materials." The work was administered under the direction of the Nonmetallic Materials Division, Air Force Materials Laboratory, Air Force Systems Command, with Mr. Robert M. Stanton, AFML/MBC, as Project Engineer.

This program was conducted in part, using Director's Discretionary Funds.

This report covers work conducted from June 1971 through June 1972, and was released by the authors for publication in November 1972.

This technical report has been reviewed and is approved.

T. J. Reinhart, Jr.

T. J. REINHART, JR., Acting Chief
Composite & Fibrous Materials Branch
Nonmetallic Materials Division

TABLE OF CONTENTS

TABLE OF CONTENTS (CONTINUED)

TABLE OF CONTENTS (CONCLUDED)

LIST OF FIGURES

LIST OF FIGURES (CONTINUED)

LIST OF FIGURES (CONCLUDED)

LIST OF TABLES

LIST OF TABLES (CONCLUDED)

SUMMARY

An analytical and experimental study designed to understand and achieve a means for predicting the thermal response of a clothing assembly and the underlying human skin tissue when exposed for short durations to a fully developed JP-4 fueled aircraft crash fire has been performed. The study has two primary objectives: first to evaluate fire-clothing-skin systems in order to determine those properties or qualities of the clothing assembly which are most important in providing protection for the skin. The goal of this objective is to provide guidance in the design of fabrics and clothing systems which may be exposed to fire environments. The second primary objective is to evaluate specifically three candidate fabrics being used or considered by the Air Force as materials for flight suits. These include Nomex, PBI, and stabilized PBI.

The approach of the study is first to collect, through literature survey and experiment where necessary, all pertinent data relating to the transient thermal response of the clothing-skin system upon exposure to a fire environment, and then to calculate the thermal response analytically for modeled fires simulating those observed in open pit tests and anticipated for aircraft crashes. The basic tool for this calculation is a sophisticated computer code which solves the one-dimensional, time-dependent heat transfer equations for a clothing-skin model which includes thermal, thermochemical (decomposition and reaction with fire and air environments), and physical (fabric shrinkage) effects. The general problem is defined as a clothing assembly (single and multiple layers of fabric) covering the human skin and exposed to a JP-4 fuel fire for a nominal 3 seconds. Heating of the clothing assembly by radiation, convection and chemical reaction between the pyrolysis gases and environment gases is considered. Heat transfer between fabric layers and the skin is assumed to be limited to radiation, conduction across layers and air gaps separating layers, and by convection of vaporized, condensible gases from the fabric to the skin.

The thermal response of the skin is determined as a function of time and depth. A burn injury model based on a temperature dependent damage rate is coupled to the code, and computes injury as a function of time and depth.

A study of pool fire data indicates that a nominal JP-4 fire has an equilibrium temperature of 1010°C, is fuel rich in the interior and radiates essentially as a black body at the equilibrium temperature with an optical depth on the order of 1 meter. Convective heating for an object moving at 4.5 m/sec

through the fire is limited to approximately 20 percent of the heating due to radiation. In the mathematical model a nominal fire is defined as one of constant heating (4.65 cal/cm^{2}sec) for the first 2 seconds of exposure with a linear decrease to zero during the final second. Calculations of thermal response are continued for a total 30 seconds, the final 27 seconds in an air environment, to include the important cooldown behavior and possible combustion of the fabric in air. Open pit fuel fire profiles are also considered; these include a linear increase in heating during the initial second of exposure, one second at constant heating (4.65 and 3.65 cal/cm^{2}sec) and a linear decrease to zero in the final second.

Characterization of the fabric extends to factors which affect the thermal response, including optical, thermal, thermochemical, and mechanical properties. Property data were collected for the candidate fabrics and other typical fabrics by literature search and test.

A thermal model of the human skin has been developed which is based upon the short response times encountered in an intense fire. Body circulatory effects are not important due to the brevity of the exposures, thus the skin transfers energy internally by conduction only. In-depth absorption of energy is shown to be important only for direct fire radiation. Since the amount of energy absorbed by the skin for threshold injuries (total loss of the epidermal layer) generally implies negligible direct transmission, the skin is assumed to be opaque to radiant energy. Skin density and specific heat are essentially equal to those for water, but the thermal conductivity increases from a value about 40 percent of that for water at the surface to near that of water in the lower dermal layer. A nominal skin profile has an epidermal thickness of about 100μm and a dermal thickness of 2mm backed up by an undefined thickness of fatty or muscle tissue.

Burn injury to skin tissue is based upon a model first proposed by Henriques and modified by Stoll. The rate of tissue destruction is taken as an exponential function of the absolute temperature only and is cumulative with time. Thus short exposures to a given total of heating are more injurious than longer exposures to the same total heating.

Using the data acquired on the fire, clothing assembly, and skin, the computer code was used to perform a parametric analysis, evaluating the relative importance of system variables and comparing the candidate fabrics. Regarding general system variables, the following conclusions were obtained:

1) Condition of the fire is a major factor in determining the response of fabric and skin primarily because the heat flux from the fire is radiation dominated and varies as the fourth power of the absolute temperature.

2) The most important fabric characteristics (these are so identified because a fabric must perform well in these areas before the influence of other characteristics becomes significant) are the dimensional, structural and thermochemical stabilities. A fabric which ignites and burns either in air or in the fire environment not only offers less protection, but becomes an additional source of heat once removed from the fire. Structural failure of a fabric, in the form of hole formation or tearing, leads to direct exposure of underlayer surfaces and greater exposure of the torn fabric. This latter effect increases the heating to the fabric and thus, the potential for ignition. If this condition develops, damage may be propagated to other locations by flame spread. Finally given that a fabric neither burns nor fails structurally, the predominant factor in the clothing system is the presence of air gaps between layers. Consequently a fabric must maintain dimensional stability to preserve the potential for formation of these gaps. Should the fabric shrink to the point of contact with the skin or with underlying layers forcing skin contact, serious burns are essentially impossible to avoid.

3) Because the fire is radiation dominated the fabric optical properties assume a significant role. Convective heating alone is not sufficient to cause injury for the short exposure periods. Thus the absorption and transmission of radiant energy represent the primary source of energy transfer into the system, and consequently, the primary threat to the system. Direct transmission through the fabric is highly undesirable, particularly in the case of a single fabric layer covering the skin, since the skin is a strong absorber. The fabrics studied are strong absorbers of fire radiant energy; absorption represents the main mechanism for introduction of energy into the system. Consequently, increasing the reflectivity of fabrics represents a significant potential for improvements.

4) Properties of the skin have essentially no effect upon the amount of heating to the skin because skin surface temperatures remain low relative to fabric temperatures. Variation in skin properties does have an effect on the response of the skin; however, skin properties were not varied from the nominal model in this study since the emphasis was on fabric evaluation.

5) Traditional thermal and physical properties including density, (fabric weight), specific heat, conductivity and thickness are generally of lesser importance. Assuming presence of air gaps, the thermal conductivity and thickness are of negligible importance because the resistance to heat transfer across the gaps is dominant. Density and specific heat in the fabrics serve as thermal capacitance and although varying these quantities does not change total heating to the skin, the larger the thermal capacitance, the longer the period of heating, resulting in a reduction in peak skin temperatures and injury.

In this latter regard, it is possible that an increase in fabric weight may result in a substantial increase in thermal protection because peak fabric temperatures will be lower for a given exposure. The improvement is not realized so much in that the fluxes are lower because the temperatures (potentials) are lower but that, indirectly, the fabric may shrink less or not at all if the weight increase is great enough thus increasing the resistance to heating. This is confirmed by fire pit evaluations which show that a 6 oz/yds fabric provides considerably more protection than a 4 oz/yds fabric of the same material. That is, in a real fire situation in which the exposure levels will vary substantially over the suit surface, and in some locations are not sufficient to cause shrinkage, the increase in fabric weight will improve the overall performance to the extent that shrinkage can be prevented. For the stable fabric increasing the weight will result in slight improvement, according to the analysis. In addition, a coupled improvement may be anticipated if the fabric weight is increased by virtue of decreasing the direct transmission of fire radiation.

6) To date, the analytical model does not include the effects of moisture transfer to skin. A laboratory analysis was conducted to determine the effects of moisture. Heat transfer measurements through fabrics exposed to direct flame contact showed conditioned fabrics (5 to 14% moisture regain) provide more thermal protection to the underlying skin than did the same fabrics in the dry state even when flow was allowed to occur between the fabric sample and the skin simulant. The effect of moisture in the fabric is to decrease the initial temperature rise thus reducing the heat transfer to the skin by radiation and convection and delaying the onset of shrinkage. It appears that the amount of energy transfer via moisture condensation on the skin is small compared to the reduction in heating provided by vaporization in the fabric. Consequently, moisture regain is believed to be a positive factor in providing thermal protection.

Conclusions of the analytical study relative to the three candidate fabrics, Nomex, PBI, and stabilized PBI (Fabric 121) are:

1) The first major difference is the chemical stability at high temperatures. Assuming equilibrium reactions between pyrolysis gases and the fire and air environments, it was found that PBI and stabilized PBI show no indication of reaction resulting in combustion. Nomex was found to ignite around 550°C in air resulting in a substantial increase in depth of burn. These predictions are consistent with the observed performance of these fabrics in the open-pit, JP-4 fuel test facility at Natick.

2) The second major difference among these fabrics is the dimensional stability factor. For exposure to the nominal fire, both Nomex and PBI, in both single layer and one layer over cotton assemblies, allow serious dermal injuries primarily because both fabrics shrink and come in contact with the skin. Stabilized PBI, which does not shrink until the temperature exceeds 600°C and then only a minimal amount provides complete protection in multilayer assemblies because predicted fabric temperatures do not exceed 600°C and the all important air gaps are maintained.

3) The third major difference is the structural integrity factor. In shrinkage tests Nomex was found to fail (melting and tearing) in the temperature range of 400 to 500°C when constrained whereas PBI and stabilized PBI maintained integrity to in excess of 600°C. Based

on observations of Natick tests and the analytical results obtained in this study, it is hypothesized that a typical response of Nomex would be initial high heating in a local region such as the front of the suit until failure occurs at the weakest (hottest) location. This failure allows the fabric to become loose from the body exposing parts of the fabric to the fire on both sides and removing the heat sink effect of underlying material and/or skin. Fabric temperatures then rise much higher than predicted for an intact fabric, leading to ignition and combustion of the Nomex either in the fire or upon egress into the air environment. How long burning continues after egress depends upon the ability of the material to sustain combustion, the amount of radiant flux from the fire, and the coupling between the fabric and underlying fabric or skin. Response of this form will result in substantial increases in injury in the local failure region and potentially, may propagate injury to other regions through the burning mechanism.

4) For the three fabrics studied, optical, thermal and physical properties are not important parameters in determining the relative performance of the fabrics because the three major factors described above are dominant. In addition, the variations in these parameters among the three candidate fabrics are relatively small, e.g., the absorptance plus transmittance varies between 0.74 and 0.83 for all fabrics in both the virgin and charred states. Stabilized PBI has the lowest transmittance but the highest absorptance, and so forth with other parameters, so that there is not much difference in the initial response of the fabrics.

5) Finally in comparing the quantitative performance of the three candidate fabrics in single layer and single layer over cotton configurations exposed to a nominal fire (11.6 cal/cm^2), the following results were obtained. Figure 1 shows the surface heating at the skin for various clothing assemblies. The curve marked Single Layer Nomex (reaction suppressed, no failure) indicates what occurs when a single layer shrinks to contact and remains intact. Heating increases rapidly upon contact and then equilibrates at a high level. PBI (not shown) provides somewhat better protection because of the added delay in contact relative to Nomex. If the Nomex were to fail, the flux to the skin would approach the fire heating level of 4.65 cal/cm^{2}sec. Single layer stabilized PBI on the other hand does not shrink to contact and keeps the heating to less than 1.0 cal/cm^{2}sec. Total injuries

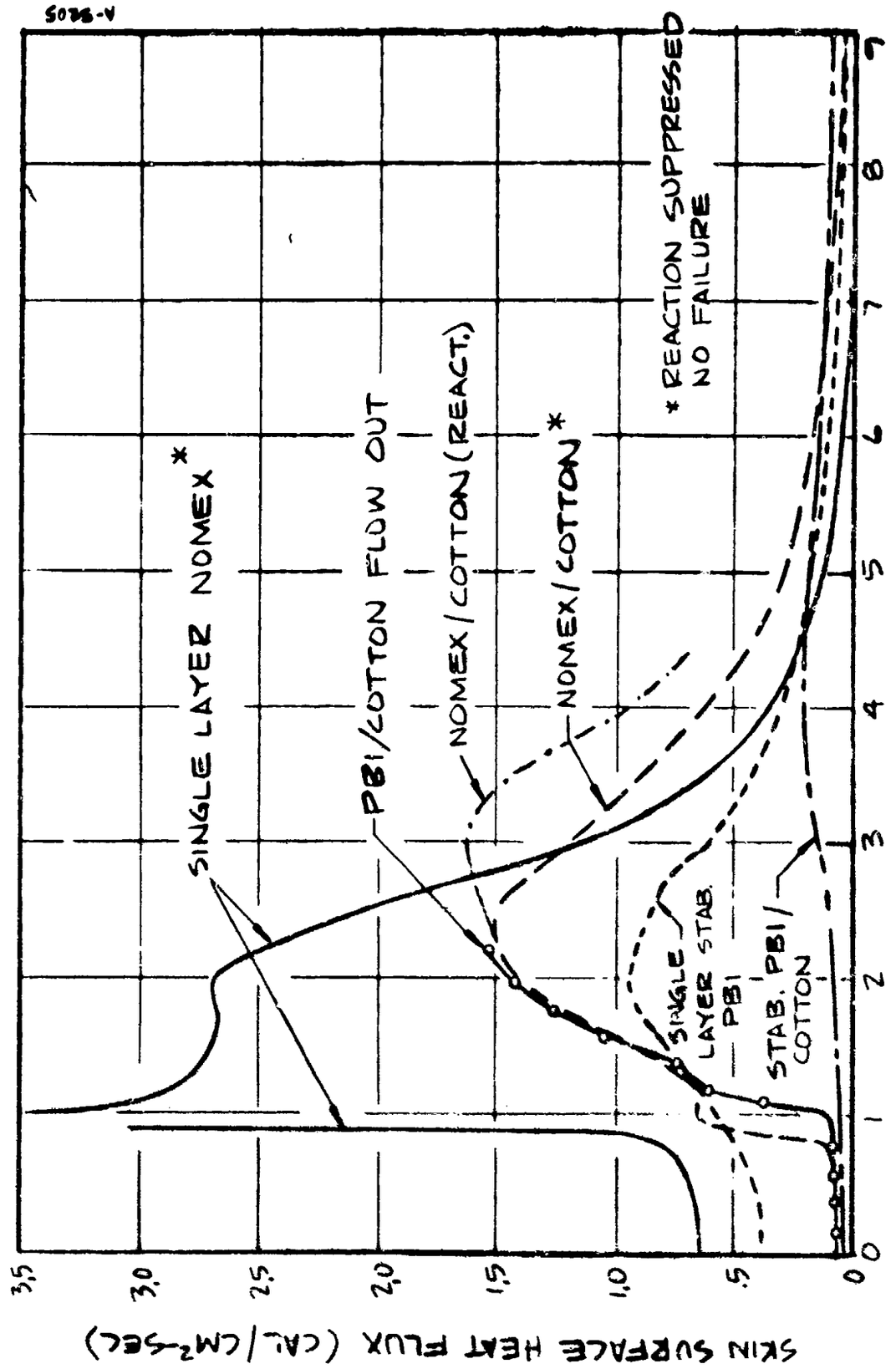

Figure 1. Heat Flux Absorbed by Skin for Various Clothing Assemblies - Nominal Fire (11.6 cal/cm²sec)

of the dermal layer are predicted for both PBI and Nomex single layers, while single layer, stabilized PBI provides considerably more protection. For multiple layers, stabilized PBI over cotton provides complete protection. PBI and Nomex again respond similarly if Nomex is not allowed to react or fail structurally. Both result in deep dermal injury (~ 3/4 thickness). Figure 1 shows the effect of allowing Nomex to react but remain intact. Injury is increased to total dermal. Not shown is the heating if failure occurs. The response in this event would depend upon the condition of the underlying layer and has not been calculated. Based on predicted temperatures failure of Nomex may occur as early as 1.0 second in the nominal fire.

In final summary, this study has shown that stabilized PBI fabrics provide substantially better protection as compared to Nomex and PBI when exposed to nominal fire conditions due to superior performance in three critical areas:

- Stabilized PBI does not shrink whereas fabric temperatures exceed shrinkage temperatures of PBI and Nomex by 200°C and 300°C.
- Stabilized PBI and PBI do not burn whereas Nomex is predicted to ignite and does show flaming in fire pit tests.
- Stabilized PBI and PBI maintain structural integrity whereas Nomex tends to lose strength and fail at temperatures 200°C below predicted peak temperatures.

PBI appears to be better than Nomex primarily because of the loss of strength and burning of Nomex at temperatures above 400°C and 550°C respectively. However, the substantial amount of shrinkage of PBI above 400°C is a serious limitation for long duration, high heating level exposures.

In concluding this study, the results obtained from the analytical model for the three candidate fabrics were compared to test data provided by the Air Force. The tests included both laboratory simulations and full scale fire pit tests using the same three fabrics. Results from these tests confirm the same relative ranking of the fabrics with respect to thermal protection. Nomex provided the least protection, with PBI offering a substantial improvement over Nomex. Stabilized PBI provided superior protection compared to both Nomex and PBI. Results of the fire pit tests obtained from thirty (30) tests for each fabric type are, in terms of body area burned*;

Nomex	49.8%
PBI	28.4%
Stabilized PBI	11.4%

*Total epidermal injury.

SECTION 1

INTRODUCTION

The following report describes the results of an analytical and experimental study designed to understand and achieve a means for predicting the thermal response of a clothing assembly and the underlying human skin tissue when exposed for short durations to a fully developed JP-4 fueled aircraft crash fire. The study has two primary objectives: first to evaluate fire-clothing-skin system in order to determine those properties or qualities of the clothing assembly which are most important in providing protection for the skin. The goal of this objective is to provide guidance in the design of fabrics and clothing systems which may be exposed to fire environments. The second primary objective is to evaluate three candidate fabrics being used or considered by the Air Force as materials for flight suits. These include Nomex, PBI (polybenzimidazole), and stabilized PBI.

In order to pursue these objectives, a complete analytical thermal model of the fire-clothing-skin system has been developed which considers the thermochemical mechanisms that determine the thermal response of both clothing and skin. This includes:

1. Heat transfer by conduction and radiation within and between fabric layers and skin
2. Decomposition (mass loss) of the fabric by pyrolysis at elevated temperatures
3. Thermochemical reaction between the pyrolysis gases and the environment including the capability for predicting ignition
4. Energy transfer by vaporization and subsequent condensation of water and other condensable vapors from the fabric onto the skin
5. Effects of possible shrinkage of fabric on the gaps between layers and skin
6. Variation of fabric properties with temperature
7. Exchange of energy with the environment by radiation and convection.

An existing, sophisticated computer code has been adapted to the solution of this problem. This code is a one-dimensional, time-dependent, finite-difference implicit solution of the energy balance equations written for a set of isothermal nodes which describe the system. The code accounts for all the above factors

and provides a thermal history of each of the nodes of the clothing and skin models.

Protection performance is based upon the burn injury levels sustained by the skin as a result of exposure to a defined, standard fire. Burn injury is determined from the thermal response of the skin, being dependent upon temperature, time, and depth into the skin. A summary of the model and description of the computer code is given in Section 2.

A major portion of this study is directed toward defining fire, clothing, and skin systems. Section 3 includes a thorough review of skin thermal, physical, and optical property data and burn assessment literature. These data have been complied and developed into a detailed thermal model of human skin. The model includes the calculation of accumulated burn injury as a function of depth and time. This model is compared to existing human and porcine burn data to establish validity of the model.

The fire environment must be understood to provide realistic boundary conditions to the clothing-skin system. This includes a description of both the radiation and convection characteristics. The spectral characteristics of the radiation and the composition of the flame gasss. Details of the fire characterization are described in Section 4. Included in this work is the development of an analytical model for the prediction of pool fire characteristics.

Results of an extensive review of fabric material properties and results of tests performed to determine necessary properties are included in Section 5. Included are results of optical property, shrinkage, and thermochemical property tests.

Section 6 describes the results of the analytical study which includes an initial, simplified parametric analysis and a detailed parametric analysis. The purpose of the initial analysis was to identify the important characteristics which would require more detailed investigation. This study did not include thermochemical and shrinkage effects. The work reported in Sections 3, 4, and 5 was guided by this initial study. Using the more detailed description of the system and the complete code, analysis was performed for each of the fabrics as a single layer and with an underlayer of cotton. Finally a detailed parametric analysis was conducted to investigate the effects of additional fire and fabric property variations. Predicted results of the analytical study are compared to laboratory and fire pit test data obtained by the Air Force in Section 7.

Conclusions and recommendations for future study are presented in Section 8.

Before proceeding, a comment about units is in order. Following the common, or natural, units used by various disciplines and investigators results in a pot-pourri of systems; yet, the understanding, or "feel" for what is happening is often deep-seated in the tranditional unit. In this report all quantities, except as

noted, are reported in metric units. In general, the quantity is first reported in the common unit and if this is not metric, is then followed by the appropriate metric conversion in parentheses. In instances in which data and figures collected from the literature are used, these data are presented in their original units. Conversion of data and scales to metric units has been added where possible.

SECTION 2

THERMAL MODEL OF THE FIRE-CLOTHING-SKIN SYSTEM

In the following section the thermal model is described including modeling assumptions, basic equations used, and properties and quantities required to solve the equations.

2.1 JP-4 FUEL FIRE

The fire as such is not part of the mathematical, thermal model, but its description does provide the time-dependent boundary condition which represents the potential or driving function for the transient response of the clothing-skin system. In section 4 of this report, JP-4 fuel fire characteristics are reviewed and nominal thermal conditions are defined. The nominal fire used in this study has a temperature of 1850°F (1010°C) and is considered to radiate as a black body at locations at least 3 feet (1 meter) from the edge. Assuming a relative velocity between fire gases and the clothed subject of 15 ft/sec (4.5 meters/sec), forced convection has been estimated to be 20 percent of the total heat flux, black body radiation at the flame temperature providing 80 percent. A nominal exposure duration of 3 seconds has been selected as consistent with the time required for egress from a burning aircraft given a 30 foot (9.2 meters) radius fire and an escape velocity of 10 ft/sec (3 meters/sec). Based on unpublished data obtained from the Army's Natick open pit fire test facility and the reduction in heat flux at the edge of the fire due to optical thickness, the nominal fire model assumed a linear decrease in flux from a maximum at 2 seconds to zero at 3 seconds. The nominal model assumes constant flux for the first 2 seconds to simulate a crash fire centered on the cockpit. The Natick fires exhibit an entry variation similar to the exit, and parametric runs have been made using a fire model based on measured Natick heat fluxes.

During the fire exposure the chemical composition of the fire is assumed to be an equilibrium composition at the fuel rich A/F ratio of 9.5. Between 2 and 3 seconds the environment is assumed to vary linearly in composition from fire to air. From 3 to 30 seconds the boundary condition is defined to be air at standard conditions with a 70°F (21°C) background radiation and a convection heat transfer coefficient based on a 4-inch (10 cm) diameter cylinder moving at 10 ft/sec (3 meters/sec).

2.2 CLOTHING-SKIN SYSTEM

The system which responds thermally to the fire environment consists of the coupled clothing assembly and skin. The thermal response is computed by the Aerotherm Chemical Charring Ablator (CMA) code which is described below.

2.2.1 Computer Code

The ASTER (Aerotherm Skin Thermal Response) program developed by Aerotherm represents a modification of the Aerotherm CMA code. The CMA code treats the heating, pyrolysis, and combustion (or chemical ablation) of charring materials. It is fully described in References 1 and 2. Section 2.2.1.1 below presents background information about the CMA code. Section 2.2.1.2 then describes the modifications made to deal with particular features of the fabric heat transfer, ignition, and combustion problems not considered in the original code.

2.2.1.1 Charring Material Ablation (CMA) Program

The CMA program is a coded procedure for calculating the in-depth thermal response of a charring, ablating material. The program is an implicit, finite-difference computational procedure for computing the one-dimensional transient transport of thermal energy in a three-dimensional isotropic material. In this respect the code resembles many transient heating or "thermal analyzer" codes. However significant elaborations are required to treat the pyrolysis or charring of material below the surface, the surface erosion or ablation by a chemically active environment.

The model consists of two basic equations, an in-depth energy balance equation written for each isothermal node and a surface energy balance equation written for a control volume including the surface of the external node.

For the purpose of writing the in-depth energy balance differential equation, we introduce the x coordinate system normal to the surface. In this system, we have the energy equation of the form

$$C_p \left.\frac{\partial T}{\partial \theta}\right)_x = \frac{1}{A}\frac{\partial}{\partial x}\left(kA\,\frac{\partial T}{\partial x}\right) + (h_g - \bar{h})\left.\frac{\partial \rho}{\partial \theta}\right)_y + \left.\frac{\dot{m}_g}{A}\frac{\partial h_g}{\partial x}\right)_\theta \qquad (1)$$

in which the individual terms have physical meanings which may be interpreted as follows (from left to right): rate of storage of sensible energy, net rate of thermal conduction, pyrolysis energy rate, and net rate of energy convected with pyrolysis gas passing a point.

In this equation, the local specific heat and thermal conductivity are formulated from input temperature functions for both virgin plastic and char, C_{pp}, C_{pc}, k_p, and k_c. In partially pyrolyzed zones ($\rho_c < \rho < \rho_p$) the specific heat is formulated with a special mixing rule

$$C_p = xC_{pp} + (1 - x)C_{pc} \tag{2}$$

where the weighting variable x is based on the convenient fiction that partially pyrolyzed material is a simple mixture of pure virgin plastic and pure char. The quantity x is defined as the mass fraction of pure plastic in this imaginary mixture which yields the correct local density:

$$x = \frac{\rho_p}{\rho_p - \rho_c}\left(1 - \frac{\rho_c}{\rho}\right) \tag{3}$$

The thermal conductivity k is weighted in the same manner.

The pyrolysis gas enthalpy is an input temperature dependent function. The quantity $\bar{h} \triangleq (\rho_p h_p - h_c \rho_c)/(\rho_p - \rho_c)$ is computed from temperature dependent h_p and h_c values determined from the input temperature dependent C_{pp} and C_{pc} values and input enthalpies of formation ΔHf_p and ΔHf_c.

The other quantities in Equation 1, T and ρ, are dependent quantities discovered during the solution process. The density ρ is determined assuming that the basic pyrolysis physics correspond to simple charring of the form

$$\text{plastic} \rightarrow \text{char} + \text{gas}$$

according to a three-component Arrhenius rate law where

$$\rho = \rho_A + \rho_B + \rho_C \tag{4}$$

and the rate of change of density as a function of temperature and density is determined from the relation

$$\frac{\partial \rho}{\partial \theta} = \sum_{i=A,B,C} B_i \rho_{o_i} \left(\frac{\rho_i - \rho_{r_i}}{\rho_{o_i}}\right)^{\psi_i} \exp(-E_{a_i}/RT) \tag{5}$$

The rate constants B_i, ψ_i, and E_{a_i} are determined for each fabric from TGA (Thermal Gravimetric Analysis) data.

The most powerful and unusual feature of the CMA program is its general coupling to a thermochemical erosion energy balance at the exposed, heated surface. This coupling involves two aspects: the surface energy balance formulation

itself, described in this section, and a chemical state program used to provide input information for the energy balance process.

The surface energy balance is derived from a consideration of the energy flux terms passing through a control volume drawn about the surface as shown in the sketch below.

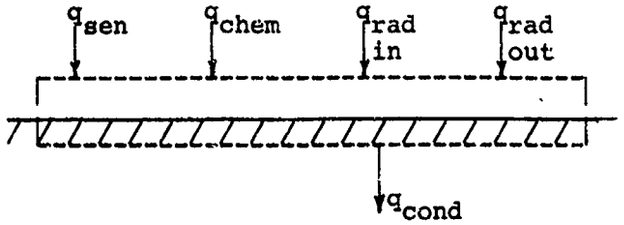

Surface Energy Balance Control Volume and Energy Fluxes

The term q_{sen} represents the "sensible convective heat flux." Physically, this is the convective heat flux which would occur for a frozen boundary layer and a non-catalytic wall in the absence of mass transfer. It excludes all chemical energy contributions, and the term q_{chem} represents the net of a number of fluxes of chemical energies at the surface. The terms q_{rad} and q_{cond} represent the radiation and conduction transfer to both the external environment and to the the interior nodes. The surface energy balance equation written in complete form is

$$\rho_e u_e C_H \left[H_r - (1 + B')h_w\right] + \dot{m}_g h_g + \alpha_w q_{rad} - F_1 \sigma \varepsilon T_w^4 - q_{cond} = 0 \qquad (6)$$

where the first term represents the exchange of energy between the surface and the external environment including both sensible and chemical energy fluxes. The term $\rho_e u_e C_H$ represents the mass and energy flux coefficient (C_M is assumed to be equal to C_H) and H_r and h_w are the recovery enthalpy and gas enthalpy at the wall respectively. The term B' is the dimensionless mass flux of pyrolysis gases. The term $\dot{m}_g h_g$ is the energy term for pyrolysis gas flow into the control volume from the material below. Radiation from the environment is $\alpha_w q_{rad}$ and that reradiated to the environment is $F_1 \sigma \varepsilon T_w^4$. Finally, q_{cond} is the conduction of energy into the material.

Before proceeding to the code modifications made for this study some general remarks concerning the surface thermochemistry model are in order. The sketch below illustrates the mass fluxes of interest at the heated fabric surface for any element k. There is a diffusive flux $\rho_e u_e C_M$ of environment gases to the surface. The rate of arrival of pyrolysis gases from below is $\dot{m}_g$. Computation of the state of the surface requires the simultaneous solution of

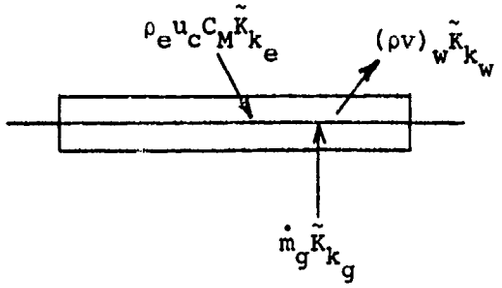

Mass Flux Terms at Surface for Element k

elemental mass balances for each element k, chemical equilibrium or kinetic relations for each species i considered, and a surface energy balance. The mass and chemistry calculations are carried out by the ACE code, as discussed above, while the surface energy balance is treated by the ASTER program.

The user himself must select the chemical relations to be employed. In high temperature problems, complete chemical equilibrium is usually a safe assumption. In addition, the equilibrium assumption is mechanically simple to effect: a standard, universally valid collection of equilibrium constants (such as those supplied by JANAF in Reference 3 for example) may be supplied to the code. Unfortunately, the fabric combustion problems of interest in this work have fabric temperatures low enough (< 800°C) that equilibrium is probably a poor assumption. As a practical matter, kinetic control renders calculations very difficult (even though the ACE code is completely general and will handle kinetically controlled reactions as easily as equilibrium laws) because kinetic data are difficult to obtain and appear to be heavily influenced by trace constituents in the environment and in the material as well as by numerous details of surface physical appearance. These complexities usually preclude useful calculations under kinetic control.

Consequently, program users frequently avoid detailed consideration of individual kinetically controlled reactions by the definition of limiting extreme cases eliminating some reactions or groups of reactions entirely. Some typical limiting cases worthy of consideration are

- Full equilibrium between environment and fabric residue, but pyrolysis gases held isolated from this equilibrium system
- Full equilibrium between pyrolysis gases and environment ("pyrolysis gas combustion"), but no reaction between this system and fabric residue
- Total isolation: pyrolysis gas, fabric residue, and environment are all isolated from each other.

In some cases it is possible, by comparing calculated results and experimental data to devise useful composite models which feature a limiting kinetic control case at low temperatures and full equilibrium at high temperatures, with an assumed transition between cases at intermediate temperatures. Such an approach avoids the detailed consideration of individual kinetically controlled reactions.

The study reported here is the first such attempt to predict the pyrolysis, ignition, and combustion of fabrics from fundamental principles. Consequently, it was desired to study limiting cases as a reasonable first step in analysis. The two cases considered are total isolation and full equilibrium, as discussed in the following subsections.

2.2.1.2 Development of the ASTER Code

The CMA program described above contained a number of deficiencies when used as a computational tool for the fabric heating problem. In order to account for the important heat transfer mechanisms and the various factors upon which they depend, modifications of the basic CMA code were undertaken. Those features which were added are discussed below.

Water. Fabrics contain an appreciable amount of water which evaporates at 100°C or in a very narrow temperature band above 100°C.* The energy effects of this evaporation are important and must be accounted for. Although use of the three Arrhenius pyrolysis reactions could be used to model this evaporation, the necessarily high activation energy required leads to numerical solution difficulties. In addition, it was desired to retain all three Arrhenius reactions to model fabric pyrolysis. Hence a new water evaporation physical model was needed.

The simplest available computing strategy was adopted. Provision was made for the user to specify the initial amount of water in each finite difference node. The program computes a thermal transient in the normal manner, except that the increased specific heat effect due to the water content of each node is noted, until any node temperature exceeds 100°C. When such an overshoot occurs, the time step is reduced so as to bring the temperature exactly to 100°C. all events during the time step being recomputed. Thereafter the node is flagged as an evaporating node. Temperatures of such nodes are damped at 100°C and amounts of water evaporated from such nodes are computed from the net thermal flux to the node. Should the remaining water content drop below zero, the time step is reduced to bring the water content exactly to zero, all events during the time step being recomputed. Thereafter the node is classified as a dry node and is excluded from the water logic. Computations proceeds as in the unmodified program.

*Based on TGA data taken at low rates. Subsequent high rate tests suggest the release of moisture may be extended to higher temperatures.

Gap Thermal Conductance. The existing CMA code treats contact resistance between finite difference nodes only as an input constant in each case. In practical fabric problems, gaps are large and the gap thermal conductance comprises temperature dependent conduction and radiation components. Consequently, a gap thermal conductance computing procedure was requested, and an appropriate procedure was added to the code.

Gap conductance is taken as the sum of conduction and radiation in parallel

$$u_g = u_c + u_r \tag{7}$$

Gap conductance is computed as (on a unit area basis)

$$u_c = \frac{k_g}{l_g} \tag{8}$$

where l_g is the current gap thickness and k_g is the gap thermal conductivity, which is taken for simplicity as the conductivity of air.

The radiation conductance is taken as

$$u_r = \frac{\sigma(T_1^2 + T_2^2)(T_1 + T_2)}{\frac{1}{\epsilon_1} + \frac{1}{\epsilon_2} - 1} \tag{9}$$

Where T_1 and T_2 are the temperatures at the fabric surfaces (determined from node temperatures by interpolation) and ϵ_1 and ϵ_2 are the emittance values for the nodes on either side of the gap.

Both u_c and u_r are recomputed during each time step, since temperatures are varying, affecting T_1, T_2, ϵ_1, ϵ_2, and k_g, and also l_g may vary due to shrinkage, as will be discussed below.

Shrinkage Effects. The shrinkage of fabrics at elevated temperature changes the local material density and reduces gap widths. The first effect must be noted in the transient heat conduction calculations and the second in gap thermal conductance calculations. The first requires only simple density changes and the second requires some bookkeeping to account for the linear shrinkage of each fabric layer compared with an assumed initial radius (such as of a limb or of the torso). Current gap widths l_g can then be employed in Equation 8 above.

Radiation Absorption. Fabrics are typically translucent and incident radiation is absorbed in all fabric layers. Appropriate changes to finite difference nodal energy balances were required. In the CMA code the incoming radiation flux is either reflected or absorbed at the surface. In the ASTER code this flux may be absorbed in all fabric layers. Changes were made to allow the user to input an absorption function for each fabric layer. The absorbtion for the layer is distributed over all nodes appearing in the layer (if more than one) and an appropriate energy term appears in each nodel energy balance equation.

The absorption function is made to be a function of shrinkage. Thus it is an implicit function of temperature. Based on shrinkage test results (see Section 5), the optical properties were assumed to vary linearly from the virgin to the charred (shrunken) condition over the range on onset of shrinkage to maximum shrinkage or the temperature at which the sample was taken in the case of no maximum in the shrinkage relation.

Skin Heating and Thermal Damage Parameters

Certain derived output quantities relating to total energy absorbed by the skin and to skin damage assessment were desired. These simple calculations involve skin node temperature and require no extended comment. Section 3 discusses the skin damage assessment model.

2.2.1.3 Solution Procedure

As in all finite difference procedures, each step of the solution is made over an incremental time step $\Delta\theta$. Each computational step has three main events: internal decomposition, internal energy balance, and surface boundary energy balance. Computation of the three events gives "new" values of nodal densities, pyrolysis gas flow, nodal temperatures, and surface temperature and ablation rate. The program is then ready for the next step.

The pyrolysis event is computed for each nodelet in the main material from Equation 5, summed over the three components. Summation over all nodelets in a node gives the nodal $\partial\rho/\partial\theta$ and contribution to $\dot{m}_g$. Note that "old" known nodal temperatures (interpolated into the nodelet locations) are used in the pyrolysis calculation.

The internal energy balance equation then is computed "implicitly" for each node, using "new" temperatures in the heat conduction terms. The energy balance is linked explicitly to the decomposition events, however, since the pyrolysis gas fluxes used in the energy balance are derived from the explicit decomposition calculation. The energy balance is also linked explicitly to the

surface boundary condition through the use of an "old" surface recession rate in all convection terms involving fluxes of solids. All other links to surface events are implicit.

The "implicit" formulation of the in-depth nodal energy equations yields a tri-diagonal set of equations which is solved for the unknown temperatures in two passes of direct elimination. The first pass eliminates one unknown from each equation and leaves the equation for the first node (at the heated surface) with only one unknown. The first node equation (the surface energy balance equation) is nonlinear and so the first nodal temperature must be discovered by an iterative procedure which assumes a temperature, calculates the error in the equation, uses this error to correct the temperature guess and repeats this process until the energy balance error is negligible compared to the major terms in the equation.

2.2.2 Fabric Model

The following subsection describes the fabric model and parametric values.

2.2.2.1 Models

Two models are considered in the detailed parametric analysis (Section 6.2); the first being a single layer of fabric with an initial gap of 0.5 cm covering the skin, the second being a two layer model with one layer of fabric and a single underlayer of cotton At the beginning of multilayer exposures, the gaps between layers are set equal at 0.25 cm so that the total gap is again 0.5 cm. These gap dimensions are based on a 10 cm diameter limb and a 10 percent oversized outer fabric layer. In each model, each fabric layer is divided into two nodes. Figure 2 shows the two layer model including the nodal structure and the energy transport terms considered in the code. At the surface each of the terms which enter into the surface energy balance are shown. Then energy is exchanged between the surface and the center of the outer node by conduction and the filtering effect of pyrolysis gas flow. In turn, energy flows from the center of the outer node to the inner node by conduction. Water vapor generated in either layer may be caused to flow outward leaving the system or inward depositing directly on the skin. Radiation from the fire is absorbed in both layers (each node is assumed to absorb half the total absorbed by the layer) with the portion transmitted passing directly to the lower layers. Any direct transmission reaching the skin is assumed to be totally absorbed in the surface node.

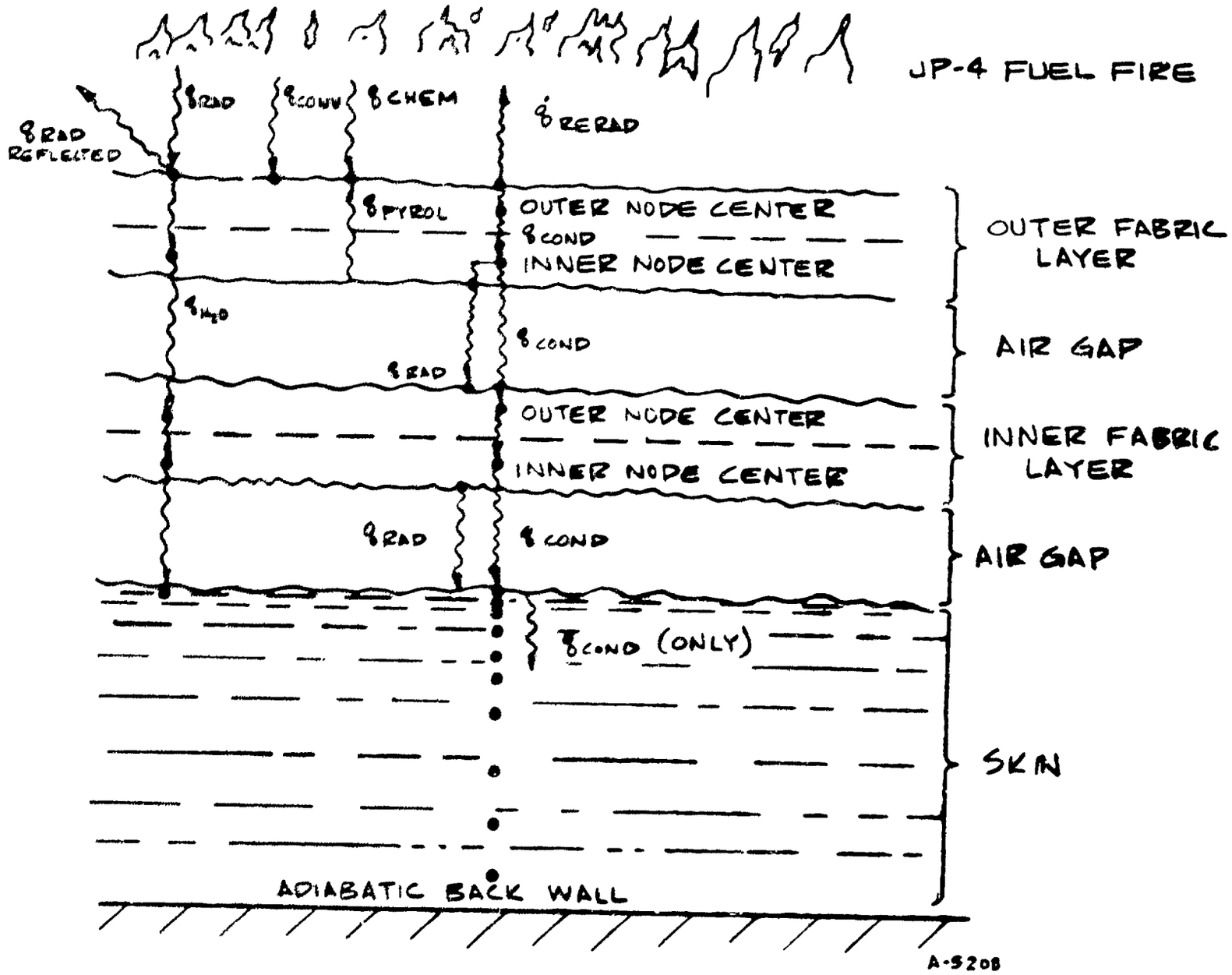

Figure 2. Two Layer Fabric-Skin Nodal Model

The air gap is assumed to have zero mass since the mass in the gap is negligible compared with the fabric layers. Thus in the model, the air gap serves as a conductive and radiative resistance with resistance to conduction proportional to the gap thickness and the radiation resistance dependent only upon the surface temperatures which are extrapolated from the node centers.

The model of the inner fabric layer is identical to the outer layer except that a surface energy balance is not required. The code is written to account for water evolution, decomposition and shrinkage of this layer. The skin receives energy at the surface by direct radiation from the fire, radiation and conduction from the inner node of the inner layer.

2.2.2.2 Summary of Fabric Property Data

Table I summarizes the fabric optical, thermal, and physical properties. Complete details are contained in Section 5 and the appendices.

2.2.3 Human Skin

Section 3 of this report contains an extensive review of the thermal, physical, and optical properties of the skin which determine the thermal response. For the thermal exposures of interest here, the skin is essentially opaque to thermal radiation and can be considered to transfer energy internally by conduction only, since exposure durations are not longer than the minimum response times reported for increased body thermoregulatory system activity. Consequently, for the skin, the in-depth energy balance equations can be reduced to the simple heat conduction (Fourier) equation

$$\rho C_p \left.\frac{\partial T}{\partial \theta}\right)_x = \frac{\partial}{\partial x}\left(k \frac{\partial T}{\partial x}\right) + q \qquad (10)$$

where ρ, C_p and k are functions of x and θ and q is the absorbed radiant energy which is a function of θ. Since the skin is assumed to be opaque, all the radiant energy incident on the surface is absorbed by the surface node, and thus the q term is included in the first skin node energy balance equation only.

In the finite difference solution scheme, an equation is written for each node i in the following form:

$$\frac{\left(T_i^{n+1} - T_i^n\right)}{\Delta\theta}\left(\rho C_{p_i}\right) l_i = \frac{T_{i-1}^{n+1} - T_i^{n+1}}{\frac{l_{i-1}}{2k_{i-1}} + \frac{l_i}{2k_i}} - \frac{T_i^{n+1} - T_{i+1}^{n+1}}{\frac{l_i}{2k_i} + \frac{l_{i+1}}{2k_{i+1}}} \qquad (11)$$

TABLE I

FABRIC PROPERTIES

Property	Nomex	Stabilized PBI	121
Weight (gm/cm^2)	0.0139	0.0146	0.0149
(oz/yd^2)	4.1	4.3	4.4
Thickness (cm)	0.0323	0.0364	0.0323
(in)	0.0127	0.0143	0.0132
Moisture Regain	5.0	12.0	13.2
Specific Heat (cal/gm°C) (5°C to 283°C)	0.30 → 0.48	0.38 → 0.45	0.38 → 0.45
Optical Properties (1010°C B.B.)			
Virgin: ρ	0.26	0.23	0.21
Virgin: α	0.57	0.62	0.73
Virgin: τ	0.17	0.15	0.06
Char: ρ	0.17	0.18	0.21
Char: α	0.72	0.76	0.78
Char: τ	0.11	0.06	0.01
Linear Shrinkage	32% max from 300 to 400°C	40% max from 400 to 450°C	2% at 500°C to 19% at 840°C

where the values of ρ, C_p, and k are the values for node i at time θ which is denoted by the superscript n on the temperatures and ℓ represents the node thickness. The skin equations are coupled to the clothing assembly equations and solved simultaneously by the ASTER code.

The skin has been modeled with 10 nodes for a total depth of 4 mm which is made up of 100 μm (0.1 mm) of epidermis, 1.9 mm of dermis and 2 mm of fatty tissue. Table II lists the values of the thermal and physical quantities which are used for each of the ten equations of the form of Equation 11 which comprise the skin set of equations. In addition to these equations, the problem is defined by assuming an adiabatic back wall condition at the tenth and final skin (fatty tissue) node. This assumption is valid for the present model which does not consider circulatory effects for short duration exposures. The initial condition is established as a uniform temperature of 32.5°C (90.5°F) for all skin nodes.

Nodes have been selected to provide optimum accuracy and efficiency and to emphasize the response at depths corresponding to the epidermal-dermal interface and to the base of the dermal layer. Burn injury is computed continuously as it accrues during the thermal transient according to the criterion hypothesized by Henriques and modified by Stoll. Details of the skin and burn injury models may be found in Section 3.

TABLE II

HUMAN SKIN NODAL QUANTITIES

Node	Thickness (μm)	Depth (μm)	Specific Heat (cal/gm°C)	Density (gm/cm^3)	Thermal Conductivity (cal/cm sec°C) * 10^{+4}	Absorptivity
1	25	12.5	1.0	1.0	5.5	1.0
2	50	50.0	1.0	1.0	6.5	0.0
3	50	100.0	1.0	1.0	7.5	0.0
4	100	175.0	1.0	1.0	9.0	0.0
5	200	325.0	1.0	1.0	11.0	0.0
6	375	612.5	1.0	1.0	12.5	0.0
7	500	1050.0	1.0	1.0	13.5	0.0
8	650	1625.0	1.0	1.0	13.8	0.0
9	100	2000.0	1.0	1.0	14.0	0.0
10	2000	3050.0	0.5	1.0	4.0	0.0

SECTION 3

SKIN THERMAL MODEL AND BURN INJURY ASSESSMENT

3.1 INTRODUCTORY COMMENTS

The effort on developing a skin thermal model and establishing criteria for assessing the amount of burn injury has been guided by the following goals as related to the purpose of this contract, i.e., the evaluation of fabrics. These goals are listed in order of importance.

1. To provide a standard method for comparing the performance of various flight suit ensembles and fabrics in terms of the relative extent of burn injury to a nominally defined human.
2. To provide an adequate thermal model of the thermal boundary condition for the inner surface of the fabric, i.e., the thermal response of the skin surface is coupled to the response of the fabric.
3. To provide a meaningful indication of the extent of burn injury. Note that this differs from 1 above in that here the emphasis is on the absolute injury, whereas in 1 above only the relative amount is necessary to compare the performance of the clothing.

3.2 SKIN THERMAL MODEL

The important properties of skin tissue fall into three categories, thermal, optical, and physical. The thermal properties are the thermal conductivity and specific heat. The optical properties include the surface reflectivity, in-depth absorptivity and the surface emissivity, while the physical properties include the density and the depth or location below the surface of various characteristic layers. All of these properties may be functions of many variables including time, temperature, pigmentation, individual human, location on the body, state of the circulatory system, form of energy transport to the surface, spectral distribution of radiant energy, and so on. The approach of the following subsections is to present a thorough review of the present state of knowledge and then to delineate the regime of importance of each property in terms of the definition of this program. Factors included in this definition are:

1. A 3 second exposure to
2. A fully developed JP-4 fuel fire
3. Use of typical flight suit fabrics and ensembles

The preliminary study (see Section 6) provides a definition of the range of heat flux levels and temperature response of the fabric and skin tissue. Results from this study have been used extensively to evaluate the importance of various parameters affecting the skin tissue properties as noted in the comments to follow.

3.2.3 General Physical Description of Human Skin

Human skin represents a sophisticated biological system which provides many functions to the support of life. Many of these functions depend upon the ability of the skin to change in some manner which may cause a change in properties. For this reason a well-defined physical description proves difficult particularly in terms of the application of standard engineering concepts and methods. The purpose of this section is to present a reasonably complete description of the skin, but one which deals only with those features which are of greatest consequence to the problem of response to short term exposure to intense heating.

Skin, as the term will be used here, is comprised of those layers of tissue which provide a covering to the subcutaneous matter such as fat or muscle tissue. It contains two major regions, the thin outer layer called the epidermis and a thicker inner layer or dermis. The epidermis consists of a series of distinguishable layers which merge into one another, the outermost consisting of loosely connected layers of highly dessicated cells. As one proceeds into the epidermis the layers become more densely packed and less dessicated. Moritz and Henriques[4] state that the outer layers of the epidermis appear to be incapable of vital reaction. Their studies indicate that the total thickness of the porcine epidermis is 80 ± 10μ. Mitchell[5] suggests a somewhat larger variability for human skin reporting values from 70 to 120μ. Buettner[6] employs a value of 120μ in his theoretical analysis and Stolwijk and Hardy[7] chose a value of 100μ for their analytical model. As for the depth of the dermal layer, Moritz and Henriques suggest a value of approximately 2 mm while the Stolwijk-Hardy model extends to only 0.8 mm. Clearly there is no single value of layer depth which is valid for all subjects and areas, in fact, biopsy cross-sections (see Moritz[8]) indicate that the layer thicknesses change over a considerable range within quite small lateral regions. The characteristic undulations of the epidermal layer occur within distances and with amplitudes on the order of the layer thickness.

In order to be consistent with the objectives of this study, it is most important to select a reasonable model of the skin; one which will reflect the average or nominal. In this spirit, the most appropriate values for the epidermal and dermal layer thicknesses are judged to be 100μ and 2mm respectively.

A general note of caution must be emphasized following this choice. It will not be possible to expect the model to predict the amount of burn injury for any given individual or specific body location. Because, as will be described subsequently, the degree of injury is often associated with observable conditions related to, for example, the state of the epidermal-dermal interface, the depth of this layer becomes a critical factor. Since it may be considerably different from the chosen average or nominal, the model will not predict the same extent of injury. A problem which contains so many variables and uncertainties must be approached statistically. Thus, it is the intent here, with layer depth as with all the properties of the skin to be discussed, to base the skin model upon consensus values derived from those reported in the literature and weighted by a judgment of the source of the data.

3.2.2 Skin Thermal Properties

3.2.2.1 Thermal Capacitance

For the purposes of a thermal model, two properties, the density, ρ, and specific heat, c, can be combined into a single equivalent property, the thermal capacitance, ρc. Few actual test data exist in the literature probably because this property does not appear to be widely variant. Most investigators describe the thermal capacitance of skin as being roughly equivalent to that of water and offer measurements to substantiate this approximation. Table III lists the values of ρc, ρ, and c as measured or used by various investigators. Although the variation in ρc is only 0.8 to 1.03, it is interesting to note that densities vary from 0.8 to 1.2, a 50 percent variation.

The accurate knowledge of the thermal capacitance is of particular concern for the short duration, transient response problem where the heat flux at the surface is the known input quantity. As an example, we know that the average tissue temperature at any time is a linear function of the thermal capacitance. The influence of ρc on local tissue temperature as a function of time and depth, is dependent upon the form of the heat flux profile. Investigation of this influence using the skin model and realistic heat fluxes will be described later.

None of the reported values include any indication of variation in depth. Moritz and Henriques[4] in describing the physical appearance of various levels of tissue, indicate that there is a progressive loss of intracellular water as the cells become older, i.e., as they progress toward the surface and away from

TABLE III

REPORTED VALUES OF SKIN THERMAL CAPACITANCE

Thermal Capacitance, ρc ($cal/cm^3 °C$)	Density, ρ (gms/cm^3)	Specific Heat, c ($cal/gm°C$)	Source (Reference)
1.0	0.8		Moritz & Henriques [18]
1.0			Buettner [6]
	1.1 → 1.2		Leider & Bunche [9]
0.8			University of Rochester [45]
0.81 → 1.0			Derksen, et al. [38]
1.03	1.2	0.86	Hardy, et al. [24]
1.0			Stoll [13]
1.0			Hardy [7]
1.0			Mitchell [5]
0.835			Hottel [69]
0.8			AFSWP [5]

the dermal layer. As stated above, the general acceptance of the nominal value of 1.0 cal/cm^3°C for ρc is based on the observations that skin tissue is composed largely of water and thus assumes the general properties of water. If the epidermal cells are dessicated relative to the dermal layers, a variation in ρc might be anticipated unless the non-water mass were also of similar ρc. Stolwijk and Hardy,[7] in their thermal model of the skin, subscribe to this approach by assigning uniform ρc to all nodes within the epidermal and dermal layers.

Following the general consensus, it seems appropriate to accept the value of skin tissue thermal capacitance as being a constant, independent of all problem variables and equal to a value of 1.0 cal/cm^{5}sec. This is not considered to be a wholly satisfactory situation as mentioned before; however, in view of the even greater uncertainties in other properties (to be described), acceptance of this value and its constancy will not represent a major source of error.

3.2.2.2 Thermal Conductivity

3.2.2.2.1 Factors

The thermal conductivity of skin tissue is of dominant importance largely because of its apparent variability with a large number of parameters and the problems encountered in its measurement. A review of the literature is discouraging if one is accustomed to well-defined thermal properties. The elusiveness of achieving this condition is the direct result of dealing with a living organism. Not only do the characteristics of the skin change from one location on the body to another and from body to body, etc., but also, they change with time and with the demands on the body's thermal control systems. Chato,[9] in his survey of thermal properties of biological systems, summarizes the problem in noting that one can not generalize about "in vivo" heat transfer and that the classical concepts of thermal conductivity and diffusivity may be inappropriate quantities for living biological systems. How does one account for the variation in blood flow that occurs as the vascular system responds to heating or cooling or the many complex chemical reactions taking place? Lipkin and Hardy[10] and others describe vasodilatation as an increase in the apparent thermal conductivity whereas in reality, energy is being convected away from the surface at a higher than normal rate. Historically, analytical modeling of the skin has not accounted for convected energy in order to simplify an extremely complex problem; thus, the concept of apparent thermal conductivity. Recent studies by Shitzer and Chato[11,12] and others have begun to include convection of energy by the blood in considering the long term transient and steady state response of the body to thermal stimuli.

Fortunately, because of the short exposure times of the current problem, we are able to ignore certain of the biological response mechanisms. Lipkin and Hardy[10] showed in their experiments on humans (in which they measured the temperature response at the surface of the skin exposed to square wave radiant heat flux pulses) that vasodilatation effects were not observed until at least 20 seconds* after the beginning of heating. This was accomplished by comparing the response of blackened skin with and without restriction of blood flow. In the case of restricted blood flow, it was shown that the thermal inertia of the skin, $k\rho c$, was constant for at least 60 seconds with a temperature rise of 15°C (27°F). The value obtained was nearly equal to that for normal skin for up to 20 seconds with significant deviation beginning at 30 seconds. By 45 seconds, the temperature at the surface of the normal skin reached a constant level even though energy was still being applied to the surface.

For 3 second exposures to a JP-4 fuel flame, results in Section 6 show that the heat flux incident on the skin surface will peak at from 3 to 10 seconds depending upon the number of clothing layers. In addition, it will be shown that if the skin is to be injured, the damage will be sustained well before the 20 second point. Consequently, the effect of vasodilatation on the thermal response will be neglected. It is noted in passing that this is a conservative assumption relative to the prediction of burn potential particularly if exposure durations tend to be longer or if there might be some preconditioning of the skin, e.g., the anticipation of a crash and/or low level exposures while egressing from the cockpit causing vasodilatation prior to direct exposure to the flame.

3.2.2.2.2 Methods of Measurement

Measurement of the skin's thermal conductivity presents a major difficulty to investigators. Various techniques have been developed; standard methods have been used on excised samples, but these results must be discounted since they are of questionable relevance to living tissue. One of the more common and successful approaches has been to measure the surface temperature during the transient response to a square wave radiant pulse. The temperature rise can be described by the equation

$$T_s - T_o = \frac{2Q\sqrt{\theta}}{\sqrt{\pi k\rho c}} \qquad (12)$$

*Buettner[6] reports that changes in the apparent conductivity did not occur for less than 30 to 60 seconds in his experiments.

enabling the solution for the product kρc, the thermal inertia, using the measured heat flux, time, and temperature. Since these quantities are all available as functions of time, the value of kρc can be determined as a function of time as well, as was done by Lipkin and Hardy[10] and Weaver and Stoll.[13] The approach is generally credited to Buettner.[14]

The measurement of surface temperature is the most critical factor. Early attempts used contact thermocouples, achieving questionable results due to the thermal conductance and capacitance of the wire, and the difficulty of insuring good contact without putting excessive pressure on the skin. Mixter,[15] Hardy,[16] Stoll and Greene[17] and others have improved this by using a radiometer to measure surface temperature. These results appear to be reasonably consistent and thus provide the best data currently available. Reported values are listed in Table IV many of which are taken from the extensive survey by Chato.[9]

3.2.2.2.3 Comments on Reported Values

There is considerable variation among these values. Unquestionably, some of this is due to the different measurement and data reduction techniques used and their associated uncertainties. However, there are definitive trends apparent as well, namely,

1. There are definite variations with location on the body. Most of the studies have used forearm skin, but measurements on the thigh and fingertip by the same techniques and investigators indicate significantly higher values at these locations.
2. The effect of blood circulation or the increase in circulation is capable of increasing the apparent conductivity by more than an order of magnitude.
3. There is a definite increase in conductivity with depth.

As noted previously, relative to this final observation Moritz and Henriques[4] have described the nature of the various distinguishable layers of skin as becoming progressively dessicated as they approach the surface. The thermal conductivity of pure water at normal skin temperatures is 14.9×10^{-4} cal/cm sec°C, a value that appears as a reasonable upper bound for most of the reported values in Table IV for living skin without increased blood flow. The measurements of Henriques and Moritz[18] and those of Hensel[19,20] clearly establish that conductivity increases with increasing depth, being on the order of 5.0×10^{-3} cal/cm sec°C in the near surface layers (epidermal) to 9 to 16 in the dermal layers. Lipkin and Hardy[10] also show the same quantitative relationship in their measurements on excised skin. Thus it appears that the non-water matter

TABLE IV

MEASURED VALUES OF SKIN THERMAL CONDUCTIVITY

Source*	Value (cal/cm sec°C)10^4	Comments
Henriques & Moritz	5.0	1947, Epidermis
"	8.85	1947, Dermis
Lomholt	5.0	1930, Skin
Roeder	8.0	1934, Skin
Buettner	9.0	1936 0-2 mm skin
"	13.0	1936 cool living skin
"	67.0	1936 warm living skin
Aschoff	8.0	1938 cold living hand
"	22.9	1938 normal living hand
Hensel	4.8 → 6.0	1952 0-0.45 mm living under arm
"	8.0 → 10.0	1952 0-0.9 mm living under arm
"	10.4 → 13.0	1952 0-1.3 mm living under arm
"	43.0 → 54.5	1952 0-1.0 mm living thigh
"	78.0 → 96.2	1952 1-2 mm living thigh
"	3.2 → 4.0	1950 0-.26 mm
"	4.8 → 6.0	1950 0-.45 mm
"	6.8 → 12.0	1950 0-.90 mm
"	7.2 → 16.0	1950 0-1.32 mm
Lipkin & Hardy	5.5 → 6.8	1954 excised dry
"	7.5 → 9.3	1954 excised moist
"	9.1 → 11.4	1954 living no flow
"	9.1 → 500.0	1954 living flow
Buettner	13.0 → 16.1	1951 living forearm
"	10.1 → 12.6	1951 living average
"	22.9 → 28.6	1951 living fingertip
Hardy	12.5 → 15.6	1951 living
Hardy	12.0 → 15.0	1938 living
Vendrich & Vos	14.0 → 17.5	1957 living forearm
Stoll & Greene	7.5 → 22.6	1959 living forearm
Derksen [38]	7.0 → 12.7	1957
Perkins [41]	18.4	
Mitchell [5]	14.3	
Hottel [69]	10.4	
AFSWP [5]	10.7	

*As reported in Reference 9 unless noted otherwise.

of skin tissue has a lower thermal conductivity than water; on the dry, dead epidermal layers this value is about 5 x 10^{-4} cal/cm sec°C. Buettner,[6] in 1952, attempted to describe this variation with depth with the equation

$$k = 7 * (1 + 3x) * 10^{-4} \text{ cal/cm sec°C} \quad (13)$$

where x is measured in centimeters. Figure 3 shows this equation together with all the known in-depth data. It should be noted that the bulk of these data are due to Hensel who used a thermocouple buried at various depths below the surface to obtain his data. As a consequence, his results have been questioned by Henriques[21] and Stoll and Hardy.[22] However, the trend is certainly established qualitatively if not quantitatively,. Spells,[23] in thermal conductivity experiments with a number of biological materials both solid and liquid, has correlated thermal conductivity with the weight fraction of water contained at normal body temperatures as,

$$k = (1.34 + 13.6 \times Wf_{H_2O}) \times 10^{-4} \quad (14)$$

which for $Wf_{H_2O} = 1.0$, gives the conductivity of pure water as noted above. Also, the non-water matter is indicated as having a conductivity about one order of magnitude less than water. If the epidermal layer's conductivity were 5 x 10^{-4} cal/cm sec°C, then according to Equation 13 the fraction of water would be about 0.27. Spells work limits the maximum real thermal conductivity of the biological material studied to that of water. Assuming that the thermal conductivity of the non-water matter of skin tissues does not exceed that of water, then, based upon the measured values of epidermal tissue and dry excised tissue, it can be stated that the real thermal conductivity of any layer of tissue will not exceed that of water at the same temperature.

Stolwijk and Hardy,[7] in an early analog computer model of the skin, used a variation in depth as shown in Figure 3 which corresponds closely to the values of Henriques and Moritz[18] and, of course, those of Hardy and coworkers.[10,18,24,25] Hardy's model assumes a total skin thickness of only 0.8 mm; the drop in k indicates a fatty tissue layer. We will return to the question of in-depth variation.

The most recent investigations, those using the radiometric measurement of surface temperature during a square wave pulse of radiant energy, appear to offer more accurate results primarily because the skin is not disturbed by the measuring device and the measurements may be made "in vivo". Nevertheless, there are some major assumptions made in this technique which must be considered.

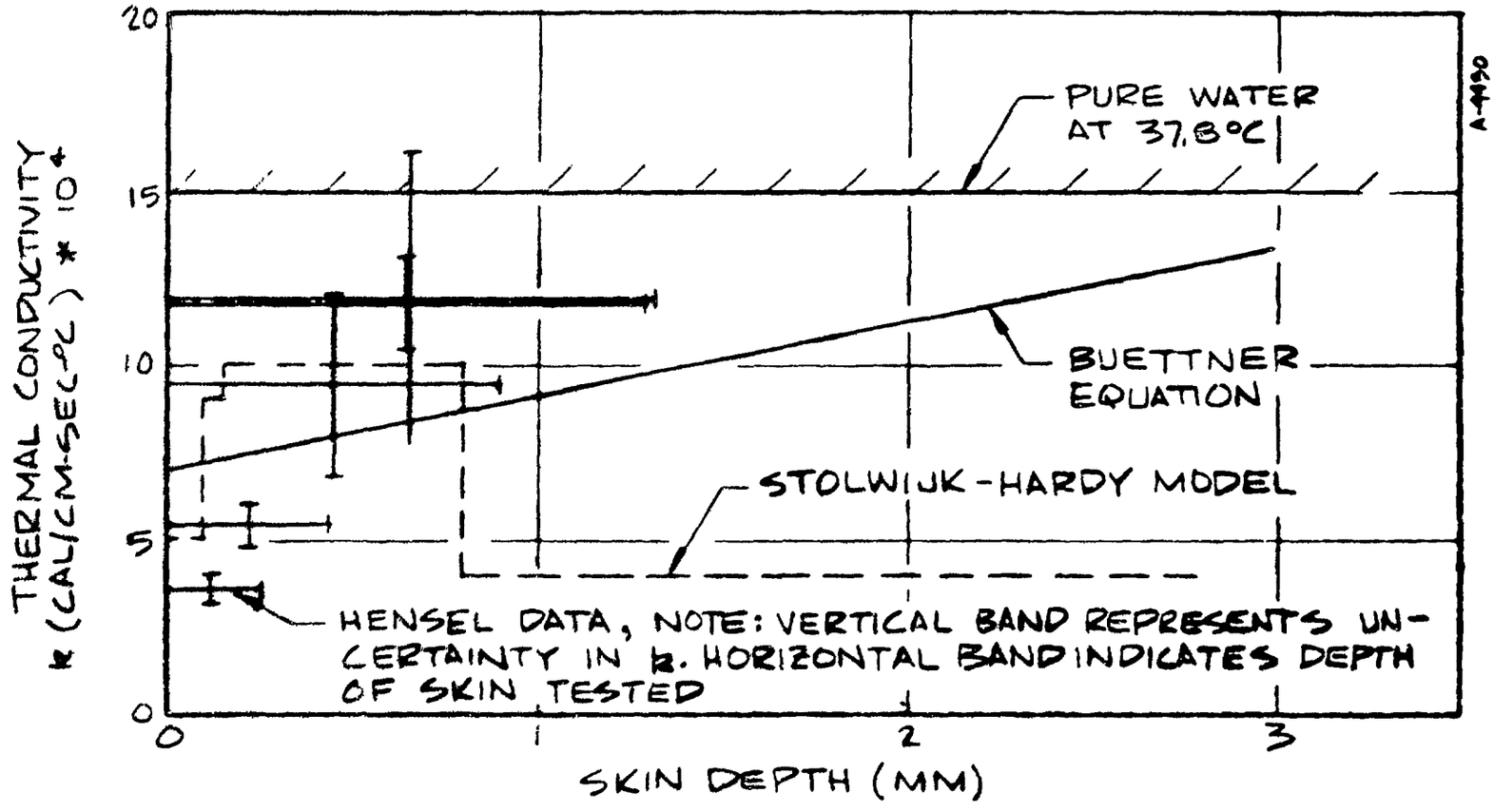

Figure 3. Variation of Thermal Conductivity with Skin Depth

The data reduction technique is based on the use of the so-called Buettner equation which is nothing more than the solution of the transient one-dimensional heat equation assuming,

1. Heat transfer within the skin by conduction only
2. Uniform thermal properties, i.e., no variation with depth or time
3. A step function of heat flux to the skin
4. All the energy is absorbed within an infinitesimally thin layer at the surface
5. Uniform initial temperature with depth
6. No in-depth generation or absorption of energy
7. Infinite thickness

In short, these are the characteristics of an opaque, passive, homogeneous, semi-infinite slab. The validity of the approach is apparently established by results such as Lipkin and Hardy's[10] which show that living skin with no blood flow and normal skin do respond with a linear temperature rise for periods less than 20 seconds just as observed for various inert materials and excised skin samples. The apparent increase in thermal conductivity for normal skin due to increased circulation is really no more than an indication that the equation is no longer valid.

Weaver and Stoll[13] using the data of Stoll and Greene[17] have suggested that the thermal conductivity is a function of irradiance level, tissue temperature and time. To provide a continuous evaluation of the thermal inertia, $k\rho c$ they used the following equation which also describes the surface response following the cessation of heating.

$$\Delta T\ (0)_{\text{surface}} = \frac{2\dot{q}}{\sqrt{\pi}\sqrt{k\rho c}} \left\{ \sqrt{\theta} - \sqrt{\theta - \tau} \right\} \qquad (15)$$

where τ is the pulse duration.

Figure 4 shows their results in terms of k (ρc = 1.0) for two different heating levels. The insert curve is a copy of the Weaver-Stoll curve. The data for the higher heating rate have been converted to a function of time in the main figure. It is difficult to understand why the conductivity should exhibit such dependence, in particular, why should the conductivity vary with the irradiance level and why should it decrease so rapidly during the initial heating and so suddenly at the end of the pulse. If, in fact, all the radiation is being absorbed at the surface, it is simply not clear what physical mechanisms are causing such variations.

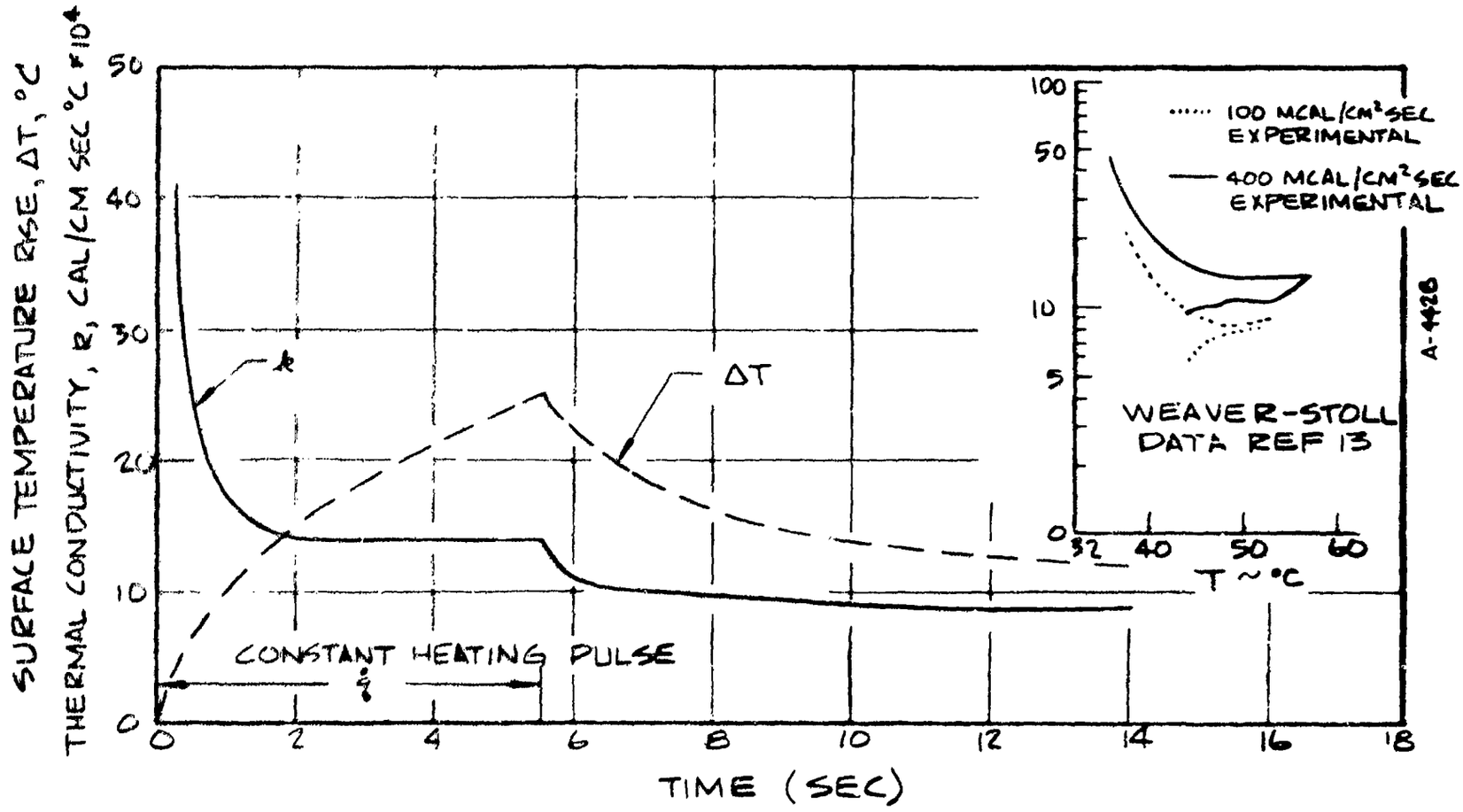

Figure 4. Thermal Conductivity and Surface Temperature vs. Time for Human Skin, Weaver and Stoll (Ref. 13)
$q = 0.376$ cal/cm²sec, $\tau = 5.55$ sec

To investigate this question further, data presented by Davies,[26] who performed similar tests on porcine skin but used a surface thermocouple to measure temperatures, were subjected to the identical method of data reduction. The results for a 2 second exposure which are representative of all exposure levels are presented on Figure 5 for direct comparison to those of Weaver and Stoll. In the case of Davies, no variations with time are evident, particularly after the end of the pulse. In both cases, the pulse durations are short compared to the response time of the circulatory system. In fact, this effect would cause the apparent conductivity to increase, not decrease as found by Stoll.

Based on the observation that both Hardy's and Davies' results follow the assumed model very closely, it is hypothesized that the Stoll measurements somehow do not satisfy one or more of the necessary conditions or assumptions behind Equation 12. The most likely of these are assumptions 4 and 6, namely, that all the energy must be absorbed at the surface. It is well established (See Section 3.2.3 to follow) that human skin is effectively opaque in the infrared beyond 3 microns, but is moderately reflective and transparent in the visible and near infrared up to 3 microns. In these radiation tests, the source is commonly a projection lamp or solar reflector which has a sizeable portion of the energy in the visible and near infrared. Thus, if the India ink coating on the surface were not sufficiently thick to absorb all the radiant energy at the surface, in-depth distribution of energy absorption would result. What does this mean relative to Equation 12.

Initially, the temperature rise at the surface would be less than for an opaque surface. Upon rewriting Equation 12 for kpc,

$$kpc = \frac{\dot{q}^2}{\Sigma} \frac{\theta}{\Delta T^2} \qquad (16)$$

it is clear that this leads to higher apparent values of kpc. Now, as the heating continues in time and into the slab, the scale of events at the surface changes. That is, an infinite slab may be transformed into a non-dimensional space by use of the Fourier number ($x/\sqrt{\alpha\theta}$) which implies that the response at a given depth approaches that at the surface as time increases. Thus if it requires 200μ of skin thickness to absorb all the radiant energy, this will have a significant impact on the early transient heating near the surface. As time increases, a greater percentage of the absorbed energy is conducted beyond the surface to the deeper layers until at some time the surface layers are in a pseudo-steady state with a fixed temperature gradient. At this point the in-depth response is essentially identical to that for an opaque surface. The gradients near the

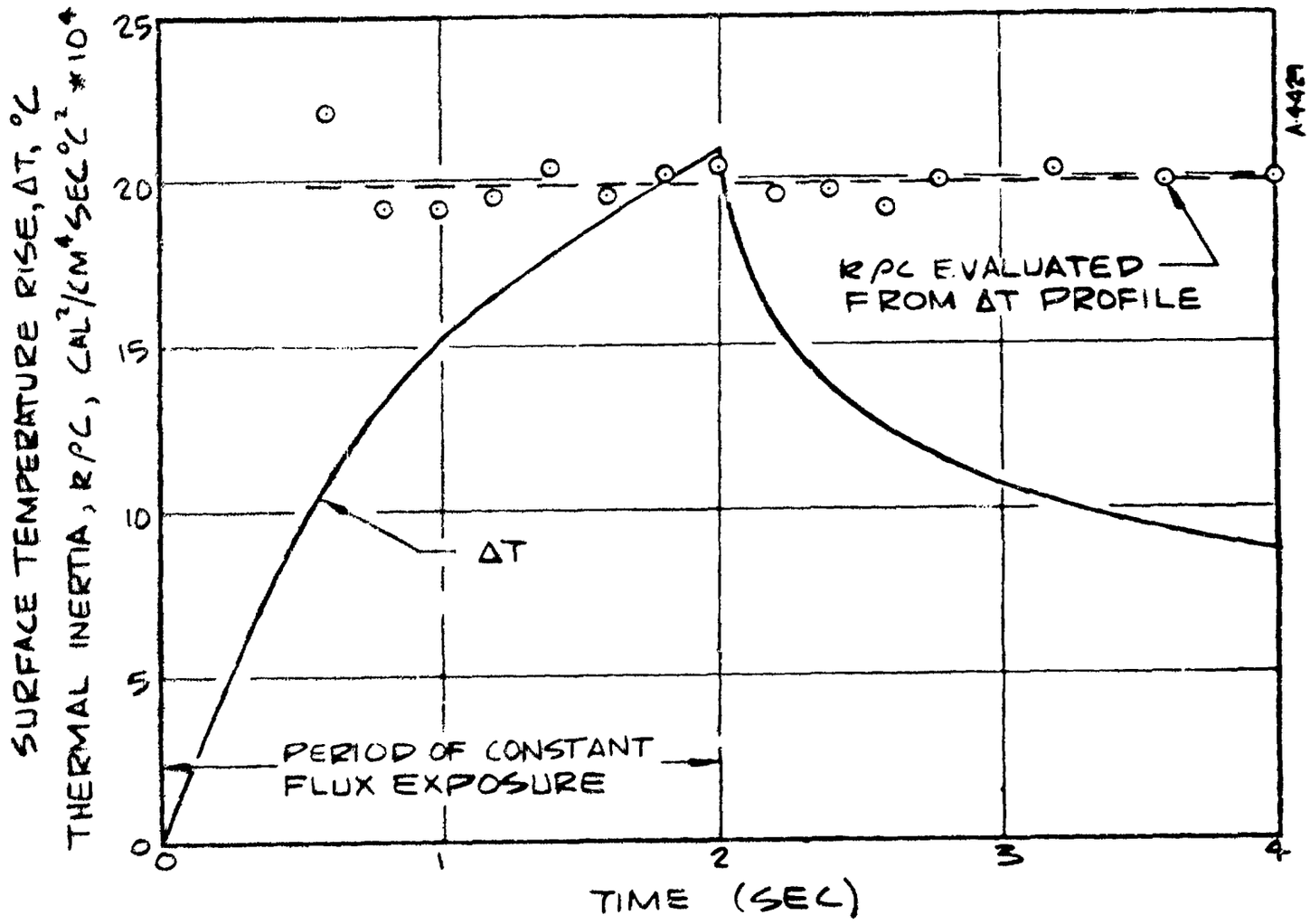

Figure 5. Thermal Inertia Evaluated from Data of Davies (Ref. 26)

surface will not be identical to the opaque case, but the temperature rise at the surface will be very nearly the same. Consequently, the response of the non-opaque case would show initially high values of kpc decreasing asymptotically to some relatively constant value if the in-depth value of kpc were constant

At the end of the pulse, the skin suddenly becomes opaque since at these low temperatures the skin is very nearly a black body radiator (See Section 3.2.3). Thus the cooldown response should satisfy the model quite well as it does for the Stoll data (Figure 4) after a short period of adjustment. This decrease is most likely due to the initial difference between the near surface temperature distributions on the opaque and diathermous slab.

One other factor must be considered relative to Equation 12 and a diathermous slab. If there is absorption, there will be reflection from the surface as well which may exceed the value used for India ink (0.94). This in turn means that $\dot{q}$ in Equation 12 may be less than expected resulting in a higher calculated value of kpc than actual. As the heating level is decreased the source temperature decreases, the spectral distribution of energy shifts to longer wavelengths and the skin becomes more opaque. This may explain the lower values of k as $\dot{q}$ decreases, i.e., the $\dot{q}$ used in the calculation is closer to the actual absorbed flux.

In summary, the above arguments are hypothetical, nevertheless, they do offer a possible explanation for results which do not appear to be consistent with either other data similarly obtained or the current understanding of the physical processes and characteristics of the skin. It is noted that Stoll estimated the India ink thickness as 10μ and according to Davies,[26] this should be more than sufficient to insure opacity. Also it would seem that a lack of opacity would be observable. Until additional data are obtained to clarify this question, it will be assumed that the conductivity is not a function of the irradiance level, time, or tissue temperature.

As a by-product of the preceding discussion, it is interesting to consider what effect the variation of conductivity with depth (due to water content) would have on the use of Equation 12. Following the previous reasoning, the calculated conductivity should increase with time because as the thermal wave progresses into the slab, the conductivity is increasing with depth. None of the available results (Lipkin & Hardy,[10] Davies,[26] Stoll & Greene[17]) exhibit this behavior to a discernable degree. It is possible that it is masked in the Lipkin & Hardy results by the low flux-long exposure durations and consequent interference with circulatory effects. On the other hand, if the main variation in conductivity occurs between the epidermis and dermis, i.e., if there is essentially a step

change in moisture content as suggested by Hardy rather than the linear model of Buettner, and the depth of the interface is 100μ, the epidermal layer will be heated to the quasi-steady state condition described above in less than 1 second for $k = 5 \times 10^{-4}$ cal/sec cm°C. This is a short time relative to most of the experiments, and since the data at short times are subject to the greatest uncertainties in the measurement of time, temperature, and the ability to provide a truly step impulse, it appears that it is not possible to observe the effect of the depth variation of k between the epidermis and dermis. The corollary states that the values of kρc observed in such tests are those of the dermal layer. Indeed, referring to Table IV, the data of Hardy and coworkers[10,24,25] and Stoll and Greene[17] are in the range of 8 to 15 x 10^{-4} cal/sec cm°C which compares quite favorably to the reported dermal values of Henriques & Moritz,[18] Hensel,[19,20] Buettner,[14] and Vendrich & Vos.[27]

3.2.2.2.4 Summation of Thermal Conductivity Data

The thermal conductivity values selected for the skin model are based upon the following factors

1. Heating durations are less than the response time of the circulatory system, thus any change in the apparent thermal conductivity will be neglected.
2. The real thermal conductivity of skin tissue will not exceed that of pure water at the same temperature.
3. The conductivity is dependent upon the amount of water content in the tissue and since water content increases away from the surface the conductivity should also increase. This is substantiated by the data; however the form of the variation with depth is not well established.
4. The conductivity may vary from body location to location and from individual to individual, however, these variations are probably within the uncertainties of the data. Most data are for the forearms and these will be used to describe the nominal skin.
5. The most important values to know accurately are those in the dermal layers because these values determine the heating response at all depths once the surface layers reach the quasi steady-state condition (less than 1 second).
6. A nominal fit of all the available data is shown in Figure 6. An attempt is made here to model the qualitative trends noted above and to correlate, as well as possible, those data which appear reasonable. The epidermal layers are assigned low values consistent with their

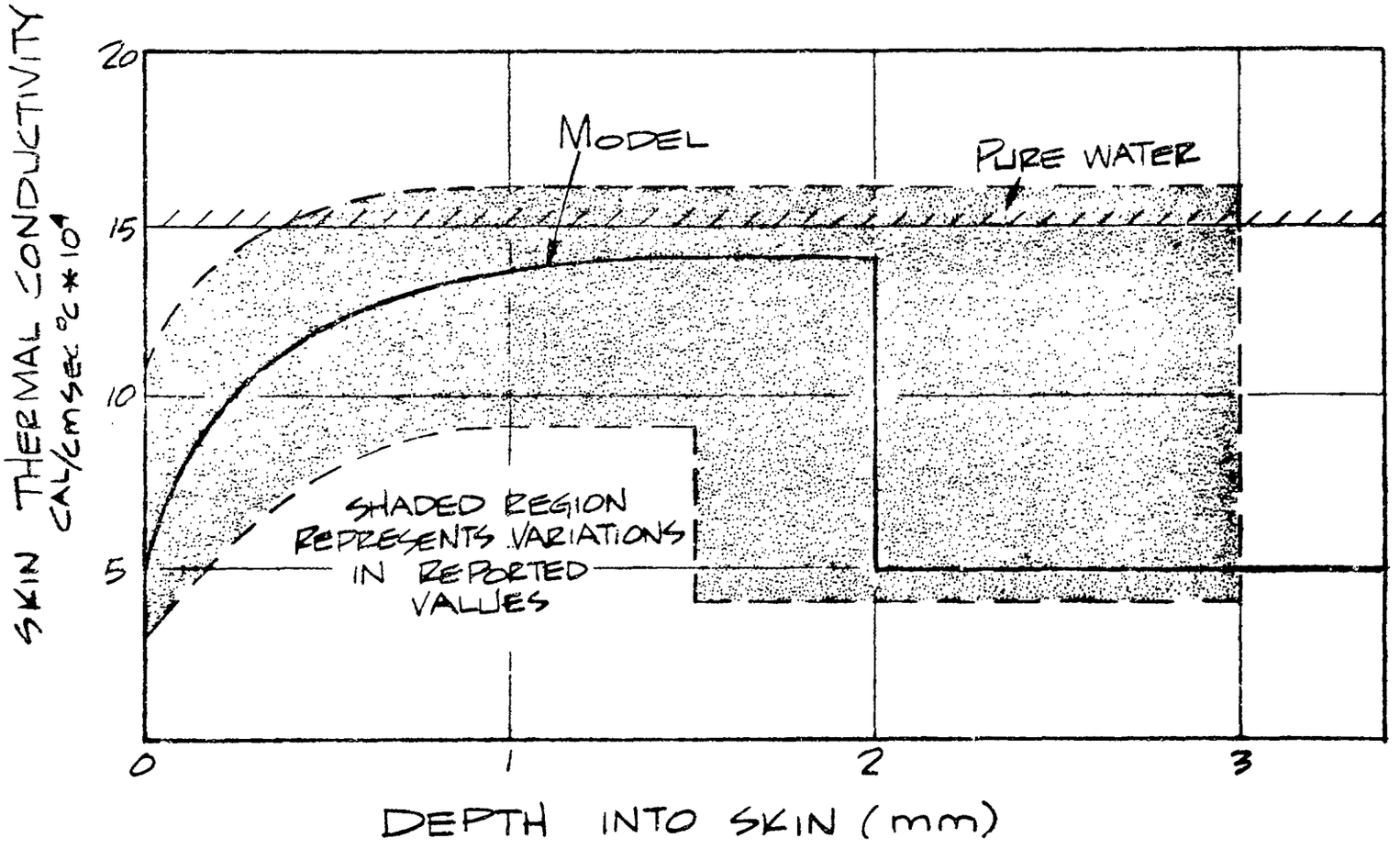

Figure 6. Skin Thermal Conductivity Model

observed dessicated state. The conductivity then increases in the dermal layers to a value of 14.0 cal/cm sec°C, slightly below the value for water, and then, at about 2 mm, decreases to a value of 4.5 cal/cm sec°C which appears to be a reasonable value for fat (see Chato[9]).

The actual shape of the curve represents more of a general impression of the data rather than a concise correlation. There are simply too many differences between the results of various investigators, and the uncertainties in conductivity and depth in their measurements are too great to permit such exacting correlation. This conductivity model is presented then in the spirit of providing a "nominal" description, one which reflects as well as possible those observed data and one which, at this point in time, is as good as these data allow.

It is noted that a number of the reported values exceed the value of pure water. This may be the result of experimental uncertainties, but more likely is indicative of the difference between the real and effective conductivities, the latter accounting for the circulatory convection which is present in some amount at all times. The current recommendation is to neglect this effect, that is, at least its variability with time, and to include any nominal effect as part of the real conductivity in order to maintain the simplicity of one-dimensional, conduction-only model. The choice of the asymptotic value of 14.0 cal/cm sec°C in the dermal layer should account for this based upon the short term exposure results presented.

3.2.3. Skin Optical Properties

A very thorough review of the investigations of the optical properties of human skin has been compiled recently by Boehm and Tuft.[28] Basically all the information presented herein is taken from this paper which also includes an extensive list of references. Some of the more intensive work has been done by Hardy and coworkers,[29-39] Derksen and coworkers,[38] and Buettner.[39] The optical properties of concern are the surface spectral reflectance, the surface spectral emittance and the in-depth absorptance or transmittance. These must be known to account for the proper amount of radiant heat transfer and how this energy is distributed. For example, during the exposure to the fire, there will be radiant flux transmitted directly through the clothing to the skin as well as reemitted energy from the back side of the fabric, yet these fluxes will not interact with the skin in the same way due to differences in the spectral distribution of the energy and differences in the optical properties. The following section presents a summary of the available data and an evaluation of the importance of these properties relative to the defined problem.

3.2.3.1 Spectral Reflectance

Figure 7 shows the average percent monochromatic reflectance of Caucasian and Negro skin as compiled by Boehm and Tuft. Caucasian skin tends to be more reflective than Negro in the visible and near infrared, but both have very low reflectances for wavelengths below 0.2μ and above 2μ. It is generally accepted that all skin has essentially zero reflectance in the far infrared although this has not been investigated extensively. Based on the reflectance values of Figure 7 the total reflectance of the skin for black body radiation incident upon the skin has been calculated for source temperatures up to 5000°R (2780°K) by Boehm and Tuft and is presented here as Figure 8.

In the preliminary analysis (see Section 6) typical temperature response curves for various fabric ensembles have been generated. Figure 11 shows the transient response of the inner surface of fabric adjacent to the skin for one, two and three layers of fabric exposed to an 1800°F (983°C) JP-4 fuel fire for 3 seconds. The peak temperature predicted is 1550° (866°K) at which the total reflectance from Figure 8 is found to be less than 2 percent. At flame temperatures of 2250°R (1256°K) about 5 percent of the total flux is reflected. For typical values of direct transmission through a single fabric layer of 10 percent and assuming the transmitted flux retains the same spectral distribution, the maximum amount of reflected energy is less than 0.02 cal/cm sec. This is less than 2 percent of the maximum flux predicted for a single layer; in addition, this reflected energy is almost totally absorbed by the fabric and thus is partially reradiated back to skin so that the error is probably less than 1 percent if the total reflectance of the skin is based solely upon the temperature of the inner fabric surface. The complete thermal model will be modified to account for this reflected energy.

3.2.3.2 Spectral Emittance

For the purpose of both fabric response and skin injury, the temperatures of the skin surface can be assumed to be bounded by the results of the preliminary analysis presented here as Figure 12. These results show that as long as there is a covering of fabric, skin temperatures will not exceed 200°F (93.4°C) to 300°F (149°C). At these temperatures, the skin will be severely injured (see Section 3.3). Figure 9 indicates the spectral emissivity of the human skin due to Elam et al.[40] If this curve is integrated with a black body spectral distribution of energy at 200-300°F (93.4-149°C), the total emissivity is 99.3 percent, that is, for this effort the skin can be assumed to radiate essentially as a perfect black body.

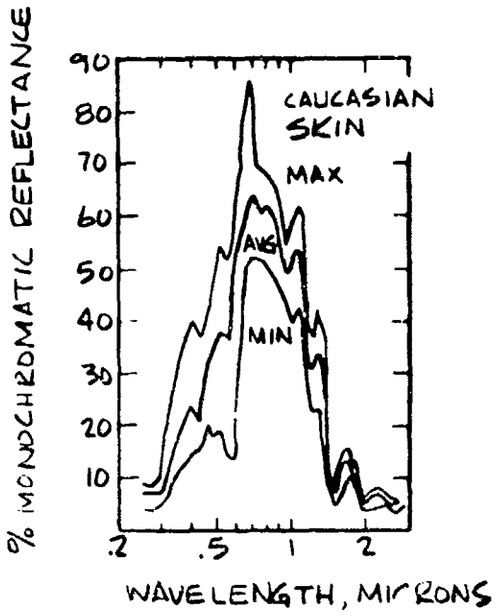

Figure 7. Envelope and Average Values of Spectral Angular Hemispherical Reflectance of Caucasian Skin, Ref. 28

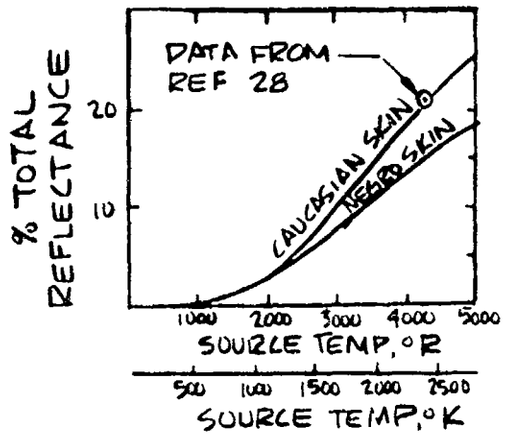

Figure 8. Variation with Source Temperature of the Average, Total, Angular-Hemispherical Reflectance of Caucasian and Negro Skin when Irradiated by a Black-Body or Gray-Body Source

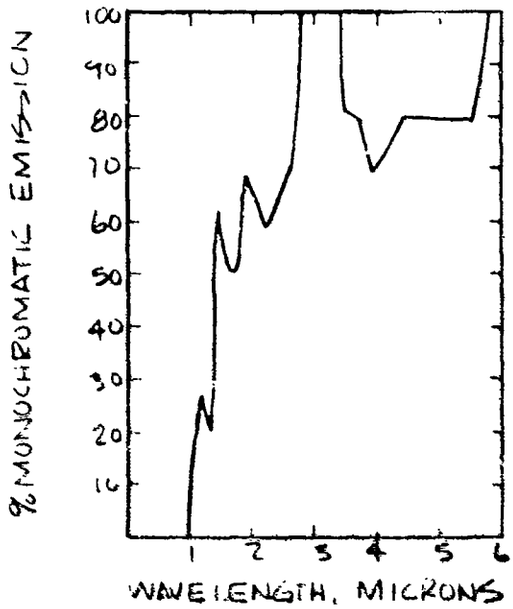

Figure 9. The Spectral Emissivity of Human Skin as Given by Elam, et al., Ref. 40

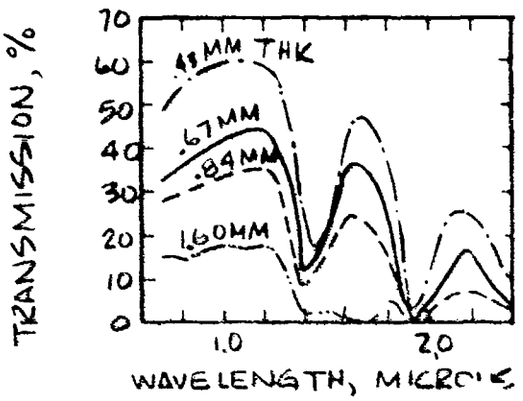

Figure 10. The Spectral Transmittance of Various Thicknesses of Human Skin as Given by Hardy, et al., Ref. 36

Figure 7 through 10. Skin Optical Properties

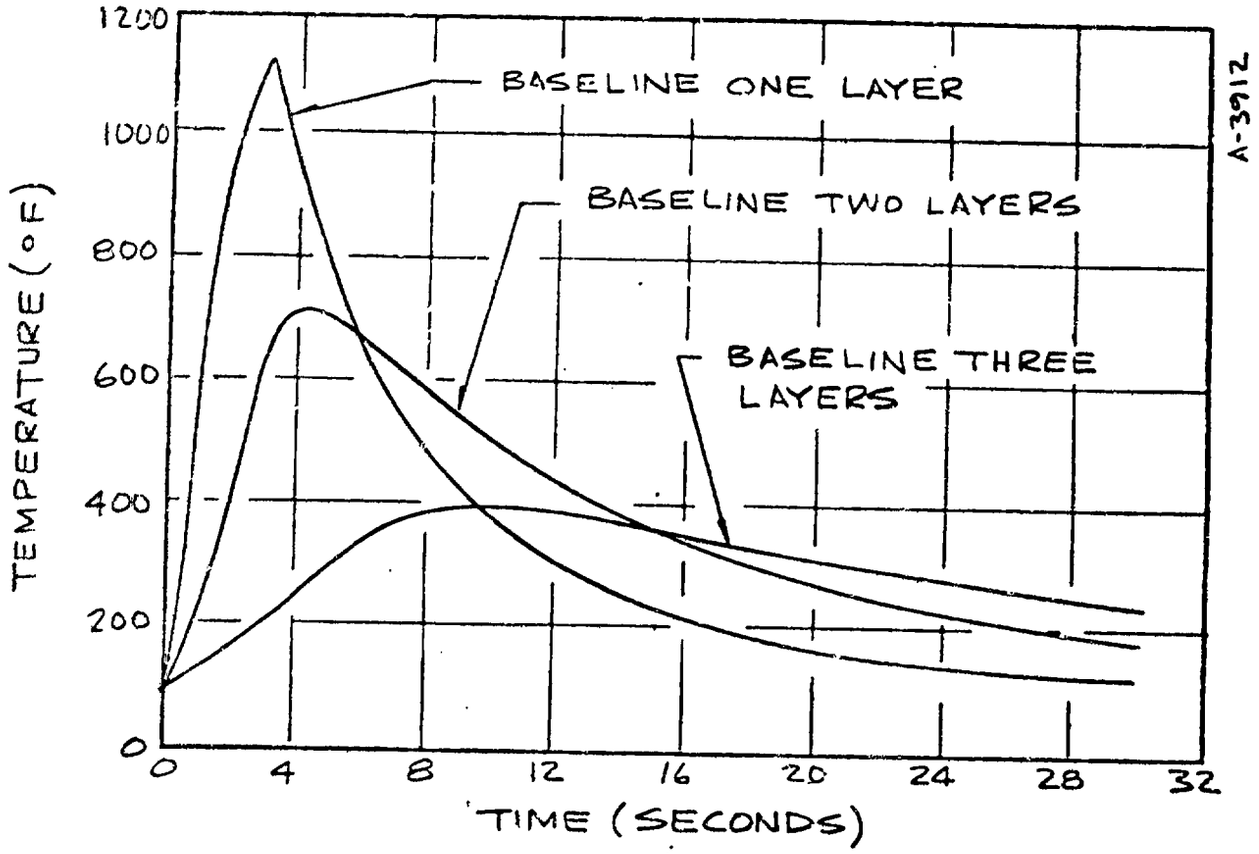

Figure 11. Temperature Time History for Innermost Surface of Fabric Assembly for Three Baseline Conditions

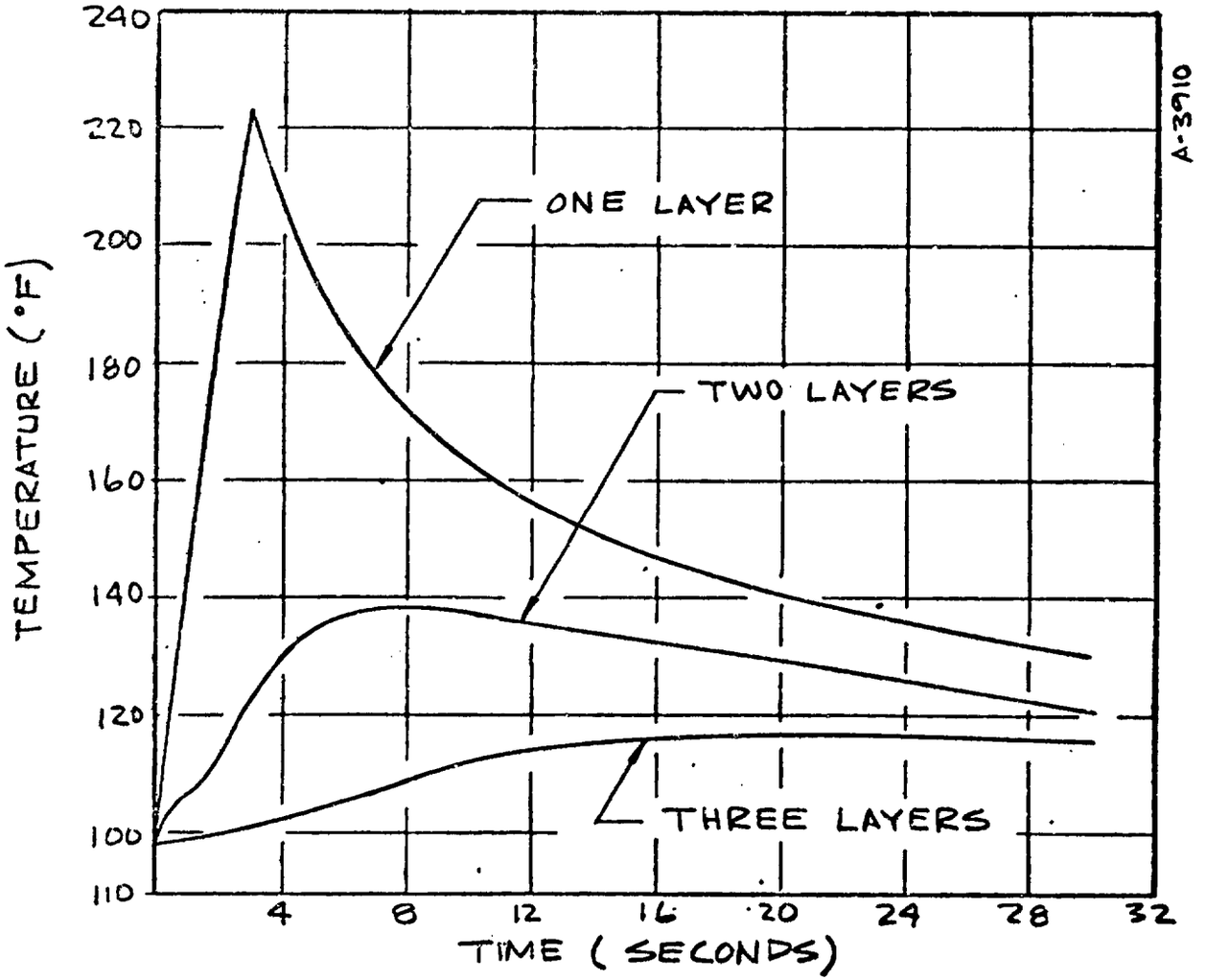

Figure 12. Skin Temperature Time History for One, Two and Three Layers of Fabric

3.2.3.3 Spectral Transmittance

In the infrared and far infrared (from 6 to 50μ) the transmittance of the skin is very low. Coupled with the low reflectance in these wavelengths, the skin is seen to be essentially opaque and totally absorbing in these wavelengths. Below 6μ and particularly in the visible and near infrared, the skin becomes much more transmissive as shown by Figure 10 which gives the results of tests by Hardy, et al.,[36] on excised, Caucasian skin. Figure 13 shows the absorption coefficient, μ*, as a function of skin thickness and wavelength used to calculate the curves of Figure 10. The values of transmittance imply that for high source temperatures, wherein a significant portion of the spectral energy is in the visible and near infrared (below 2.5 to 3.0 microns), the skin can not be modeled as an opaque body (absorbing all the energy within an infinitesimally thin layer at the surface).

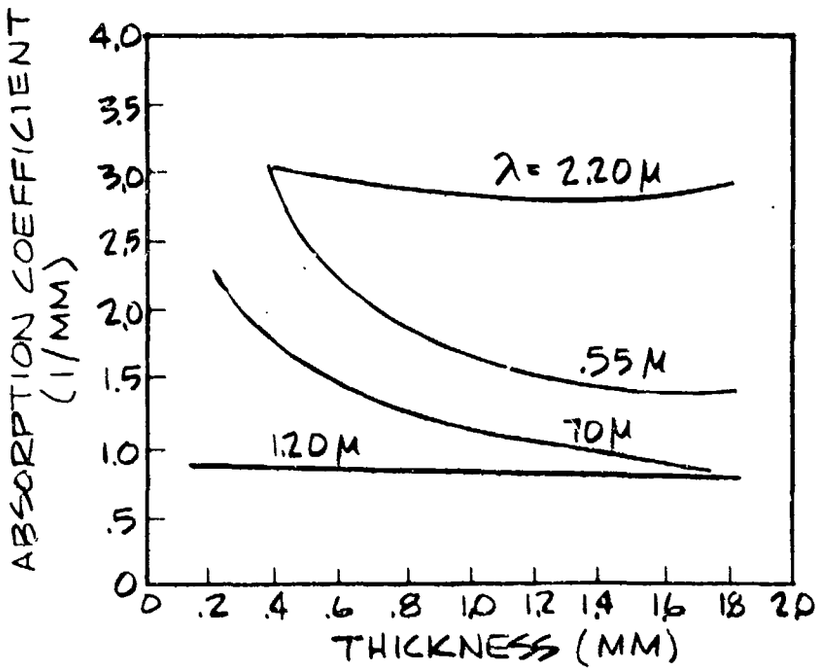

Figure 13. Absorption Coefficients for Excised White Human Skin of Different Thickness (from Ref. 36)

*The percent transmission at some depth x in a one-dimensional uniform slab is given by $100\ e^{-\mu x}$ where μ is the absorption coefficient.

If such were the case, the determination of the thermal response of the skin would become much more complex, not because it would be difficult to account for in-depth absorption of energy in the computer code, but because the amount of absorption is a combined function of the spectral distribution of the incident radiation (which will be a composite of direct radiation from the fire and re-radiation from the fabric) and the variation in the absorption coefficient with depth and wavelength.

The significance of transmission of radiant energy at these wavelengths is apparent from the work of Buettner,[39] Derksen, et al.,[40] and others who have shown substantially lower surface temperatures for normal skin as compared to blackened skin on exposure to high intensity sources such as carbon arc lamps, tungsten lamps and solar collectors. At the temperatures of these sources (~3000°K and higher), at least 85 percent of the total energy is at wavelengths below 2.6μ. For a given heat flux, considerably longer exposures are required to cause a given burn level for normal skin, and in some low flux level cases, where blackened skin is burned after short exposures, no burn is experienced at all with normal skin even with very long exposures. A steady state temperature distribution is established (due to absorption of flux below skin levels and to onset of increased circulation) which does not exceed the threshold tissue damage temperature (~ 44°C). In effect, the mechanism of in-depth absorption serves to enhance the ability of the skin to transfer energy away from the surface, an ability the normally low thermal conductivity of the skin does not provide. Figure 14 shows the percentage of total absorbed energy which has been absorbed within the distance of 100μ and 200μ for source temperatures up to 2250°R (1256°K). These values were obtained using the transmission curves given in Figure 10. If the spectral distribution incident on the skin were that of an 1800°F (983°C) fire, only 70 percent of the total absorbed energy would be absorbed within 100μ. The actual spectral distribution at the skin surface will depend upon the amount and spectral distribution of flame energy transmitted by the clothing ensemble and by the temperature and emissivity of the inner fabric surface. Assuming:

1. that the relative spectral distribution of the transmitted energy is not affected by the fabric,
2. each fabric layer has the same transmittance,
3. the inner fabric layer radiates as a black body,
4. the maximum inner fabric temperatures are those predicted in Figure 11,

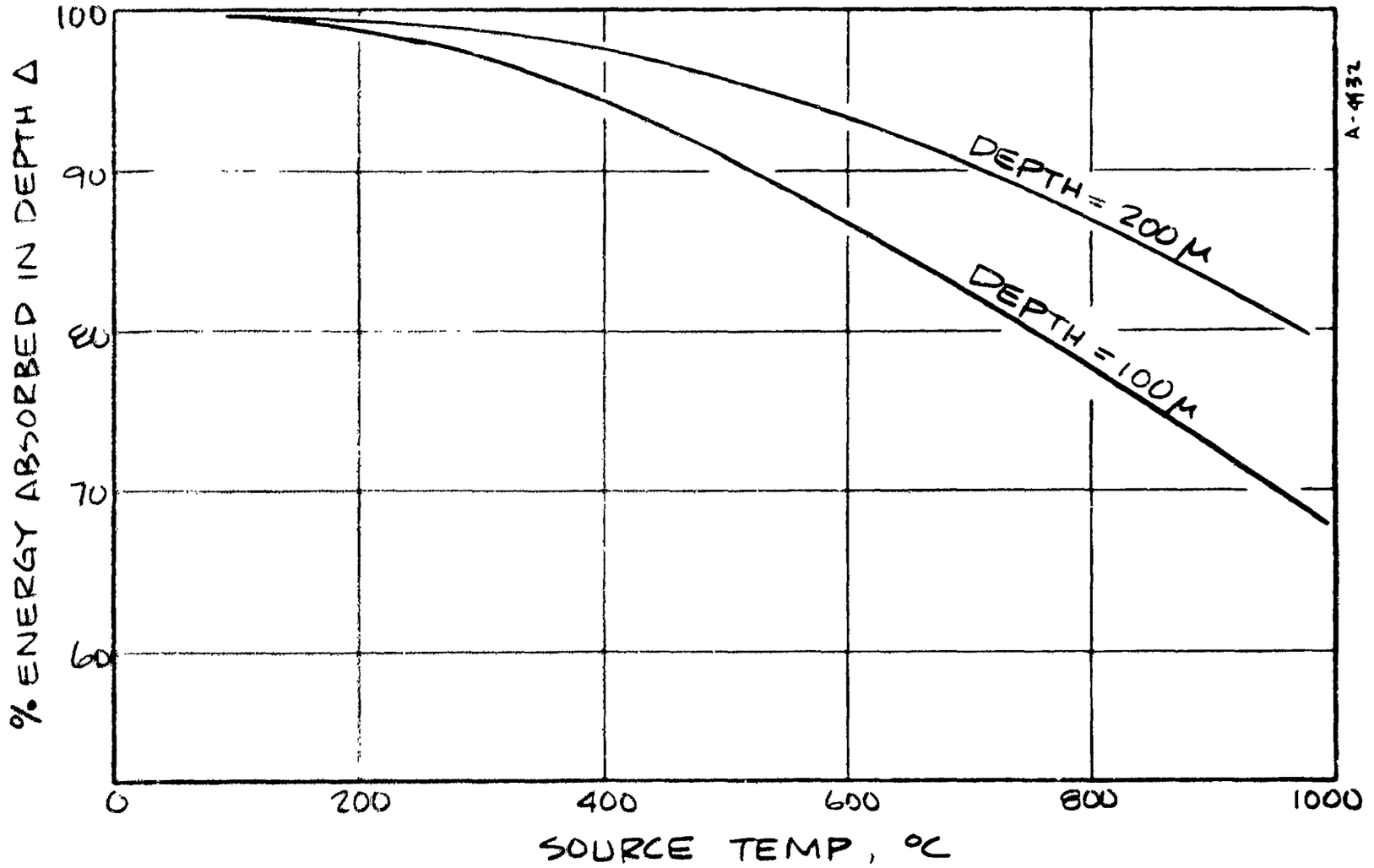

Figure 14. Percentage of Total Absorbed Energy Absorbed In Depth for Black Body Radiation up to 983°C (2250 R)

an estimate can be made of the percentage of the total absorbed energy absorbed within 100μ. Figure 15 shows the results as a function of the transmittance of a single fabric layer. The percent absorbed increases with increasing layers of fabric for two reasons, first the amount of flame energy is decreasing by the percent transmission raised to the power of the number of layers and secondly, by the shift of the spectral distribution of the reradiated energy to higher wavelengths as the fabric temperatures decrease. However, Figure 15 does not tell the complete story. It is based on the distribution of energy at peak heating, i.e., at the end of the 3 second exposure. In fact, a significant portion of the heating of the skin occurs after this time and during this period none of the energy is coming from the flame. Figure 11 shows that for the 3-layer case, peak heating does not actually occur until 8 to 10 seconds after beginning of exposure. If the contributions of direct flame and fabric radiation energy are determined over a 20 second duration, the value for a single layer and 10 percent transmission increases from 82 to 86 percent. Values for 2 and 3 layers increase from 92 to 95 percent and 98 to 99 percent respectively. These values are shown as squares on Figure 15.

The implication of this must be taken in context with the assessment of burn injury to the skin. Subsequent sections will show that injury to skin tissue is determined by the temperature and the length of time the tissue is exposed to that temperature. In addition it will be shown that at temperatures above 137°F (58.3°C) less than 1 second exposure will result in irreversible damage to the epidermal layer. Since temperatures at the 100μ level are generally within a few degrees of the surface temperature even for the higher flux levels, the temperatures predicted for a single layer, (see Figure 12), strongly suggest that that the surface and near surface temperatures will far exceed 137°F (58.3°C) even if in-depth absorption were considered. In this case, epidermal tissue will be irreparably injured; however, accurate assessment of damage to the deeper layers of dermal tissue will not be significantly impaired because

1. effectively all the energy will be absorbed above these layers and
2. the thermal response at deeper levels is considerably dampened relative to that near the surface i.e., the amount of damage is much more dependent upon total duration at elevated temperature than upon the temperature level. This point will be discussed further in subsequent sections.

As the number of layers of protection increases, the amount of energy transmitted beyond 100μ is limited to a few percent, levels which, considering the magnitude of other uncertainties in the total problem of predicting tissue injury, are not of sufficient importance to warrant increasing the complexity of

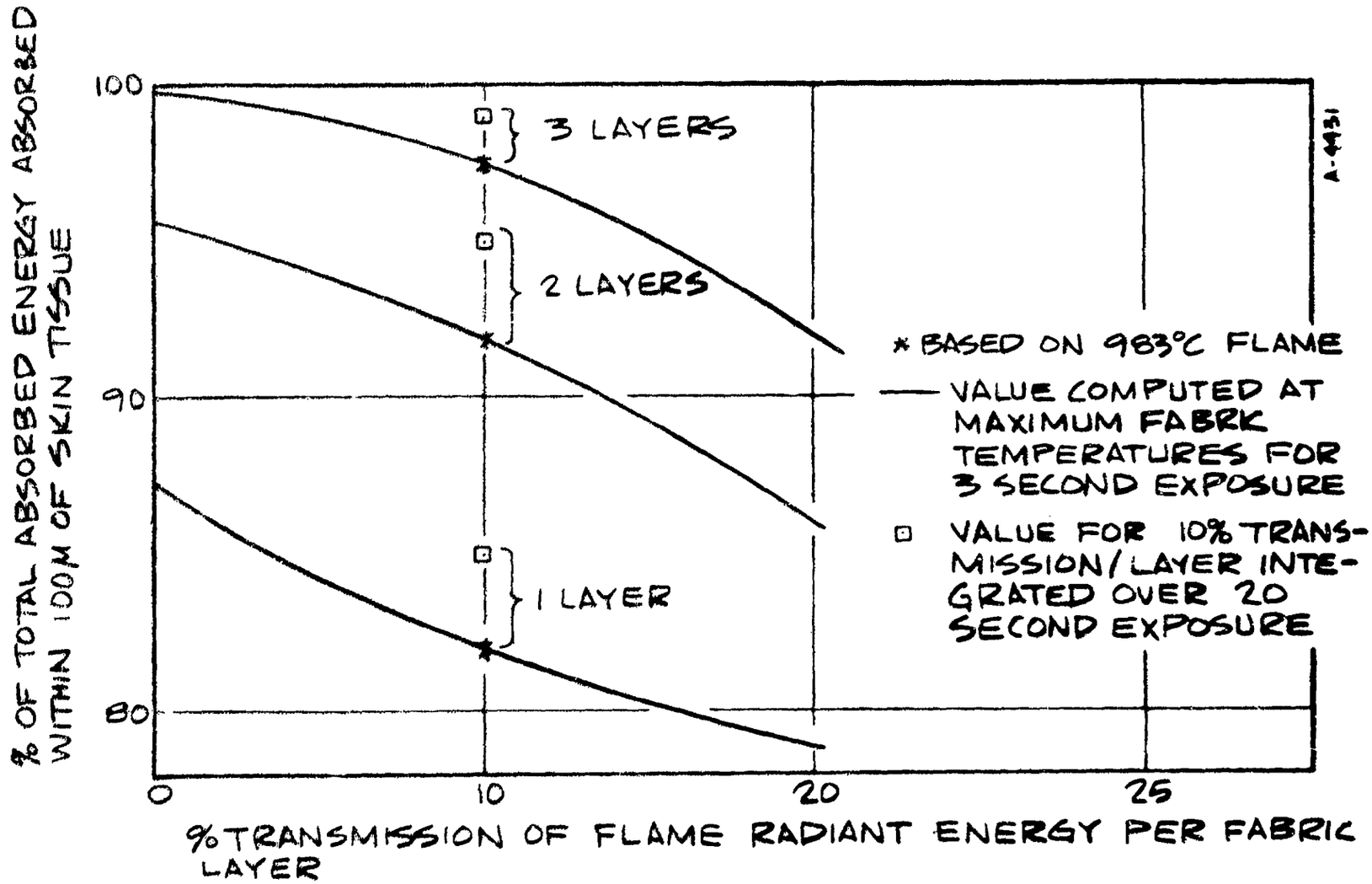

Figure 15. Percent of Total Absorbed Energy Absorbed within 100μ of Tissue as a Function of Fabric Transmission

the model. Thus, for all hypothesized heating conditions it is recommended that the skin be assumed to be opaque, in the meantime noting that this assumption will tend to predict higher temperatures at the surface particularly for the higher flux levels.

3.3 BURN INJURY ASSESSMENT

Assessing the amount of burn injury to skin tissue is definitely not a precise practice. There is no universally accepted method for classifying burns, although the clinical terminology of first, second, and third degree is by far the most common. Within this and the other systems, there is considerable potential for subjective judgment and owing to the differences in tissue and the fact that injury is a continuous function both in time and space, this situation is understandable. The remainder of this section will consider first the various methods of classifying burns which have been proposed and then how to relate the measured or predicted thermal response to tissue injury.

3.3.1 Classification of Burn Injury

Moritz and Henriques[4] subscribed to the standard "Degree" method proposing the following definitive structure. They divided injuries basically into two groups, those which failed to cause complete transepidermal necrosis (complete and irreversible damage to the entire epidermis with subsequent loss of this layer) and those which did. The first degree designation was applied to the sub-threshold group with second and third degree burns falling into the second or supra-threshold group. Mild first degree reactions were noted as transient dilatation of near surface blood vessels, i.e., a slight reddening. Stronger first degree response was indicated by prolonged hyperemia (reddening due to increased amount of blood), while severe first degree injury resulted in some exfoliation of the epidermis after a few days.

Blistering was always an indication of a suprathreshold burn but was not sufficient; if the epidermis could be displaced by friction in a few days or if an encrustation developed within a week, the injury was definitely at least of second degree. Suprathreshold injuries were classified as second or third degree primarily upon the amount of penetration into the dermal layer. The only criterion indicated for a third degree burn was that a significant portion of the dermis was irreversibly damaged.

In their experiments on porcine skin, Perkins, et al.[41] developed the University of Rochester method which is presented in Table V.

TABLE V

UNIV. OF ROCHESTER CLASSIFICATION OF BURNS

Burn Classification	Description	Human Equivalent
0	No Burn	No Burn
1+	Reddening, erythema	1st Degree
2+	Patchy white coagulation	2nd Degree
3+	Solid white coagulation	3rd Degree
4+	Steam blebs	3rd Degree
5+	Carbonization	3rd Degree

According to Davies,[26] the Quartermaster Research and Engineering Center, Natick, Massachusetts, has modified this by adding the following criteria for 2+ and 3+ burns.

2+ The epidermis can be pushed aside and removed rather easily. The underlying dermis is pink.

3+ The epidermis can be removed but not as readily. The underlying dermis is grayish white.

Davies actually used this with the additional classification based on the areal extent of injury as described by Wight and Robinson.[42] This simply enabled Davies to distinguish subgrades of 1+, 2+, and 3+ burns but applies only to the specific tests performed at Natick.

Table VI presents the grading system used by Knox, et al.,[43] at the U.S. Army Aeromedical Research Laboratory at Fort Rucker, Alabama, in assessing damage to porcine skin. This system is quite similar to that of the University of Rochester including one extra grade between steam blebs and carbonization.

Basically the various systems exhibit similarity in the definition of the lower grades of burns. First degree and 1+ both imply that complete transepidermal necrosis has not occurred. 2+ is similar to second degree in that the epidermis has been completely destroyed. Knox, et. al., provide some qualititative correspondence between the extent of in-depth injury and surface appearance, but none of the methods provides a clear definition of what depth or what percentage of thickness of the dermal layer the dermis must be irreversibly damaged to cause a 3+ or third degree injury. Stoll and Greene[17] used the onset of blistering within a 24 period following exposure as the criterion for complete transepidermal

TABLE VI

GRADING SYSTEM FOR GROSS BURN EVALUATION*

Laboratory Grade	Surface Appearance	Additional Information	Descriptive Term	Human Equivalent
0	Normal Skin	Normal Skin	Normal Skin	No Burn
1	Erythema	Painful Pliable Hyperemia No Blisters Skin hot to touch	Red Burn	Epidermal
2	Patch Coagulation (Mottled Red)	Painful Pliable Cap. Refill Possible No blisters Skin hot to touch	Spotted White Burn	Superficial Intradermal
3	Uniform Coagulation (Pearly White)	Pliable Little Pain + Blister (early) Skin Temp Normal	White Burn	Deep Intradermal
4	Steam Bleb early blebs ruptured blebs ruptured blebs with charring	Blisters Moderately Pliable No Pain Skin Temp Normal	Blebbed White Burn	Superficial Subdermal
5	Leathery Brown	Nonpliable Cold, Hard Insensitive Thrombosed Vasculature	Leathery Brown Burn	Deep Subdermal
6	Carbonization	Hard - Fat or Muscle Burned	Charred Black Burn	Very Deep Subdermal

*Used by U. S. Army (Fort Rucker) on Porcine Skin

necrosis in their tests on human skin following the approach of Moritz and Henriques.[4] The other investigators have classified burns both immediately and some period latter finding that some burn characteristics do not develop immediately. A 24 hour period is generally accepted as sufficient.

In summary, although classification of burn injury does not lend itself to precise definition, it appears that it is possible to identify several critical factors which are of primary concern to the current study. First, the thickness of the epidermal layer and total tissue destruction at the base of this layer determine the onset of injury to the more critical tissues of the dermis. Secondly, the depth of the dermal layer and the degree of damage near the base of this layer determine the ability of the tissue to regenerate the upper destroyed layers. If the dermis is completely destroyed, the reproduction can only proceed from the edges of the wound; consequently, surgical repair is generally required. This condition appears to be that described as a third degree or 3+ burn. Less serious injuries are able to grow new tissue spontaneously unless secondary factors such as infection or interference with circulation occurs.

3.3.2 Effects of Skin Thickness

The impression established concerning the classification of burn injury above is that the thickness of two major skin layers is a primary factor in the determination of the extent of the injury. As discussed previously in Section 3.2.1 these thicknesses are not uniquely defined quantities, varying as much as 50 to 100 percent over the body and between individuals. Thus two areas of skin exposed to identical heating may not sustain identical injury classifications. This factor, by itself, must account for a significant amount of the spread in test results both within a given experimental sequence and among various investigators. The only viable approach to this problem is to define a nominal model which is consistent with the conditions encountered in the experiments and to limit consideration to those experiments which include a large enough sample to define adequately these nominal conditions.

3.3.3 Theories of Tissue Injury

The other major factor in the determination of extent of injury is the mechanism of tissue damage. Several hypotheses have been advanced; investigators at the University of Rochester[41] developed an empirical approach which does not attempt to explain the actual physical and chemical processes that occur during an exposure. They note that a certain critical enthalpy or energy is required to produce a burn of a given grade, but it is also noted that this quantity is

a function of time. Figure 16 shows the results of University of Rochester tests on porcine skin giving the critical total energy for a 2+ burn, EE_{50}^{2+}, as a function of the exposure time to a square wave pulse for durations of 0.3 to 30 seconds. This figure also includes the work of Davies on porcine skin.

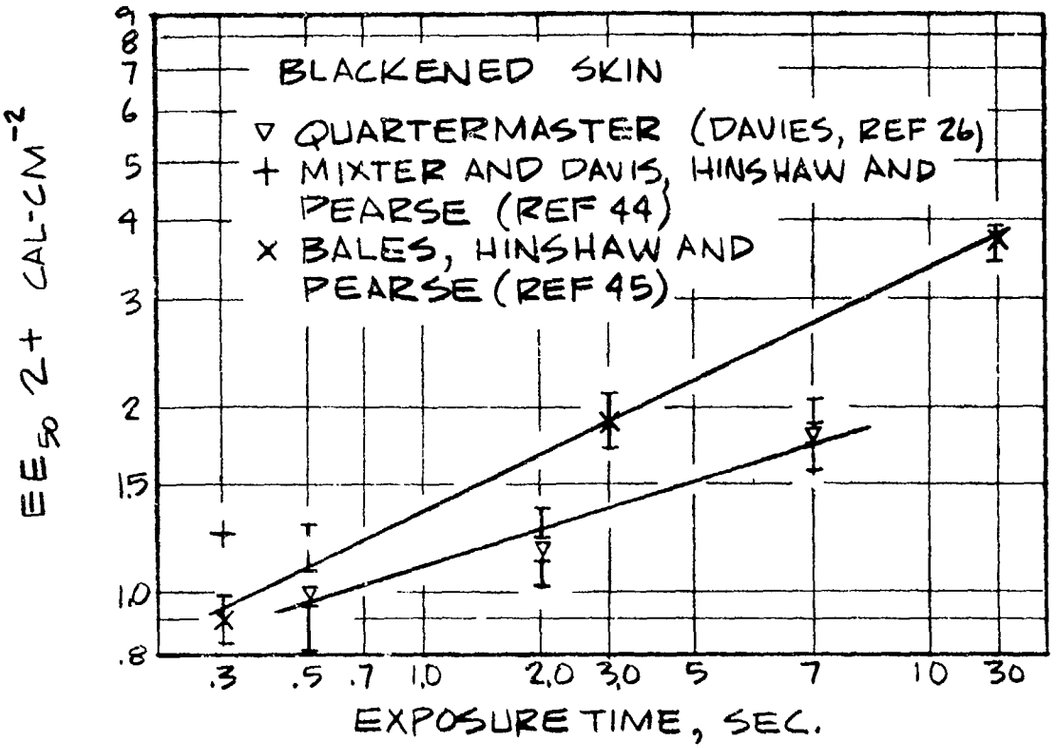

Figure 16. Critical Energy for Burning Pig Skin as a Function of Exposure Time (from Ref. 41)

Although these results are not in particularly close agreement, both indicate that increasing amounts of energy are required to produce a given burn with increasing duration. Goldsmith and Takata have attempted to correlate these data in terms of tissue temperature at 160μ depth suggesting that the threshold levels between the indicated burns are reached when the tissue temperature rises to the values in the following table.

Critical Temperature	Threshold Burn Level
50°C (122°F)	0, 1+
70°C (158°F)	1+, 2+
90°C (194°F)	2+, 3+

The lack of description of and relation of tissue damage to the fundamental processes of the above approach detracts from the ability to use these data to extrapolate to different conditions, especially heat flux profiles of other than square wave shape. Considering the order of 4 variation in critical energy shown in Figure 16 over the exposure duration, it is simply not apparent how the type of heat flux pulses to be encountered in JP-4 fire exposures (see Figure 11 for example) can be related to these data with a satisfactory degree of confidence. For this same reason, the critical temperature values proposed by Goldsmith and Takata are not satisfactory; variations in the shape of the heating pulse will result in significantly different temperature response at varying depths such that the observation of the observation of the temperature level at one depth is not necessarily a valid indicator of conditions at other depths.

The most believable hypothesis at this point in time is that of Henriques[47] who has attempted to relate the tissue injury to fundamental chemical and physical processes. He first assumes that thermal effects upon living protoplasm follow the kinetics of many well known chemical and physical processes which depend upon the total energy of the constituents. The rate of such a process is determined by the relation between this energy and some critical energy level unique to the process. This latter energy is often termed the activation energy, and the rate of the process is given by

$$\text{rate} = Ce^{-\frac{\Delta E}{RT}} \tag{17}$$

where C is rate constant

ΔE is the activation energy

and RT represents the energy level of the constitutents according to the Maxwell-Boltzman energy distribution law

Henriques presents an extensive investigation of the magnitude of the activation energy and concludes that "one can place considerable confidence in the statement that thermally induced injury of living epidermal protoplasm is primarily due to changes in some of the nuclear and cytoplasmic proteins which have activation energies for thermal degradation in the order of 150,000 calories per mol."

This finding is then combined with the data from the Moritz and Henriques[18] tests on porcine and human skin to arrive at the expression

$$\frac{d\Omega}{d\theta} = 3.1*10^{98}e^{-\frac{75,000}{T(^{\circ}K)}} \tag{18}$$

where the parameter Ω represents the total thermal damage and $d\Omega/d\theta$ is the rate at which damage occurs at temperature, T. The damage rate constant was chosen such that the value of $\Omega = 1.0$ at the base of the epidermis was equivalent to complete transepidermal necrosis, i.e., a second degree burn as defined by Moritz and Henriques. Further correlation of their results indicated $\Omega = 0.53$ as the threshold value for a first degree burn or the onset of epidermal necrosis.

The constants in Equation 17 relate only to epidermal injury. The convincing nature of Henriques arguments and the success in correlating the test data would seem to imply that his criterion can be applied to dermal tissue as well. This of course assumes that dermal tissue sustain injury in a similar manner and have the same activation energy as the epidermal tissue. It will be assumed that all skin tissue exhibits similar behavior; however, it is noted that there is neither specific evidence to support or deny this contention.

3.3.4 Selection of the Burn Assessment Criteria

The work of Stoll and coworkers[13,17] has extended the approach of Henriques[47] by considering the effect of radiation heating (Moritz and Henriques' tests were performed using conduction heating only). The results of Stoll and Greene[17] did not correlate well with the Henriques expression (Equation 17) and following extensive discussion of this point, Stoll and Greene suggested that there is a duality to the damage process which can be explained in terms of steady state vs. unsteady heating. For long term, low temperature steady state heating, it is possible that regeneration processes are occuring at rates of the same order as the heat injury process. Henriques notes, in studies of latent injury, that if some period of time intervenes between application of heating pulses to the same location and the tissue damage is not total, there is at least partial recovery of the thermally altered proteins between pulses. On the other hand, in high rate heating cases, the damage rate is predominant.

To account for this and the fact that a significant portion of the injury may occur after the cessation of the pulse as the temperature returns from its peak value to normal, Stoll and Greene have modified the Henriques equation as shown in Figure 17. The two portions of the radiative heating curve represent the steady-state (low temperature) and unsteady (high temperature) heating. For the current problem with a maximum exposure duration of 10 to 30 seconds, only the unsteady portion is of primary importance. Note that at the knee in the curve at 50°C (122°F) that more than 20 seconds exposure is required to reach $\Omega = 1.0$.

This hypothesis clearly establishes the dependence of injury on both temperature level and time, a dependency which is also apparent in data of the

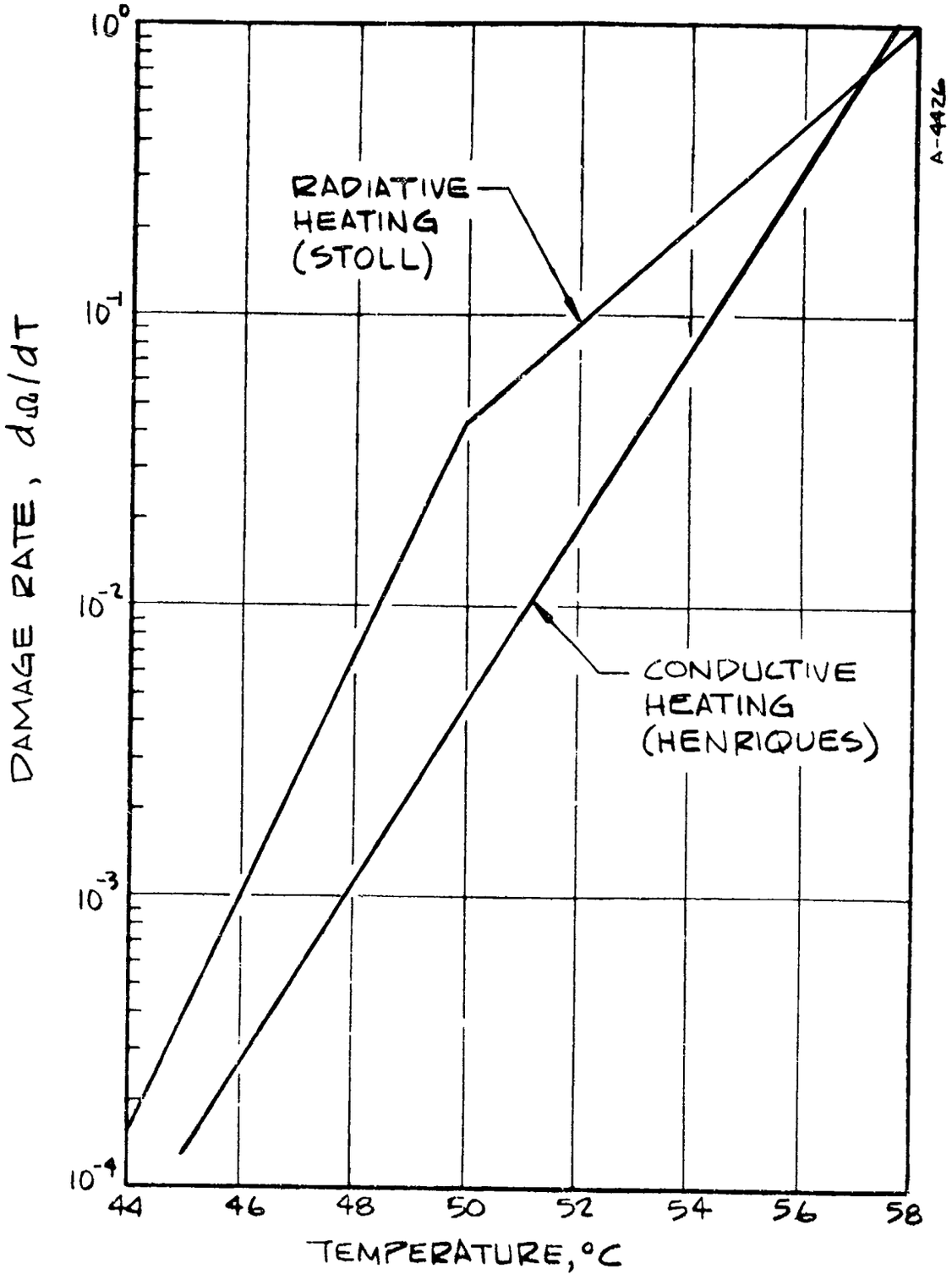

Figure 17. Comparison of Damage Rates Derived from Conductive and from Radiative Data

University of Rochester[15,44,45] and Davies[26] but is not explicitly accounted for by their methods of burn prediction. The virtue of the Henriques approach is that it is only necessary to know the temperature-time history at a given cell location to determine the amount of injury; it is independent of how the energy was applied to the skin. Since the skin model enables us to predict this response, this method for assessing injury is especially well suited.

3.3.5 Comparison of Skin Model - Burn Assessment Criteria to Experimental Data

As a verification of the choice of both the skin model and the burn assessment criteria, all the known pertinent experimental burn data on porcine and human skin have been collected and correlated in terms of the heat flux of a square wave pulse versus the exposure duration which is necessary to produce a second degree of a 2+ burn. To present the constant surface temperature data of Moritz and Henriques[4] in this manner, it was necessary to determine the average heat flux applied during an exposure by dividing the total flux by the exposure time. This alone is not sufficient to relate the two types of tests since the transient response to a constant temperature boundary condition is considerably different from that due to a constant flux. For the same total flux absorbed in the same total duration, the temperature profiles at the base of the epidermal layer for the two boundary conditions will appear as in the sketch.

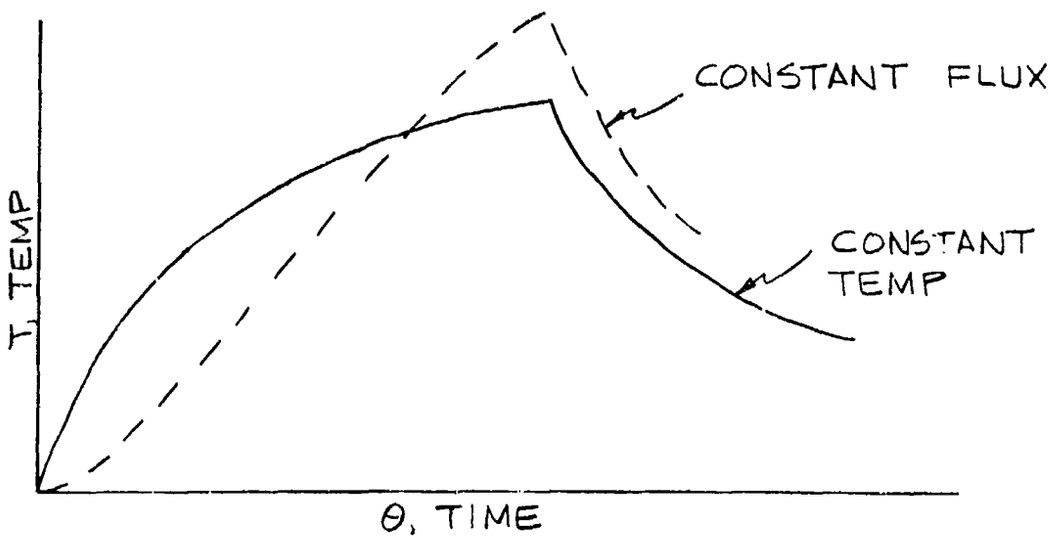

Typical Skin Temperature Response for Constant Surface Flux and Temperature

Note that the maximum temperature is greater for the constant flux case. This occurs because most of the energy is applied early in the pulse for constant

temperature; consequently, this energy has more time to be conducted away. In the constant rate case, energy is still being absorbed at the surface at the average rate at the end of the pulse meaning that more of the total energy is located near the surface at pulse end. Since the damage rate is exponential with temperature, greater damage will be inflicted by the constant flux pulse. To correct for this effect, the computer code (skin model) was run for a range of total durations with both constant flux for both conditions with the flux-duration combination selected to obtain $\Omega = 1.0$ at 100μ nominally. The flux level of the constant flux runs was then adjusted until the total damage, Ω, was equalized for both boundary conditions at the same total duration. The net result was that the constant temperature data of Moritz and Henriques when converted to constant flux form required an additional downward correction in flux of 10 percent at 1 sec duration and 20 percent at 10 seconds. This means that for the same degree of injury and the same total exposure, less total energy is required with constant flux than with constant temperature. The Moritz and Henriques data presented in this manner in Figure 18 correlate quite well with the radiation data of Stoll and Greene[17] and Bales, et al.,[45] (University of Rochester). Only the longer duration data of Davies[26] show any substantial deviation. The extent of the agreement is particularly significant in view of the many potential sources of difference and uncertainty, e.g., different investigators, methods for grading burns, methods of applying heat flux, subjects (porcine and human), and methods of measuring the thermal response.

A possible explanation for the Davies data is that the initial temperature distribution may have been higher than that experienced by Stoll and Greene and Bales, etal. Stoll and Greene report initial surface temperatures of 32.5 ± 1°C (tests outside this range were normalized to 32.5°C) whereas Davies does not report the initial value but notes that 37°C was assumed when relating his tests to the Henriques damage integral. If, in fact, Davies initial temperatures were 4.5°C higher than for the Stoll Greene tests, the heating rate necessary to produce a 2+ burn at 2 and 10 seconds would be decreased relative to those of Stoll Greene by 16 percent and 20 percent respectively. If these corrections are applied to these two data points, the solid triangle points result. The consequence is an almost total collapsing of the data; however, the fact that such changes may result from such small differences emphasizes the sensitivity of such a correlation to the many possible variables previously mentioned.

Verification of the skin model and the burn injury criterion must be in terms of a comparison with the data presented in Figure 18. To do this, the skin model, as described in Section 3.2 was run with square wave heat flux pulses for total durations from 1 to 30 seconds. For each duration selected, the heat flux level was varied until the total injury, Ω, at the base of the

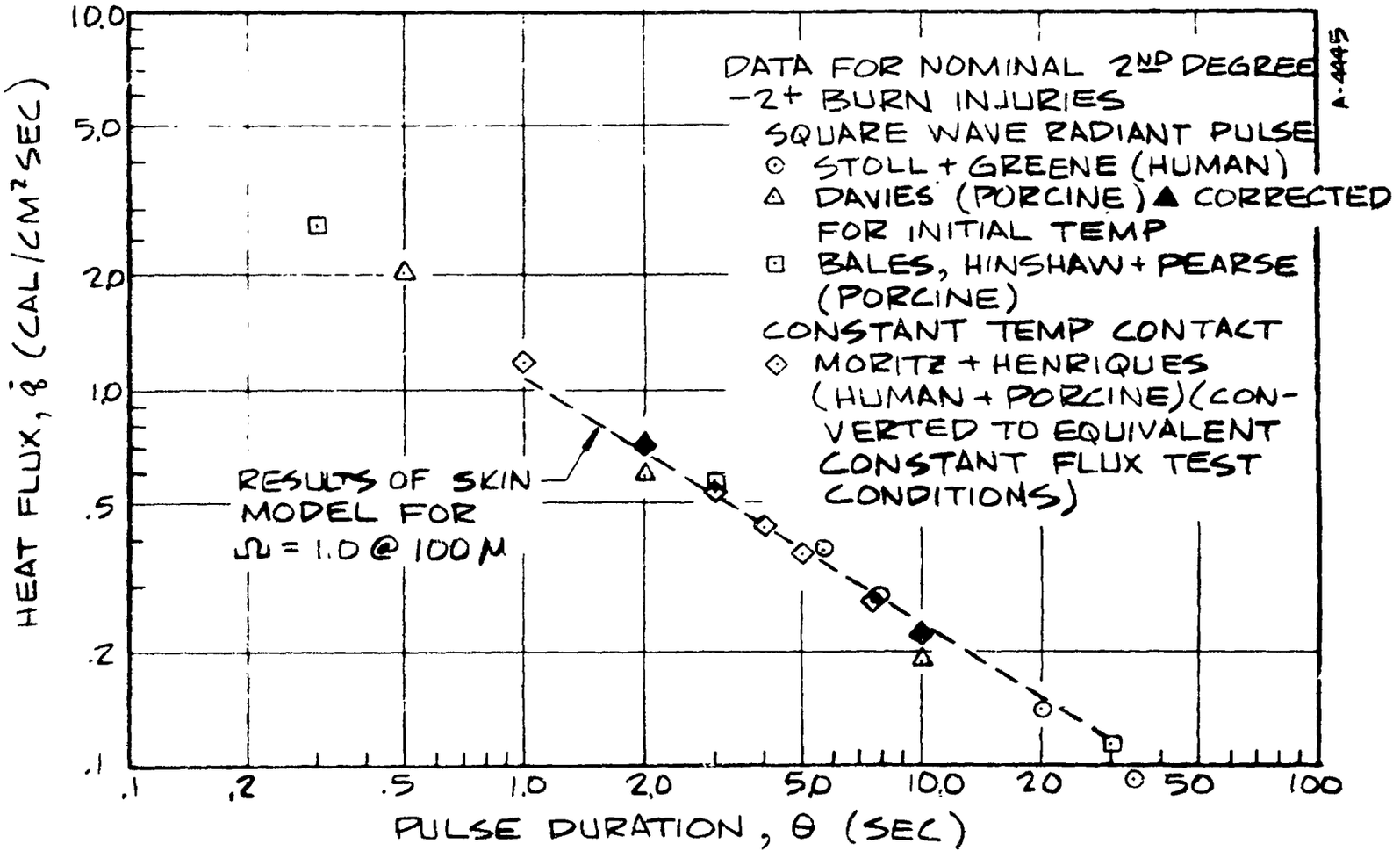

Figure 18. Correlation of Skin Burn Tests with a Comparison to Results of the Skin Model - Burn Assessment Model

epidermal layer (100μ) was equal to 1.0. The result is the dashed line appearing on Figure 18.

The correlation with the data is considered excellent and thus confirmation of the validity of both the skin thermal model and the modified Henriques damage rate criterion, particularly in the range of greatest interest, i.e. for pulses from 1 to 10 seconds long.

Several additional encouraging facts are noted relative to the correlation of the data and the comparison of the skin model results to these data. First, the fact that the corrected Moritz-Henriques data agree so well with the square pulse data implies that the burn damage criterion is equally suited to non-square pulse heating. This is consistent with Henriques hypothesized temperature dependent rate behavior. Secondly, the Stoll-Greene modified form of the criterion which is employed here appears to be valid at temperatures in excess of those encountered in the Weaver-Stoll tests. Their shortest duration test was 5.6 seconds with a peak temperature of about 57°C (135°F) whereas for the one second duration condition of Figure 18, the peak temperature was 61.2°C (142°F).

Investigation has been made into the validity of the extension of the damage rate relation to the prediction of higher level burns, although because very little data exist here, it is not possible to provide a comparison similar to that for the second degree case. In the Moritz and Henriques tests a limited number of experiments were made at high temperature and sufficiently long exposures to result in what they judged to be third degree reactions. In their words these were "Reactions indicating that a significant degree of irreversible injury to the dermis has occurred - - -"*. As stated before they report dermal thicknesses of 1 to 2mm. The exposure values used in the tests were input in the Aerotherm model to predict the resulting extent of burn with total irreversible injury to all tissue above $\Omega = 1.0$. The results are shown in Table VII. The predictions are consistent with the observed results showing only minimal penetration into the dermal layer for the two tests judged to be second degree and at least 1.0mm penetration for those judged to be third degree, i.e., at least half of the dermal layer in these cases was destroyed. Thus it is concluded that there is nothing inconsistent, so far, with the extension of the Henriques approach to higher level injury and dermal damage; however, the accumulation of more data is required to provide a true test for this hypothesis.

Therefore; it is concluded that both the skin model and the burn injury criterion represent valid descriptions of the thermal characteristics and response to thermal stimulation of nominal human skin tissue.

TABLE VII

BURN INJURY PREDICTIONS COMPARED TO MORITZ-HENRIQUES DATA
FOR THIRD DEGREE BURNS
(Reference 4)

Test Conditions		Observed Degree of Burn		Predicted Depth for $\Omega = 1.0$
Surface Temp.	Exposure Duration	2nd	3rd	
65°C	3 sec.	X		0.37mm
70	2	X		0.36mm
75	5		X	1.0 mm
80	5		X	1.2 mm
85	5		X	1.45mm
90	5		X	1.7 mm
95	3		X	1.3 mm
100	3		X	1.4 mm.

SECTION 4

DEFINITION OF THE FIRE ENVIRONMENT

Knowledge of the thermochemical and geometric characteristics of large open pool fires is required before the response of fabrics immersed in such fires can be predicted. The parameters of importance in establishing a definition of the fire environment are:

- Temperature
- Chemistry
- Emissivity and Emission Spectrum
- Fire Dimensions
- Convective Velocities

Once the magnitudes of these quantities are known for particular test conditions, the energy transfer mechanisms can be deliniated and the heating and chemical environment seen by the test fabric can be estimated.

The discussion in the present section will be limited to fires in large pools of JP-4 fuel. A literature survey revealed that the number of existing experimental and analytical investigations of large pool fires is quite limited. Furthermore, none of these investigations was found to provide sufficient information about JP-4 fuel fires in particular. Consequently, it became necessary during the course of the present study to develop a pool fire model which could be used to calculate values of the important fire parameters. In Section 4.1 the available experimental data and theoretical results considered in this study are summarized. The new pool fire model is described in detail in Section 4.2, and in Section 4.3, the fire environment predicted by the new model is presented and compared with the available experimental measurements and theoretical predictions.

4.1 CRITICAL REVIEW OF PERTINENT LITERATURE

Three experimental studies and one analytical model were selected from the literature for consideration in the present investigation. The experimental studies are summarized first in Section 4.1.1, and the analytical model is reviewed in Section 4.1.2.

4.1.1 Experimental Studies

In Reference 48 JP-4 fuel pool fires were studied for the purpose of determining the effects of accidental fires enveloping shipping containers for radioactive wastes. The fires were approximately 18 feet (5.5 meters) square and were conducted with wind velocities less than 5 mph (2.25 m/sec). The fuel was contained in nine steel pans each six feet (1.83 meters) square. In a few of the tests the fuel was poured directly into the pans, while in the remaining tests the fuel was floated on several inches of water in the bottom of the pans. Temperatures were monitored by thermocouples located in the fire 10 to 50 inches 25.4 to 127 centimeters) above the fuel surface. Total heat fluxes were measured by heat meters located in the fire 19 to 34 inches (48.3 to 86.5 centimeters) above the fuel surface.

After an initial transient of less than one minute, the fires were observed to reach an approximate steady state. Figure 19 illustrates the range of temperature profiles measured after steady state was achieved. The asymptotic temperatures are seen to vary from fire to fire over the range 1725°F to 2100°F (941°C to 1150°F) which reflects the typical irreproducibility exhibited by large pool fires. A temperature of 1850°F (1010°C) was determined to be the "average" temperature which characterizes the typical JP-4 fuel pool fire.

The heat meters indicated total heat fluxes varying from 35,960 to 47,540 Btu/hr ft^2 (2.71 to 3.58 cal/sec cm^2). To further substantiate the heat meter readings, an analytical expression was derived relating the measured fire temperatures to the theoretical irradiation which should exist at the heat meter face. The heat flux evaluated from this integral expression was within 10 percent of the value obtained directly from the heat meter. Also, if all the heat flux were due to black body radiation, the corresponding temperature range would be 1680 to 1835°F (915 to 1002°C). On the basis of these results, it can be concluded that the dominant mode of energy transfer within the fire is radiation from a source which is essentially black.

The major conclusion for Reference 48 was that exact predictions of temperatures expected in a particular fire cannot be made because many of the parameters affecting the fire temperature, such as wind velocity and fuel burning rates, are uncontrollable. On the other hand, an "average" temperature of 1850°F (1010°C) for the typical large JP-4 fuel pool fire (under the condition of negligible wind velocity) was recommended.

Reference 49 describes the results of a dry ground field fire test which was performed to study parameters affecting the design of a fire simulation facility. The test pool was comprised of 500 gallons (1.89 x 10^3 liters) of JP-4 fuel spread over an 18' x 30' (5.50 m x 9.15 m) area lined entirely with a canvas. Temperatures were measured in the fire by thermocouples located at

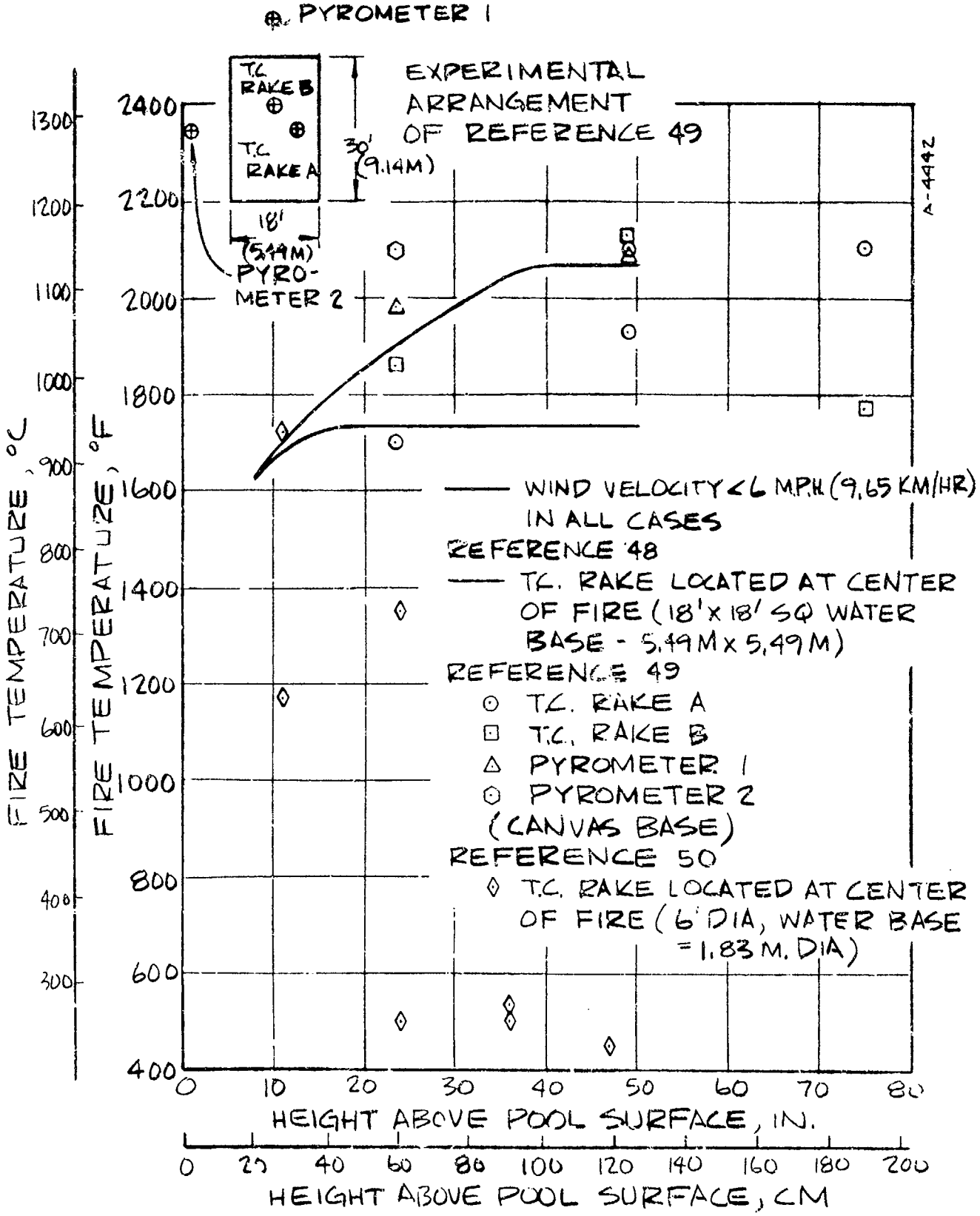

Figure 19. Experimentally Measured Temperature Profiles in Large JP-4 Fuel Pool Fires

heights above the fuel surface of 75, 49, and 23.5 inches (190.6, 124.5, and 59.7 centimeters). In addition to these thermocouple measurements, temperatures were also measured using two optical pyrometers located outside the fire.

The test was conducted with wind velocities low enough that the effects of wind were essentially negligible.

The thermocouples indicated approximately steady temperatures after an initial transient of about twenty seconds. These temperatures are included in Figure 19 and range from 1700 to 2100°F (927 to 1150°C). It appears that the variation in the indicated temperatures cannot be correlated with the position of the thermocouple above the pool surface. The temperatures indicated by the pyrometers are also presented in Figure 19 and vary from 1990 to 2100°F (1089 to 1150°C). These readings do indicate that the fire temperature at 23.5 inches (59.7 centimeters) above the fuel surface is 1990°F (1089°C), slightly lower than that at 49 inches (125.4 centimeters) above the surface, 2090-2100°F (1142-1150°C). Since the optical path through the fire for the two pyrometers differed by a factor of 1.67 (one pyrometer was located on the long side of the rectangular pool, and the other was located on the short side), the close agreement between the two pyrometer measurements at 49 inches (124.5 centimeters) confirms that the fire behaved as a black body radiation source.

Since both fire size and wind effects are comparable in the tests conducted in References 48 and 49, the slightly higher temperatures observed in Reference 49 are probably due to the fact that the JP-4 fuel was spread over a dry surface, in contrast to the water base used in most of the tests of Reference 48. The difference in pool bases is assumed to explain the differences between the average fire temperature recommended by Reference 48, 1850°F (1010°C) and that recommended by Reference 49, 2100°F (1150°C).

In the investigation described in Reference 50, the characteristics of large pool fires were studied for the purpose of producing information useful in the design of protective clothing for fire fighters. The effects of wind velocity, ground conditions, orientation relative to wind direction, distance from the fire, and fire area were investigated. The pools were circular and varied in diameter from 3 to 18.67 feet (0.92 to 5.7 meters). Water, concrete, and ground bases were considered. Thermocouples were placed in the fire at heights above the fuel surface varying from 11 to 47 inches (28 to 119 3 centimeters). Heat meters were located at various positions outside the fire, including several locations at the edge of the fuel pool. Infrared radiation at six different wavelengths was detected by radiometers located about 50 feet (15 meters) from the fire site.

The results reported in Reference 50 tend to disagree with the findings described in References 48 and 49. This is indicated in Figure 19 which compares the thermocouple measurements of Reference 50 (for winds of less than 6 mph) (2.7 m/sec) with those of References 48 and 49. The maximum temperature observed was 1720°F at 11 inches (938°C at 28 centimeters) above the pool surface. Temperatures measured at 36 and 47 inches (91.5 and 119.3 centimeters) above the surface were only 535 and 350°F (280 and 177°C), respectively. The only significant difference between the test conditions of Reference 50 and those of References 48 and 49 is the pool area; in the former study, thermocouple measurements are presented only for the six foot (1.83 meter) diameter pool. However, experimental results presented in Reference 51 indicate that the burning rate of most fuels is constant for pool diameters exceeding roughly 3.5 feet (1.0 meters). Therefore, thermocouple conduction losses (admitted to in Reference 50), rather than the smaller pool area, are most likely the cause of such low indicated temperatures.*

The radiometer measurements of Reference 50 are inconsistent with both the thermocouple measurements made in the same study and the general findings of References 48 and 49. The six wavelengths considered in the radiometer measurements were 1.1, 1.55, 2.2, 2.7, 4.0, and 5.55 microns. Figure 20 is a reproduction of Figure 19 of Reference 50 and shows the measured spectral distribution for large and small JP-4 fuel pool fires with a water base and wind velocities less than 5 mph (2.24 m/sec). These radiometer results indicate strong non-black body behavior; for $\lambda \leq 1.55\mu$, the data appear to coincide with the black body curve at an unusually high temperature of 1600°K (2420°F), while for $\lambda > 1.55\mu$, strong absorption is indicated for almost all wavelengths. These measurements were accepted at face value in Reference 50 and, in addition, calculations were performed there which indicated the maximum total emittance of the JP-4 fuel pool fire was 0.625 at a diameter of 13 feet (3.96 meters).

The radiometer data of Reference 50 were examined closely in the present study and, as a result of several significant discrepancies exhibited by this data, it is felt to be unreliable. First, since $\varepsilon_\lambda = \alpha_\lambda$ from Kirchoff's law and

$$\alpha_\lambda = 1 - e^{-a_\lambda s} \simeq a_\lambda s$$

for small $a_\lambda s$ (a_λ = spectral absorption coefficient and s = path length),

*In further support of this conclusion, the analytical model described in Section 4.2 predicts a temperature of 1720°F (938°C) at distances up to 32 inches (81.2 centimeters above the surface of a six foot (1.83 meter) pool.

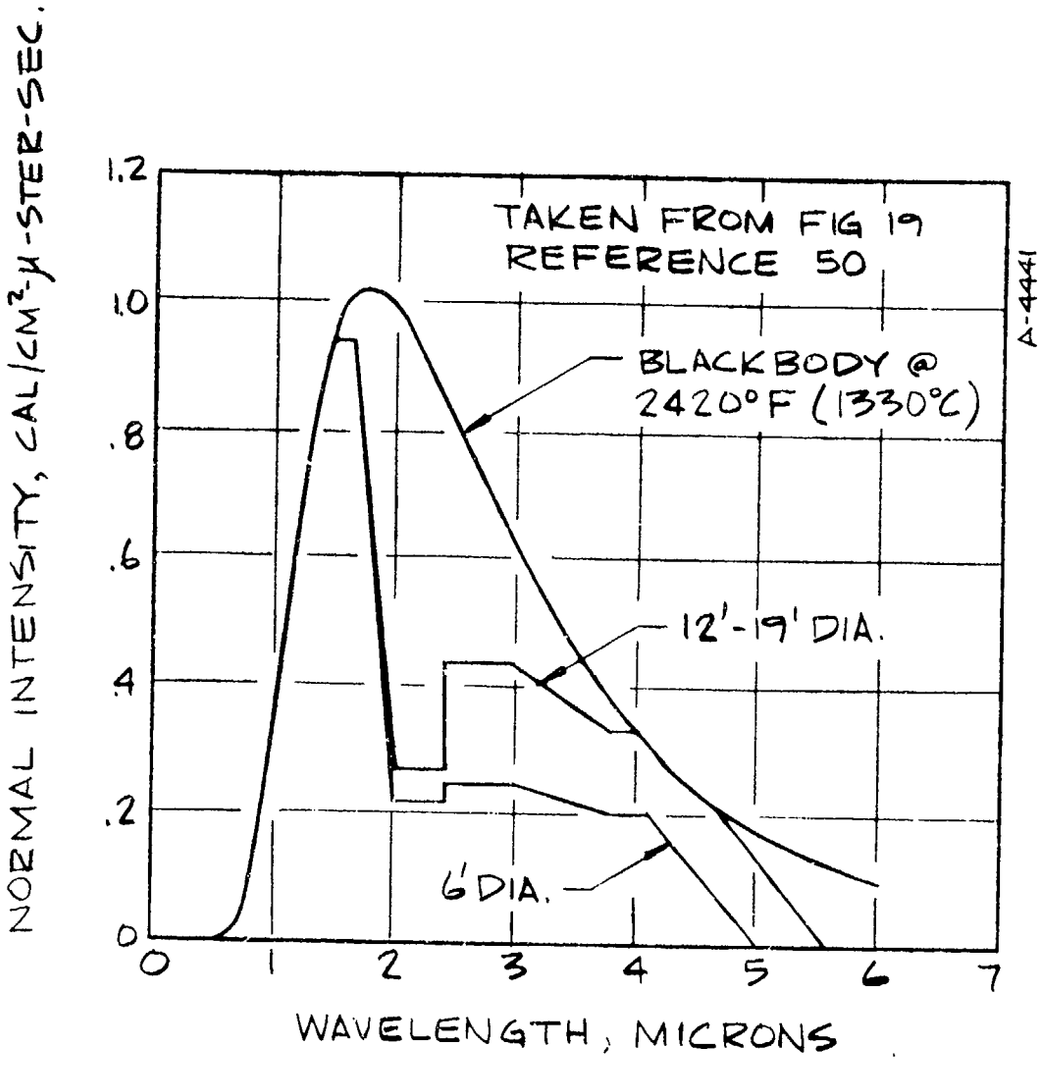

Figure 20. Experimentally Determined Radiation Spectrum for Large JP-4 Fuel Pool Fire

it is evident that intensity is approximately a linear function of path length when the radiating medium emits substantially less than a black body at the same temperature. Examination of Figure 20 reveals that this linearity is not followed at $\lambda = 2.2\mu$ (i.e., α_λ for the 6 foot diameter (1.83 meter) is approximately equal to α_λ for the 12 to 19 foot diameters (3.66 to 5.80 meters). It must be concluded, therefore, that radiation was possibly absorbed either by the atmosphere separating the fire and the radiometer or due to non-uniform concentrations of absorbing species within the fire (assuming, of course, that no errors were made in performing the radiation measurements). The only specie with an emission-absorption band at 2.2μ is CO (Reference 52); as indicated in Section 4.3, the concentration of CO is appreciable. Most likely the CO concentration is significantly higher in the core, where the supply of air is relatively low, and is dominated by CO_2 in the fire periphery, where air is more accessible. Correspondingly, the core temperature is probably somewhat lower than the temperature closer to the periphery since the local air/fuel ratio is lower in the former region. This core of CO could absorb a large portion of the 2.2μ radiation emitted from regions on the back side of the fire (relative to the radiometer).

Absorption at the other wave lengths is even more probable. Water vapor has strong absorption-emission bands at 2.7 and 6.3μ and CO_2 has strong absorption-emission bands at 2.7 and 4.3μ (Reference 52). Thus, absorption due to H_2O vapor either in the fire or between the fire and radiometer and CO_2 nonuniformities within the fire could possibly explain the nonblack body behavior in the 2.7, 4.3, and 6.3μ bands. In any event, these arguments pertain to the fire as it appears to be an observer 50 feet (15.3 meters) from the fire site. For the observer at the center of a large pool fire, emission and absorption in all wavelength bands would most likely appear to be in equilibrium locally; that is, black body behavior would prevail.

Finally, the heat meter data of Reference 50 also seem somewhat inconsistent with that of the other two references. The heat meter at the edge of the 6 foot (1.83 meter) diameter pool indicated 22,600 Btu/ft^{2}hr (1.7 cal/cm^{2}sec). This is roughly half of the heat flux observed in Reference 48. In addition, if the fire were assumed to be a gray body with $\epsilon_{max} = 0.625$ as computed in Reference 50, the corresponding temperature would be about 1700°F (927°C) if all energy transfer were due to radiation. This is considerably lower than the temperature of 2420°F (1330°C) which was recommended based upon the radiometer results.

In view of the conflicts between the data of Reference 50 and those of References 48 and 49, it is evident that either the former or the latter must be eliminated from further consideration. Because the data of Reference 50

contain a number of internal inconsistencies, as pointed out above, it was decided to ignore these data for the remainder of the present study. Considering only the data of References 48 and 49, then, it is concluded that the following features characterize large JP-4 pool fires:

1. Fire temperatures vary from 1850°F (1010°C) (water base) to 2100°F (1150°C) (ground base).
2. Heat transfer within the fire is radiation dominated.
3. The fire exhibits black body behavior.

The results presented in Section 4.3 provide further substantiation of the above conclusions.

4.1.2 Analytical Models

In addition to performing an experimental investigation, the study described in Reference 49 includes the development of an analytical model for large pool fires. An excellent review of the literature treating large pool fires analytically is provided in this reference. It was found there that the major weakness of all available models was the lack of a proper treatment of the fire chemistry. Therefore, an effort was made to develop a model which provided a realistic prediction of the chemical composition of the fire.

It was assumed in Reference 49 that the major portion of a pool fire is characterized by a uniform temperature and composition. Hence, a control volume approach was initiated wherein it was assumed that the thermochemical state of the hot combustion gases within the control volume could be specified by a single temperature and set of species mole fractions. The vaporized fuel coming off the pool surface was injected at the bottom of the control volume. Air was fed by entrainment through the sides of the control volume according to an empirical turbulent entrainment formula. The combustion products were allowed to exit through the top of the control volume. Under these constraints, the model reduced to essentially two equations and two unknowns. The unknowns were fuel rate and entrainment mass rate, and the equations were the empirical entrainment formula and a conservation-of-energy equation. The only heat transfer mechanism allowed was radiation, with fire emissivity taken to be unity. Both the fire temperature and the fire size and geometry were assumed to be known. Chemical composition was obtained from the temperature and known pressure (atmospheric) in conjunction with the standard equilibrium chemistry relations (law of mass action) and the computed fuel and air rates. However, the allowed species were restricted to H_2O, CO_2, CO, H_2 and N_2; that is, the formation of soot particles, which is observed to occur in most pool fire experiments, was not considered.

There are a few major weaknesses associated with the model just described. Two fundamental laws not satisfied by the model are conservation of mass and conservation of momentum. In other words, the model does not require that the fuel burning rate plus air entrainment rate equal the rate of production of combustion products. Nor does it require that all forces on the control volume balance in the vertical direction. Finally, the model does not allow for the formation of soot.

Due to the inadequacies, especially with respect to fire chemistry, inherent in all fire models available in the literature, including that of Reference 49, it was deemed necessary to develop a new model during the present study. This model is described in detail in the following section. In Section 4.3 the predictions of the new model are compared with those of the model described in Reference 49 and briefly summarized above.

4.2 DESCRIPTION OF THE NEW POOL FIRE MODEL

The assumptions inherent in the model and the governing equations are presented in Section 4.2.1, and the technique used for solving the governing equations is illustrated in Section 4.2.2.

4.2.1 Assumptions and Governing Equations

The new model developed in the present study is an extension of the model described in Reference 49. As pointed out in Section 4.1.2, the latter model has three basic deficiencies. The extension in the present work is concerned with eliminating these deficiencies.

Consistent with the approach taken in Reference 49, we assume that the combustion zone over the pool is characterized by a uniform thermochemical state. This means that a single temperature and a single set of species mole fractions will define the fire thermochemistry. Furthermore, we assume that the shape of the combustion zone can be idealized as the frustrum of a right cone; hence, the configuration of the control volume used to develop the conservation equations is dictated by this geometry. Fuel enters through the base of the cone, air is entrained through the side of the cone, and the combustion products exit through the top of the cone. The control volume surrounding the combustion zone and various mass and energy fluxes crossing its surfaces are depicted in Figure 21.

The following is a list of assumptions used in the control volume analysis:

1. The combustion zone is thermochemically uniform.

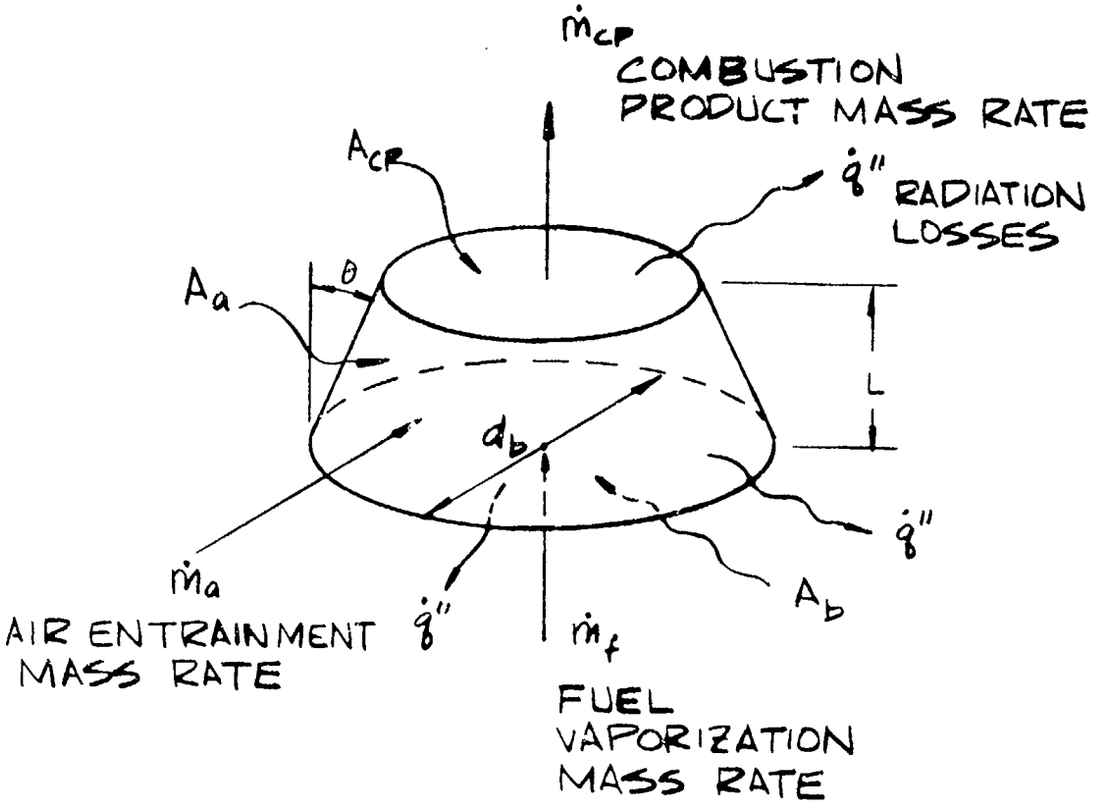

Figure 21. Control Volume Used to Represent Combustion Zone

2. The combustion zone is approximately the shape of the frustrum of a right cone.

3. All chemical reactions in the combustion zone are in equilibrium; soot is formed due to incomplete air-fuel mixing rather than chemical kinetics.

4. The only heat transfer mechanism by which the fire loses energy is radiation, and the fire behaves as a black body.

5. Air is entrained into the combustion zone via a turbulent entrainment mechanism.

6. The fuel burning rate is known from experimental measurements.

7. The effective pool area and angle of inclination of the conical combustion zone are known from experimental observations.

The assumptions listed above deserve durther discussion. Assumption 1. is valid for most of the volume of a large pool fire. However, there are vertical gradients near the surface, as indicated by the temperature gradients in Figure 19. Also calculations have been carried out which indicate the existence of horizontal gradients in the first three feet of the fire periphery. Assumption 2. is used to reduce the number of variables required to specify the volume and surface areas of the fire control volume. Also, it is consistent with experimental results which indicate the fire assumes roughly a conical shape even when the pool base is non-circular.

With regard to assumption 3., experimental results indicate that the rate of combustion in large pool fires is limited by the fuel-air mixing process rather than chemical reaction rates (see Reference 49). The fuel-air mixing process is, in turn, governed by the turbulent entrainment characteristics of the fire plume. Due to this diffusion limit on the combustion process, the mixture in the reaction zone is on the average fuel rich. In fact, it is possible that certain regions of the combustion zone are completely devoid of oxygen. Therefore, any free carbon which has originated due to fuel decomposition at the pool surface and which is present in an oxygen-deficient region will transverse the entire combustion zone without undergoing further reactions. It will be shown in Section 4.3 that the requirement of chemical equilibrium dictates that the majority of this free carbon be in the condensed phase at typical fire temperatures 1850°F (1150°C).

Assumption 4. is justified on the basis of the experimental results presented in References 49 and 49 (see Section 4.1.1).

Assumption 5. is based upon the experimental observation that the fire plume over a large pool is strongly buoyant and turbulent in nature (see References 49 and 53).

Assumption 6. relies on the experimental fact that burning rates for pools of JP-4-like fuel are independent of pool size when the pool diameter exceeds roughly 3.5 feet (1.07 meters) (see Reference 51).

Assumption 7. implies that the height of the fire need not be specified; indeed, in the new model this quantity is treated as an unknown. In the case of rectangular or square pools, an effective pool diameter is obtained by setting the actual area equal to $\frac{\pi}{4}d_b^2$. The angle of inclination is a rather difficult variable to determine from observation of field tests. Nevertheless, photographs of circular pool fires presented in Reference 50 indicate that this angle is somewhere between 10 and 35 degrees (the angle θ in Figure 21).

The governing equations are now presented. From Reference 53 an empirical correlation for turbulent entrainment in strongly buoyant fire plumes is obtained:

$$\dot{m}_a = 77.0\left[(\rho_a\rho_{cp})^{1/2} A_a v_{cp}\right] \tag{20}$$

where

$\dot{m}_a$ = Air entrainment rate, g/sec

ρ_a = Ambient air density, g/cm^3

ρ_{cp} = Density of combustion products, g/cm^3

A_a = Side area of conical control volume, cm^2

v_{cp} = Mean vertical velocity of the combustion products at the top of the conical control volume, cm/sec

Conservation of mass for the conical control volume requires that

$$\dot{m}_{cp} = \dot{m}_f + \dot{m}_a \tag{21}$$

where

m_{cp} = Combustion product flow rate out of conical control volume, cm/sec

m_f = Fuel vaporation rate at pool surface, g/sec

and $\dot{m}_a$ has the same meaning as in Equation 20. A force balance on the control volume requires that the weight of the combustion products within the control volume balance the momentum flux through the top (assuming that the momentum flux associated with the injection of the vaporized fuel at the base is negligible and the velocity vectors for air entrainment lie entirely in the horizontal plane):

$$\rho_{cp} V g = \rho_{cp} v_{cp}^2 A_{cp} \tag{22}$$

where

V = Total volume of the control volume, cm^3

g = Gravitational acceleration 980 cm/sec^2

A_{cp} = Top area of conical control volume, cm^2

and ρ_{cp} and v_{cp} have the same meaning as in Equation 20. Finally, conservation of energy dictates that the following equation be satisfied:

$$\dot{m}_a h_a + \dot{m}_f h_f = \dot{m}_{cp} h_{cp} + Q \tag{23}$$

where

h_a = The specific enthalpy of the entrained air, cal/g

h_f = The specific enthalpy of the JP-4 fuel, cal/g

h_{cp} = The specific enthalpy of the combustion products, cal/g

Q = Total radiation energy loss, cal/sec

and the $\dot{m}$'s have the same meanings as in Equations 20 and 21. The enthalpies in Equation 23 are total enthalpies; that is, sensible plus chemical.

The four equations above can be reduced to three equations in the three unknowns:

T_{cp} = Combustion products temperature, °K

$\dot{m}_a/\dot{m}_f$ = Air-fuel ratio

L = Height of combustion zone (conical control volume), cm

In order to perform this reduction, the following equations are needed:

$$\dot{m}_{cp} = \rho_{cp} V_{cp} A_{cp} \tag{24}$$

$$Q = \sigma(A_b + A_a + A_{cp}) \varepsilon_{cp} T_{cp}^4 \tag{25}$$

where

σ = Stefan-Boltzman constant, 1.354×10^{-12} $cal/cm^2 sec °K^4$

ε_{cp} = Total emissivity of combustion gases

Equations 20, 21, and 24 are combined to give:

$$\dot{m}_a/\dot{m}_f = [5.89(\rho_{cp}/\rho_a)^{1/2} A_{cp}/A_a - 1]^{-1} \quad (26)$$

Equations 21, 22, and 24 are combined to give

$$\dot{m}_a/\dot{m}_f = (\rho_{cp}/\dot{m}_f)\sqrt{gVA_c} - 1 \quad (27)$$

Equations 21, 23, and 25 are combined to give

$$(\dot{m}_a/\dot{m}_f)h_a + h_f = \left(1 + \frac{\dot{m}_a}{\dot{m}_f}\right)h_{cp} + \left(1/\dot{m}_f\right)[\sigma(A_b + A_a + A_{cp})\varepsilon_{cp}T_{cp}^4] \quad (28)$$

The volume and areas can be expressed in terms of the known base diameter, d_b, known angle of inclination, θ, and unknown fire height, L:

$$A_b = \frac{\pi}{4} d_b^2 \quad (29)$$

$$A_a = \pi(d_b - L\tan\theta)L\sqrt{1 + \tan^2\theta} \quad (30)$$

$$A_{cp} = \frac{\pi}{4}(d_b - 2L\tan\theta)^2 \quad (31)$$

$$V = \frac{\pi}{3} L(d_b - L\tan\theta)^2 \quad (32)$$

In Equations 26, 27, and 28 the quantities $\dot{m}_f$, ρ_a, h_a, h_f, ε_{cp}, d_b, and θ are presumed to be known. The quantities ρ_{cp} and h_{cp} are unique functions of T_{cp}, $\dot{m}_a/\dot{m}_f$, and pressure (which is assumed to be atmospheric in the fire plume), by virtue of the assumption of chemical equilibrium. In other words, the equilibrium constants for all possible reactions depend upon only T_{cp} for a fixed pressure, and the relative amounts of the elements present in the plume gases depend upon only $\dot{m}_a/\dot{m}_f$. (Precisely how the chemical state, including the formation of soot, is evaluated in terms of T_{cp} and $\dot{m}_a/\dot{m}_f$ is outlined in Section 4.2.2). Since A_b, A_a, A_{cp}, and V are functions of L only, it is evident that Equations 26, 27, and 28 are, indeed, functions of the three unknowns T_{cp}, $\dot{m}_a/\dot{m}_f$, and L.

Although the model just described represents a substantial improvement over that of Reference 49 and is probably the most complete model available from the viewpoint of flame chemistry, there are several features which could be improved with further study. The most crucial assumption is that the fuel burning rate $\dot{m}_f$ can be specified a priori. In actuality, the rate of fuel vaporization is dependent on the net rate of energy transfer to the pool of liquid

fuel, which includes contributions due to radiation and convection from the fire plume and conduction losses through the pool base. Therefore, a more rigorous model would treat $\dot{m}_f$ as an unknown and introduce an additional equation, such as an energy balance on the fuel pool. Secondly, the model as just presented can predict only the steady-state fire characteristics. A more complete model would include time-dependent terms which would allow for the prediction of the initial transient behavior of the fire. Thirdly, the present model relies on a specification of the angle of inclination θ which is difficult to determine from field tests except under conditions of virtually zero wind velocity. It might be possible to introduce an additional equation which would allow treating θ as an unknown. Finally, the model utilizes the assumption of a thermochemically uniform fire in both vertical and horizontal directions. This is not truly satisfactory with respect to the vertical direction, since experimental measurements indicate the presence of vertical temperature gradients near the pool surface (see Figure 19). A more realistic model would therefore involve differential conservation equations which would enable these vertical thermochemical gradients to be determined.

4.2.2 Solution Technique

Equations 26, 27, and 28 are three nonlinear algebraic equations in the three unknowns T_{cp}, $\dot{m}_a/\dot{m}_f$, and L. Ideally, the solution method would involve developing a computer program which utilizes any one of several standard iteration techniques for solving sets of nonlinear algebraic equations. In the present study, however, time restrictions did not permit such a computer code to be developed. Hence, a simple graphical technique was developed which has the main disadvantage of being rather tedious in application. This graphical technique is now briefly outlined.

Equations 26 and 27 can be combined to eliminate the variable ρ_{cp}, resulting in

$$\dot{m}_a/\dot{m}_f - \left(\frac{5.89}{\sqrt{\rho_a}} \frac{A_{cp}}{A_a}\right) \left[(\dot{m}_a/\dot{m}_f + 1) \frac{\dot{m}_f}{\sqrt{gVA_c}}\right]^{1/4} - 1\Bigg)^{-1} = f_1 (\dot{m}_a/\dot{m}_f, L) = 0 \qquad (33)$$

Given arrays of values for $\dot{m}_a/\dot{m}_f$ and L, the function f_1 can be computed and plotted versus L with $\dot{m}_a/\dot{m}_f$ as a parameter. By determining through interpolation the value of L which gives a zero value of f_1 for a given value of $\dot{m}_a/\dot{m}_f$, the function $L = L(\dot{m}_a/\dot{m}_f)$ can be established.

The energy equation, Equation 28, can be manipulated to the following form:

$$(1/\dot{m}_f)[\sigma(A_b + A_a + A_{cp})\varepsilon_{cp}T_{cp}^4] + (1 + \dot{m}_a/\dot{m}_f)h_{cp} - h_f - (\dot{m}_a/\dot{m}_f)h_a$$

$$= f_2[T_{cp}, \dot{m}_a/\dot{m}_f, L(\dot{m}_a/\dot{m}_f)]$$

$$= f_2(T_{cp}, \dot{m}_a/\dot{m}_f) = 0 \qquad (34)$$

The reduction of f_2 from a function of three variables to a function of two variables is made possible because L is a known function of $\dot{m}_a/\dot{m}_f$ through solution of Equation 33. The combustion product enthalpy h_{cp} was computed for arrays of values of T_{cp} and $\dot{m}_a/\dot{m}_f$ (assuming atmospheric pressure) by utilization of the Aerotherm Chemical Equilibrium (ACE) computer program. ACE is an extremely general and versatile tool for calculating the equilibrium chemical composition and associated thermochemical properties of a system containing an arbitrary number of elements. Both gas and condensed phase species are allowed. In the present problem, which involves the elements C, H, O, and N, ACE considered a total of 59 gas and condensed phase species. The basic species thermodynamic data such as heat of formation, specific heat, and standard state entropy were obtained from sources such as Reference 54, in which the thermochemical base state is taken as the elements in their most natural state at 298°K and one atmosphere.

The formation of soot is treated in a rather arbitrary manner by ACE. If x pounds of fuel and $x\dot{m}_a/\dot{m}_f$ pounds of air are taken to be the chemical system, equilibrium chemistry predicts that all carbon in the system will react to form CO, CO_2, and trace amounts of other carbon compounds, even when the mixture is fuel rich. Such a calculation effectively assumes that the air-fuel mix is infinitely well mixed. In reality, however, the turbulent entrainment mechanism does not result in perfect mixing. This imperfect mixing can be simulated in the ACE program by allowing a prespecified fraction of the carbon in the fuel to remain chemically frozen throughout the combustion process. In Section 4.3, it is shown that all frozen carbon tends to condense even at the combustion temperature. The only drawback to this approach is that the magnitude of the fraction of carbon to be frozen must be selected a priori.

For arrays of values of T_{cp} and $\dot{m}_a/\dot{m}_f$, the function f_2 can be computed and plotted versus $\dot{m}_a/\dot{m}_f$ with T_{cp} as a parameter. Using graphical interpolation to determine the value of $\dot{m}_a/\dot{m}_f$ which gives a zero value of f_2 for a given value of T_{cp}, the function $\dot{m}_a/\dot{m}_f = \dot{m}_a/\dot{m}_f\ (T_{cp})$ can be determined.

Finally, Equation 34 can be arranged to the form

$$(1 + \dot{m}_a/\dot{m}_f) - \left(\rho_{cp}/\dot{m}_f\right)\sqrt{gVA_c}$$

$$= f_3 \left\{T_{cp},\ \dot{m}_a/\dot{m}_f(T_{cp}),\ L[\dot{m}_a/\dot{m}_f(T_{cp})]\right\}$$

$$= f_3(T_{cp}) = 0 \qquad (35)$$

The reduction of f_3 from a function of three variables to a function of one variable is made possible through the parametric solutions of f_1 and f_2. Note that ρ_{cp} is computed, in addition to h_{cp}, by the ACE program for each set of values of T_{cp} and $\dot{m}_a/\dot{m}_f$. For a range of values of T_{cp}, the function f_3 can be computed and plotted and its root thereby obtained graphically. Once this unique value of T_{cp} has been determined, values of $\dot{m}_a/\dot{m}_f$ and L automatically follow from the previously determined functional relationships. The values of T_{cp} and $\dot{m}_a/\dot{m}_f$ determined in this manner are then used by ACE to compute the exact chemical composition of the fire.

4.3 PREDICTIONS OF THE NEW MODEL AND COMPARISON WITH AVAILABLE EXPERIMENTAL AND THEORETICAL RESULTS

The input parameters $\dot{m}_f$ and d_b were determined from observations of a JP-4 fuel pool fire test conducted at the Natick Army Test Facility in November, 1971. For this experiment it was observed that 25 gallons (95 liters) of fuel were consumed during a fire that lasted approximately 30 seconds, including initial and final transients. Assuming that the initial transient was approximately six seconds, (based on visual observation) during which the rate $\dot{m}_f$ increased linearly from zero to its steady state value, and assuming that the final transient was also six seconds during which the rate decreased linearly from its steady state value to zero, the steady state value of $\dot{m}_f$ was determined to be 3175 g/sec (the specific gravity of JP-4 fuel was taken to be 0.82).

The pool was rectangular in shape with dimensions of 20' x 30' (6.10m x 9.15 m). The effective diameter for a pool area of 600 square feet (56.7 square meters) is d_b = 27.7 ft (8.4 m). However, it was found that using this value for d_b resulted in unrealistically high values of T_{cp}. Since the fire plume attains an approximate conical shape even though the pool geometry is rectangular, it was assumed that the actual vaporizing portion of the fuel surface can be more accurately described as an ellipse with major and minor axes equal to the long and short dimensions of the rectangular pool. The effective diameter for a vaporization area of this size is d_b = 24.5 ft (7.5 m).

Using $\dot{m}_f$ = 7.0 lbm/sec (3175 g/sec) and d_b = 24.5 ft (7.5 m), the rate of recession of the pool surface due to fuel vaporization can be computed. This rate is 5.31 mm/min, which compares well with the burning rates presented in Reference 51 for various hydro-carbon fuels in pools of large dimensions.

In Reference 49 the effective molecular configuration for JP-4 fuel is determined to be $C_{9.64}H_{2(9.50)}$, and the corresponding heat of formation is given as h_f = -137,253 BTU/lb mole (-76302 cal/g mole) (this value is consistent with the thermochemical base state used by the ACE program). Since the air entering the combustion zone is entrained from an environment at approximately standard state conditions, we conclude that $h_a = 0$ to a good approximation and $\rho_a \approx 0.07$ lbm/ft^3 (1.12×10^{-3} g/cm^3). Consistent with the findings of References 48 and 49, it is also concluded that $\varepsilon_{cp} = 1.0$. Finally, photographs presented in Reference 50 indicate that $\theta \approx 25°$ for large pool fires under windless conditions.

Tables VIII and IX present solutions of the governing equations for seven different sets of input variables. The first solution is a baseline calculation, and the remaining solutions involve varying the magnitude of each input variable in order to assess the degree of sensitivity of the final solution to changes in that variable. Table VIII presents the resulting values of T_{cp}, $\dot{m}_a/\dot{m}_f$, and L. Table IX presents $\dot{m}_{cp}$ (molecular weight of the combustion products), ρ_{cp}, v_{cp}, and the mole fractions of the most prominent species.

Note that the baseline solution does not consider the formation of soot. The resulting values of T_{cp}, $\dot{m}_a/\dot{m}_f$, and L are 2050°F (1393°K), 9.53, and 7.77 ft (2.38 m), respectively. The T_{cp} value agrees quite well with experimentally measured values for JP-4 fuel pool fires with a ground base. This agreement is appropriate since no attempt was made to include in the model the effects of a water base on the fuel vaporization rate, the enthalpy of combustion, or the elemental constituents of the fuel. The $\dot{m}_a/\dot{m}_f$ indicates that the combustion zone is quite fuel-rich, since the stoichiometric value of $\dot{m}_a/\dot{m}_f$ is 14.6 (Reference [49]). The value of L indicates that the ratio L/d_b is about 0.32, which agrees well with photographs of large circular pool fires presented in Reference 50.

The results presented in Table VIII indicate that the solution is much more sensitive to changes in $\dot{m}_f$, d_b, and θ than to changes in ρ_a, ε_{cp}, or the presence of soot. Thus, fuel rate and fire geometry are the most important parameters to measure and control in field tests. Note that the change in $\dot{m}_f$ causes large changes in T_{cp} and $\dot{m}_a/\dot{m}_f$ and only a small change in L, while the changes in d_b and θ cause large changes in all three parameters. Also, when soot is allowed to form, the value of T_{cp} is changed significantly.

In the seventh solution where the presence of soot is considered, the ACE calculations were made with 25 percent of the carbon present in the fuel

TABLE VIII

JP-4 FUEL FIRE PARAMETRIC STUDY RESULTS

	$\dot{m}_f$ (g/sec)	d_b (m)	θ (deg)	ρ_a (g/cm^3)	ε_{cp} (-)	Soot (-)	T_{cp} (°K)	$\dot{m}_a/\dot{m}_f$ (-)	L (m)
1. Baseline	3175.	7.47	25	1.12×10^{-3}	1.0	No	1393	9.53	2.37
2. Fuel Rate	3630. +14%	7.47	25	1.12×10^{-3}	1.0	No	1330 -4.5%	8.35 -12.5%	2.37 -0.1%
3. Pool Area	3175.	6.70 -10%	25	1.12×10^{-3}	1.0	No	1250 -10.0%	7.37 -22.7%	2.12 -10.4%
4. Angle	3175.	7.47	35 +40%	1.12×10^{-3}	1.0	No	1266 -9.0%	7.67 -19.5%	1.86 -21.4%
5. Ambient Conditions	3175.	7.47	25	1.28×10^{-3}	1.0	No	1408 +1.1%	9.72 +2.0%	2.29 -3.5%
6. Emissivity	3175.	7.47	25	1.12×10^{-3} +14%	0.9 -10%	No	1398 +0.3%	9.26 -2.8%	2.35 -0.9%
7. Soot	3175.	7.47	25	1.12×10^{-3}	1.0	Yes	1460 +4.5%	9.40 -1.4%	2.36 -0.4%

TABLE IX

THERMOCHEMICAL RESULTS OF JP-4 FUEL FIRE STUDY

	M_{cp} (g/g mole)	ρ_{cp} (g/cm³)	V_{cp} (m/sec)	Mole Fraction (Molecules/Gas Phase Molecule)					
				CO	CO_2	H_2O	H_2	N_2	C*
1. Baseline	26.14	2.28×10^{-4}	6.73	.1094	.0679	.0993	.0755	.6478	0
2. Fuel Rate	25.24	2.31×10^{-4}	6.75	.1381	.0547	.0807	.1094	.6171	0
3. Pool Area	24.36	2.37×10^{-4}	6.40	.1638	.0441	.0603	.1446	.5872	0
4. Angle	24.64	2.37×10^{-4}	6.25	.1551	.0479	.0665	.1336	.5969	0
5. Ambient Conditions	26.28	2.67×10^{-4}	6.72	.1053	.0698	.1021	.0705	.6523	0
6. Emissivity	25.95	2.26×10^{-4}	6.57	.1166	.0641	.0963	.0818	.6412	0
7. Soot	27.27	2.27×10^{-4}	6.64	.0614	.0791	.1394	.0453	.6749	.0468

prevented from reacting with other elements. That is, this portion of the carbon was allowed to reside in the combustion zone only as C, C_2, C_3, C_4, or C*. Freezing 25 percent of the available carbon logically implies that the actual turbulent mixing in the combustion zone is 25 percent less effective than hypothetical perfect mixing. As indicated in Table IX, ACE predicts that virtually all of this carbon goes to C*. As an auxillary calculation, the tables of Reference 55 were used to estimate the total emissivity of a soot suspension with soot concentration identical to that of the seventh solution. According to ACE, the volume fraction of soot in the seventh solution is 2.09×10^{-6}. The path length is d_b = 24.5 ft = 748 cm. Using the resultant volume fraction path length product in conjunction with the tables of Reference 55 indicates that the total emissivity is essentially unity. Using the same procedure it is estimated that if the fraction of carbon frozen were reduced from 25 percent to 2.5 percent, the total emissivity of the corresponding soot suspension would be roughly 0.85.

The chemical composition of the fire for the seven conditions is given in Table IX. As indicated, the dominant species are CO, CO_2, H_2O, H_2, N_2, and C*. It is important to note that virtually all of the free oxygen entrained into the fire zone is consumed in chemical reactions, even when imperfect mixing is considered. According to ACE, the mole fractions for all other possible species are several orders of magnitude lower than those for the six dominant species. For the purpose of comparison, the predictions of the model of Reference 49 are mentioned here: assuming a fire temperature of 2100°F (1150°C), the mole fractions of CO, CO_2, H_2O, and H_2 were computed to be 0.1340, 0.0600, 0.0765, and 0.1145, respectively. The ratio $\dot{m}_a/\dot{m}_f$ was found to be 8.33. These results agree well, with the exception of T_{cp}, with solution 2. of the present study.

Another auxiliary calculation was performed to assess the relative importance of radiative and convective heating on an object in the fire plume. The radiative heat flux emitted by a black body at 2510°R (1393°K) is 18.9 BTU/ft^2sec (5.13 cal/cm^2sec). Assuming the object immersed in the fire is cylindrical with a diameter of two inches and is located at the top of the fire plume where V_{cp} = 22 ft/sec (6.70 m/sec), a convection heat transfer coefficient of 4.24×10^{-3} BTU/ft^2sec°R (2.07×10^{-3} cal/cm^2sec°K) is obtained from a correlation available in Reference 56. This is a worst-case value, since the convection coefficient decreases with increasing object diameter and decreasing convective velocity; a diameter of two inches is a reasonable minimum, and the vertical convection velocity in the fire is a maximum at the top of the combustion zone. The resulting convective heat transfer is roughly 8 BTU/ft^2sec (2.17 cal/cm^2sec). We conclude that convection will never amount to more than 30 percent in the typical large JP-4 fuel pool fire.

In summary, the following major conclusions can be made based upon calcualtions utilizing the pool fire model developed in the present study:

1. The value of T_{cp} for a ground-base fire is within 10 percent of 2510°R (1393°K); based on experimental results, for a water-base fire T_{cp} is probably 200 - 300°F (111 - 167°C) lower.
2. The only molecular species present in appreciable amounts are CO, CO_2, H_2O, H_2, N_2, and C*; there is virtually no uncombined oxygen present.
3. The value of $\dot{m}_a/\dot{m}_f$ is 9.53, with an uncertainty of 23 percent.
4. The combustion zone height is L = 7.77 ft (2.37 m), with an uncertainty of 21 percent.
5. The maximum vertical convective velocity in the combustion zone is 22 ft/sec (6.70 m/sec), and this maximum occurs at the top of the zone.
6. Convection heat transfer to an object immersed in the fire will not exceed 30 percent of the total heat transfer to the object.
7. Due to the large path lengths and appreciable soot concentrations, the fire radiates as a black body.
8. The parameters most important in predicting the thermochemical characteristics of the fire are fuel burning rate, pool area, and angle of inclination; exact knowledge of ambient conditions is much less important.

These conclusions agree with the conclusions presented in Section 4.1.1 which are based entirely on experimental data.

SECTION 5

FABRIC PROPERTIES

The final and most complex part of the system is the clothing assembly. Any one of a number of different types of fabric properties is capable of playing a dominant role in the determination of protection potential. In this section, each of the following property categories is discussed relative to the candidate fabrics.

1. Optical Properties - determine how much of the radiant heat flux from the fire is reflected, absorbed, transmitted directly to inner layers, and reradiated. Since the fire heating is predominantly radiation, the optical characteristics of the fabric determine the amount of energy entering the clothing-skin system.

2. Dimensional Stability - gas or air gaps between layers provide the major resistance to the flow of heat within the system, thus the ability of a fabric to maintain dimensional stability at elevated temperatures is an important characteristic.

3. Thermal and Physical Properties - this category includes fabric density (weight), specific heat, thermal conductivity, thickness, and moisture regain, quantities which control the thermal response within the fabric layer.

4. Thermochemical Properties - considers the mass and energy transfer events occurring at elevated temperatures as the fabric decomposes. Included is the loss of mass as a function of time and temperature, the description of pyrolysis gases for possible reaction with the ambient environment (possible ignition and combustion), and the heat of formation of the fabric.

5. Fluid Mechanical Considerations - the flow of ambient gases (primarily flame) and pyrolysis gases including water vapor through the fabric depends upon the permeability of the fabric and the configuration of the assembly as well as the dynamic factors of relative motion and rate of generation of vapor. An order of magnitude analysis based on nominal conditions is described.

Candidate materials considered in this section include Nomex, PBI, and stabilized PBI. Relative to the stabilized PBI, data for two separate fabrics are reported; the fabric designated L represents an intermediate development stage in the stabilizing of PBI whereas the fabric designated 121 represents the latest version of a stabilized PBI. As such, emphasis is placed on this latter fabric. Data for fabric L are included for the record.

5.1 OPTICAL PROPERTIES

The results in Section 4 for the fire characteristics indicate that radiation is the dominant mode of heat transfer from the fire to the fabric. Consequently, the optical properties of the materials are of major importance in determining the thermal response of the fabric and underlying materials. Energy may be transferred from the fire to the skin in one of two ways, either directly by transmission through the fabrics or by absorbtion with resulting reradiation and conduction from fabric to skin. Desirable characteristics for a fabric then would include both minimal transmittance and absorptance, i.e., simply prevent the energy from entering the fabric - skin system. In addition, given a certain reflectance value, it is also desirable that the fabric absorb the remaining energy keeping the transmitted portion to a minimum. This is because energy once absorbed within the skin tends to stay within the skin whereas energy absorbed within the outer layer of fabric is reradiated both inward and outward, thus some fraction of the energy absorbed by the fabric will not reach the skin.

In order to determine the needed properties, samples of each of the candidate fabrics were subjected to radiant heating (in the shrinkage facility described in 5.2) until they reached the point of total shrinkage or onset of the charred state. These samples together with samples of the virgin materials were sent to the Thermophysics Section of the TRW Systems Group for optical property testing. Table X contains the integrated values of reflectance, absorptance, and transmittance at each of two black body temperatures, 1800°F (980°C) and 4500°F (2480°C), accounting for the spectral energy distributions of the JP-4 fire and the quartz lamp source radiation facility respectively. Values are given for both the virgin and charred (shrunken) state. The latter state was based on the maximum shrinkage condition. In all cases discoloration had occured and some degree of char existed.

Spectral reflectance and transmittance measurements were made in a Gier-Dunkle integrating sphere reflectometer with a Beckman DK-2A spectrophotometer between 0.5 and 2.5μ. For the PBI and Nomex fabrics, total reflectance in the region beyond 2.5μ was measured directly on the Gier-Dunkle model DB100 portable

emissometer. Since reflectance in this region was found to be quite low for these materials, the lack of spectral data is not significant. Spectral transmittance beyond 2.5μ for PBI and Nomex were made with a goniometric bidirectional reflectometer in which the transmitted energy is measured at several angles and then integrated. Subsequent analysis of the data and the test method and comparison with data obtained using another technique on other fabrics suggested that there were errors in the transmittance results beyond 6μ where very high values were measured. Measurements made on other fabrics indicate the transmittance is effectively zero beyond 6μ for both the virgin and charred (shrunken) state. Consequently, the total transmittance to the two black body spectra were recomputed by TRW for the PBI and Nomex fabrics. The effect is significant only for the virgin state at 1800°F resulting in a decrease in transmittance (increase in absorptance) of .04 and .05 for PBI and Nomex respectively. The corrected values are reported in Table X.

For the remaining materials, an alternate technique to measure spectral reflectance and transmittance beyond 2.0μ was employed to eliminate the uncertainties encountered in the infrared region. Directional reflectance was measured in a paraboloid reflectometer with two different backings behind the fabric, one of low reflectance and the other of high. Based on these measurements and a reduction technique described in Appendix I, both the reflectance and transmittance of the fabric can be determined. The resultant optical property data indicate the necessity for knowing the spectral characteristics of the source energy to be used in an analysis. A high temperature source (4500°F) emits more of its total energy at much shorter wavelengths than does a lower temperature source (1800°F). Thus the amounts of energy transmitted, absorbed, and reflected by a given fabric exposed to a given source will depend upon both the optical characteristics of the fabric and the spectral content of the source.

Additional details of the measurement technique employed and the spectral data for the fabrics have been edited from the TRW reports and are included in Appendix I.

5.2 FABRIC SHRINKAGE

The existence and maintenance of air gaps in the clothing assembly are significant factors in providing thermal protection; thus, the dimensional stability of fabrics must be known. Since such data were not available, a testing method was devised to obtain the required information for the candidate fabrics. The heating durations and levels used for the shrinkage tests were selected to determine the amount of fabric shrinkage as a function of maximum fabric temperature achieved during the test. These data would then be used in the fabric

TABLE X

OPTICAL PROPERTIES OF CANDIDATE FABRICS

Fabric	Virgin State						Charred (Shrunken) State					
	1800°F (980°C) B.B.			4500°F (2480°C) B.B.			1800°F (980°C) B.B.			4500°F (2480°C) B.B.		
	ρ	α	τ	ρ	α	τ	ρ	α	τ	ρ	α	τ
PBI	.23	.62	.15	.41	.36	.23	.18	.76	.06	.24	.68	.08
Nomex	.26	.57	.17	.43	.32	.25	.17	.72	.11	.30	.52	.18
Stabilized PBI												
Fabric L	.21	.73	.06	.41	.45	.14	.21	.78	.01	.19	.80	.01
Fabric 121	.17	.74	.09	.34	.46	.20	-- Measurements Not Made --					

model to determine shrinkage (air gap closing) as a function of temperature. Consequently, a range of test conditions were required to generate data over a fully descriptive range of temperatures. As such, not all of these tests are representative of conditions encountered in crash fires. Since the tests were conducted with a high temperature quartz lamp source, higher incident heat flux levels and, in some cases, longer durations than found in typical crash fires were required due to the lower fabric absorptance to a 4500°F source (see Table X).

5.2.1 Test Purposes

The purpose of the shrinkage tests was to determine the dimensional change as a function of temperature and to examine the influence of the following parameters on shrinkage.

- Temperature
- Heat Flux
- Environment - inert or oxidizing
- Tensile loading
- Exposed side

5.2.2 Test Technique

Samples of the fabric materials were exposed to radiant heating on one side in the Aerotherm 10 kw quartz lamp facility. The back side of the fabric was exposed to ambient temperature. The fabric was supported such that it remained in a flat plane throughout the exposure. The tension imposed was kept at a low level to reduce the influence on shrinkage. Capability was provided for performing the tests in a ambient temperature non-oxidizing (N_2) environment simulating the inert quality of the fire environment.

The fabric temperature history and the pre- and post-test dimensions of the fabric were recorded. By running tests of different duration, it was possible to obtain the relationship between shrinkage and maximum fabric temperature achieved in each test.

5.2.3 Test Setup

The test configuration is depicted schematically in Figure 22. Figures 23 and 24 are photographs of the test equipment. Not shown are a CEC Model 5-119 Recording Oscillograph used to record the pyrometer output and a nitrogen bottle connected to the facility.

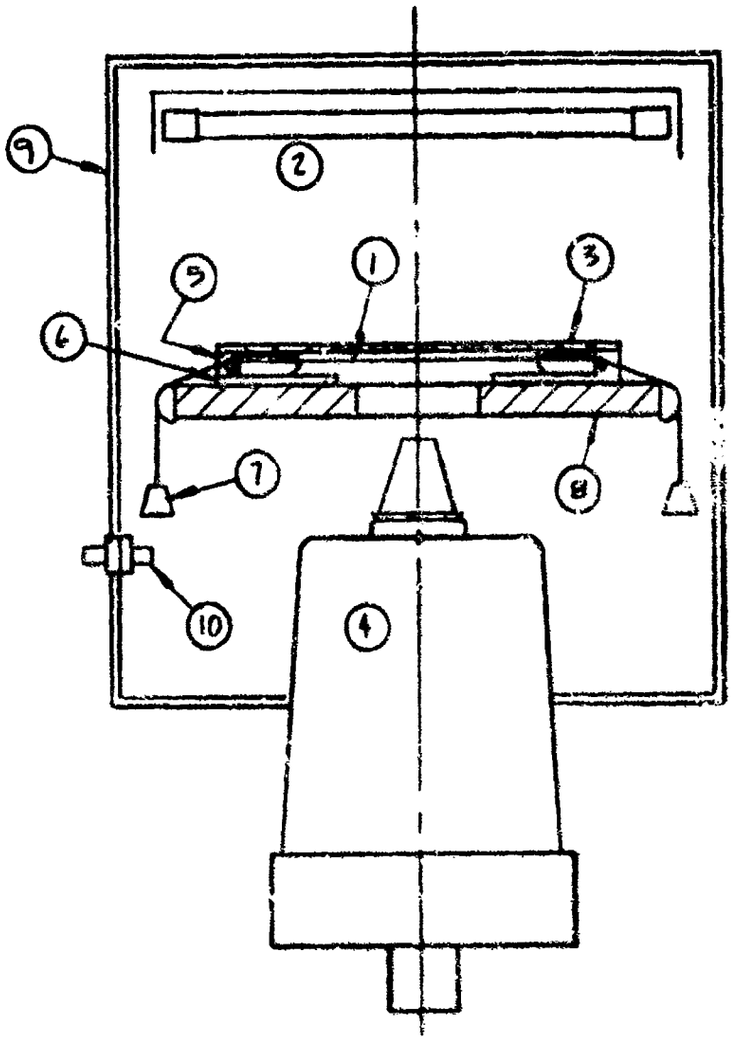

1. Fabric Sample, 10 cm x 13 cm
2. Quartz Lamp Array
3. Aperture Plate, 6.4 cm x 6.4 Opening
4. Barnes IT-4A Pyrometer
5. Fabric Clamps (Aluminum)
6. Runner Plates (Teflon)
7. Tension Weights
8. Water Cooled Mounting Plage
9. Air Tight Enclosure
10. Inert Gas Bleed-In Port

Figure 22. Fabric Shrinkage Test Facility

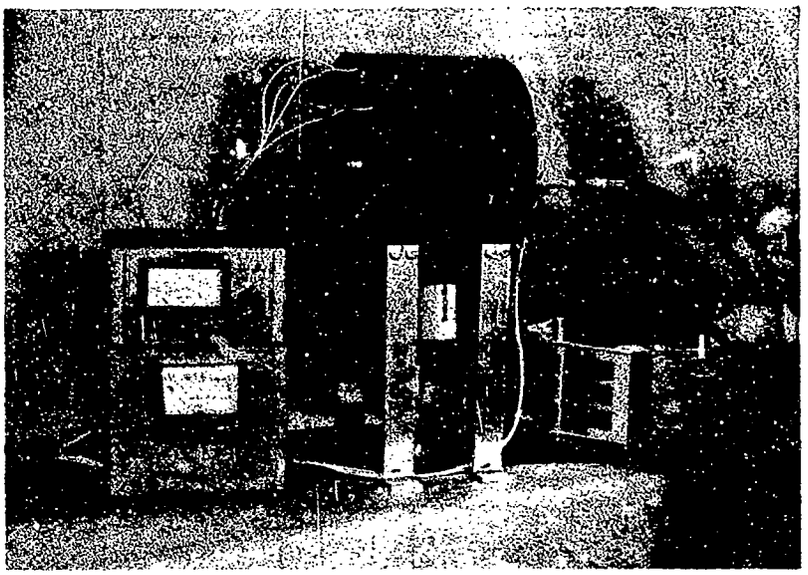

Figure 23. Total Shrinkage Test Facility

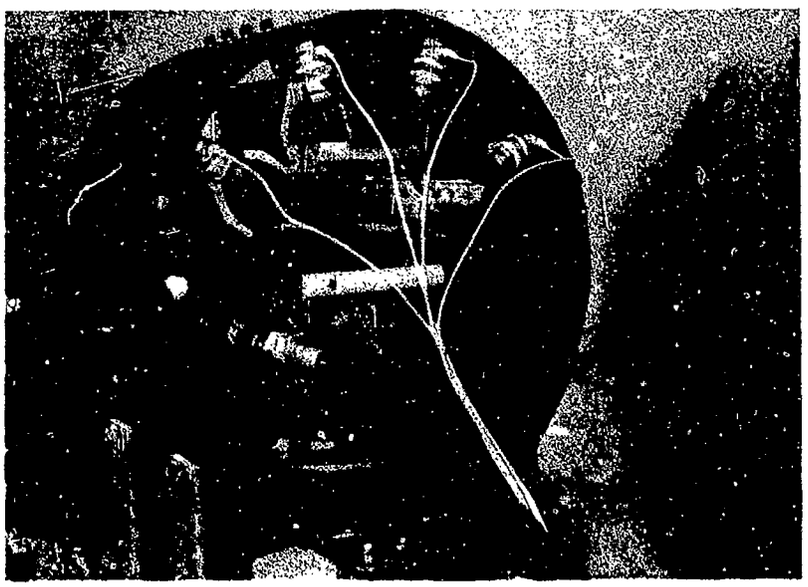

Figure 24. Radiant Lamps

LAMP ARRAY

The lamp array is composed of four 155V - 1200W tubular quartz lamps, each mounted in an elliptical reflector, and arranged in a cylindrical array above the test panel. The flux uniformity at the aperture within the 6.4 cm x 6.4 cm zone is ±6 percent. Since the aperture is displaced slightly above the fabric, some shadowing occurs at its perimeter. For that reason the fabric controlled zone in which temperature and shrinkage were measured was a 2.5 cm square. Within that region, the flux uniformity on the fabric is ±2 percent.

A shutter was not employed since lamp heat-up time was less than one second as indicated by a Gardon gauge calorimeter.

PYROMETER

The pyrometer was a Barnes Engineering Company IT-4A Thermalmaster which is sensitive to radiation within the spectral bandwidth of 8μ to 15μ. The pyrometer has a 50 millisecond response in going from 10 percent to 90 percent output for a stepped input. Since the factory-calibrated full-scale reading of the IT-4A is 570°F, it was necessary to install a filter in the light path and recalibrate at 100°F steps between 400°F and 1400°F with a Barnes Model 11-201T Infrared Radiation Source. The long wave-length range of the pyrometer eliminated the influence of quartz lamp energy transmitted through the fabric. Beyond 4μ, the quartz envelope is opaque to energy radiated from the tungsten filament. Energy radiated directly from the quartz envelope is a small fraction of the filament energy.

Emittance measurements made at the TRW thermophysical properties laboratory on PBI and Nomex yielded the following emittance values:

Fabric	ε
PBI, virgin	.89
PBI, charred	.90
Nomex, virgin	.88
Nomex, charred	.91

(Further information on the radiation properties measurements may be found in Subsection 5.3). In converting the pyrometer black body measurement to a true surface temperature, an emittance of $\varepsilon = .90$ was used for all fabrics, virgin or charred.

The pyrometer was aligned to the center of the aperture. The pyrometer face was located 13 cm below the fabric, resulting in a 1.9 cm diameter field of view on the fabric.

Pyrometer calibration and alignment were checked for accuracy in the following manner. A 3.8 cm x 3.2 x .080 cm blackened flat plate slug calorimeter was instrumented with a chromel-alumel thermocouple and suspended at the position normally occupied by the fabric sample under test. The rectangular dimensions of the calorimeter corresponded to the region of uniform char observed in the fabric samples in the longer test runs.

The calorimeter was exposed to lamp flux while the thermocouple and pyrometer signals were recorded. Figure 25 presents a comparison of the temperature results, indicating an average bias of 14°C which is within 3 percent of the absolute temperature. The variation in bias was ±3.5°C over the range measured indicating an uncertainty of ±0.6 percent of the absolute temperature. The bias was not corrected for in the fabric test results because it was not large.

DIMENSIONS

Critical fabric dimensions were measured before and after each test to determine shrinkage. Pre-test measurements of the dimensions in the exposed region were accurate to ±.020 cm and post-test measurements had an accuracy of ±.050 cm. Thus the probable error in measurement of shrinkage was ±2 percent of the virgin length.

5.2.4 Test Procedure

The tested fabrics were supplied by AFML, one type each of PBI, Nomex and stabilized PBI (L and 121). Fabric weights as measured at Aerotherm were 149 gms/m^2 (4.4 oz/yd^2) for PBI, 136 gms/m^2 (4.0 oz/yd^2) for Nomex, 173 gms/m^2 (5.1 oz/yd^2) for L and 148 gms/m^2 (4.4 oz/yd^2) for 121.

The fabrics were washed once prior to use. Each fabric sample was cut into a 10 cm x 13 cm rectangle. Parallel marks, 3mm long, were speced 2.54 cm apart in orthogonal directions from the sample center on the back surface (away from the lamps). The marks were made with ink or a knife cut. The sample was mounted in the clamps along the short side and positioned in the facility under the aperture.

Tension weights were 16 grams for all runs. It was found that when less weight was used, the sample tended to sag, which was undesirable. Assuming a coefficient of sliding friction of $\mu = 0.2$ between the aluminum clamp and the teflon plate, the additional sliding load was 11 grams. Some friction occurred in sliding of the tension weight support wires over teflon capstans. Therefore

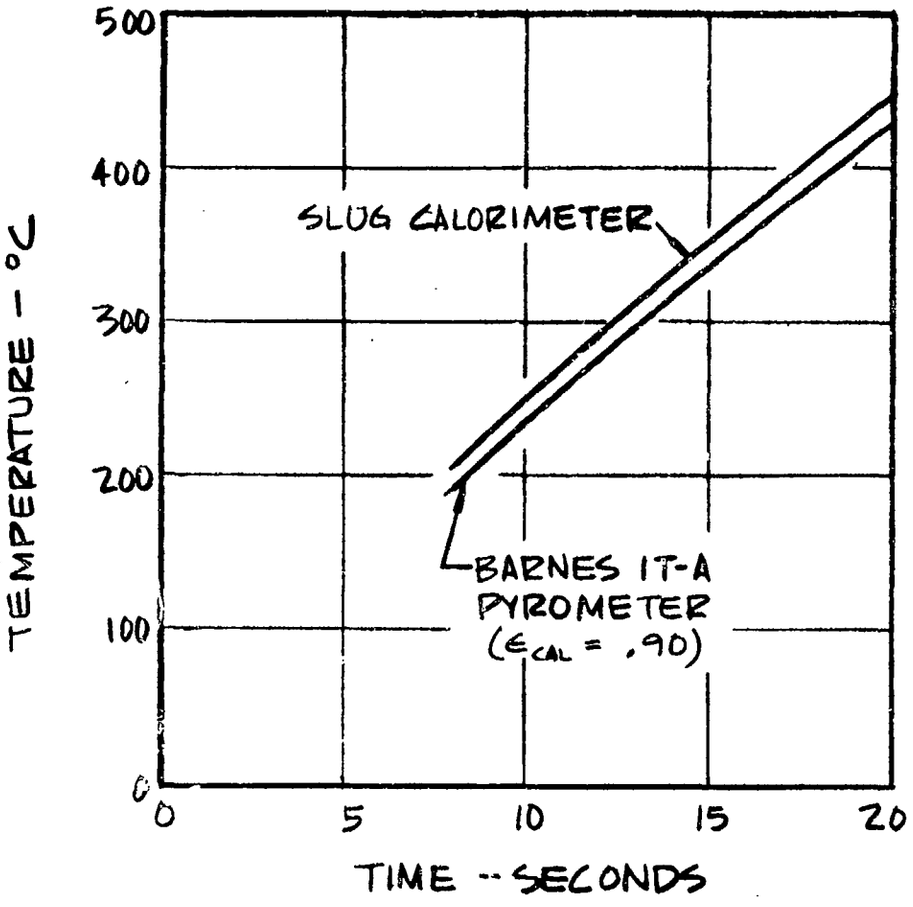

Figure 25. Pyrometer Calibration and Alignment Test Results

the total tensile load was approximately 30 grams distributed over the 10 cm side of the fabric. In the other axis, a small restraint was transmitted from the clamped ends. The clamps were displaced about 5 cm from the controlled dimensions in the heated area of the sample; thus, restraint in the unclamped direction was very low.

The test sequence was as follows: 1. pre-test dimensions were recorded; 2. voltage level was established; 3. facility was purged with N_2 for 3 minutes; 4. oscillograph on; 5. lamps on 6. lamps off at a predetermined run duration; 7. oscillograph off 5-10 seconds after lamps and 8. post-test dimensions were recorded.

5.2.5 Test Results

The results of the fabric shrinkage tests are presented in Tables XI through XIII for PBI, Nomex and Fabric L, respectively. Typical temperature histories are presented in Figure 26. A discussion follows of the test results and the influence of the various parameters examined.

5.2.5.1 Temperature and Flux Level

The magnitudes of shrinkage in all fabrics was found to be strongly influenced by temperature and weakly affected by flux level within the range of flux studied. Figure 27 shows the relationship between shrinkage and measured temperature that resulted for PBI. It is significant that the major shrinkage occurred within a relatively narrow temperature band; 400°C to 450°C. The magnitude of shrinkage was large, with a plateau value of roughly 44 percent in the axis in which tension was not directly imposed and 36 percent in the axis under tension. Fabric at the plateau level was stiff, but had not lost structural integrity. A sample of PBI, approximately 3 cm in width by 10 cm long, was placed in the facility and fully constrained at both ends, then heated to in excess of 600°C. Although lateral shrinkage was severe, no structural failure of the material was noted. Above 600°C onset of brittleness was found.

The shrinkage mechanism was found to be more complicated in Nomex as exhibited in Figure 28. Shrinkage began to occur 100°C earlier than in PBI but the increase was less abrupt so the major shrinkage took place in the band; 300°C to 400°C. At 400°C an interesting phenomenon took place; the Nomex proceeded to re-expand. The fabric would have expanded even more than indicated if it had not been restrained by a rigid "frame" of lower temperature cloth surrounding the hottest region. Therefore. in the sample 2-4, for instance, rigid wrinkles had formed, the post-test sample was quite brittle and the reduction in shrinkage was

TABLE XI

PBI FABRIC SHRINKAGE TEST RESULTS

Test No.	Lamp Voltage (volts)	Incident Heat Flux ($cal/cm^2 sec$)	Run Duration (sec)	Orientation	Environment	Shrinkage (%) X Axis	Shrinkage (%) Y Axis	Maximum Temperature °C (°F)	Comments
1-1	151	2.1	7.5	A	N_2	0	3	357 (674)	
1-2			10.3			31	34	434 (814)	
1-3			13.2			-	-	524 (976)	Shrinkage scale not visible
1-4			13.4			35	40	544 (1012)	Rerun of 1 - 3
1-5			9.3			23	25	419 (787)	
1-6			8.3			6	10	403 (758)	
1-7	224	4.2	3.8			20	25	419 (787)	
1-8			4.9			36	42	531 (987)	
1-9	151	2.1	10.9		Air	34	41	494 (922)	
1-10			14.9		N_2	34	43	525 (979)	Temperature not valid - fabric warped bringing low temp. fabric into pyro. view.
1-11	224	4.2	6.4			36	44	640 (1184)	
1-12	151	2.1	10.5	B		34	35	452 (846)	
1-13			11.1	C		34	42	484 (903)	
1-14			11.1	B		38	37	482 (899)	Rerun of 1-12 for verification

Orientation:

A Side 1 toward lamps, tension in X direction.

B Side 1 toward lamps, tension in Y direction.

C Side 2 toward lamps, tension in X direction.

NOTE: Y is the warp direction
Side designation is arbitrary

TABLE XII

NOMEX FABRIC SHRINKAGE TEST RESULTS

Test No.	Lamp Voltage (volts)	Incident Heat Flux ($cal/cm^2 sec$)	Run Duration (sec)	Orientation	Environment	Shrinkage (%) X Axis	Shrinkage (%) Y Axis	Maximum Temperature °C (°F)
2-1	151	2.1	7.7	A	N_2	20	31	378 (713)
2-2			6.3			9	11	333 (631)
2-3			9.1			27	39	405 (761)
2-4			10.7			23	14	446 (835)
2-5			9.8			23	30	422 (792)
2-6	224	4.2	3.9			28	38	406 (763)
2-7			3.2			14	23	359 (678)
2-8	151	2.1	9.0		Air	25	40	410 (771)
2-9			4.6		N_2	1	3	279 (535)
2-10			9.1	B		29	30	407 (762)
2-11			9.0	C		25	38	397 (746)

Orientation:

A Side 1 toward lamps, tension in X direction.

B Side 1 toward lamps, tension in Y direction.

C Side 2 toward lamps, tension in X direction.

NOTE: Y is the warp direction
Side designation is arbitrary

TABLE XIII

STABILIZED PBI FABRIC SHRINKAGE TEST RESULTS

FABRIC	TEST NO.	LAMP VOLTAGE (VOLTS)	INCIDENT HEAT FLUX ($cal/cm^2 sec.$)	RUN DURATION (SEC.)	ORIENTATION	ENVIRONMENT	SHRINKAGE		MAXIMUM TEMPERATURE (°C)
							X AXIS	Y AXIS	
Fabric L	3-1	151	2.1	10.0	A	N_2	3	4	430
	3-2			14.3			17	15	543
	3-3			12.3			4	5	485
	3-4			16.2			17	15	610
	3-5			13.2			11	10	519
Fabric 121	4-1	160	2.2	8.0	A	N_2	3	4	510
	4-2			9.0			6	8	570
	4-3			10.0			10	12	690
	4-4			12.2			13	13	720
	4-5			16.0			13	14	740
	4-6	240	4.3	8.0			16	20	845

NOTE: X direction is the warp and tension direction

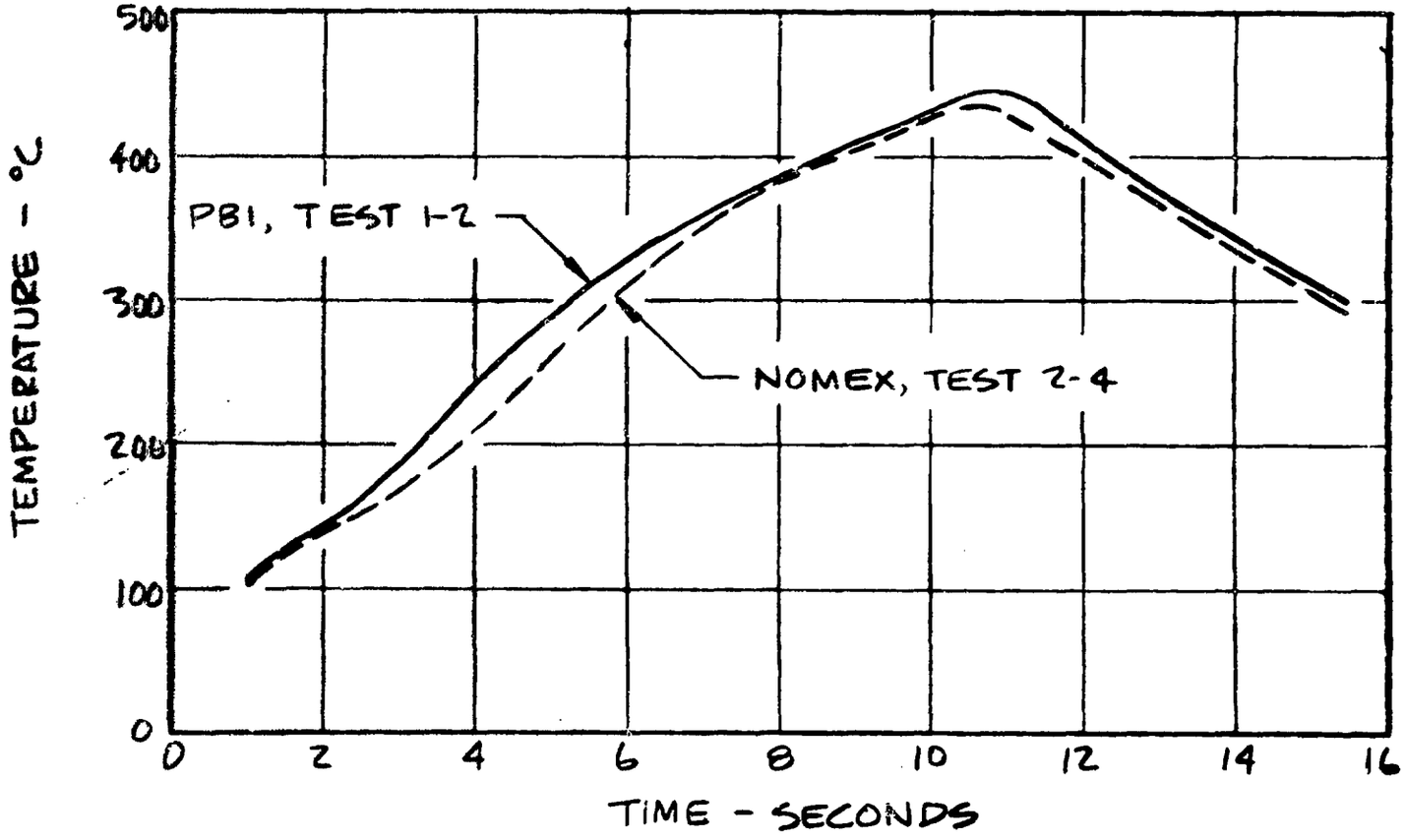

Figure 26. Fabric Temperature Histories in a Nitrogen Environment
Incident Flux = 2.1 cal/cm^{2}sec

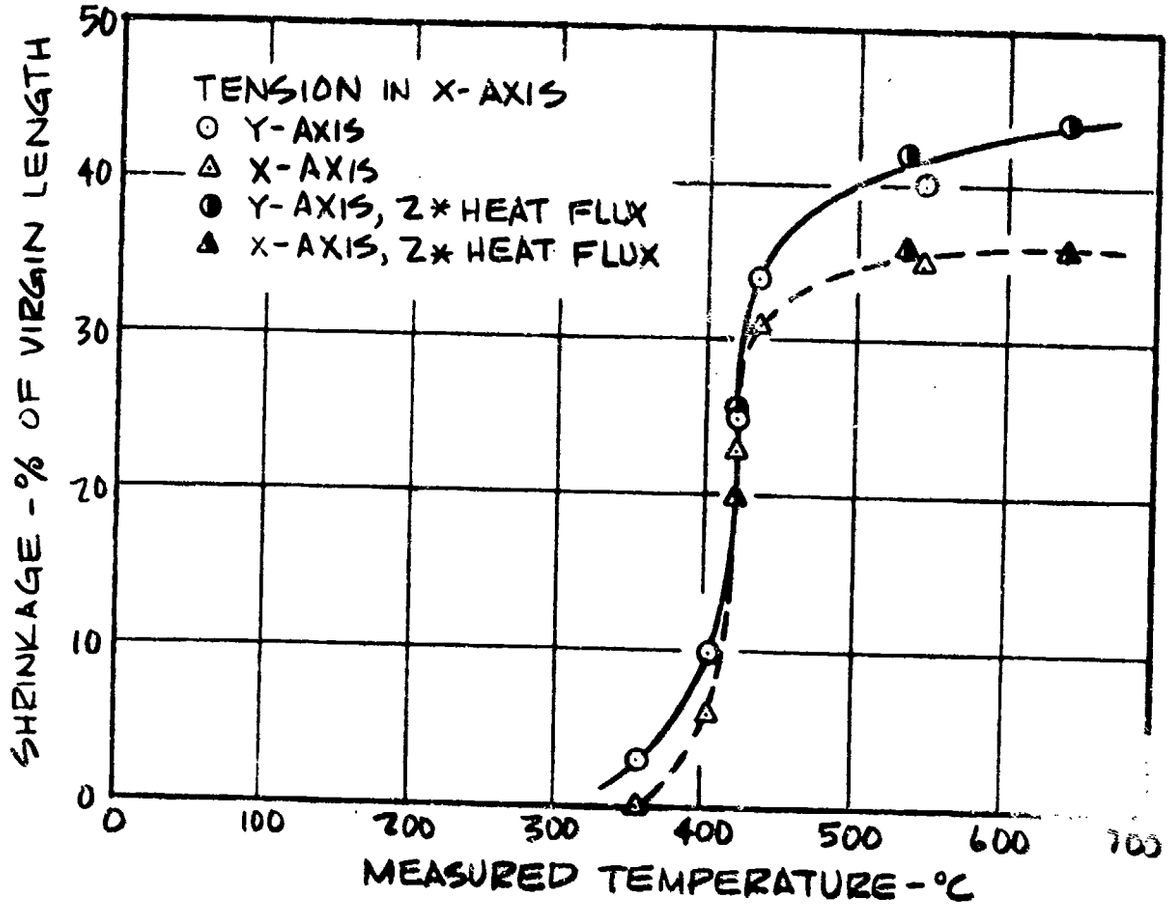

Figure 27. PBI Shrinkage Test Results in a Nitrogen Environment

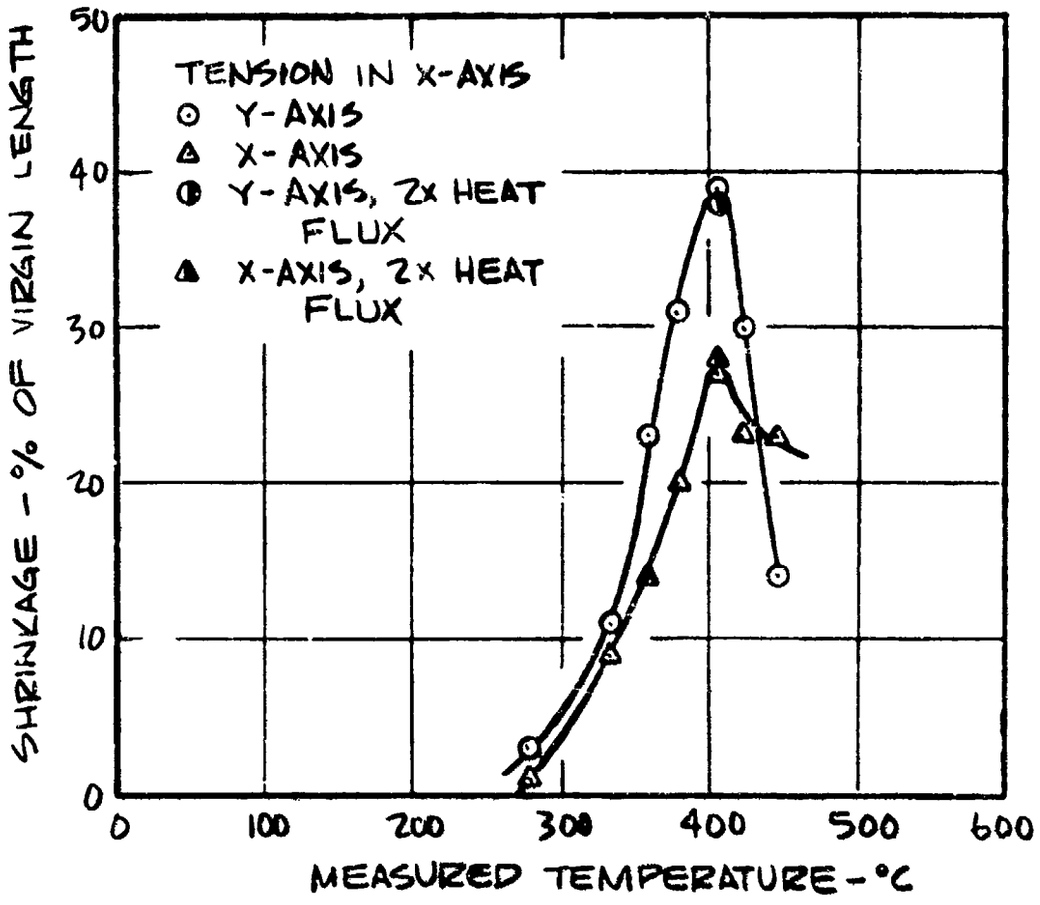

Figure 28. Nomex Shrinkage Test Results in a Nitrogen Environment

not as great as it would have been if unrestrained to expand. Under a 15 power microscope the yarns appeared swelled and distorted. In comparison, PBI did not exhibit yarn swelling under the microscope.

In the fully restrained test described for PBI above, the Nomex sample failed in the center of the sample by developing a hole which enlarged to 1.5 cm in length and extended across nearly the complete sample width. Upon cooling the material near the failure appeared to be melted and indicated flowing in the tension direction. This is significant because the cooled sample is quite strong and not brittle. Thus the failure occurred at relatively low temperatures, 400 to 500°C, near the peak in the shrinkage curve (Figure 28). This behavior was noted also when 10% linear shrinkage was allowed before the fully constrained condition was applied. At 550°C, Nomex has lost about 50% of its original mass and will literally fall apart if folded or pulled. Therefore, although Nomex exhibits a lower maximum shrinkage than PBI in the unrestrained shrinkage tests, the results of the restrained tests, together with the fact that on the order of 10 to 15 percent linear shrinkage of a uniform will result in full contact with the wearer, show that in actual use the Nomex can be expected to shrink to contact and then break apart allowing direct exposure of the underlying fabric or skin, and, as will be described later, the loose fabric may then ignite causing additional damage.

The test results on Fabric L appear in Figure 29. Comparison with Figure 27 for PBI shows that the shrinkage regime is elevated by 100°C and the maximum shrinkage is roughly 40 percent of the shrinkage in PBI.

Results for stabilized PBI (Fabric 121) are shown in Figure 30. For fabric 121 shrinkage begins to occur at approximately 450°C and the originally green colored material appears slightly brown-black. By 570°C the coloration is totally black with shrinkage of 5-7 percent, and the fabric begins to lose softness and flexibility but is not brittle. It does not crack on flexing but can be broken only under strong tension. At 700°C the material is still not brittle and can be easily rolled between the fingers without breaking; however, it will break moderately easily in tension; at 750°C the fabric has become brittle and will break if bent or pulled.

Finally, Figure 31 is a composite presentation of the shrinkage results for all fabrics tested. The dimensional stability superiority of the stabilized PBI fabrics, particularly 121, is readily apparent. As will be shown by the results discussed in Section 6, this is a dominant factor in determining the protection potentials for these fabrics. With maximum fabric temperatures calculated at the 600°C level for exposure to the nominal, 3 second JP-4 fire, only stabilized PBI is able to maintain an air gap throughout the exposure. In

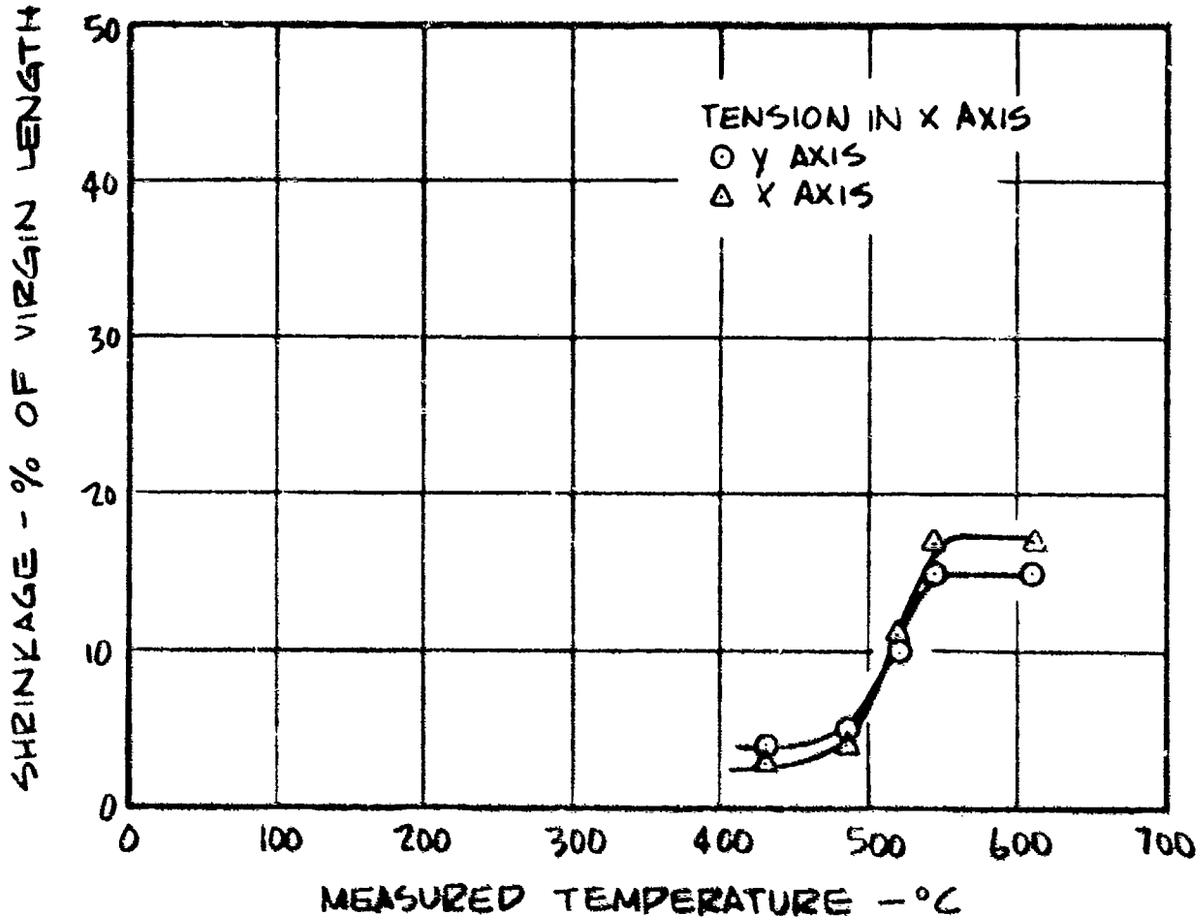

Figure 29. Stabilized PBI (Fabric L) Shrinkage Test Results in a Nitrogen Environment

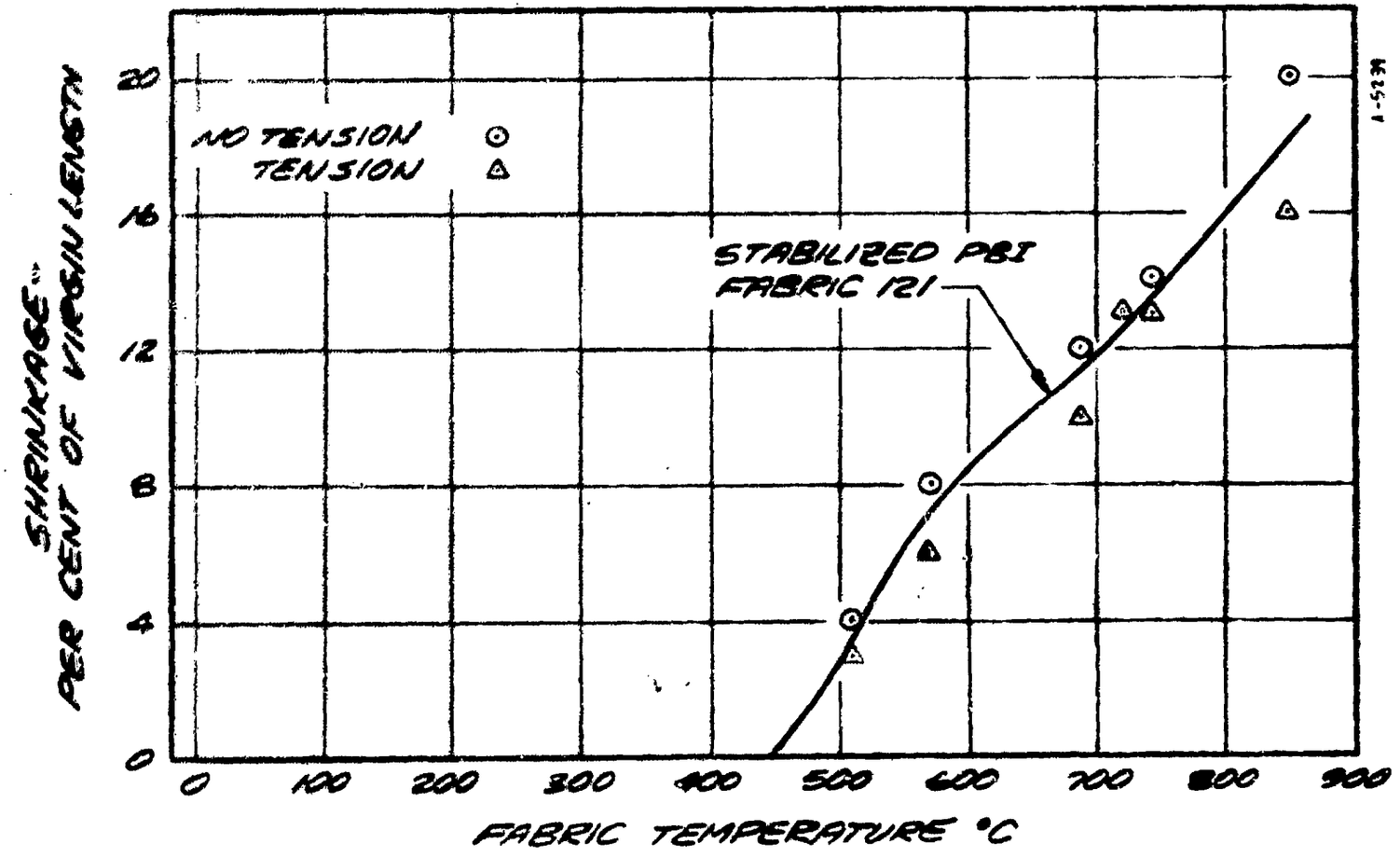

Figure 30. Stabilized PBI (Fabric 121) Shrinkage Test Results in a Nitrogen Environment

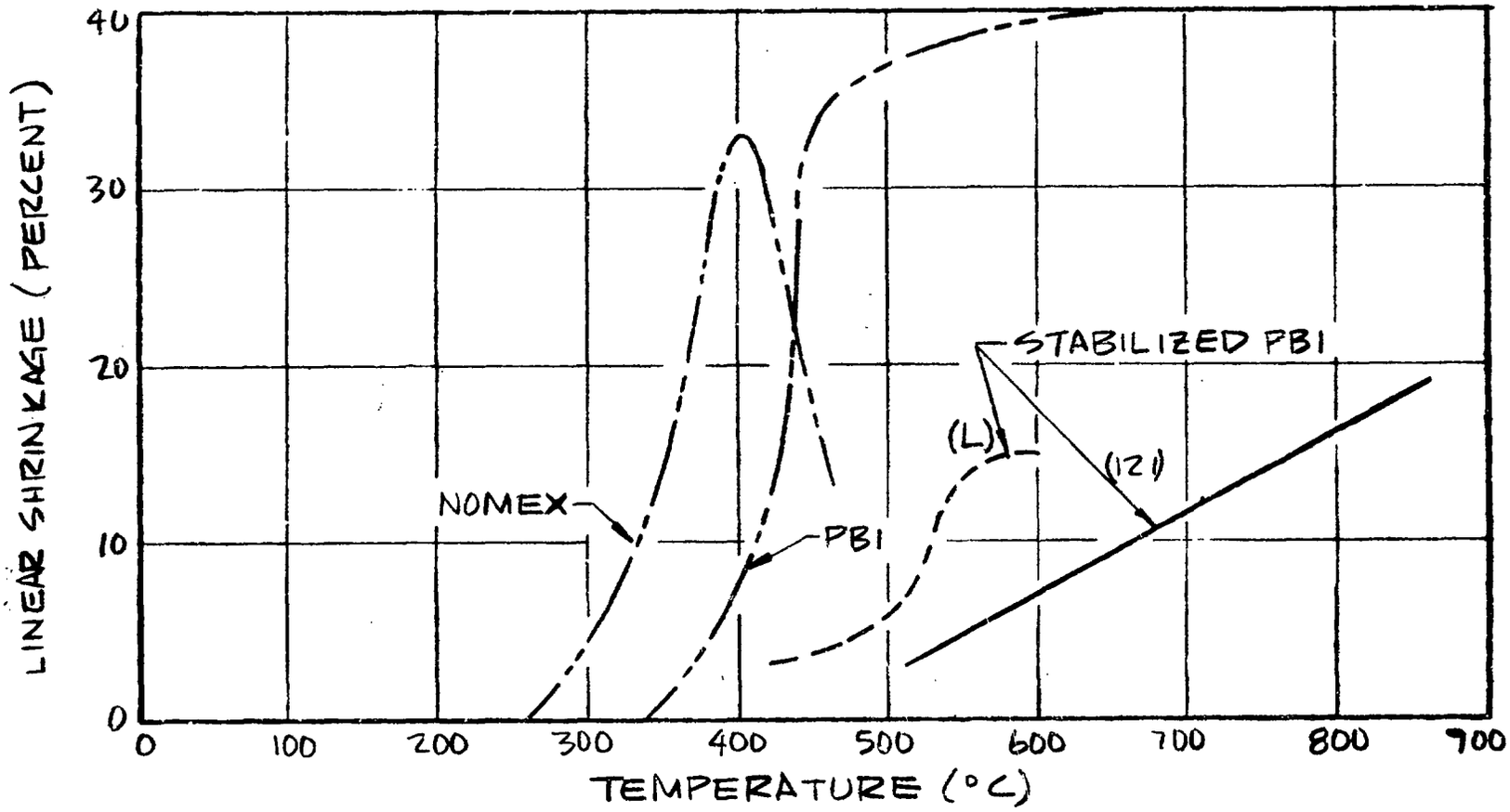

Figure 31. Shrinkage Test Results for Various Fabrics in a Nitrogen Environment

addition, the stabilized materials maintain structural integrity until at least 600°C and as high as 700°C for 12l.

Except for the fully restrained strip tests mentioned above, most judgments concerning structural integrity have been made qualitatively, essentially by feel and handling and should not be construed as quantitatively accurate particularly since these impressions are of the cold, post-test fabric. Since the structural integrity of the fabric can have a significant impact upon the thermal response of the fabric and skin, more quantitative testing under heating conditions should be added to the criteria for comparing materials.

It should be noted that the measured temperature in all runs was nominally that of the back surface and that the average temperature of each fabric was higher than the back surface. However the lack of influence of heating rate indicates that the pyrometer-measured temperature was not appreciably different from the mean. Otherwise, shrinkage at the higher flux would have appeared to occur at a lower temperature due to the larger temperature gradient through the fabric. The pyrometer tended to measure an in-depth temperature due to fabric porosity. Porosity would also tend to reduce the actual gradient. Even on careful examination, it was difficult to identify which surface on the post-test samples had been exposed to the radiation.

5.2.5.2 Mass Loss

In order to obtain a better understanding of the weight loss, simple weight change tests were run on PBI and Nomex in the radiant lamp facility. A square region 2.54 cm x 2.54 cm was marked off on a sample of each fabric. The samples were exposed in the facility for durations that would result in maximum shrinkage. The marked-off areas, now reduced in size, were then cut out and weighed on an analytical balance. The results of the tests are presented in Table XIV.

TABLE XIV

FABRIC WEIGHT LOSS RESULTS

Fabric	Maximum Temperature (°C)	Pre-test Weight (gms/cm^2)	Post-test Weight (gms/cm^2)	Weight Loss (%)
PBI	455	.0149	.0133	10.7
Nomex	404	.0136	.0113	16.9

In neither material was the weight loss nearly as large as the volume reduction observed. So the shrinkage in length is evidently observed primarily in closing up the weave spacing. Transmittance measurements performed at TRW show that the transmittance of charred PBI, for instance, is reduced to 1/3 the virgin transmittance.

5.2.5.3 Environmental Effects

PBI and Nomex were both tested in air for a relatively long duration in order to compare the shrinkage in air versus nitrogen. It was necessary to heat the PBI fabric to higher temperatures than was Nomex in order to demonstrate the environmental effect on shrinkage at a maximum shrinkage. For the maximum temperatures achieved, equivalent shrinkage values in nitrogen were taken from Figures 27 and 28. The comparative results appear in Table XV.

TABLE XV

COMPARISON OF SHRINKAGE IN AIR AND N_2 AT THE SAME TEMPERATURE

Fabric	Maximum Temperature (°C)	Incident Heat Flux (cal/cm sec)	Run Duration (sec)	Shrinkage - %			
				X Axis		Y Axis	
				N_2	Air	N_2	Air
PBI	494	2.1	10.9	34	34	40	41
Nomex	410	2.1	9.0	27	25	38	40

The onset of shrinkage for PBI occurs at approximately 100°C higher as compared to Nomex in both environments. The table indicates that the difference between shrinkage in air and N_2 at the indicated temperature is not detectable within the accuracy of the measurement. It is therefore probable that the shrinkage-temperature profile in air is similar to that in the inert environment.

5.2.5.4 Tensile Loading

Tensile loading of PBI and Nomex during heating, even at the low levels required to support the fabric samples in the tests, had an influence on the maximum shrinkage levels achieved. As discussed in Section 5.2.4, the samples were restrained in one axis by approximately 30 grams of tension distributed over the 10 cm side and virtually unrestrained in the other axis.

The unrestrained axis is of primary interest because of the similarity to a garment of normal fit. In most tests on each fabric, the X axis was loaded. In tests 1-12, 1-14, and 2-10, tension was applied in the Y axis. For the maximum temperatures achieved, equivalent shrinkage values were taken from the correlations in Figures 27 and 28 for PBI and Nomex respectively. A comparison of the directional effects is shown in Table XVI.

TABLE XVI

EFFECT OF TENSION DIRECTION

Fabric	Maximum Temperature (°C)	Shrinkage - %			
		X Axis Loaded		Y Axis Loaded	
		X	Y	X	Y
PBI	452	33	37	34	34
	482	34	39	38	37
Nomex	407	27	38	29	30

Again, the PBI fabrics had to be exposed to higher temperatures to attain maximum shrinkage. In the case of Nomex the warp yarns were more numerous and Y was identified as the warp axis. When the warp yarns were clamped, shrinkage in both directions was about the same. As might be expected the warp yarns, due to their greater tension in weaving (and greater number in the case of Nomex), dominate the dimensional stability of the fabric.

5.2.5.5 Effect of Inverting Fabric

In order to determine any effects of directionality normal to the fabric surface, tests 1-13 and 2-11 were run with the fabric sample inverted.

For the maximum temperatures, equivalent shrinkage values were chosen from Figures 27 and 28. Table XVII shows that for both fabrics there is no apparent dependence on which side was exposed.

TABLE XVII

INFLUENCE OF ENERGY DIRECTION

Fabric	Maximum Temperature (°C)	Shrinkage - %			
		Side 1 Exposed		Side 2 Exposed	
		X	Y	X	Y
PBI	484	34	39	34	42
Nomex	397	27	38	25	38

5.3 THERMAL AND PHYSICAL PROPERTIES

Thermal and physical properties which affect the thermal response of the fabric and skin include:

- o Heat capacity
- o Thermal conductivity
- o Thickness
- o Water content

The data presented in Reference 57 show that, in general, the specific heat of a given fabric is essentially the same as the virgin material from which the fabric is constructed. The variation in material specific heat with temperature and material is presented in Table XVIII for several typical fabric materials. Specific heat data for candidate fabrics other than PBI have not been found, but as indicated by the tables, variations among materials appear

TABLE XVIII

FABRIC SPECIFIC HEAT

Material	Specific Heat (Btu/lb°F)	
	500°R	1000°R
PBI	0.30	0.45
Cotton	0.32	0.48
Rayon	0.32	0.49
Nylon	0.36	0.54
Nomex	0.29	

to be small. As noted in the discussion of the preliminary analysis parametric results in Section 6, the affect of thermal capacitance of protection capability is complicated, nevertheless, a higher value seems desirable in that it tends to result in lower fabric temperatures and a spreading out in time of the transfer of energy to the skin even though total heating after the cooldown period is not significantly affected. Because synergistic effects may occur for the pyrolyzing material, thermal capacitance will be treated as a parameter in the final parametric analysis.

The density of the various fabrics varies as the fraction of air voids in a given material. The amount of air void varies from a low of 60 percent to a high of 80 percent as demonstrated by the data presented in References 57, 58, and 59. Summarized in Table XIX are reported fiber volume fractions for various materials. All the materials of interest show the same variation and range of possible fiber volume fractions.

A study of the data presented in References 57, 58, 59, and 60 indicates that material thickness varies from a low of .008 inches to a high of .020 inches. Data presented in these references indicate also that water content for most fabrics will vary from 3 to 15 percent by weight. Data for weight, thickness, and equilibrium water content (moisture regain at 72°F (22°C) and 65 percent RH) are given in Table XX for various candidate fabrics.

The results of Reference 57 indicate that the thermal conductivity of fabrics can be correlated with the following equation:

$$K = x(V_f K_f + V_a K_a) + y \frac{K_f K_a}{V_a K_f + V_f K_a} \tag{36}$$

where

V_f, V_a Volume fractions of fiber and air

K_f, K_a Thermal conductivity of fiber and air

In this equation

$$x + y = 1 \tag{37}$$

and

$$V_a + V_f = 1, \tag{38}$$

TABLE XIX

MATERIAL THERMAL CONDUCTIVITY CORRELATED WITH VOLUME FRACTION

Material	Density gm/cc	Thermal Conductivity cal/cm sec°C x 10^5		X	Y	V_f	Thermal Conductivity Fabric* cal/cm sec°C x 10^5
		21°C	260°C				
Cotton	1.51	5.38	6.2	0.2	0.8	.21 to .30	.84
PBI	1.31	4.97	5.8	0.3	0.7	.20 to .37	.91
Nomex	1.38	4.55	5.38	0.3	0.7	.20 to .38	.81
Air	.00119	0.58	1.07	-	-	--	.58

*For V_f = .3 and T = 21°C

TABLE XX

PHYSICAL PROPERTY DATA OF CANDIDATE FABRICS

Material	Weight		Thickness		Moisture Regain
	oz/yds^2	gm/cm^2	inches	cm	% dry basis
Nomex	4.1	.0139	.0127	.0323	5.0
PBI	4.3	.0146	.0143	.0364	12.0
L	5.2	.0176	.0127	.0323	12.0
121	4.4	.0149	.0132	.0335	13.2

thus allowing the equation to represent the proper limit. Summarized in Table XIX are the x and y factors for this equation. These constants were obtained from the thermal conductivity data presented in References 57 and 58.

It is noted that the resultant fabric conductivities are nearly the same, but more importantly are not much greater than that of air alone. Thus conduction of energy through the fabric layer is controlled primarily by the gas and not the fiber. Thus significance of this fact is that in clothing assemblies with gaps between layers which are at least as thick as the fabric layers, the fiber conductivity will have minimal effect upon the total heat transfer. These effects are shown in the preliminary parametric results discussed in Section 6.

5.4 THERMOCHEMICAL PROPERTIES

5.4.1 Thermogravimetric Analysis Data (TGA)

As the fabrics are heated to elevated temperatures their thermal response becomes dependent upon the pyrolysis phenomena which occur. Thus it is essential to know how mass is lost as a function of temperature and time. This information can be obtained by performing a thermogravimetric analysis on the material. This test is simply a continuous measure of the mass of an isothermal sample which is being heated such that the rate of change of temperature is a constant. The resulting mass versus time plot is differentiated to determine a mass loss rate as a function of time. In practice, this results in the identification of several major reactions which can be used to describe the behavior of the material. These reactions conform to the Arrhenius relation

$$-\frac{d\rho}{d\theta} = Ae^{-\frac{E}{RT}}\left(\frac{\rho - \rho_f}{\rho_o - \rho_f}\right)^n \qquad (39)$$

where A is the rate constant, E is the activation energy, R is the gas constant, T is the absolute temperature and ρ is the instantaneous density (mass) with o and f indicating initial and final (complete reaction) values. By conducting TGA tests at several different rates, it is possible to evaluate the values of A, E, and n quantities which then are independent of rate (see Reference 61).

The ASTER code is designed to accept up to three separate reactions per material. For any fabric then, the TGA tests are run, major reactions identified and lumped into three resultant reactions if more than three are found.

TGA data for each of the candidate fabrics was obtained by Dr. Ivan Goldfarb of the Air Force Materials Laboratory at Wright-Patterson AFB, Ohio. These data, in reduced form are included as Appendix II.

5.4.2 Pyrolysis Gas Composition

Combustion calculations at the heated surface require that the elemental compositions of charred material and pyrolysis gas be known. Virgin compositions for PBI and Nomex materials were taken from References 62 and 63 respectively. To compute pyrolysis gas compositions, char yields were taken to be 0.709 and 0.387 respectively, from the TGA data of Goldfarb. The fully charred material is assumed to contain only carbon; pyrolysis gas elemental composition can be determined by difference. The resulting composition data are summarized in Table XXI.

TABLE XXI

COMPOSITION BY MASS FRACTION

	Nomex			PBI		
	Virgin	Char	Gas	Virgin	Char	Gas
H	0.042	0.0	0.069	0.039	0.0	0.134
C	0.707	1.0	0.522	0.780	1.0	0.242
N	0.118	0.0	0.191	0.181	0.0	0.624
O	0.134	0.0	0.218	0.0	0.0	0.0

Some qualitative composition data have been obtained by Dr. Goldfarb for Nomex and PBI using a mass spectrometer/TGA apparatus. A description of his findings may be found in Reference 70. These results indicate that different species are coming off at various temperature levels and that there are small amounts of unidentified species which have been related to the dyes.

The ASTER code has a limitation in that in its present form, only one pyrolysis gas composition can be specified, i.e., it is independent of the temperature. Thus it is currently not possible to account for the variations in composition observed in the mass spectrometer experiments.

5.4.3 Pyrolysis Gas Specific Heat and Enthalpy

It is necessary to specify absolute enthalpy levels of virgin material, charred material, and pyrolysis gas in order to characterize the amount of energy associated with pyrolysis events and with pyrolysis gas combustion. Since the char residue is known to be mostly carbon, its reference enthalpy or heat of formation may be assumed zero. The heats of formation of virgin material and pyrolysis gas are much more elusive.

In the case of h_p, the heats of formation* were initially assumed to be -2050 cal/gm for PBI (Reference 62) and -556 cal/gm for Nomex (Reference 64). The absolute pyrolysis gas enthalpy was computed from the assumed elemental make up and the assumption of full chemical equilibrium with condensed phases excluded. The necessary calculations were made with the Aerotherm ACE code.

Subsequently it was discovered that these heats of formation did not yield accurate predictions of sample temperatures during pyrolysis in code comparisons to fabric temperature histories measured during the shrinkage tests described in Section 5.1.

It was desired, therefore, to "tune" the energy involved in pyrolysis to cause a better match of data and predictions. The amount of net sensible energy release during pyrolysis may be denoted q_p. During the pyrolysis of a unit volume of virgin material we have

$$\rho_p \text{ units of virgin material} \rightarrow \rho_c \text{ units of char residue} + (\rho_p - \rho_c) \text{ units of pyrolysis gas} \tag{40}$$

The associated energy statement is

$$\rho_p h_p \rightarrow \rho_c h_c + (\rho_p - \rho_c) h_g + q_p \tag{41}$$

If it is desired to change q_p, we can change any or all of h_p, h_c, and h_g. However, since the char residue is generally almost entirely carbon, with a zero heat of formation, h_c may be regarded as known. The quantities h_p and h_g are not at all well known. In the case of h_p, the specific heat is usually known to acceptable accuracy, but the datum enthalpy or heat of formation is quite uncertain, due primarily to the practical difficulties of making the necessary heat of combustion measurements with sufficient accuracy. The pyrolysis gas enthalpy is doubly uncertain. Heat of formation data are not available, and no quantitative experimental specification of the gas molecular composition is available to allow a calculation of the heat of formation. Furthermore, gas specific heat data are generally lacking. The method of determining the heat of formation described above can provide data to use in lieu of experimental data, but the assumption of equilibrium species is a dubious one at typical pyrolysis temperatures.

Consequently, an investigator would have little objection to varying either virgin material or pyrolysis gas enthalpy in order to match temperature traces during pyrolysis. In non-combustion experiments, it would make no real difference

*At 536°R.

which was varied, as only the net pyrolysis energy is of significance. As will be discussed below, the virgin material heat of formation was selected for variation in this work. The choice has certain implications for later calculations involving combustion of the pyrolysis gases as they appear at the heated surface. since alterations of pyrolysis gas enthalpy would damage the net combustion energy evolved at the surface. Usually this effect would be minor, however, since combustion energy release amounts are much larger than the enthalpy variations needed to match specimen temperatures in pyrolysis experiments.

The shrinkage tests provide an excellent source of data for comparison to code results. The heat flux is all radiation with a minimal amount of convective cooling, and the output of the radiometer is a temperature-time history for the fabric. Given the pyrolysis gas enthalpies determined above plus the other thermal and optical properties of the material, iterative code predictions were made varying the heat of formation (pyrolysis) of the fabric until a "best" fit with the test data was achieved. It was found that the response of the prediction was quite sensitive to the value of Δh_f selected, and it is believed that the values determined by this method are within several hundred cal/gm of the proper value (relative to the enthalpies of the pyrolysis gases).

Figures 32 through 34 show the results of these tests and predictions for each of the candidate fabrics. The values of Δh_f are given in Table XXI.

TABLE XXII

HEAT OF FORMATION RESULTS FOR CANDIDATE FABRICS

Fabric	Heat of Formation (cal/gm)
Nomex	-473
PBI	0
121	-167

The significant outcome from these comparisons is that very good agreement with test data has been achieved by the code. Comparisons are good at low temperature where thermochemical events are not important, indicating that quantities such as specific heat and absorptance are sufficiently well known. In the case of the fabrics with higher water content there is more difficulty at the low temperatures probably due to the high heating rates. At these high rates, the assumption that the water is all removed at 100°C is no doubt inadequate. If water is retained at temperatures above 100°C, it can be expected

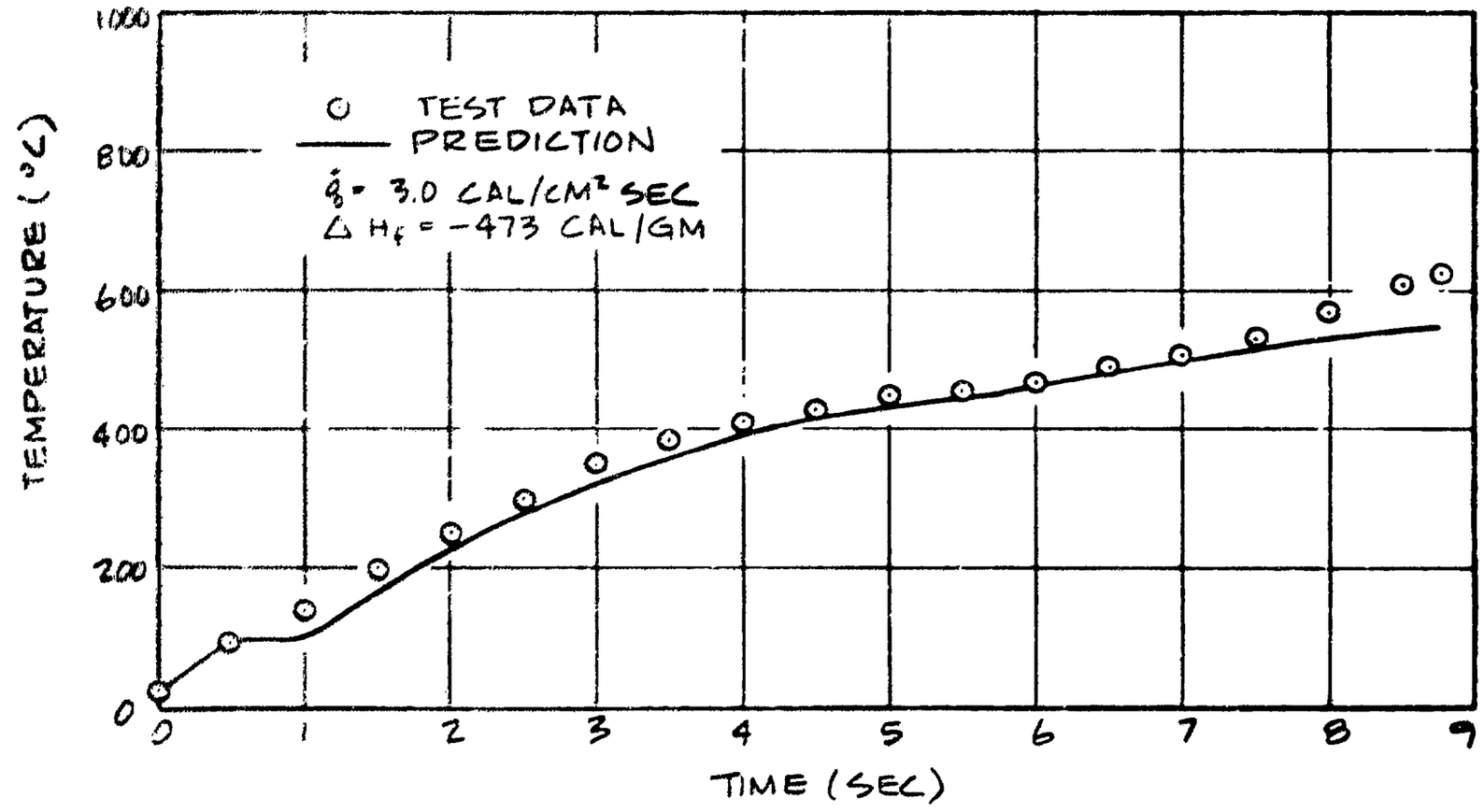

Figure 32. Comparison of Fabric Model Prediction of Shrinkage Test Data - Nomex

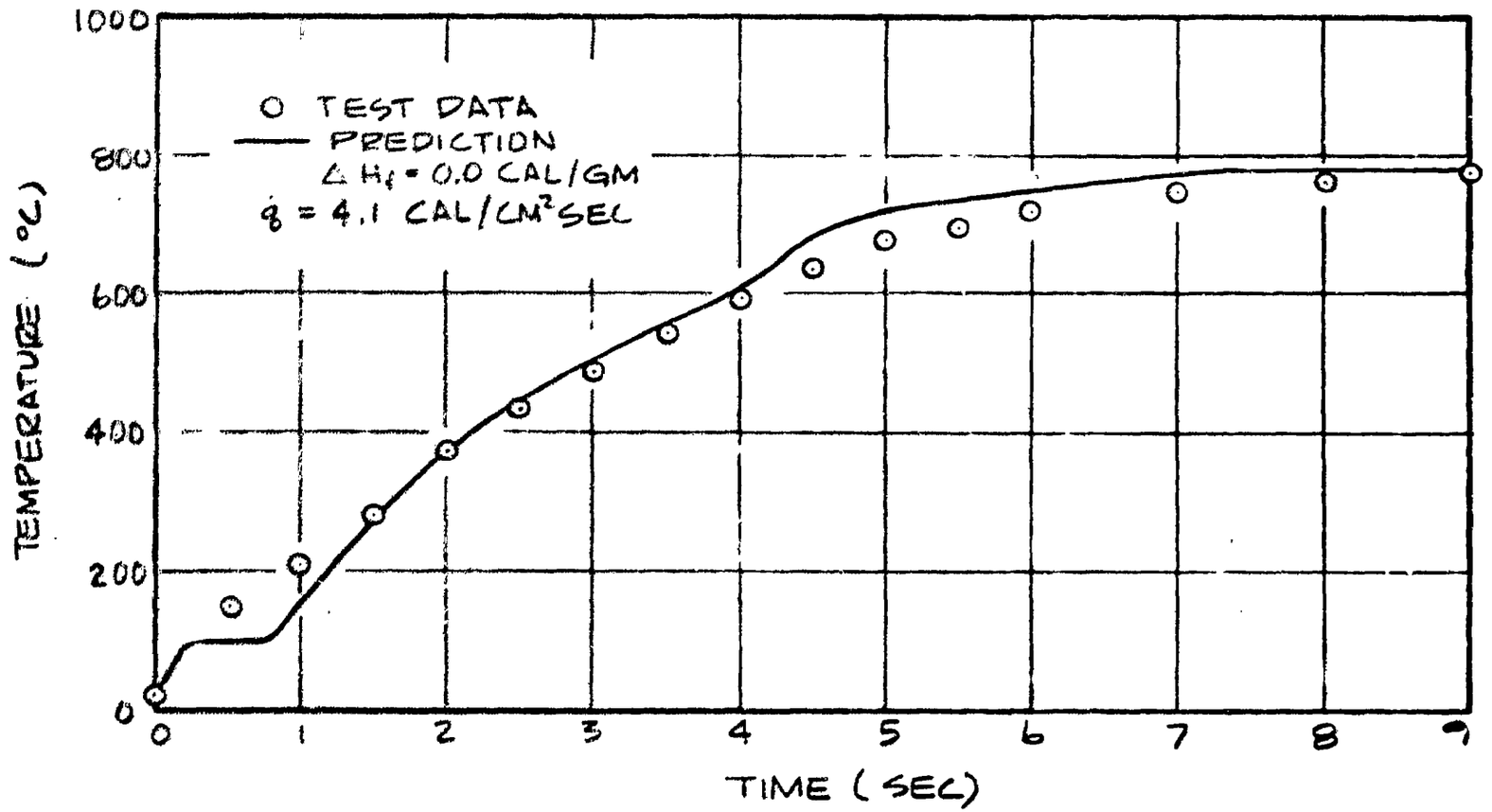

Figure 33. Comparison of Fabric Model Prediction to Shrinkage Test Data - PBI

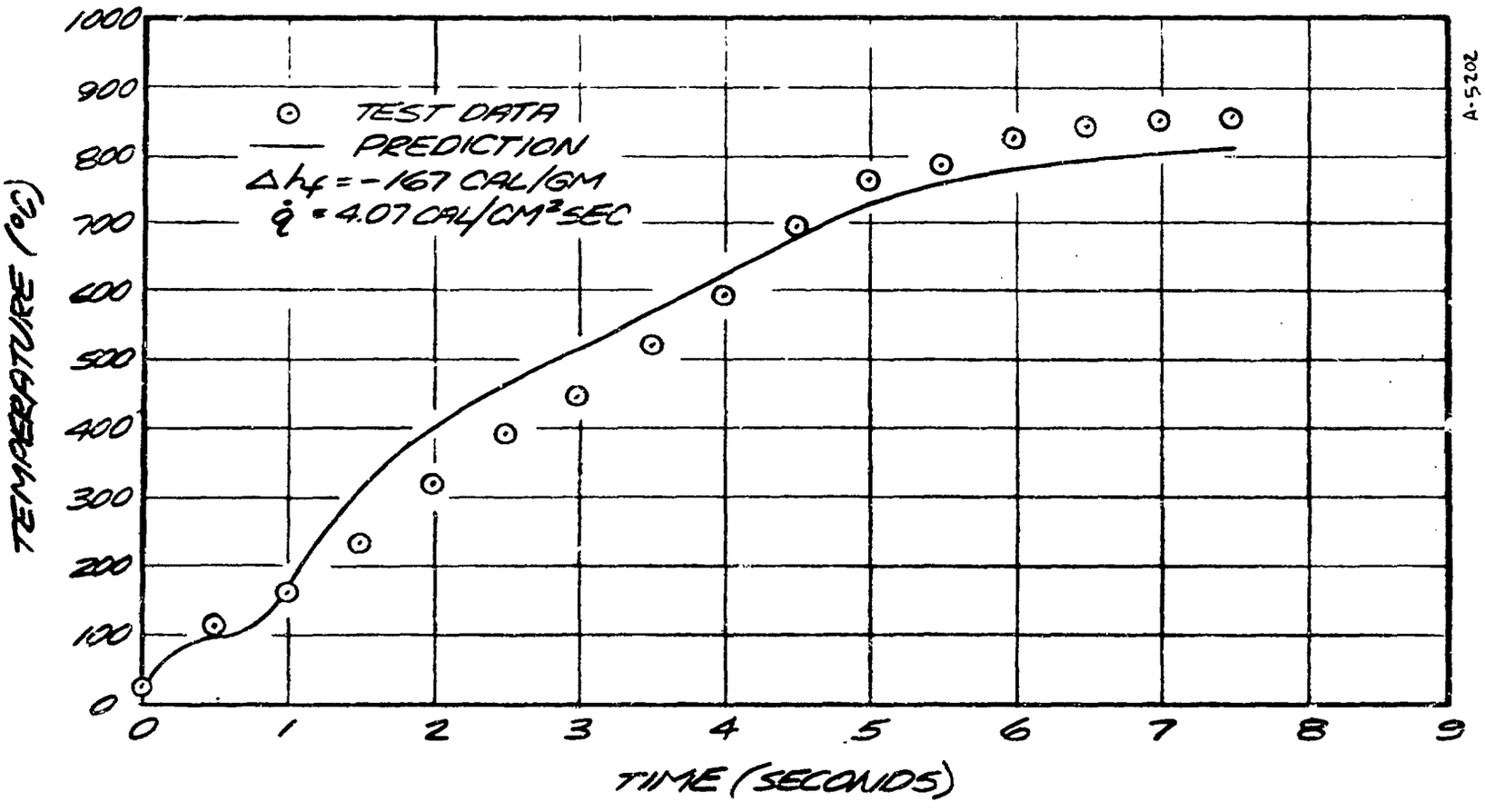

Figure 34. Comparison of Fabric Model Prediction to Shrinkage Test Data - Stabilized PBI (Fabric 121)

to slow the rate of temperature rise due to its high specific heat relative to the basic polymer.

At the higher temperatures and with the selected Δh_f values good agreement was found between the predicted and measured mass loss of the sample. Although this latter measurement was somewhat crude, the measured and computed values were within 10 to 20 percent. This provides confidence in the TGA data and the modeling of pyrolysis events in the code. Also the treatment of shrinkage and optical property variations are accounted for in the prediction and appear to be adequately modeled. For example, as Nomex and PBI shrink, there is roughly a factor of 2 increase in the mass per unit area. The excellent agreement found for these fabrics through the temperature range for shrinkage is very encouraging.

Different heat flux levels were used for the Nomex and PBI fabrics because of the differences in fabric absorptance and because the pyrolysis events occur at higher temperatures for the PBI fabrics thus requiring higher heating levels to achieve the temperature range of interest.

5.5 FLUID MECHANIC CONSIDERATIONS

5.5.1 Fabric Gas Blow Through

As the clothed subject traverses the fuel fire, the potential for gases being blown through the fabric to the skin surface exists. This investigation evaluates the relative contribution of this heat transfer mechanism compared to the others that exist during the flame exposure. The gas which enters the fabric outer surface will exchange energy with the fabric and then exit the back surface exposing the subsequent layer to the hot gases. This investigation will evaluate the extremes in the following parameters:

- Maximum dynamic pressure for gas blow through
- Maximum expected gas blow through flow rate and energy transfer
- Maximum energy transfer between gases and fabric
- Maximum energy transfer to the fabric surface
- Maximum energy flux to the skin surface for a single layer of fabric.

The effort described will not consider blowing of the hot gases parallel to the fabric skin surface such as would occur if the gases enter a cuff. This energy transfer method is more dependent upon clothing configuration rather than fabric design. With proper clothing design, flow through the wrist, ankle or neck should be kept to a minimum.

5.5.1.1 Analysis

The basic mechanism to be studied is the flow of gas through the porous fabrics caused by the dynamic pressure of the fabric moving relative to the flame environment.

Dynamic Pressure Range

The velocity of the fabric relative to the ground during flame exposure is approximately 10 ft/sec (3 m/sec). (In mannikin tests at Natick, this velocity is used for clothing tests.) As noted in Section 3, the estimated upward fire velocity is also approximately 10 ft/sec. Therefore, it is estimated that the maximum relative velocity between the fabric and the bulk flame is approximately 15 ft/sec (4.5 m/sec). This velocity is a maximum on the front surfaces of the mannikin; however, it does not include the additional velocity that occurs as the subject moves arms or legs during egress from the fire. The mean velocity of the limbs will also be in the range of 15 ft/sec.

In order to calculate the dynamic driving pressure, the density of the gases in addition to the velocity must be evaluated. The flame gas can be treated as a perfect gas and the density can be calculated using the equation of state for a perfect gas. The pressure during flame exposure is a maximum under sea level condition of 14.7 lb/in^2 (1 atm). The expected range in flame temperature is between 1600°F and 2200°F (870°C to 1200°C). (The lowest temperature will give the maximum density and therefore highest dynamic pressure.) The molecular weight of the flame gas is approximately 30 based upon the results summarized in Section 3. Using these quantities the maximum expected density of the flame gas is 0.018 lb/ft^3 (2.9×10^{-4} gm/cc).

The dynamic pressure experienced during the flame exposure can be calculated from the following equation:

$$p = \frac{1}{2} \frac{\rho V^2}{g_c} \qquad (42)$$

where

g_c = Gravitational constant

U = Relative velocity

Using the quantities suggested above, the maximum available dynamic pressure is 0.012 in H_2O (2.96×10^{-5} atm). This is the maximum pressure difference which can be expected to exist across the fabric and represents the potential for flow through the fabric. In general, the actual pressure difference will be somewhat

less than this since additional pressure drops will exist when the gas flows through the rest of the clothing assembly.

Porous Media Flow

The flow through the fabric can be idealized as flow through a porous media which is expressed by the following equations obtained from Reference 65.

$$\frac{\Delta p}{L} = \frac{\alpha \mu V}{g_c} + \frac{\beta \rho V^2}{g_c} \tag{43}$$

where

L = Length

Δp = Pressure difference

μ = Viscosity

V = Flow velocity in fabric

ρ = Density

α = Constant for given media

β = constant for given media

If the constants of this equation (α,β) are known for a given material, the velocity or flow rate of the hot gases can be determined for the known maximum pressure difference (Δp). Data available in Reference 66 gives velocity through various fabric types for a given pressure difference of 0.5 in H_2O (1.2×10^{-4} atm). In order to evaluate the two constants of Equation 43, data at two different test conditions should be known. However, an investigation of literature on porous material flow indicates that in general there is a unique relationship between the value of α and β. The values for α and β from References 59, 67, and 68 for various porous materials have been plotted in Figure 35. These data show that the following approximate ratio between α and β exists.

$$\frac{\beta}{\alpha} = 1.2 \times 10^{-4} \text{ft } (3.66 \times 10^{-3} \text{cm}) \tag{44}$$

The data of Reference 66 along with these results allow the evaluation of α and β in Equation 44 for various fabrics. The maximum air permeability presented in Reference 66 is 121 $ft^3/ft^2 min$* (3690 cm^3/cm min). This value will be used

*Measurements made by AFML on Nomex, PBI, Fabric L and stabilized PBI indicate permeability values of 99, 124, 22, and 134 $ft^3/ft^2 min$, respectively.

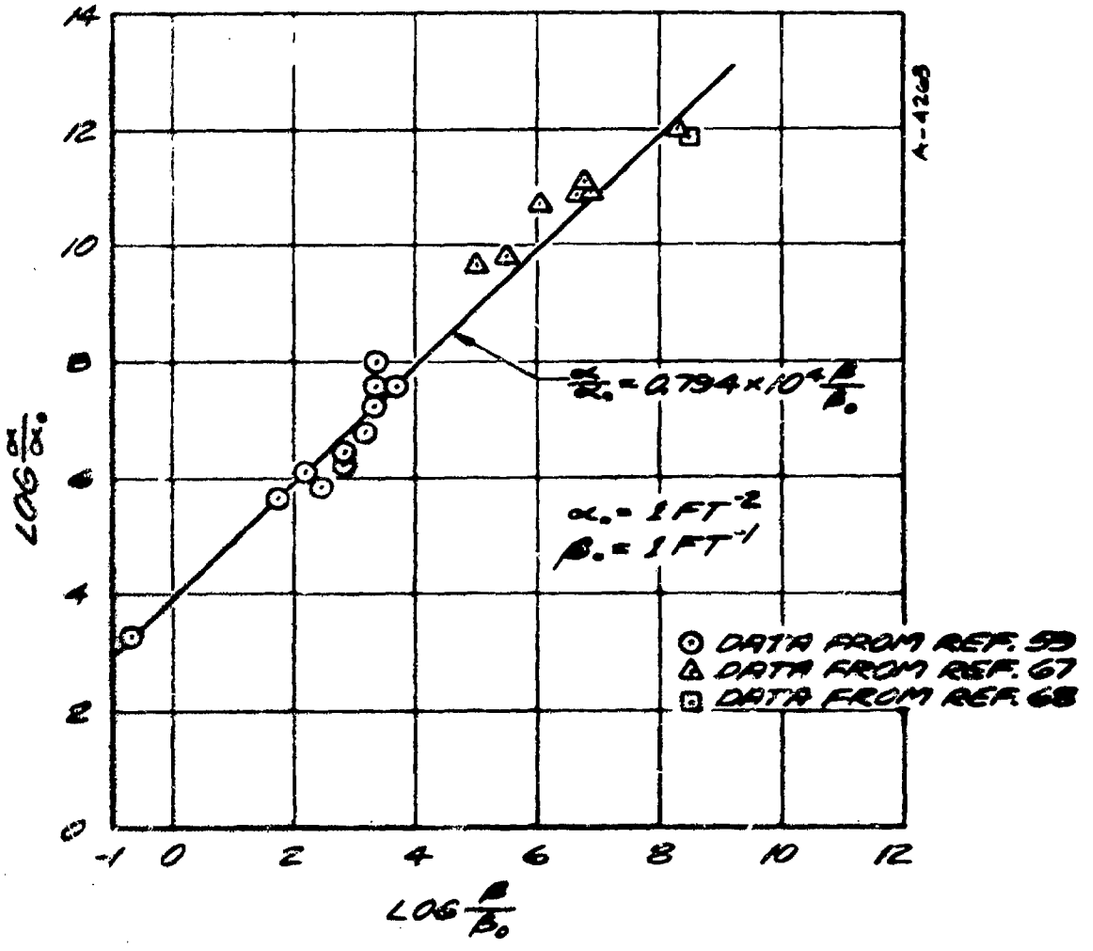

Figure 35. Experimentally Determined Coefficients in Equation for Flow Through Porous Media $\Delta p/L = a\mu V/g_c + \beta\rho V^2/g_c$

for subsequent evaluation of energy transfer. The use of this permeability value in Equation 44 results in the following values of α and β

$\alpha = 1.2 \times 10^{+9}$ 1/ft^2 (1.29×10^{6} 1/cm^2)

$\beta = 1.4 \times 10^{+6}$ 1/ft (4.6×10^{3} 1/cm)

The maximum dynamic pressure of 0.012 in H_2O results in a flow velocity of 0.04 ft/sec (1.2 cm/sec) for the flame exposure conditions.

Blown Gas Energy Rate

The maximum energy rate due to flow of the gas through the fabric can be expressed as

$$q = \rho V C_p \Delta T \tag{45}$$

where

c_p = Gas specific heat

q = Heat flux

ΔT = Temperature difference

The temperature difference to be used in this equation is the difference between the ambient flame gases and the fabric or skin surface. For an average fire this difference would be approximately 1700°F (925 °C). The blow-through energy flux for this condition is approximately 0.35 Btu/ft^{2}sec (0.095 cal/cm^{2}sec). If this flux were absorbed at the surface of the fabric it would be only 3 percent of the incident flame heat flux, thus making it a small contributor to the total heating of the fabric. It is, however, possible that not all the energy in the gas will be removed during the passage of the gas through the fabric, and therefore, a large heat flux will be incident on the skin or subsequent fabric layer. If the fabric is assumed to be constant in temperature during the passage of the hot gases through the fabric (Fabric temperature change is small relative to gas temperature change), the following equation can be used to evaluate the gas temperature as it traverses the fabric thickness.

$$\frac{(T_{g_x} - T_F)}{(T_{g_{in}} - T_F)} = e^{-\frac{h4}{\rho C_p V}\left(\frac{x}{D}\right)} \tag{46}$$

where

D = Fabric effective flow passage diameter

h = Hot gas heat transfer coefficient to fabric surface

x = Distance through fabric

T_P = Fabric temperature

$T_{g_{in}}$ = Initial temperature of gas on entering fabric

T_{g_x} = Gas temperature at position x in the fabric

The distance which the gas travels through the fabric before it is in equilibrium with the fabric can be evaluated from Equation 46. If for an 1800°F (980°C) temperature difference the gas is assumed to be in equilibrium, then by solving Equation 46 for x, the following equation can be used to calculate the passage distance.

$$x = \frac{3\rho C_p VD}{4h} \tag{47}$$

where the terms in this equation are the same as those of Equation 46. The quantities in this equation which have not been evaluated are D and h. The values calculated for α and β can be used as an estimate of the characteristic dimension of the fabric pores (D). If these values are used, the dimension D is in the order of 0.0003 inches (.00075 cm). The value of h for flow of gases at low velocities should be on the order of 1 Btu/hr ft²°F (.488 cal/cm²hr°C). If these values are used in Equation 47, the gases will be in equilibrium with the fabric after traversing the fabric on the order of only 0.001 inches (.0025 cm). This dimension is much smaller than the normal thickness of the fabric. This result indicates that the gas upon leaving the fabric is at fabric temperature and that at short times, the gas has very little energy content for transfer of energy to the skin. With most of the energy absorbed from this effect at the surface of the fabric, the energy rate contribution to fabric heating is quite small relative to the flame radiant heat flux. (As indicated above, about 3 percent).

Heating of the Skin

An estimate of the temperature rise of the skin surface when exposed to an increment in the value of constant heat flux can be expressed by Equation 12 written in differential form

$$\Delta T = \frac{2\Delta q\sqrt{\theta}}{\sqrt{\pi k\rho c}} \tag{48}$$

The energy rate to the skin surface would be a maximum of 0.35 Btu/ft^{2}sec for the 3 second flame exposure. This would result in an 8°F (4.5°C) rise in skin temperature. This rise in temperature is a maximum, and in general, will be much less for the following reasons.

- Energy absorbed by fabric
- Additional layers of fabric

5.5.1.2 Conclusion

The results of this investigation indicate that the effects of gas blow through on fabric or skin heating is small. In general, the heating to the fabric surface is less than 3 percent of the flame incident radiant energy. This variation is much smaller than that expected from variations in flame environment. At short time, most of the energy from blow through is absorbed in the fabric allowing a small fraction of the energy to be transferred to the skin. For a single layer of fabric the temperature rise during a 3 second exposure would be less than 8°F. This value is small relative to that predicted in the preliminary parametric analysis (see Section 6) for a single layer of fabric exposed to a nominal flame environment. The rise in temperature during this condition was predicted to be approximately 110°F compared to the maximum of 8°F for gas blow through. For any multiple layer case, the increase will be very small since the resistance to flow is increased and the inner layers tend to remain cooler so that any fire gas which does penetrate to the skin will be at a greatly reduced thermal potential. For these reasons blow through will not be considered in the final model.

5.5.2 Fabric Pyrolysis Products

The previous subsection was concerned with the transfer of energy to the skin resulting from the flow of external gases (fire combustion gases) through the material due to dynamic forces. The following subsection will attempt to deal with the effect of the gases generated within the fabric, i.e., pyrolysis products. As in the case of flow of the external gases, the flight suit-man system represents an extremely complex flow system with time and space variant flow passage dimensions and distributed regions of entry and exit as well as potential orifices at penetrations for limbs and neck. Consequently, the first approach to the general problem will be to establish the limits and to ascertain the probable modes of mass and energy transfer.

In a 1951 study at the Fuels Research Lab at MIT, Hottel, et al., Reference 69 investigated the possibility of moisture condensation on the skin surface due to heating of various clothing materials. They developed an analytical model of

moisture (vapor) generation within the material and transport both to the skin surface and to the external environment. The model considered transport by diffusion only; generation and transport being determined by the vapor partial pressure states of the material, internal gas, external gas, and skin surface. Bulk flow of vapor was not considered. The net result of this study, which included experimental evaluation with a skin simulant measuring the response due to heating of both "wet" (normal wear conditions) and "dry" fabrics, indicated that moisture transport to and condensation on the skin surface is possible and may represent a significant form of heat transfer to the skin.

Following the approach of MIT study, a simple, one-node fabric model has been developed to evaluate the relative importance of the diffusive and bulk transport mechanisms. In this model, vapor was assumed to be generated within the fabric node at some selected rate and then to flow, by diffusion only, either to the skin through a nominal air gap where it condensed on the skin if the vapor pressure exceeded the saturation pressure at the skin temperature or to the external environment, the relative amounts of flow being determined by the diffusive resistances.

In the example selected, the following values were used:

Fabric thickness	15 mils	(.038 cm)
Air gap thickness	100 mils	(.254 cm)
P_{H_2O} External	0.35 psi	(.024 atm)
P_{H_2O} Skin Surface	1.00 psi	(.068 atm)

In addition, a fabric weighing 4.5 oz/yd^2 (.0152 gm/cm^2) with 10 percent moisture was assumed to evaporate all the water uniformly over a 0.5 second duration. The resistance/unit length to diffusive flow (tortuosity factor) in the fabric was assumed to be twice that in air. The result was an over pressure within the fabric of 8.5 psi (.58 atm) clearly indicating that bulk flow cannot be ignored. in the case of the short duration, rapid heating experienced in crash fires. This conclusion remains true even for the lower moisture content fabrics and for the more realistic case in which the moisture is released over a longer period of time as will be shown subsequently.

In addition, the simple model showed that less than 10 percent of the moisture would be transported to the skin because of the resistance to diffusive flow across the air gap. However the fact that high over pressures are predicted suggest that, in the real case, bulk flow cannot be ignored, i.e., the vapor

within the fabric-gap may be purged of the non-water molecules thereby reducing the diffusive resistance to the limit of bulk flow resistance.

Proceeding on then, the next question is, if the transport of the water vapor is by bulk flow, which direction does it flow? By analogy to the diffusive flow analysis above, in a static situation, the relative amounts flowing outward to the external environment and flowing inward to condense on the skin (or inner fabric layers) will be determined by the relative resistances to bulk flow. This in turn will be dependent upon the actual internal flow geometry which, as noted before, is a complex matter. Assuming the water to be uniformly distributed and that resistance to flow varies with the distance within the material, at least 50 percent of the total water should flow outward. The additional flow resistances encountered internally should increase this value. However, in the dynamic situation, with a man running on the order of 10 ft/sec (3 m/sec), the result may be quite different.

Referring back to Equation 43 for flow through a porous media, it is possible to determine the pressure drop across a layer of fabric as a function of the velocity of flow through the fabric. Using an air permeability of 121 ft^3/ft^2min (3700 cm^3/cm^2min), a viscosity of 10^{-5}lbm/sec ft (1.5×10^{-4}gm/cm sec), and a density of 0.075 lbm/ft^3 (1.2×10^{-3} gm/cm^3) gives:

$$\frac{\Delta P}{L} = 1.2 \times 10^{4} \frac{V}{g_c} + 1.05 \times 10^{4} \frac{V^2}{g_c} \qquad (49)$$

For a thickness, L, of .015 inches (0.038 cm) this becomes

$$\Delta p = 3.2 \times 10^{-3} V + 2.8 \times 10^{-3} V^2 \qquad (50)$$

This function is plotted on Figure 36 along with the dynamic pressure, ΔP, as a function of relative velocity, U, in the flame. For example, for velocity U of 15 ft/sec (4.5 m/sec) the dynamic pressure is 4.4×10^{-4}psi (3×10^{-3}atm) With this potential, the effective flow velocity through the fabric is 0.12 ft/sec (3.6 cm/sec).

Returning to the generation of water vapor in the material, if we assume that there is 10 percent water in a 4.5 oz/yd^2 (0.15 gm/cm^2) fabric, all the water is evaporated in 0.5 sec, and that within the fabric the gas is pure water at 373°K, the effective flow velocity required to remove the water in that time is:

$$V = \frac{\dot{m}}{\rho_a}$$

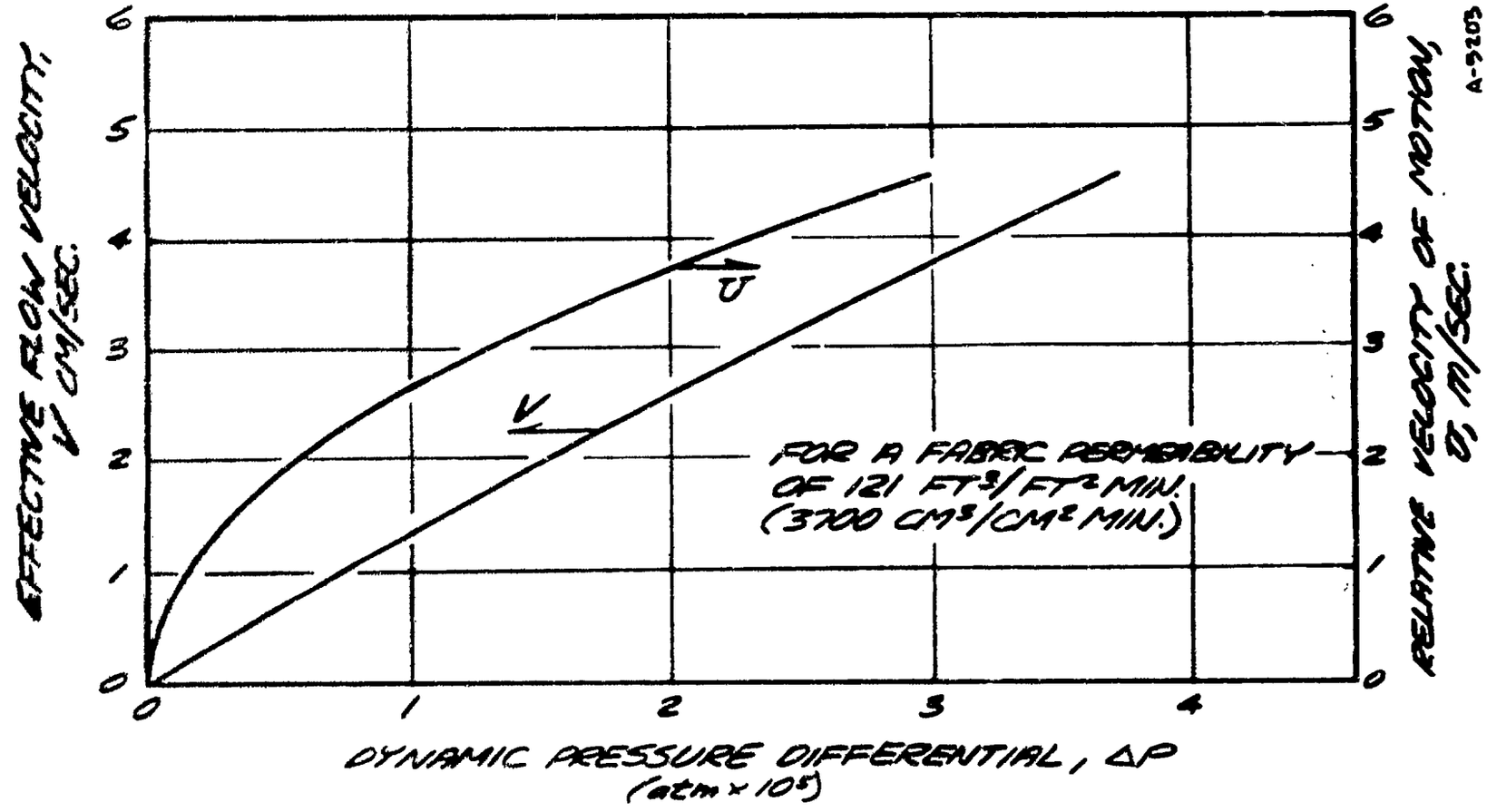

Figure 26. Gas Blow Through as a Function of Relative Velocity

where

$$\rho = \frac{p}{RT}$$

and, the pressure, p, is assumed to be the local atmospheric value. Upon substitution of values, the effective velocity is found to be equal to 0.164 ft/sec (5.0 cm/sec) which is seen to be of the order of the effective velocity resulting from a dynamic pressure for a man running with a relative velocity of 15 ft/sec (4.5 m/sec). Thus, the generation of water vapor is capable of developing a pressure within the material of the order of the dynamic pressure applied externally. With this being the case, it is not clear which direction the vapor will flow, although more will flow inward than for the static case. For fabrics with lower regain moisture and for the more realistic case in which the generation of water is over a longer period, the dynamic pressure becomes more dominant and a larger percentage of the water should flow inward if the maximum potential dynamic pressure is realized across the fabric.

In conclusion, this simplistic analysis has shown that the dynamic pressure across a layer of fabric and the internal pressures developed by moisture evaporation are of the same order of magnitude. Consequently, the direction and relative amount of flow of these vapors will be very sensitive to the characteristics of the total flow system. For example, if the resistance to flow through the fabric is small relative to the resistance of the rest of the system, most of the vapor should go outward. If the opposite is true, most of the vapor should go inward for realistic generation rates. Such a result is not very satisfactory since it serves neither to eliminate the need to consider condensation nor to refine the limits of this effect. Consequently, the next approach could be to consider the limiting cases in the parametric analysis, i.e., all the water goes to the skin or all the water goes outward, and then compare the resultant effects upon skin temperatures and injury levels. First, however, consider that for each 1 percent of moisture by dry weight in a 4.5 oz/yds^2 fabric, the potential heating value of condensation is about 0.1 cal/cm^2, the moisture in fabrics of 5 to 15 percent moisture regain represents potential heating of 10 to 25 percent of the total exposure of the typical 3 sec fire (6 to 8 cal/cm^2). Thus, it is readily apparent that in considering the extreme limiting cases, significant differences in the protective potential of fabrics may be anticipated, and it is not clear by physical reasoning that either limiting case is more likely to be representative of the real situation. Consequently, since it is not within the scope of this present work to provide a more satisfying answer, laboratory analysis will be used to provide the best available answer to this question.

SECTION 6

PARAMETRIC ANALYSIS

The parametric analysis for this study was conducted in two stages. The initial or preliminary stage was undertaken at the beginning of the program with an immediate goal of identifying the important parameters, thus serving as a guide in the more detailed literature search, test programs and parametric analysis to follow. Consequently, the initial analytical model used for the computer code thermal response predictions was simplistic relative to the final model. The differences in models are described in Section 6.1. The results of the detailed parametric analysis and predictions of the protection provided by the candidate fabrics are summarized in Section 6.2.

6.1 INITIAL INVESTIGATION OF PARAMETER SIGNIFICANCE

The first step in the identification of the important parameters in the fire-fabric-skin model which affect heat transfer and thermal injury to the skin was to perform a computer analysis making parametric variations about a defined nominal model. Initial study and literature survey were performed to arrive at this nominal model, consequently, values used in the preliminary study may not be exactly those used in the final model. Nevertheless, the values used in the initial model are quite satisfactory for the preliminary screening process. The nominal or baseline case parameters are described in Section 6.1.1. A description of the preliminary fire-fabric-skin model is given in Section 6.1.2.

6.1.1 Preliminary Nominal Fire-Fabric-Skin System

6.1.1.1 JP-4 Fire

The nominal fire was described by:

Flame temperature:	1600°F (990°C)
Flame spectrum:	Black body at flame temperature
Flame emittance:	1.0
Flame convective heat transfer coefficient: (based on a 2 diameter cylinder)	$2 \cdot 10^{-3}$ Btu/sec-ft^2-°F ($0.98 \cdot 10^{-3}$ cal/cm^{2}sec°C)
Exposure duration:	3 seconds

Thus the nominal exposure was a square wave pulse lasting 3 seconds followed by a cooldown exposure to a 70°F (21.1°C) environment with radiation and convection cooling for an additional 27 seconds. The 3 second duration was chosen to represent the nominal exposures experienced in the open fire pit tests performed at the U.S. Army test facility at Natick, Massachusetts. A convection/radiation heat flux distribution of 20%/80% was used. Total heat flux was 16.4 Btu/ft^{2}sec (4.45 cal/cm^{2}sec).

6.1.1.2 Clothing System

The basic parameters considered included those related to the fabric and those associated with the clothing assembly. The former included the number of layers and the gaps or spacing between layer(s) and skin, while the latter included thermal capacity, thermal conductivity, thickness, absorptance, transmittance, emittance, and water content. Following a review of the available fabric data (see Section 5) the nominal fabric properties were chosen as:

- o Absorptance: 0.70
- o Transmittance: 0.20
- o Emittance: 0.85
- o Specific heat: 0.30 to 0.45 Btu/lb°F (cal/gm°C) from 500 to 1000°R (5 to 283°C)
- o Thickness: (single layer) 0.015 inches (0.038 cm)
- o Thermal conductivity: 0.022 Btu/ft-hr°F (0.33 cal/cm hr°C)

A nominal gap of 0.100 inches was selected, and the number of layers in the clothing assembly was varied from one to three layers.

6.1.1.3 Initial Skin Parameters

In the preliminary analysis, the skin was considered primarily from the point of view of a back-up material to the fabric. That is, the emphasis was on providing the proper boundary condition for the fabric as opposed to calculating the in-depth response of the skin. Both goals are satisfied by an exact description of the skin, but, as will be shown by the results, an adequate description of the boundary condition for the fabric is provided by nominal estimates of skin properties since skin temperatures do not increase significantly relative to fabric temperatures. Consequently, the nominal skin properties used in the preliminary analysis are less refined but substantially equivalent to those described in Section 3 of this report.

The skin thermal properties of primary concern and the nominal values selected were:

Thermal capacitance:	54.0 Btu/ft^3-°R (0.865 cal/cm^3-°C)
Thermal conductivity:	$9.2 * 10^{-3}$ Btu/ft-sec°F) ($1.36 * 10^{-3}$cal/cm-sec-°C)
Absorptance:	0.95
Transmittance:	0.00

Thus the skin was assumed to be opaque with properties similar to those of water. The rear wall boundary condition was assumed to be insulated.

6.1.2 Preliminary Thermal Model-Computer Code

The thermal model selected for the preliminary analysis was similar to the final model described in detail in Section 2 with several significant exceptions which will be described. The basic code used was the Aerotherm, one-dimensional, time-dependent conductive heat transfer code, CMA which is described in Section 2. The basic differences between the preliminary and final models are that, in the preliminary model, the following phenomena were not included:

1. Shrinkage of material with consequent change in gap dimensions
2. Variation of optical properties of the fabric as a function of temperature
3. Pyrolysis of the fabric
4. Thermochemical interaction between the fabric, pyrolysis gases and environmental gases, both of fire and standard air compositions

Thus, the fabrics were first treated as thermochemically inert materials whose thermal response was dependent upon the change in the sensible enthalpy ($\rho C_p \Delta T$) of the material and the energy transferred into the material by radiation, conduction, and convection. The evaporation of free water was included, but this water vapor was assumed to flow outward, leaving the system. In addition, there was no calculation of thermal injury to the skin. Relative assessment of fabric protection potential was based on the total heat load to the skin at the end of 3 and 30 seconds.

Figure 37 shows a pictorial of the model including the heat transfer mechanisms considered. The fabric layers and skin were divided into a series of homogeneous isothermal nodes with thermal properties being defined as functions of temperature only.

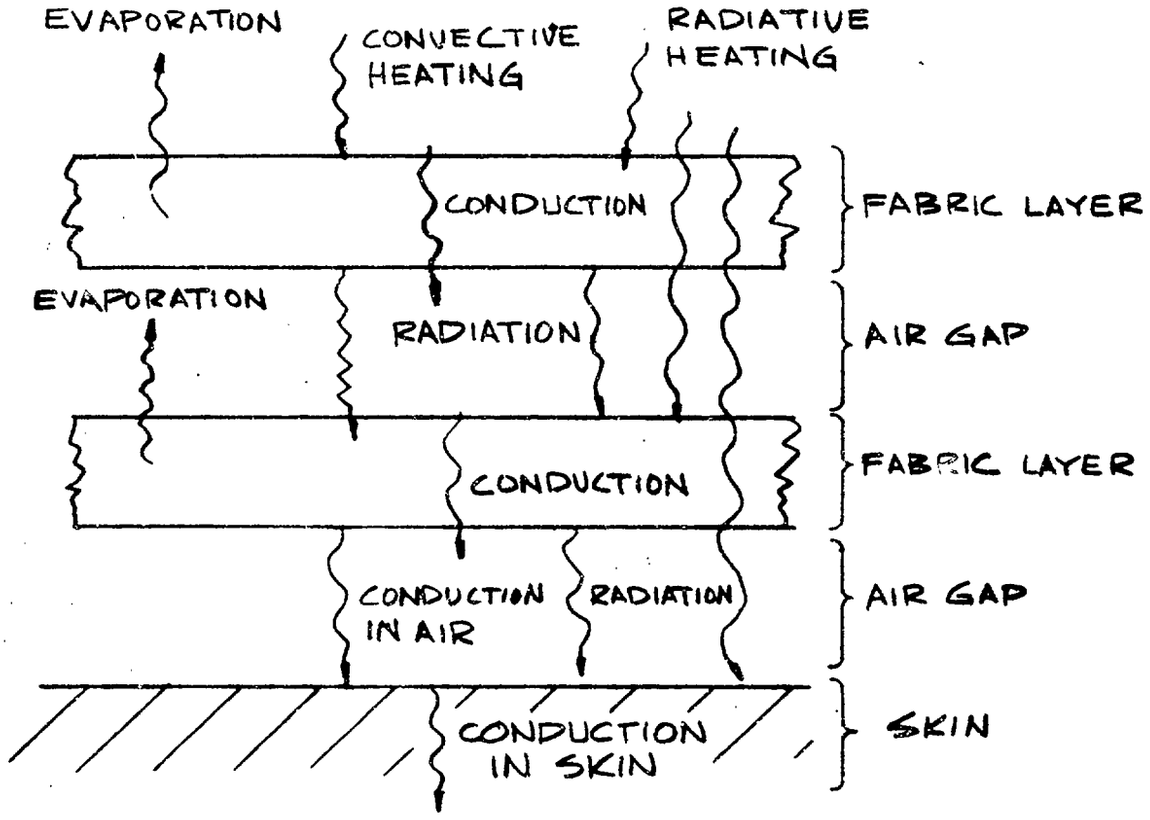

A-3905

Figure 37. Preliminary Heat Transfer Model

6.1.3 Parametric Variations - Preliminary Analysis

A number of variations about the nominal system description of 6.1.1 were made in the preliminary studies. The cases run are tabulated in Tables XXIII through XXVI for the flame environment, clothing assembly, fabric properties, and skin thermal properties respectively. The parameters of interest have been listed in Section 6.1.1 and the range of variations are presented in the tables. Parametric values and the results which follow are given here in English units only as the study was done prior to the conversion to metric units in this program. These results have not been converted because their main value is relative not absolute.

6.1.4 Results of Preliminary Parametric Analysis

Results of the preliminary analysis are given in Tables XXVII through XXIX. The performance indicators used at this stage of the program were 1) skin surface temperature, 2) total heat to the skin at the end of the full 30 second computational period and, 3) total heat to the skin at 3 seconds, the end of the fire exposure. In the preliminary analysis there was no attempt to relate any of these indicators to skin injury; they serve only as relative figures of merit for the various cases run.

Table XVII shows results for variations using one fabric layer. The first results are for the baseline case described in Section 6.1.1. These results indicate that the skin properties and back surface boundary conditions are not significant parameters. Basically, skin temperatures are low relative to fabric temperatures and thus do not affect the heat transfer between fabric and skin. This does not say that skin thermal properties are not important to skin injury, only that they do not affect the fabric response.

Flame temperature obviously has a major impact with variations of only 200°F resulting in 40% variations in heating. Reduction of the convective coefficient has only a minor affect owing to the low percentage of convective heating rate to the total heating rate.

Adiabatic cooldown substantially increases the total heating to the skin emphasizing how much energy and thus potential for damage remains in the fabric after the exposure has ended. Pursuing this point, a cooldown using -200°F gaseous CO_2 can reduce the total heating by a modest 15%, but of course, cannot reduce the heating at 3 seconds.

TABLE XXIII

FLAME ENVIRONMENT PARAMETERS

Case No.	1*	2	3	4	5	6	7	8
Flame Temperature (°F)	1800	1800	1800	1800	1800	1600	2000	2200
Flame Spectrum	Correspond to Black Body Spectrum at Flame Temperature							
Flame Emittance	1.0	1.0	Time Function	1.0	1.0	1.0	1.0	1.0
Flame Convective Coefficient Btu/sec ft^2°F	2×10^{-3}	5×10^{-4}	2×10^{-3}	2×10^{-3}	2×10^{-3}	2×10^{-3}	2×10^{-3}	2×10^{-3}
Exposure Time (Seconds)	3 Seconds for All Cases							
Cool Down Mode	2	3	2	1	3	2	2	2

*Baseline Case

Cooldown Mode

1) Adiabatic
2) Radiation and Natural Convection to 70°F
3) CO_2 Blown on Fabric

TABLE XXIV

CLOTHING ASSEMBLY PARAMETERS

Case No.	1*	2	3	4*	5	6	7	8	9	10	11	12
Number of Layer of Fabric	1	1	1	1	1	1	2	2	2	2	2	2
Gap Dimension(1) (Inches)	.100	.010	.250	.100	.010	.250	.100	.010	.250	.100	.010	.250
"T" Shirt	None	None	None	Yes	Yes	Yes	None	None	None	Yes	Yes	Yes

*Baseline Case

(1) Constant Dimension for all Gaps

TABLE XXV

FABRIC PARAMETERS

Case No.	1*	2	3	4	5	6	7	8	9	10	11
Emittance	0.85	.95	.85	.85	.85	.85	.85	.85	.85	.85	.85
Transmittance	.20	.20	.05	.20	.20	.20	.20	.20	.20	.20	.20
Absorptance	.70	.70	.70	.60	.70	.70	.70	.70	.70	.70	.70
Water Content (Percent)	3	3	3	3	15	3	3	3	3	3	3
Material	PBI	PBI	PBI	PBI	PBI	PBI	PBI	PBI	PBI	Cotton	Nomex
Thickness (inches)	.015	.015	.015	.015	.015	.008	.020	.015	.015	.015	.015
Fiber Volume Fraction	.30	.30	.30	.30	.30	.30	.30	.20	.40	.20	.30

*Baseline Case

TABLE XXVI

PRELIMINARY SKIN THERMAL PROPERTY PARAMETERS

Case No.	1*	2	3	4
Heat Capacity ($Btu/ft^3°F$)	54	54	54	54
Thermal Conductivity (Btu/hr ft°F)	0.33	0.20	0.50	0.33
Absorptance	0.95			
Transmittance	0			
Back Wall Boundary Condition	1	1	1	2

*Baseline Case

Back Wall Boundary Condition

1) Adiabatic
2) Constant Temperature (98.6°F)

TABLE XXVII

SUMMARY OF RESULTS FOR ONE LAYER OF FABRIC - PRELIMINARY ANALYSIS

Case	Outer Surfaces Temperature at 3 Seconds (°F)	Inner Surface Temperature at 3 Seconds (°F)	Skin Temperature at 3 Seconds (°F)	Total Heat to Skin Including Cooldown (Btu/ft^2)	Total Heat to Skin After 3 Seconds (Btu/ft^2)
Baseline Case	1396	1125	222	20.6	11.6
K_{SKIN} = 0.5 Btu/ft hr°F	1396	1124	200	20.7	11.6
K_{SKIN} = 0.2 Btu/ft hr°F	1398	1127	257	20.4	11.6
Constant Temp Back Wall	1396	1125	222	20.6	11.6
Flame T = 2200°F	1829	1448	342	36.1	23.1
Flame T = 2000°F	1612	1288	275	27.6	16.6
Flame T = 1600°F	1188	962	183	15.1	7.9
Flame e = f(Time)	1394	1121	221	20.3	11.4
Low Flame Convective Coef.	1338	1073	214	19.3	10.9
Adiabatic Cooldown	1396	1125	222	26.4	11.6
CO_2 Cooldown	1396	1125	222	17.6	11.6
GAP = 0.25 (fabric-skin)	1412	1157	215	19.3	11.0
GAP = 0.010 (fabric-skin)	1261	823	281	26.7	17.1
15% Water in Fabric	1358	1077	211	18.9	10.3
Fiber Transmission = 0.05	1396	1122	174	15.4	6.4
Fiber Fraction = 0.2	1504	1140	230	19.6	12.6
Fiber Fraction = 0.4	1306	1038	209	21.0	10.4
Fabric Emittance = 0.95	1387	1112	222	20.2	11.5
Fabric Absorptance = 0.6	1333	1073	215	19.5	11.0
Fabric Thickness = 0.008 in	1439	1395	264	21.5	16.0
Fabric Thickness = .020 in	1341	974	204	20.0	9.7

TABLE XXVIII

SUMMARY OF RESULTS FOR ONE LAYER OF FABRIC BACKED UP A "T" SHIRT - PRELIMINARY ANALYSIS

CASE	Outer Layer Front Surface Temp (°F)	Outer Layer Back Surface Temp (°F)	Second Layer Front Surface Temp (°F)	Second Layer Back Surface Temp (°F)	Skin Temperature at 3 second °F (Max. Temp °F)	Total Heat to Skin (Btu/ft^2)	Total Heat To Skin at 3 seconds (Btu/ft^2)
Baseline Case	1438	1226	853	634	124 (138)	12.4	2.27
K_{SKIN} = 0.5 Btu/ft hr°F	1438	1226	853	635	132 (149)	12.3	2.26
K_{SKIN} = 0.3 Btu/ft hr°F	1438	1226	853	634	120 (131)	12.5	2.27
Flame T_∞ = 2240°F	1900	1540	1210	980	158 (178)	22.3	5.00
Flame T_∞ = 2040°F	1764	1429	1073	801	138 (156)	16.9	3.41
Flame T_∞ = 1540°F	1317	1031	655	483	115 (125)	8.9	1.48
Flame α = f(Flame)	1433	1220	844	626	124 (137)	12.3	2.21
Low Flame Convective Coef.	1379	1168	813	605	123 (135)	11.7	2.20
Adiabatic Cooldown	1438	1226	853	634	124 (150)	10.4	2.27
CO_2 Cooldown	1438	1226	853	634	124 (135)	9.7	2.27
GAP = 0.2% (fabric-skin)	1445	1243	839	637	120 (132)	10.9	2.02
GAP = 0.010 (fabric-skin)	1578	1302	905	528	159 (181)	19.6	4.89
Fiber Fraction = 0.2	1550	1282	910	684	127 (149)	11.8	2.42
Fiber Fraction = 0.4	1335	1112	778	579	122 (135)	12.4	2.14
15% Water	1384	1143	637	384	116 (126)	9.2	1.75
Fiber Transmission = 0.05	1433	1188	613	428	105 (125)	8.54	.62
Fabric Emittance = 0.95	1427	1218	869	632	124 (137)	12.1	2.26
Fabric Absorptance = 0.6	1370	1161	775	574	122 (134)	11.3	2.10
Fabric Thickness = 1.000 in	1568	1488	1199	1069	159 (166)	13.8	4.92
Fabric Thickness = 0.020 in	1361	1042	685	425	117 (129)	11.1	1.78

TABLE XXIX

SUMMARY OF RESULTS FOR MULTIPLE FABRIC LAYERS - PRELIMINARY ANALYSIS

Cloth	Outer Layer Front Surface Temperature at 3 seconds (°F)	Outer Layer Back Surface Temperature at 3 seconds (°F)	Second Layer Front Surface Temperature at 3 seconds (°F)	Second Layer Back Surface Temperature at 3 seconds (°F)	Third Layer Front Surface Temperature at 3 seconds (°F)	Third Layer Back Surface Temperature at 3 seconds (°F)	Skin Temperature at 3 seconds (°F) Maximum skin temp °F	Total Heat to Skin Including Cooldown (Btu/ft²)	Total Heat to Skin at 3 seconds (Btu/ft²)
Two Layers Fabric - .043 inch Air Gap	0.043	833	--	--	--	--	181 (201)	26.7	17.1
Two Layers Fabric - .080 inch Air Gap	0.080	0.135	--	--	--	--	222 (232)	20.6	11.6
Two Layers Fabric - .180 inch Air Gap	0.418	0.591	--	--	--	--	215 (215)	19.3	11.0
Two Fabrics Gun "B" Shield + .043 Air Gaps	0.070	0.103	695	870	--	--	139 (181)	19.6	6.89
Two Fabrics Gun "B" Shield + .080 Air Gaps	0.038	0.030	693	634	--	--	131 (130)	13.4	3.27
Two Fabrics Gun "B" Shield + .180 Air Gaps	0.045	0.063	830	837	--	--	130 (132)	10.9	2.82
Two Fabrics + .043 Air Gaps	0.083	0.108	844	913	--	--	156 (181)	19.9	6.55
Two Fabrics + .080 Air Gaps	0.031	0.039	762	666	--	--	131 (135)	13.3	3.05
Two Fabrics + .180 Air Gaps	0.040	0.038	965	861	--	--	118 (127)	20.5	1.85
Two Fabrics Gun "B" Shield + .043 Air Gaps	0.080	0.086	823	894	816	312	111 (146)	15.3	.99
Two Fabrics Gun "B" Shield .180 Air Gaps	0.1.	0.113	672	787	842	363	103 (116)	8.7	.43
Two Fabrics Gun "B" Shield + .018 Air Gaps	0.046	0.050	781	876	851	353	103 (112)	9.1	.38

One of the major factors is the separation or gaps between fabric layer(s) and skin. Gaps greater than 0.100 inches (.254 cm) do not show substantial improvement because as shown in Figure 38, beyond that distance, the transfer of energy across the gap is predominantly by radiation. However, as the gap decreases, the resistance to heat flow is significantly reduced by the increasing dominance of the conduction mode. Thus, shrinkage of a fabric becomes of primary importance.

Changing the fabric transmittance from 0.20 to 0.05 has a significant affect upon the total heating primarily because 20% of the incident radiant flux is a substantial portion of the total heating at 3 seconds (7.2 of the 11.6). Surface emittance of the fabric is not too important as it is a high value in either case (0.85 and 0.95). Absorptance is actually more important than indicated by the results since a variation of only 0.1 from 0.7 to 0.6 was made. Basically, it is desirable to minimize as much as possible both the absorptance and the transmittance, the first to keep energy out of the system, and the second to keep it from being directly absorbed into the skin. If the energy which is not reflected can be fully absorbed by the fabric, some percentage of it will be reradiated outward so that less than 100% reaches the skin.

Variations in fiber fraction constitute changes in two fabric parameters, in this analysis, thermal conductivity and density, both quantities increasing with increasing fiber fractions. Increases in thickness while maintaining the same bulk density result in an increase in mass per unit area and no change in thermal conductivity, but a decrease in the conductance. Considering the relative resistances to conductive heat flow across the various fabric layers and gaps, it is noted that the thermal conductivity of the fabric is not a significant factor as long as the gaps are at least as thick as the fabric layers, and when the gaps become this small, the total resistance is so low that the protective capability is substantially reduced. Since the effective conductivity of a fabric cannot be decreased below the value for the gas, it is concluded that the thermal conductivity of the fabric is not a significant parameter. The other variable, density (or lumping this with specific heat to form thermal capacitance) has a more complicated affect. Total heating values including cooldown show little difference for rather sizeable changes in the thermal capacitance whereas the differences at 3 seconds are significant. This occurs because the larger thermal capacitance provides a greater heat sink initially, thus fabric temperatures rise less and less energy is transferred to the skin. However, given enough time, the energy absorbed by the fabric is transferred to the skin in about the same ratio relative to that reradiated or convected to the environment independent of the thermal capacitance. From Section 3 we

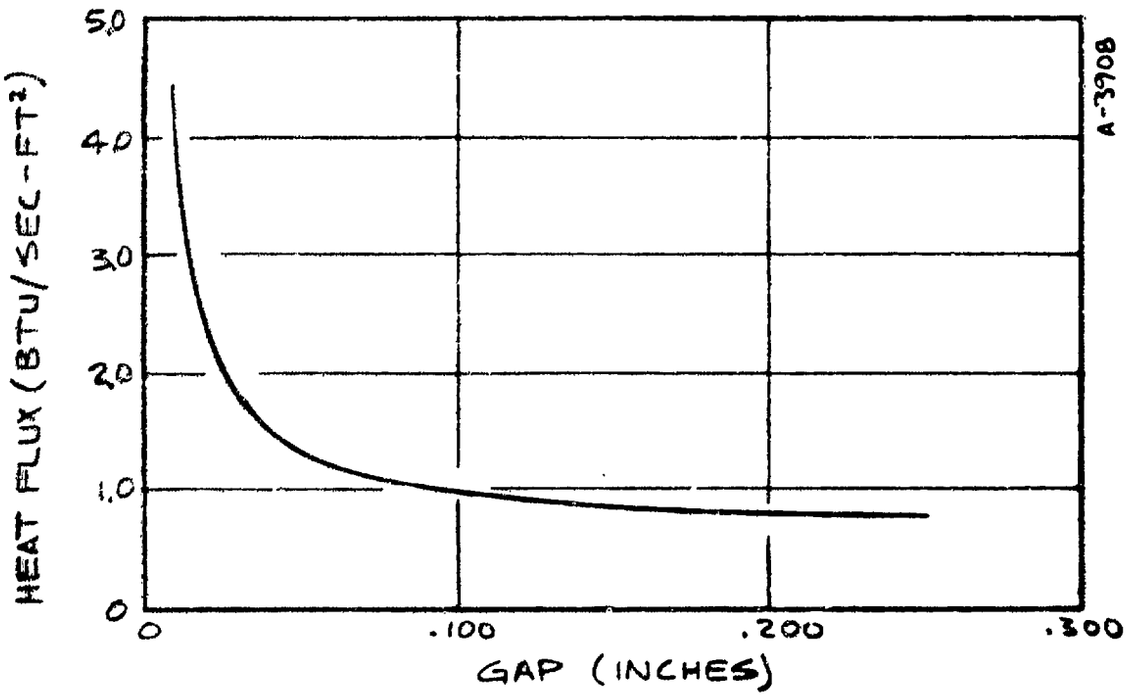

Figure 38. Heat Flux Across Air Gap as a Function of Gap Width for a 500°F Temperature Difference

know that skin injury being temperature dependent is very sensitive to the man ner in which a given amount of energy is received. Thus any factor which can spread the energy over a greater period of time can be considered desirable.

Table XXVIII includes the same variational cases as Table XXVII, but now a cotton T-shirt has been added, also with a gap of 0.100 inches (0.254 cm) between T-shirt and skin. We see that both skin temperatures and total heating levels have been reduced substantially, primarily because the radiation resistance across the clothing assembly has been effectively doubled by the introduction of another absorbing surface, and also because the baseline direct transmission to the skin has been further reduced by 80% to 0.04. Relative effects of the variation of parameters with the T-shirt added are basically the same as discussed above for the single layer cases.

Finally Table XXIX summarizes the results for various layers of fabrics and the three gap values 0.01, 0.1 and 0.25 inches (0.025, 0.25 and 0.63 cm). The only new results here are those for two layers of fabric and for two layers plus a T-shirt. There is little difference between 1 layer plus T-shirt and 2 layers. The added protection of a third layer is apparent for the same reasons described above.

6.1.5 Summary and Conclusions from the Preliminary Parametric Analysis

The following conclusions from the preliminary analysis have been drawn and will be used to select the final model and to guide the final parametric analysis.

1) The fire temperature, or more generally, the level of the thermal environment is a major factor in the protective capability of clothing due to the dominance of radiation and the fourth power variation of radiant flux with temperature. Consequently, substantial difference in performance of the same fabric may be found for different fires if these fires exhibit variations in flame temperature.

2) Skin properties do not affect fabric response

3) Substantial heating of the skin may occur following egress from a fire as the energy stored in the fabric is released.

4) Gaps between layers are of primary importance. It is desirable to maintain these gaps sufficiently large to insure near radiation limited heat transfer between layers.

5) Likewise it is desirable to increase the number of layers of material (and to maintain some gap between them) to increase the overall resistance to radiation heat transfer.

6) Optical properties of the fabrics are very important in that in a radiation dominated environment, they represent the primary mechanism for transfer of energy into the clothing skin system. High reflectance and minimal transmittance are desirable to keep energy out of the system and to prevent its direct absorption by the skin.

7) Water content in a fabric is favorable if the water vapor flows out of the system.

8) Thermal conductivity of the fabric is not significant since heat transfer is controlled mainly by radiation and by the conductivity of the gas in the gaps and within the fabric.

9) Thermal capacitance affects the response of the fabric and thus the heat flux - time history of skin heating. Although the total heating to the skin is not affected significantly by varying the capacitance, a higher capacitance will spread out the heating with a possible reduction in injury (see discussion of Section 3) depending on the total heating levels.

10) Fiber fraction does not appear to be important relative to its role in determining the thermal conductivity (see 8 above). It may be of some significance, however, if variation of the fiber fraction simultaneously varies the thermal capacitance and/or the optical properties.

11) Fabric thickness is similar to fiber fraction in that variations will change the thermal conductance, but unless thicknesses become of the order of the radiation dominated air gap thickness (~ 50-100 mils), the maintenance of an air gap is far more essential for protection and thus fabric thickness, as it effects conductance is not of primary importance. Again, it may be more important if it effects thermal capacitance and optical properties.

12) An active means of providing cooling such as a CO_2 spray represents a potential for reducing the level of injury by removing much of the residual energy in the fabric and minimizing the post fire heat soak load to the skin. However, it must be recognized that time is critical. Most of the heat soak occurs within the first few seconds following egress. Active cooling applied by some external agent which commences more than 5 to 10 seconds after egress will have negligible beneficial effect.

Finally, it is to be recalled that these studies did not consider some properties of real fabrics which are undoubtedly of significance, e.g., shrinkage and pyrolysis, and it may be anticipated that some of the above parameters

may become more or less important in the more complete model. Also, the parameters used as figures of merit will be replaced by the burn injury model which will account for the actual, time dependent thermal response of the skin.

6.2 DETAILED PARAMETRIC ANALYSIS

The more detailed parametric analysis has two primary objectives. First, specific candidate fabrics are to be considered. Section 5 of this report describes the results of the literature search and test which defined the necessary, thermal, optical and physical properties for the three fabrics considered: Nomex, PBI, and stabilized PBI. In this section only the stabilized PBI fabric designated as fabric number 121 will be considered, thus excluding fabric L. These fabrics will be evaluated for protection capacity against a nominal fire environment (described below) as single layers and as double layers, one of the specific fabrics over an underlayer of cotton.

The second objective is to investigate the effect of variation of various fabric and fire parameters which have indicated potential importance in the preceding preliminary analysis. Before discussing results of the analysis, the environment and skin models used will be described.

6.2.1 Fire and Skin Models

6.2.1.1 Fire Models

6.2.1.1.1 Fire

The nominal fire model selected is shown in Figure 39. It is assumed that the fire is fully developed and that exposure begins in the middle of the fire, as the cockpit of an aircraft would be. For a total 3 second period in the fire, the first 2 seconds are assumed to be of uniform flux (4.65 cal/cm^{2}sec) whereas for the final second, the flux decreases linearly to zero. This is based upon unpublished data from Natick tests and from considerations of A/F variations fire coning, and optical path effects at the edge of a fire, discussed in Section 4. A standard sea level environment is assumed to exist upon egress.

6.2.1.1.2 Natick Fire Profile

The Natick fire profile used in the detailed parametric analysis differs from the nominal fire in that during the first second, the flux is increased linearly from zero to the maximum level. For both fire models, the fire is assumed to be radiating an 1850°F (1010°C) black body flux at 13.7 Btu/ft^{2}sec (3.7 cal/cm^{2}sec) with an additional convective contribution equal to 20 percent of the total heating when the fabric is at the initial temperature, i.e.,

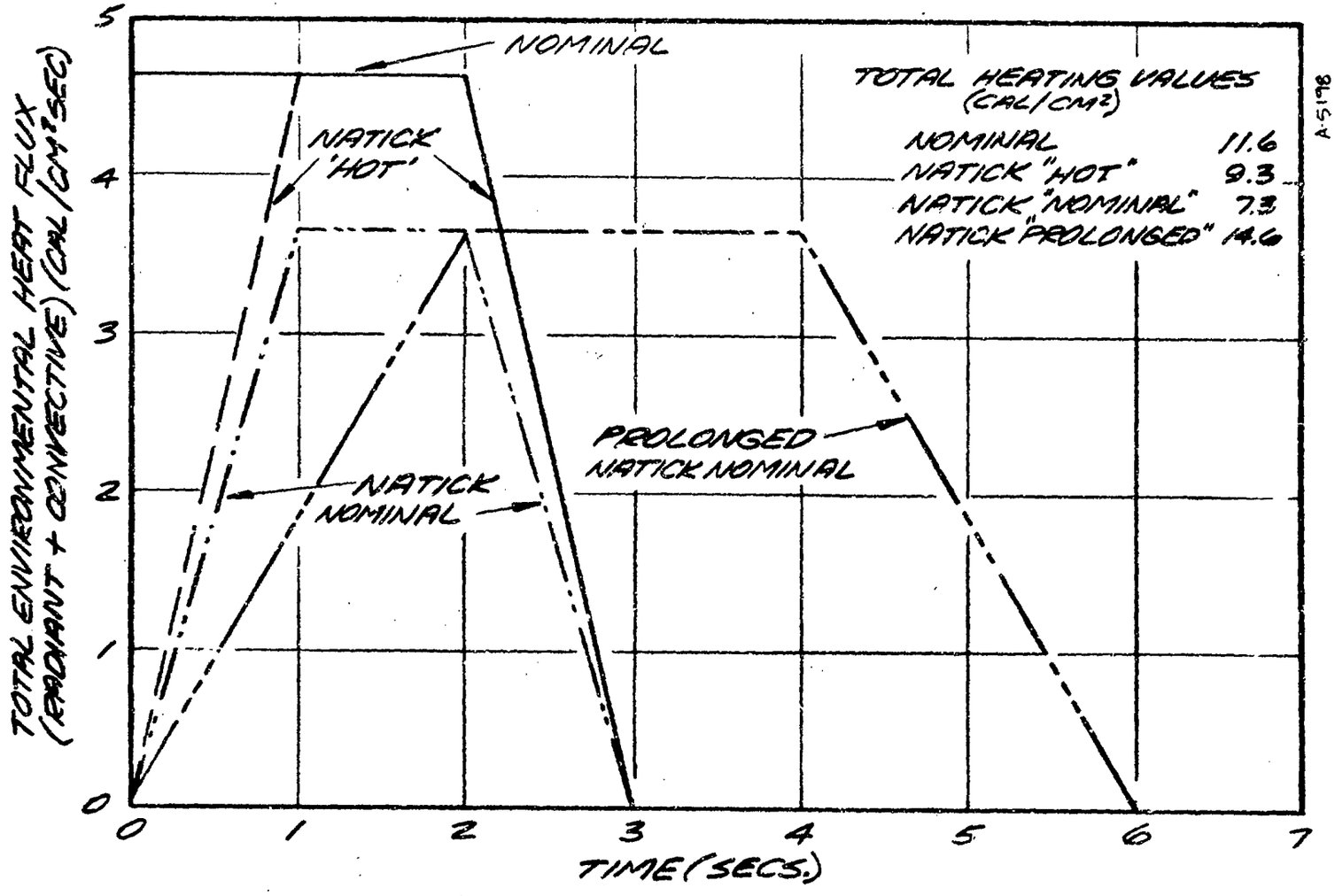

Figure 39. Fire Profiles

3.4 Btu/ft^{2}sec (0.92 cal/cm^{2}sec) of a total 17.1 Btu/ft^{2}sec (4.65 cal/cm^{2}sec). Again, based on unpublished and incomplete data from Natick tests, this appears to represent a "hot" fire, with a more nominal fire indicating a maximum value around 13.5 Btu/ft^{2}sec (3.68 cal/cm^{2}sec) when spread over the trapezoidal profile assumed herein. The "nominal" Natick fire is considered as well as a 6.0 sec "nominal" flux level, Natick trapezoidal profile with ramps from 0.0 to 2.0 sec and from 4.0 to 6.0 sec.

Convective coefficients for the fire and air environments are based on a relative velocity of 15 ft/sec (4.5 m/sec) and a four inch (10 cm) diameter cylinder. Computer runs are terminated after 30 seconds. All fire profiles considered are shown in Figure 39.

6.2.1.2 Skin Model

The skin model used is that described in Section 2 (Table II) and Section 3. The surface is assumed to be totally absorbing, circulatory effects are assumed to be invariant during the period of heating, and an adiabatic back wall boundary condition is used following the 2 mm thick final node of fatty tissue.

6.2.2 Results of Analysis- Comparison of Candidate Fabrics

6.2.2.1 Single Layer

The results for single fabric layers exposed to a nominal fire are presented in Table XXX and Figures 40 and 41. One factor stands out above all others in the comparison of results, namely, the dimensional stability of the fabric. The nominal model assumed for all fabrics is a four inch (10 cm) diameter cylinder covered with a 10 percent larger diameter layer of fabric. Air gaps, initially 0.200 inch (0.5 cm) in diameter are decreased linearly with shrinkage up to 10 percent at which time the fabric is restrained from further shrinkage, and the air gap is reduced to zero.

In Table XXX results are given in terms of

1. Time to $\Omega = 1$ at the base of the epidermal layer
2. Time to $\Omega = 1$ at the base of the dermal layer
3. Depth of penetration of $\Omega = 1$ at end of 30 seconds
4. Total skin heating at end of exposure and 30 seconds

For the 11.6 cal/cm^2 (nominal fire) all three fabrics, in the single layer cases, allowed total damage of the epidermis. Nomex and PBI both shrink within the first second of the exposure, PBI about 0.2 seconds after Nomex due

TABLE XXX

SINGLE LAYER FABRIC ASSEMBLIES - NOMINAL FIRE (11.6 cal/cm^2)

Fabric (% H_2O)	$\theta_{\Omega=1}$ (sec)*		$D_{\Omega=1}$ (μm)	Total Skin Heating (cal/cm^2)	
	Base of Epidermis	Base of Dermis		Max	θ = 3.0
Nomex (5.0)	0.8 → 1.0	12.0 → 13.5	> 2000	6.9	6.0
PBI (12.0)	1.0 → 1.2	13.5	> 2000	6.85	6.2
121 (14.0)	2.3	∞ (.000)	450	3.1	2.1

*If Ω < 1, value of Ω is given in parentheses, the symbol ∞ indicates total injury did not occur at this depth.

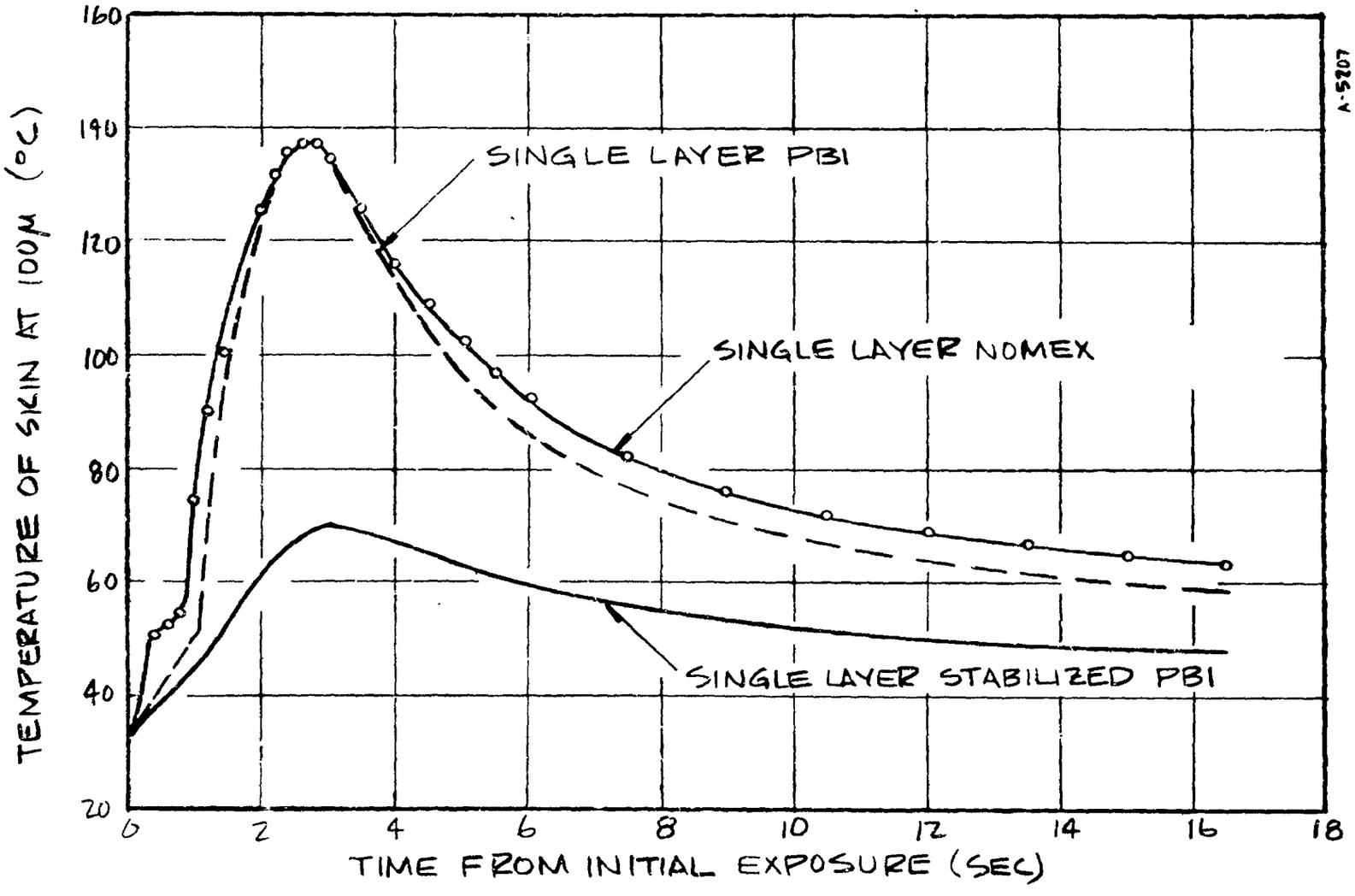

Figure 40. Skin Temperature Response for Single Fabric Layers - Nominal Exposure

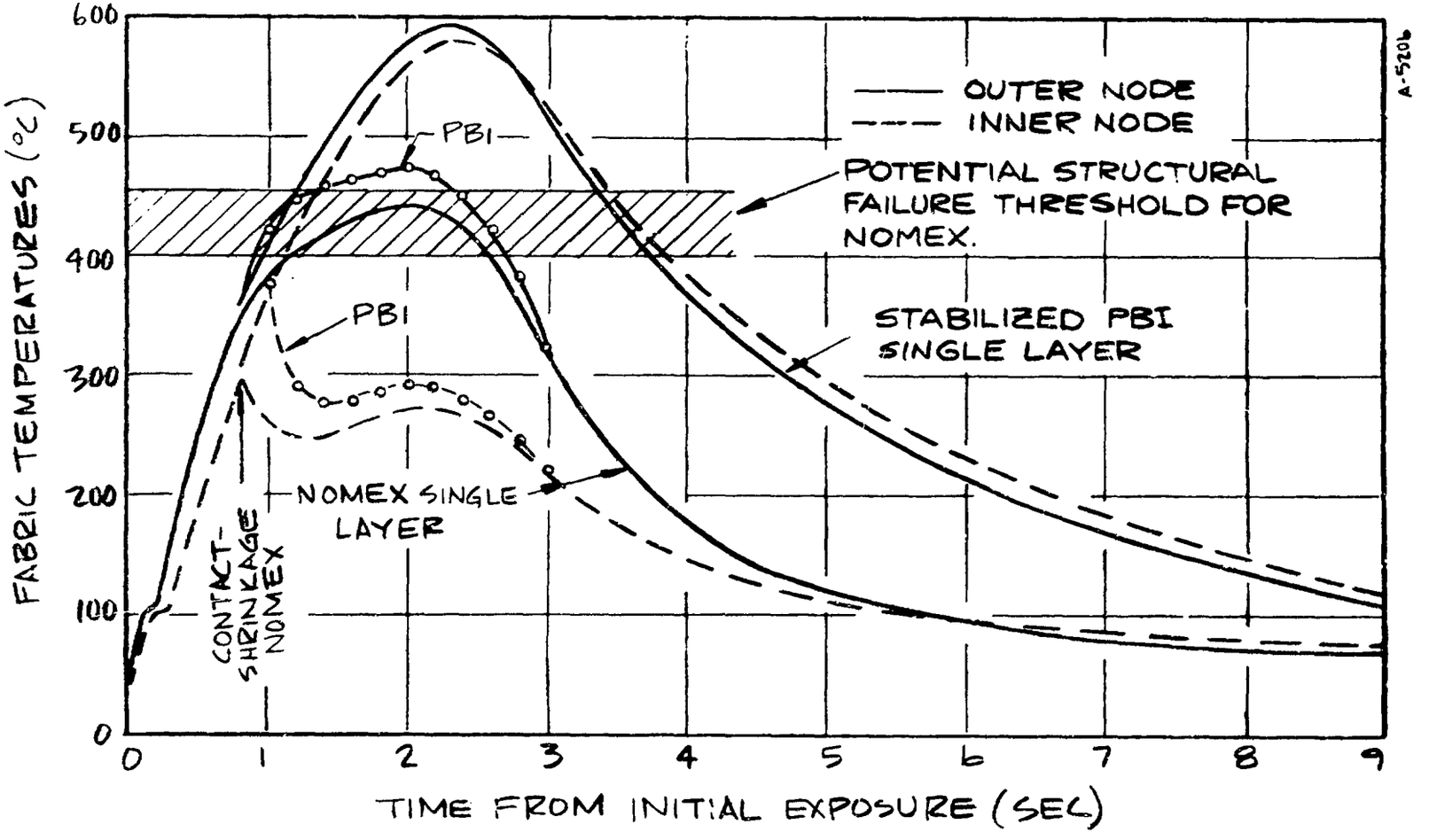

Figure 41. Fabric Temperature Response for Single Fabric Layers - Nominal Exposure

to the greater water content and higher temperature required for onset of shrinkage for PBI. The dermal layer is totally injured in 12.0 to 13.5 seconds for Nomex and PBI, and as shown by the total heating values, essentially all heating has occurred within the first 3 seconds. On the other hand, stabilized PBI which maintains dimensional stability to 600°C and above, does not close the gap and consequently reduces the total heating by a factor of 2 to 3 overall, and 3 to 4 at 3 seconds. The epidermal layer is totally damaged in about 2.0 seconds.

Figures 40 and 41 show some of the salient details of the thermal response of the skin and fabrics respectively for single layers. The skin temperature response is given at 100 μm, the nominal base of the epidermal layer. The effect of shrinkage is shown dramatically in Figure 40. Nomex and PBI exhibit rapid increases around 0.8 to 1.0 seconds as the fabric almost instantaneously shrinks to total contact. Shrinkage is simply the overwhelmingly dominant factor. Stabilized PBI maintains gaps which are sufficiently large to keep the heat transfer across the gaps effectively limited to radiation.

Figure 41 shows the response of the fabrics. Here the single layer is represented in the computer code by two nodes, thus, the figure shows the temperature of each node indicating the general heat transfer situation. Stabilized PBI is nearly isothermal because there is very little heat transfer across the gap. Nomex and PBI, on the other hand, have large gradients within the fabric once shrinkage has caused contact with the skin. All fabrics having similar properties tend to respond similarly until shrinkage occurs. At this point, stabilized PBI temperatures proceed to a maximum more than 150°C higher than Nomex and 100°C higher than PBI.

In all cases the fabrics were allowed to react with air upon egress from the fire. None indicated a tendency to ignite because they did not attain high enough temperatures during the single layer runs. When the double layer cases were run only Nomex exhibited a tendency to ignite while PBI and stabilized PBI did not. The difference is that in the single layer case Nomex comes in contact with the heat sink (skin surface) which prevents Nomex from reaching high enough temperatures to ignite. However in actual test at Natick, Nomex was found to break apart upon shrinking, thus separating from the heat sink and igniting. This burning fabric could result in further burn damage. In the computer model, the shrinking materials are not allowed to break apart and thus protect themselves from ignition by coming in contact with a heat sink, the skin or underlying layer. As the resistance to the heat sink is increased by adding low conductivity underlayers, the outer fabric becomes hotter and in the case of Nomex, ignites. Under the worst possible conditions, PBI and stabilized PBI attain a maximum temperature to 580°C.

One final observation relative to the Natick type fires is in order. The code does not consider structural response of the materials. The shrinkage test results discussed in Section 5 indicate that simultaneous with the charring of these fabrics is a loss of strength and increasing brittleness. Although quantitative tests were not conducted, qualitative judgements and the TGA data suggest loss of strength at lower temperatures for the Nomex fabric. This is further substantiated by Natick results. Nomex uniforms frequently fail in the limb regions suggesting that shrinkage has occurred until contact is made, but the fabric has a potential for and will continue to shrink applying tension to weakened fabric causing the material to break. In the simple, restrained shrinkage tests described in Section 5, it was found that the Nomex material failed structurally around 400 to 450°C whereas PBI did not fail to temperatures in excess of 600°C. The predicted peak temperatures for Nomex from Figure 41 indicate that Nomex temperatures are between 400 to 450°C from one to two seconds following the initial exposure. Thus, it is highly probable that the Nomex fabric will break or flow apart during the peak heating portion of the exposure. Once the fabric is free to move away from the body, heating to the fabric increases since there is no heat sink and the fabric is totally enveloped, resulting in much higher temperatures than computed herein. These conditions are far more conducive to ignition and burning. Once the fabric has ignited, the flame may propagate to portions of the uniform which remained intact. PBI material does not exhibit this tendency to fail structually even though shrinkage is severe.

In its present form, the computer model does not account for loss of the outer fabric layer. Thus it must be noted that the results for Nomex will indicate less skin injury than would actually occur if loss of fabric took place. In the case of the single layer where damage is already quite severe for the nominal fire, additional local heating to the skin will not be important; the concern is that this failure can cause propagation of injury to other regions by virtue of afterflaming and direct exposure.

6.2.2.2 Multiple Layers

Table XXXI and Figures 42 and 44 give results for multilayer comparisons of the various candidate fabrics. Here we see a significant improvement in protective capability even to some degree for the fabrics which shrink. In all runs, cotton was used as the underlayer.

Table XXXI and the figures again indicate the dramatic effect of dimensional stability. Figure 42 shows skin temperature response for stable and unstable fabrics and Figures 43 and 44 indicate the thermal response of the

TABLE XXXI

MULTILAYER ASSEMBLIES FABRIC/COTTON - NOMINAL FIRE (11.6 cal/cm^2)

Fabric	$\theta_{\Omega=1}$ (sec)*		$D_{\Omega=1}$ (μm)	Total Skin Heating (cal/cm)	
	Base of Epidermis	Base of Dermis		Max	θ = 3.0
Nomex/Cotton†	2.0	∞ (.108)	1300	4.55	2.7
Nomex/Cotton (react)	2.0	12.5	> 2000		
PBI/Cotton	2.1	∞ (.152)	1400	4.7	2.95
Stabilized PBI/ Cotton	∞ (.005)	∞ (.000)	0.0	1.70	0.31

*If Ω < 1, value of Ω is given in parentheses; the symbol ∞ indicates that total injury did not occur at this depth

†Not allowed to react with air

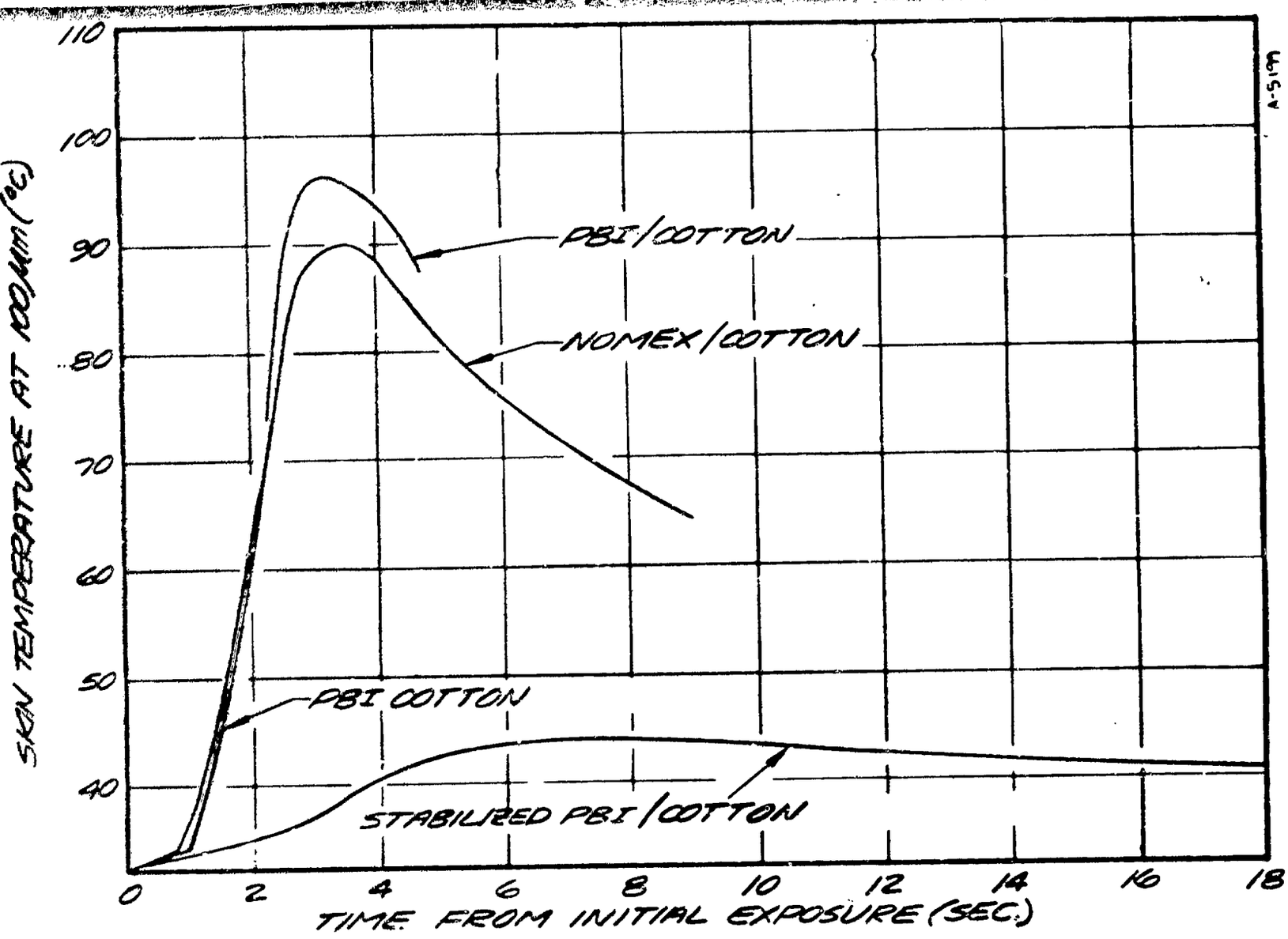

Figure 42. Skin Temperature Response for Two Fabric Layers - Nominal Exposure

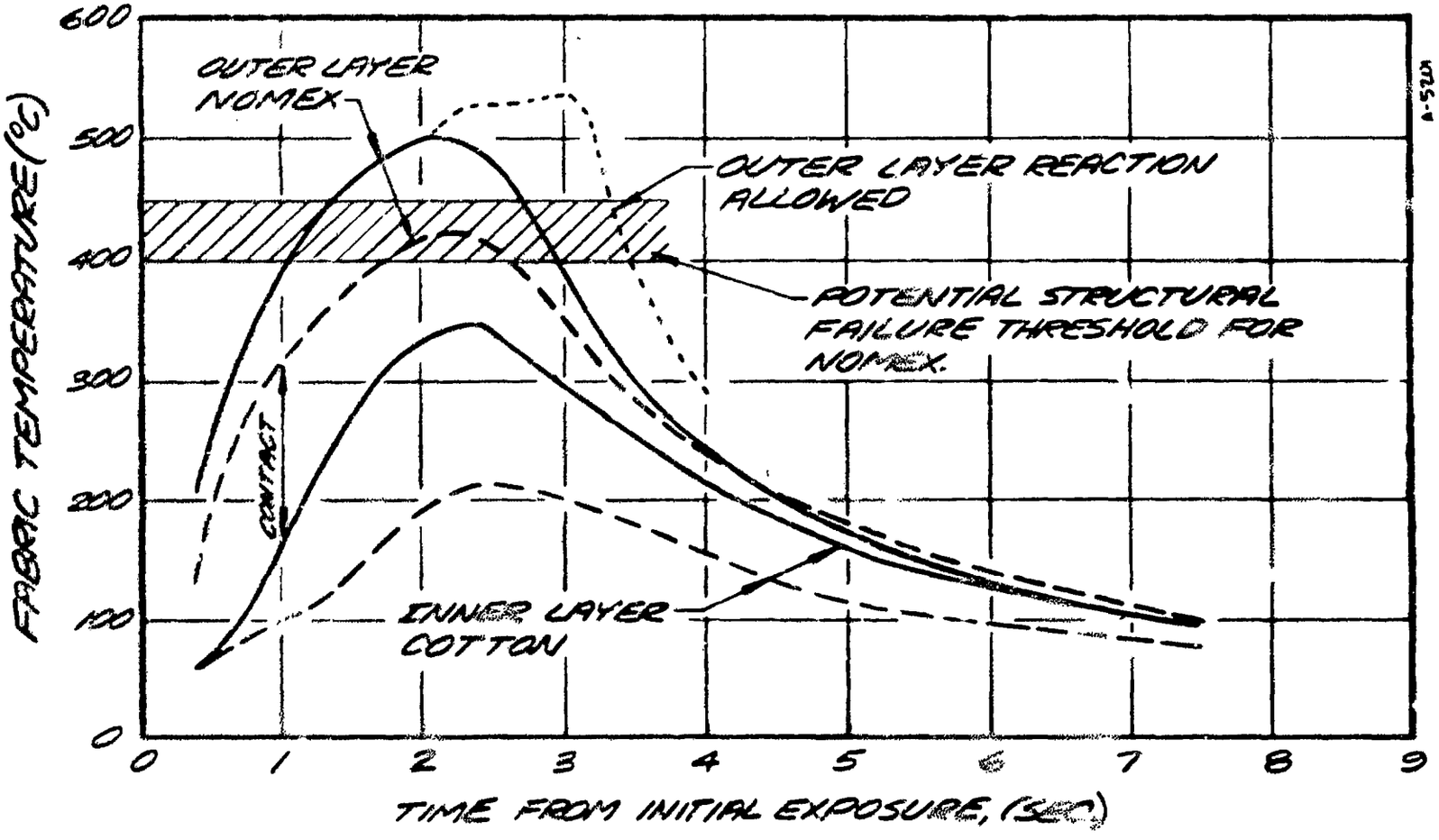

Figure 43. Typical Fabric Temperature Response for Two Layers for Shrinking Fabrics, Nomex/Cotton - Nominal Exposure (11.6 cal/cm²)

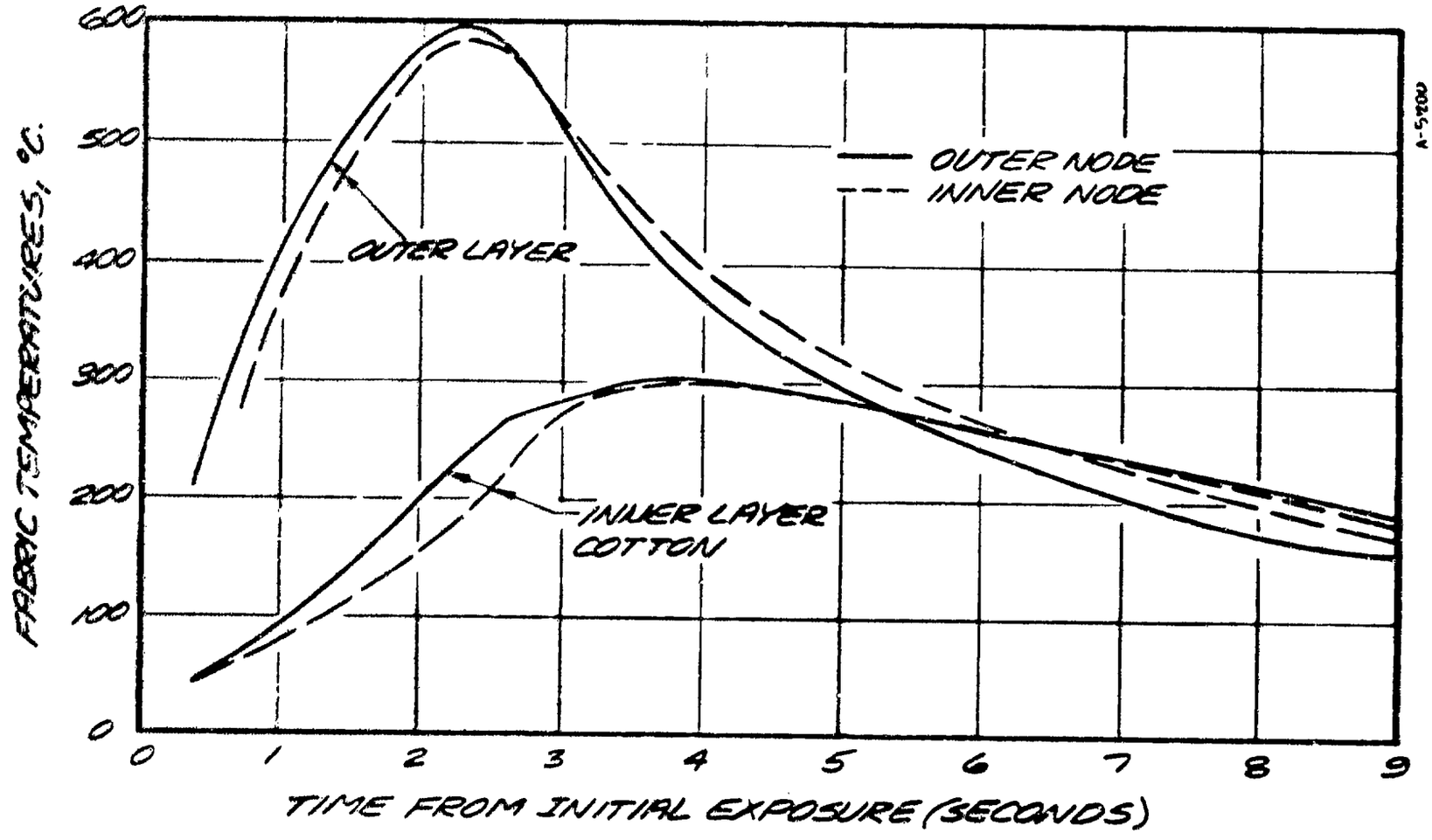

Figure 44. Typical Fabric Temperature Response for Two Layers for Stabilized Fabrics, Stabilized PBI/Cotton,- Nominal Exposure (11.6 cal/cm^2)

fabric including the cotton underlayer. Note the large gradients which exist once contact has been made with Nomex compared to the nearly isothermal outer and inner (cotton) layers with stabilized PBI. Nomex/cotton (reaction with air suppressed) and PBI/cotton still show substantial injury with epidermal destruction occurring after 2.0 seconds and penetration of total injury from over half to nearly the entire dermal thickness.

For Nomex/cotton, ignition and combustion were predicted to occur during the egress portion of the exposure as the fabric is encountering a mixed fire and air environment. The effect of this as shown in Table XXXI was to extend the depth of injury beyond the base of the dermal layer at 12.5 seconds compared to the 1300 μm penetration which occurred when reaction with air was suppressed. Combustion ceased upon entry into the air environment due to the low fabric temperature and the lack of radiant heating. The exposure profile chosen simulates the exposure to the front of the uniform in that upon egress from the fire, the radiant and convective heating from the fire goes to zero. For the rear surfaces of the uniform, this model ignores the continued radiant heating which exists. In Natick tests, these are the surfaces which are observed to afterflame; consequently, the predicted extinguishing of the "front surface" Nomex at 3.0 seconds is understandable, and it may be expected that proper modeling for a rear surface would predict sustained combustion beyond 3.0 seconds until the radiant flux became insufficient to support the combustion or the reaction was completed. In either event, the possibility of structural failure of the Nomex was not addressed in the computer predictions. Figure 43 indicates that the predicted Nomex temperatures exceed the probable failure threshold level of 400-450°C. Thus if sufficient tension exists due to the integrated shrinkage around the periphery of a limb or the torso, failure of the material at the point of maximum heating should occur under these conditions. This is more significant in the multilayer case than in the single layer since an intact outer layer of Nomex exposed to a nominal fire does provide some protection whereas a single layer of Nomex will not. In the case of less demanding environments such as the Natick profile results to be discussed, the structural integrity factor for Nomex may be even more important since intact outer layers would provide protection approaching the threshold epidermal injury level as the total heating is reduced. Total heating values in all cases of Nomex and PBI over cotton exceed the heating values experienced for single layer stabilized PBI. Double layer, stabilized PBI/cotton provided complete protection for the nominal 11.6 cal/cm^2 modeled, post-crash fire.

6.2.3 Results of Analysis - Parametric Variations

6.2.3.1 Fire Model Variations

In order to compare effects of variations in the fire model, a case which resulted in roughly a threshold injury of the epidermal layer was selected, this being the single layers stabilized fabric. Since dimensional stability has been shown to be the dominant factor, a case where complete loss of gap did not occur was chosen in order to allow sufficient sensitivity of response to variation of other factors. At this point the clothing assembly represents only a convenient standard against which to compare variations in both fire and fabric property parameters. The fabric property variations will be discussed in the following subsection.

Table XXXII presents the results for the four fire models shown in Figure 39. The nominal fire results are similar to those described above for single layer fabrics. By assuming a ramped buildup to maximum flux for the first second, the "hot" Natick profile, some improvement is obtained in that the depth of injury is reduced from 450 to 250 μm, but the injury level is still greater than threshold epidermal injury. By reducing the peak flux level to 3.65 cal/cm²sec to represent the heating profiles measured in recent Natick tests, injury is reduced slightly below the threshold level.

This latter result indicates that, basically, any fabric which can maintain a gap between itself, as a single layer, and the skin and which does not react with the environment, has the potential for providing sufficient protection in the cooler Natick type fire. Variations in optical and thermal properties among fabrics may result in greater or lesser injury; however, the point is, subthreshold injury is possible for single layer fabrics in Natick type fires. Clearly, for multilayer assemblies which are dimensionally stable, injury will be substantially subthreshold with the cooler Natick profiles. The results of the Natick test show that there are large variations in heating over the total suit area. Some are to show large burn damage; others show no damage, demonstrating the large variation in heating which can exist within a given fire.

Finally, by increasing the fire duration to 6 seconds and using the lower maximum flux of 3.65 cal/cm²sec, injury of the epidermis occurs in 3.5 seconds and the dermal layer is totally destroyed to over half depth. A stable fabric with an underlayer of cotton is capable of providing subthreshold protection for this exposure as shown by the final table entry.

6.2.3.2 Fabric Property Variations

As stated above, a single layer of stabilized, 5.2 percent moisture regain fabric is used to provide a comparison for fabric property variations. In

TABLE XXXII

FIRE MODEL VARIATIONS*

Fire Model	Total Exposure (cal/cm²)	$t_{\Omega=1}$ (sec)†		$D_{\Omega=1}$ (μm)	Total Skin Heating (cal/cm²)	
		Base of Epidermis	Base of Dermis		max	θ=3.0
3.0 sec Standard Fire Maximum q = 4.65 cal/cm²sec	11.6	2.1	∞ (.000)	450	3.1	2.15
3.0 Natick Fire Profile Maximum q = 4.65 cal/cm²sec	9.3	2.75	∞ (.000)	250	2.55	1.67
3.0 sec Natick Fire Profile Maximum q = 3.65 cal/cm²sec	7.3	∞ (0.691)	∞ (.000)	85	2.06	2.06
6.0 sec Natick Fire Profile Maximum q = 3.65 cal/cm²sec	14.6	3.5	∞ (.086)	1200	4.6	3.75 (θ=6.0 sec)
Stabilized Fabric/ Cotton 6.0 sec Natick Profile	14.6	∞ (0.755)	∞ (.000)	70	2.66	0.87 (θ=6.0 sec)

* The basic fabric model used is a single layer of stabilized fabric with initial gap of 0.5 cm.

† If Ω<1, value of Ω is given in parentheses; the symbol ∞ indicates that total injury did not occur at this depth.

addition, the hotter (4.65 cal/cm^{2}sec) Natick profile defines the baseline exposure. Table XXXIII includes results for several property variations of possible importance relative to the improvement of materials. The baseline case results in a threshold injury at 2.75 seconds and a penetration depth of 250 μm.

Finally, the moisture content is increased by 100 percent from 5.2 to 10.4 percent by dry weight. Interestingly, the improvement is not very great; total heating is reduced only 4 percent and injury depth is reduced only 60 μm to 190 μm. Peak temperature at 100 μm depth is reduced 2°C which in turn reduces the damage rate $d\Omega/d\theta$ by 50 percent.

The effect of increasing the fabric thickness by 50 percent while maintaining the same bulk density which also increases the mass per unit area and the conductive resistance across the fabric by 50 percent, is to reduce the injury to slightly subthreshold with a penetration depth of 85 μm. Note that the total heating has not been changed, but that heating at 3.0 seconds has been reduced by 20 percent, i.e., the additional mass has the effect of spreading out the heat load. Peak temperature at 100 μm is reduced by 8°C which is an order of magnitude reduction in injury rate. The improvement results essentially from the increase in mass since the conductive resistance across the fabric is small relative to the heat transfer resistance across the gap. This means that the same results can be achieved by increasing the mass while maintaining the same thickness.

Variations in optical properties indicate that significant improvement can be achieved by reducing absorptance and transmittance. In two cases the sum of fabric absorptance and transmittance was held fixed while the transmittance was increased and reduced by a factor of 2. Clearly, it is desirable to minimize transmittance. This is one reason why multiple layers offer improved protection, i.e., the direct transmittance to the skin is reduced to a negligible amount. For the baseline case about 40 percent of the heating during the first 3 seconds is due to direct transmittance. For single layer cases, the analysis is somewhat conservative in assuming all direct transmitted energy to be absorbed at the surface (see Section 3) so that injury at 100 μm for stable fabric cases will be somewhat less than predicted although depth of penetration, if well into the dermal layer, is not significantly affected by in-depth absorption.

In the final case, both α and τ were reduced by 20 percent with a net effect nearly equal to that of increasing the mass by 50 percent. Note that total heating is actually less than that for the mass increase case, but because the heating is more concentrated in time for the decrease in $(\alpha + \tau)$ case, the injury to the epidermal layer is greater.

TABLE XXXIII

FABRIC PROPERTY VARIATIONS* - NATICK FIRE MODEL (11.6 cal/cm^2)

Parametric Condition	$\theta_{\Omega=1}$ (sec)†		$D_{\Omega=1}$ (μm)	Total Skin Heating (cal/cm^2)	
	Base of Epidermis	Base of Dermis		Max	θ = 3.0
Baseline: 5.2% Moisture	2.75	∞ (.000)	250	2.55	1.67
100% Increase Moisture from 5.2 to 10.4%	3.0	∞ (.000)	190	2.45	1.57
50% Increase in Thickness and Mass	∞ (.753)	∞ (.000)	85	2.57	1.37
100% Increase in τ from .101 to .201; (α + τ) the same	1.9	∞ (.000)	450	3.12	2.26
50% Decrease in τ from .101 to .50; (α + τ) the same	3.9	∞ (.000)	150	2.22	1.32
20% Decrease in α and τ	∞ (.856)	∞ (.000)	95	2.10	1.26

*The basic fabric model used is a single layer of stabilized fabric with initial gap of 0.5 cm. This case was selected since it results in approximately a threshold epidermal burn and thus will provide sensitivity for comparison of parametric variations.

†If Ω < 1, value of Ω is given in parentheses; the symbol ∞ indicates that that injury did not occur at this depth.

SECTION 7

EXPERIMENTAL EVALUATIONS OF FABRICS

To provide a basis for comparison to verify the validity of fabric model results, laboratory scale evaluations and full scale JP-4 fuel fire pit tests were conducted by the Air Force using the three fabrics, Nomex, PBI and stabilized PBI. This section presents a brief description of the tests, a summary of the results and a comparison of the analytical and experimental findings. All of the evaluations described in this section were conducted as in-house programs by the Air Force Materials Laboratory under the direction of Mr. Robert Stanton.

The fabric model was designed primarily as a tool to be used in the identification of fabric design parameters that are most critical in providing thermal protection against direct flame exposure. These parameters are evaluated against a nominal definition of a fire environment and physical description of a clothing ensemble including, e.g. well defined gaps. In actual experience, fires and dimensions will not be so "ideally" behaved, consequently, the model is not expected to predict the performance of a particular test which is subject to temporal variations of many of the parameters. Therefore the approach will be to compare results only to see if the same relative differences exist between the fabric model results, the laboratory heat transfer data, and the full-scale fire pit evaluations of the same three fabrics. In order to evaluate the effects of moisture on the thermal protection characterisitcs of the fabrics, a series of laboratory tests were conducted by AFML. These tests are described in Section 7.1.

7.1 LABORATORY EVALUATION

7.1.1 Test Technique

Fabrics were exposed to a JP-4 fuel fire in the configuration shown in Figure 45. The average heat flux was 2.6 cal/cm^2-sec and each exposure was 3 seconds in duration. The exposure time was controlled by a solenoid activated shutter with an opening and closing time of 0.1 seconds. The fabric to be evaluated is mounted with an initial .05 cm air gap between the fabric and the sensor. The exposed area of the circular fabric sample is 4.5 in^2 (24.6 cm^2). The burner has a circular cross-section with a 2 in. (5.1 cm) diameter. The heat flux profile across the sample surface is at its maximum of 2.6 cal/cm^2-sec at the edge to within approximately 0.5 in. (1.3 cm) from the center where the heat

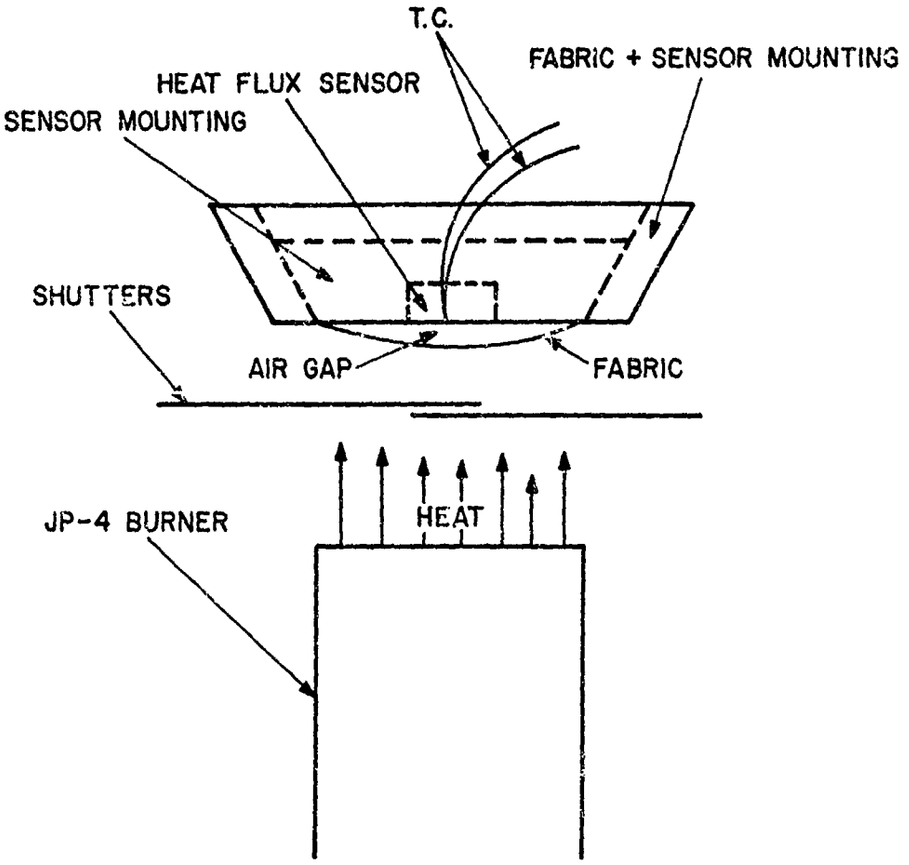

Figure 45. Laboratory Heat Transfer Device

flux level drops to 2.1 cal/cm^2-sec. During a given exposure energy delivered to the sample remains constant within ± 0.1 cal/cm^2. The burner consists of a fuel reservoir within the burner barrel shown in Figure 45. An air plenum below the fuel reservoir feeds a constant supply of air to the fuel bed surface through stainless steel tubes that project up through to the fuel surface

The heat transmission through the fabric absorbed at the surface of glass/epoxy, Teflon "S" coated total heat flux transducer is determined by measuring the thermal response with a copper/constantan thermocouple imbedded 6 mils (0.015 cm) beneath the surface. The temperature-time profile is then input into an Aerotherm, one-dimensional heat transfer code which first solves for the absorbed heat flux and then, using the skin thermal and burn assessment model described herein, predicts the thermal and injury response of human skin.

Experiments conducted with the laboratory device are static experiments in that the fabric is stationary and air flow around the heat sensing device is blocked by the sample mounting configuration. The effect of the fluid mechanics between the sensor and fabric upon the heat transfer is investigated briefly in the following section.

7.1.2 Results of the Laboratory Evaluation

The laboratory fabric exposures were based on a nominal Natick fire of 2.6 cal/cm^2-sec or a total heat load of 7.8 cal/cm^2. It is recognized that this exposure level is below that of the fabric computer evaluation, however only relative differences between the fabrics will be examined. The results of The laboratory evaluation are given in Table XXXIV. The laboratory evaluation showed the same ranking of the three fabrics which the fabric model predicted. Nomex and PBI fabrics allowed complete destruction of the epidermis while stabilized PBI provided complete protection. The degree of damage predicted by the model was more severe than that indicated by the laboratory test data, which is explained by the more severe exposure conditions used in the computer evaluations. There appears to be one major difference between the model predictions and the laboratory data, which is evidenced in the resultant time versus temperature profiles shown in Figure 46. The Nomex shrank to the sensor in 1.2 seconds, as indicated by the rapid change in temperature response. PBI shrank to the sensor in 2.4 seconds indicating a 1.2 second difference in shrinkage time for the two fabrics compared to the 0.2 seconds predicted (0.8 second for Nomex, 1.0 for PBI).

There are two probable explanations for the differences in shrinkage times. First, since the heat flux levels are different (4.65 cal/cm^2-sec in the model to 2.6 in the test), the fabric temperature rise is much faster in the prediction,

TABLE XXXIV

AIR FORCE MATERIALS LABORATORY DATA
HEAT TRANSMISSION THROUGH FABRICS
JP-4 Fuel Fire - Average flux 2.6 cal/cm²sec - 3 second exposures

Fabric	Percent Moisture Regain	Ω at 100μ at End of Exposure	Time to Ω = 1 at 100μ sec	Total Heat Btu/ft²	(Cal/cm²)
Nomex	5.5	218.0	2.0	12.3	(3.33)
PBI	12.0	20.0	3.6	10.4	(2.82)
PBI	0.0	54.3	2.9	10.3	(2.79)
Stabilized PBI	13.2	0.0	---**	5.4	(1.46)
Stabilized PBI	0.0	0.1	---**	6.8	(1.85)
Nonshrinking* Fabric	5.5	0.3	---**	8.6	(2.33)
Nonshrinking* Fabric	0.0	1.1	7.7	10.7	(2.90)
Nonshrinking Fabric	5.5	0.1	---**	6.7	(1.82)
Nonshrinking Fabric	0.0	1.3	6.5	8.9	(2.41)

* Test conducted with holes in sensor to allow flow between fabric and sensor.

** Injury would not occur.

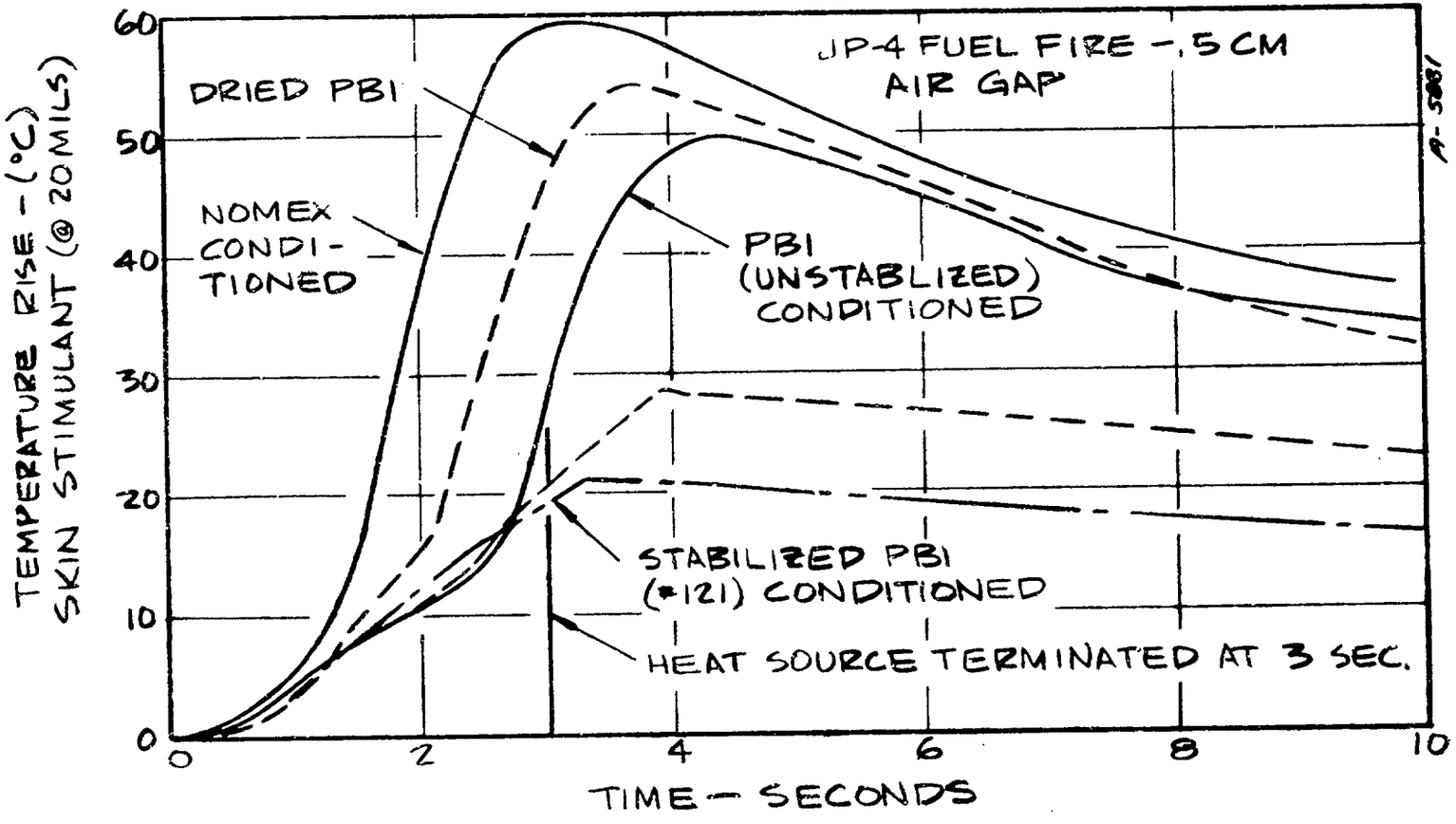

Figure 46. Temperature Response of Skin Simulant Covered by Various Fabrics Exposed to JP-4 Flame (Air Force Materials Laboratory Data)

leading to the earlier shrinkage times. In addition, the rate of change of fabric temperature as the fabric temperature reaches the shrinkage level is considerably greater for the prediction because the radiation equilibrium temperature is higher (830°C at 4.65 cal/cm^2-sec versus 680°C at 2.6 cal/cm^2-sec with shrinkage temperatures of 320°C for Nomex and 400°C for PBI). Thus at the lower flux level, the PBI will require greater time to reach the shrinkage temperature and the difference in contact time between the two fabrics is amplified (see sketch).

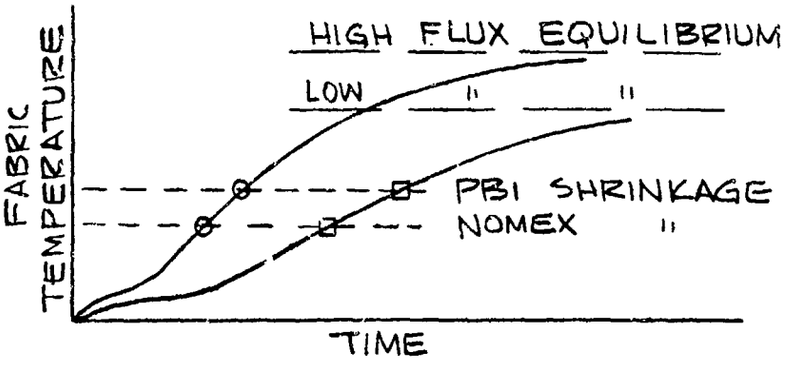

Effect of Incident Flux on Shrinkage Time

The second reason is that the amount of regain moisture in the PBI tends to suppress the early response to a greater degree than predicted since the water is not completely vaporized at 100°C. This effect was shown and discussed in Section 5.4. Finally, it must be pointed out that the temperature traces of Figure 46 lag the surface response since the thermocouple is 6 mils deep in a low conductivity material; thus, several tenths of a second delay are expected.

7.1.3 Effect of Fabric Moisture

To help clarify the effect of fabric moisture on heat transmission through fabrics, two test cases were evaluated. The first five samples were run dry (placed in a circulating air oven for two hours at 104°C). The second set of five fabrics were conditioned for forty-eight hours at 65% relative humidity and at 72°F (28°C) and were exposed exhibiting 12% moisture regain. The results are shown in Figure 46. Due to the lack of moisture, the dried PBI fabric shrank to the sensor surface in 1.8 seconds as compared to the conditioned sample which shrank in 2.6 seconds. Thus the moisture delayed the shrinkage process. The same analysis was conducted with stabilized PBI and the conditioned samples showed considerably more protective capability than did the same fabric in the dried state. Neither stabilized sample shrank to contact the sensor. The resultant data

from these evaluations are provided in Table XXXIV. In each case, the conditioned samples allowed less damage to occur by blocking more heat indicating that in those tests the bulk of the energy absorbed by the moisture in evaporating flowed from the fabric to the external environment. Thus in this situation data indicate that moisture aids the thermal protective qualities of a fabric.

To further investigate the effects of moisture, and more closely identify with the analytical effort, a nonshrinking, fabric with a moisture regain of 5.5% was evaluated in the laboratory device in the dry state and conditioned. The test set-up was the same as previously defined, except that gas flow between the sensor and the fabric was allowed by drilling holes in the sensor housing. This was done to provide a more realistic model of the fluid mechanics of a moving system. The results of the above evaluation are shown in Figure 47. Initially the conditioned sample yields moisture which adds heat to the sensor from about 0.5 to 1.5 seconds as shown by the more rapid rise in temperature for the conditioned sample than for the dried sample. After 1.5 seconds the moist sample appears to be superior due to the lower fabric temperature resulting from the moisture vaporization. Table XXXIV indicates that both total heating and injury are predicted to be less for the sample with 5.5% moisture. The final two entries in Table XXXIV are for the nonshrinking fabric without the holes in the sensor housing. Total heating values are reduced by approximately 20% as compared to the same tests with holes. However, it is noted that this reduction occurred for both the moist and dry samples implying that a mechanism other than water vapor condensation was involved, e.g., loss of the stagnation volume which may support the gap for the no hole case. The total heating value of 5.5% by dry weight of water in a 4.4 oz/yds^2 material is about 1.7 Btu/ft^2 (0.4 cal/cm^2) which is the order of the difference in total heating between moist tests with and without holes, (1.9 Btu/ft^2), but since the difference between dry tests is 1.8 Btu/ft^2, it appears that the effect of the moisture condensation is small.

Since in tests both with and without hole the presence of moisture reduces the total heating and resulting injury, the presence of moisture apparently provides increased thermal protection. However the experimental results are incomplete in that it is not clear that the tests properly represent the real situation since quantifying the real situation is difficult (dimensions of flow passages and time variations). These experiments do point out the need to model both the fluid mechanics and thermodynamics in both the analytical and experimental investigations.

7.2 POST CRASH FIRE EVALUATION

Simulated post crash fire exposures of the three fabrics were conducted at the U.S. Army Natick Laboratories in Natick, Massachusetts. The tests were conducted for the Air Force Materials Laboratory by Mr. Earl T. Waldron of Natick Labs.

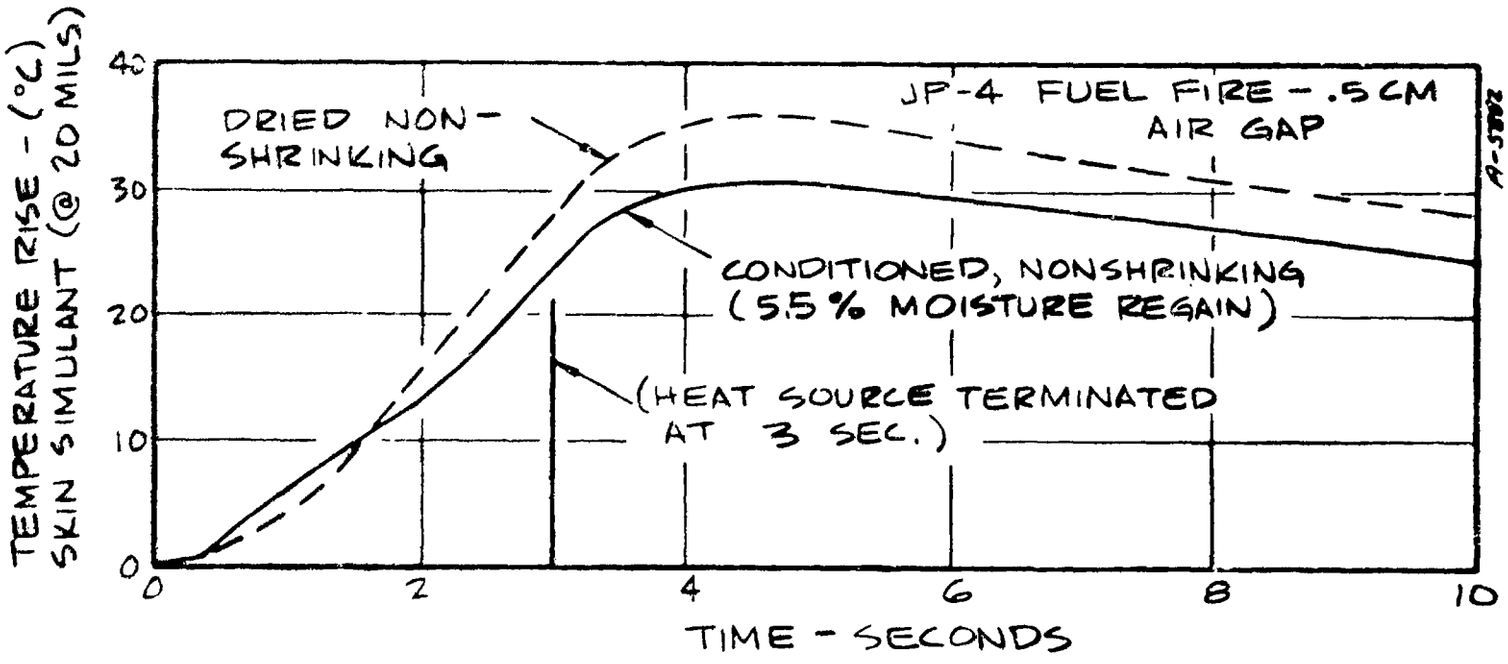

Figure 47. Effect of Moisture Regain on Simulant Response
(Air Force Materials Laboratory Data)

7.2.1 Test Procedure

Mannikins clothed in the candidate fabrics were exposed to a nominal 3 second fire. The test set-up is shown in Figure 48. The front suit in the figure is Nomex and the rear suit is PBI. Twenty-five gallons of JP-4 fuel is used for each fire. The mannikins are moved through the fire at 10 feet per second across the 30 foot pit length. The mannikins enter the fire pit through a set of doors at the front of the pit which are used to prevent pre-exposure of the suits while the fire is building to its peak intensity. Upon exiting the fire pit the mannikins are protected from post-exposure by a spray of water. The mannikins are dressed in standard cotton boxer shorts, cotton t-shirts, flight suits made from the candidate fabric and Nomex gloves and booties. Damage incurred by the mannikins is measured by temperature sensitive tapes at 61 locations throughout the mannikin torso. When the paper tapes attain a temperature of 221°F, a burn is indicated. A more thorough description of the test is provided in Reference 71. The evaluations included thirty suits made from each fiber type.

The paper tapes used in the fire pit evaluation were examined for burn prediction accuracy. To check the validity of the tapes, experiments were conducted using the test configurations shown in Figure 49. First, the time to trip the tapes at the 221°F level was determined by exposing configuration A to the quartz lamp/meker burner combination. Time to trip the tapes was also established using the JP-4 burner. Once these times were established the experiments were rerun with a heat flux sensor in place of the paper tapes, and the exposure time required to cause a second degree burn ($\Omega = 1.0$ at 100μ) was established. The exposure times required to trip the 221°F tape indicator also were measured with the tape covered by a fabric. As shown in configuration A, the tape damage indicator was placed on a section of a mannikin used in the Natick fire pit test. Under normal test conditions at Natick, the mannikin substrate would have an air backing as was the case for the lab experiments. The mannikin section was circular with 3.8 in^2 (24.5 cm^2) surface area. For configuration B, a heat flux sensor developed by Aerotherm was used to measure the incident heat flux that would be seen by the underlying skin. The skin-burn injury computer model was then used to determine the resultant burns. The results of this evaluation are shown in Table XXXV. Each data point is an average value for five tests. For the paper tapes, exposure time was increased until a trip was indicated. The indicated trip time was then used for five exposures and in all five cases a trip occurred. Exposure time was then decreased by 0.1 seconds and five more test conducted for each fabric and energy source. With the exposure time decreased by 0.1 seconds, 18 out of 20 exposures indicated indicated no burn while in two instances the tapes were tripped. These data indicate that the burn predictions of the paper tapes are reproducible. For the

Natick Fire Pit Test

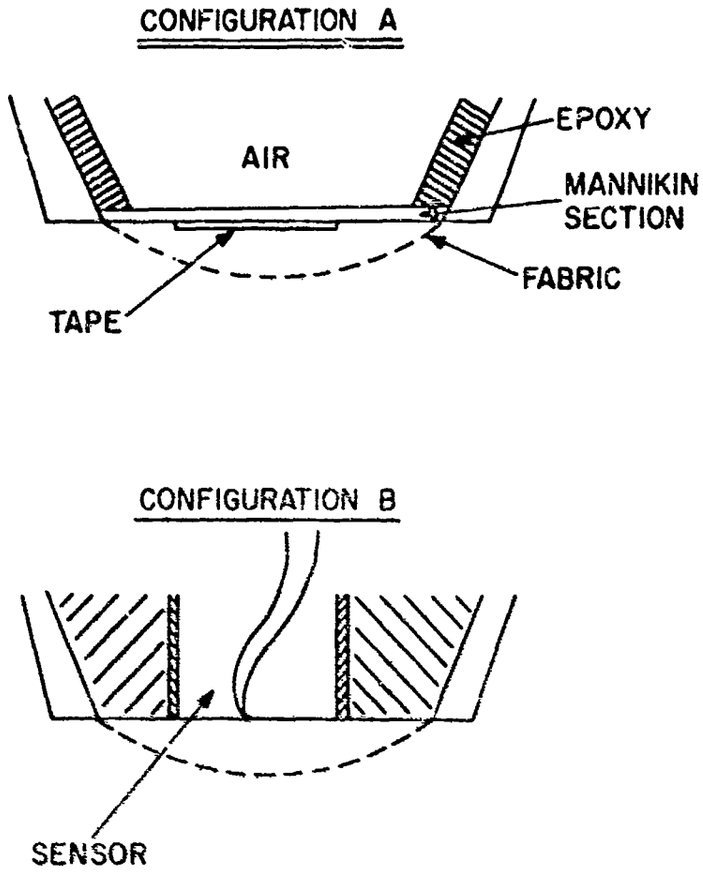

Figure 49. Test Configurations for Paper Tape Sensor Calibration

TABLE XXXV

COMPARISON OF RECORDED BURN DAMAGE AND BURNS INDICATED BY NATICK TAPES

Fabric	Source of Energy (2.1 cal/cm²sec)	Exposure Time Required to Indicate a Burn by Natick Paper Tapes (seconds)	Exposure Time to Cause a 2nd Degree Burn as Measured by Heat Flux Sensor (seconds)
PBI, Stabilized	Quartz Lamps & Meker Burner	4.0	4.2
Nonshrinking Fabric	Quartz Lamps & Meker Burner	3.9	3.8
PBI, Stabilized	JP-4 Burner	5.9	6.0
Nonshrinking Fabric	JP-4 Burner	4.9	5.0

five exposures with each fabric and energy source recorded with the heat flux sensor, data points along the five time temperature curves were within several degrees centigrade. The net effect on the resultant total heat absorbed for each test indicated 3.0% variation in the actual data. The results of the evaluation demonstrate excellent correlation between the burn indication of the Natick paper tapes and burns predicted from recorded time-temperature profiles.

7.2.2 Results of the Fire Pit Analysis

The results of the fire pit analysis are given in Table XXXVI. The relative ranking of the three materials for thermal protection are the same as indicated by both the fabric model and the laboratory evaluation. On the average Nomex allowed the greatest amount of body area damaged. Nomex consistently continued to burn upon egress from the fire. PBI flight suits exhibited a marked improvement over Nomex for thermal protection while the stabilized PBI fabrics were superior to both Nomex and PBI. The Nomex suits were also found to fall away from the mannikin and form large holes throughout the suit while both the PBI and stabilized PBI fabrics remained intact.

As the fabric model predicted, stabilized PBI provided the best protection, because it did not break apart nor did it shrink, and it did not exhibit any afterflaming. In the fabric model the PBI fabric was found to shrink to contact with the skin, as was the case in the fire pit test. As a result the unstabilized PBI provided less protection than the stabilized PBI. The lack of protection provided by the Nomex fabric was demonstrated to be due to severe afterflaming, lack of fabric integrity and shrinkage of the fabric to the skin. From the above results it is evident that efforts should be directed to use nonflammable, non shrinking and thermochemically stable fabrics in all Air Force flight suits. Of the fabrics considered in this report stabilized PBI is clearly superior in satisfying these objectives.

TABLE XXXVI

NATICK FIRE PIT TEST RESULTS

25 Gallons of JP-4 Fuel - Average 2.76 Cal/cm^2- sec

Fabric	Average* Percent Body Area Damaged
Nomex	49.8
PBI	28.4
Stabilized PBI	11.4

* Average of 30 suits (tests) per fabric.

SECTION 8

CONCLUSIONS AND RECOMMENDATIONS

8.1 CONCLUSIONS

The analysis effort performed has considered in detail the in-depth thermal response of various fabrics when exposed to JP-4 fuel fire heating environments. The results presented have identified many of the important parameters in a fabric skin system which provide improved protection against skin burn damage. The investigation has also pointed out where additional analysis and testing are required in order to develop a more complete and accurate fabric analytical model. The effort described herein has followed a path in which first the many parameters of importance have been identified, then an analytical model was developed which included these parameters, and finally analysis was performed to define the relative importance of each identified parameter. The analytical model results were then compared to laboratory and field test results and areas identified where analytical model and tests show differences.

The investigation into the parameters of interest included the following areas:

- Skin thermal-optical properties and burn damage assessment
- JP-4 fuel fire thermal chemical environment
- Fabric thermal-mechanical-optical properties

These investigations have indicated some important conclusions which are independent of the parametric analysis results and are summarized below.

Skin Model and Burn Assessment

- The assumed model for the skin will have no effect upon the thermal response of the fabric cover.
- The burn damage analytical model developed by Henriques and modified by Stoll seems to be the best model available for damage assessment.
- The thermal capacity of the skin (ρc_p) is very near that of water.
- The thickness of the skin layers is critical when determining burn damage.

- The reported literature shows extensive variations in measured skin thermal conductivities.
- Human skin when covered by a fabric layer exhibits relatively high absorptance and emittance to radiation from the fabric.

Fuel Fire Environment

- The chemical environment of the JP-4 fire is relatively inert with only small amounts of oxygen present.
- The fuel fires are in general fuel rich with accompanying large amounts of carbon particles.
- The heating from the fire is predominately radiant with up to 30 percent of the heating coming by convection.
- Due to the large path lengths and appreciable soot concentrations the fire radiates as a black body.

Fabric Properties

- The porosity of the fabric limits the amount of energy that can be transferred to the skin from the hot fuel fire gases by convection to an insignificant level.
- The shrinkage data indicate that both Nomex and PBI shrink to contact with the underlying skin during a nominal (11.6 cal/cm^2) fire while stabilized PBI does not attain high enough temperatures to allow shrinkage to occur. For Nomex, PBI and stabilized PBI 10% shrinkage occurs at fabric temperatures of 330°C, 410°C and 660°C respectively. Since the fabric temperature does not exceed 600°C, stabilized PBI is the only fabric evaluated that maintained the protective air gap between the fabric and skin.
- For an 1800°F black body source, exhibiting properties of a JP-4 fuel fire, the optical property data indicate that stabilized PBI fabrics have lower direct transmission compared to Nomex and PBI but that reflectance values are both higher and lower depending on the material and the state of the material. In general these differences appear to be minor in the comparison of predicted results with the exception of the improvement due to lower transmittance.
- The fabrics considered, consisting of fiber and air, seem to have specific heats which are near the solid material.
- The thermal conductivity of the fabric is determined mainly by the amount of air voids. As the air voids increase the thermal conductivity is reduced.

- Fabrics containing moisture (5 to 14%) have a thermal protection advantage as compared to dry fabrics.

In addition to these conclusions about the parameters of interest the following general conclusions relative to any fabric-skin system have been identified.

- The environment heating level and duration are of primary importance in the determination of burn severity.
- Multiple layers of fabric provide substantial improvements in protection even for fabrics which shrink; however, the realization of this potential requires the maintenance of the air gaps.
- Increased fabric thermal capacitance provides improved protection by spreading the heating pulse to the skin over a longer time thus lowering peak temperatures.
- Fabrics with low transmission or high reflectance in general will provide better protection by isolating the skin from the flame environment.
- Fabric thermal conductivity has a small effect upon burn damage due to the small thicknesses which result in small temperature differences across the fabric layer if gaps are maintained. That is, the air gaps provide the dominant resistance to conduction.
- Fabrics which are dimensionally stable provide much improved protection over fabrics which shrink and bring hot material in contact with adjacent fabric or skin layers. The air gap between the fabric and the skin is an important parameter to the ultimate protection provided. Reduced air gaps substantially increase the heat to the skin.

The materials studied in the analysis included PBI, Nomex and stabilized PBI fabric. The first two materials, as shown by the shrinkage results of Section 5, exhibit considerable dimensional change at relatively low temperatures while the stabilized PBI is stable to temperatures in excess of 600°C. This characteristic of stabilized PBI enables it to demonstrate a much better protection potential compared to PBI and Nomex. Dimensional changes in which the material shrinks to a level where gaps are reduced to near zero, limit the protection by bringing hot fabric in contact with the skin or adjacent fabric layers and by reducing the resistance to external heat flux provided by the air gaps. Moisture in the fabrics tends to delay the onset of fabric shrinkage.

The analytical results also show that neither PBI fabric exhibits any potential for combustion when exposed to the air environment at elevated temperatures but that the Nomex, if equilibrium chemical reactions are assumed,

shows a potential for combustion or burning. Around 550 to 600°C stabilized PBI did not combust when equilibrium reactions were considered.

Summarizing the results of the three fabrics exposed to the nominal fire (11.6 cal/cm^2), it can be stated that:

1. Single layer Nomex and PBI both cause serious burns exceeding total dermal injury due primarily to shrinkage of the fabrics. However, the results of the analysis suggest that the greater moisture content of PBI provides a thermal protection assist; this contention is supported by the results of the laboratory tests which show improved protection with the moist sample compared to the dry even when flow between the sample and simulant was allowed. Also, PBI does not ignite and is stable at higher temperatures than Nomex, therefore, it is concluded that PBI would provide better protection than Nomex for the following reasons:

   - Nomex ignites where PBI does not.
   - The Nomex tends to shrink at a temperature approximately 100°C below that of PBI. This characteristic would allow better protection with PBI in fire environments where the heating levels are lower than that considered in this analysis.
   - Laboratory tests and the Natick tests have shown that if the Nomex material is heated above 400°C to 450°C and is restrained from shrinking, the material will fail structurally resulting in total loss of coverage. This, in turn, can lead to higher probability of combustion of the surrounding fabric due to stronger coupling to the environment and less to the skin.

2. An outer layer of Nomex or PBI over an inner layer of cotton reduces the injury, but it is still a serious dermal injury (~1.5 mm deep) again primarily due to shrinkage. These results do not allow for breakage of the outer fabric, which has been found to occur for Nomex at temperatures 50°C to 100°C below those predicted. Such failure will clearly result in a more serious burn at the point of failure than predicted and creates a potential for the fabric to ignite and propagate the damage to other regions. In addition Nomex, assuming equilibrium reaction between pyrolysis gases and air was found to afterflame in the prediction. This is a worst possible reaction assumption; however, the result is consistent with Natick test observations.

3. PBI and stabilized PBI did not ignite in any of the predictions.

4. A single layer of stabilized PBI provides significant improvement compared to Nomex and unstabilized PBI due to its dimensional stability. Injuries are limited to approximately a 0.4 mm penetration of the dermis, for a nominal 11.6 cal/cm^2 fire exposure.

5. Multilayer assemblies with stabilized PBI provide complete protection.

The analysis studied the effects of the fire environment on the burn damage using a 5% water, stabilized fabric as the baseline. These results confirm that with reduced fire environment, burn damage is reduced dramatically. By reducing the fire from the standard model (11.6 cal/cm^2 total) to a Natick profile with the same peak heating (9.3 cal/cm^2) and then to a Natick profile with a peak heating consistent with recent heat flux measurements on Natick fires (7.3 cal/cm^2), injury for a single layer of fabric was reduced from an 0.5 mm penetration of the dermis to a subthreshold epidermal injury. Thus, it is quite possible, due to the large variation in heating from fire to fire and within a fire (level above surface, direction etc.), to find adequate protection afforded by single layer fabrics. If the heating is at a low enough level such that PBI and Nomex do not reach shrinkage temperatures, they also will provide adequate protection. However, it should be noted that the exposure level must be much lower for Nomex than PBI because of the 100°C difference in shrinkage temperatures.

8.2 RECOMMENDATIONS

The following list of recommendations are provided to define additional tasks that should be performed in order to improve the developed capabilities to evaluate various fabrics relative to their ability to provide protection when exposed to aircraft crash fires. The proposed additional tasks would also allow identification of potential areas for fabric improvement in order to porvide better fire protection. The recommendations are divided into the three major areas of investigation skin, fire, and fabric.

Skin Properties and Damage Assessment

1) Tests should be performed to verify the proposed skin model at conditions which simulate actual temperature-time histories experienced when the fabric-skin system is exposed to fuel fire environments. These tests can be performed, for example, using an electrically heated plate in conjunction with radiometric skin surface temperature measurements. The tests can be designed such that uncertainties in optical properties of the skin are eliminated.

   Such tests would eliminate many of the questions and uncertainties found among the available burn injury data associated with the use of high temperature sources (to which the skin is not opaque) and to step function, heat flux exposures.

2) Burn damage assessment should be determined as a function of location on the body. As has been indicated, thickness and thermal conductivity of skin are both a function of the particular subject and body location. The determination would allow assessment of burn damage for a given exposure at various locations on the body, thus providing a means for evaluating the protection requirements as a function of body location.

Fire Environment

1) The question of the level and make-up of the heat flux from fires continues to be of concern. It is recommended that additional and highly relevant data be obtained by running the instrumented mannikin uncovered through several fires. This would provide a considerable quantity of data covering effectively all directions within the fire.

2) In addition to providing more data, a more extensive investigation of existing data is recommended, particularly in the evaluation of the adequacy of certain instrumentation. For example, it appears that some data used to establish the relative magnitude of convective and radiative flux may be misleading because of the size of the sensor, i.e., the convective heat transfer coefficient is considerably higher for small objects. This is the primary reason for recommending a nude mannikin test which provides the proper scale for convection.

3) With mannikin heat flux data from actual pool fires now available, it is recommended that these data be evaluated in order to improve the nominal description of a pool fire for analytical evaluation of fabrics and to add to the collection of knowledge required to perform the other recommended tasks related to the flame environment and the fire model.

4) The development of the JP-4 fuel fire environmental model has pointed out the important features of these fires and the controlling parameters on fire temperature. The investigation has indicated that it might be quite fruitful to extend the efforts in order to better define parameters which can and should be controlled in order to develop fires which are more repeatable. The two most important parameters identified are:

   - Fuel mass flux
   - Entrainment and mixing

The fuel mass flux is controlled by many parameters which can be modeled by extending the work described. A few of these parameters are: fuel bed temperature, fuel heat of vaporization, energy loss to fuel container. All of these parameters can be modeled quite easily analytically and the importance of each can be identified.

The entrainment and mixing phenomena will depend primarily upon:

- Wind velocity
- Turbulence and buoyancy.

These characteristics can be modeled in detail as well. Control of entrainment can be implemented, for example, through the use of screens or other turbulence controlling systems.

The results of these analytical investigations would be the identification of the important controllable parameters and the specification of an experimental program to measure and control these parameters.

Fabric Thermal Modeling

1) A test facility should be constructed to provide a satisfactory method for screening and evaluating fabrics at a level prior to building up flight suits and running full-scale fire tests. This facility will be subscale, similar to the shrinkage test facility developed at Aerotherm, but will include the capabilities to provide 1) a radiant spectrum and intensity equivalent to that of a fuel fire, 2) hot gas convection over the fabric, 3) a pressure gradient across the fabric to investigate blow through and vapor deposition on, 4) an instrumented skin simulant, and 5) continuous front and back fabric surface temperature measurements using a radiometer as in the existing Aerotherm facility. In summary, this facility would enable a more detailed investigation of the various heat transfer machanisms, as well as a means to compare and screen fabrics at a laboratory level in a well simulated environment.

2) Studies to date indicate that one of the most important factors is the optical nature of the fabric. Since a significant portic of the heat flux at the outer surface is radiative, an obvious goal would be to reduce the absorption characteristics of the fabric. Thus, it is recommended that additional investigation be made into understanding the interaction between the radiant spectrum and the fabric; to determine what effect weave, color, material, etc. have upon

absorption and transmission of radiant energy and to seek to identify ways to reduce the absorption of radiation in the predominant wavelengths of the fire.

3) Other materials might offer promise as fire protective fabrics. The general computing capability developed under the present program can be used to evaluate the ability of numerous candidate materials to resist thermal degradation and oxidation. An analytical screening survey could identify promising hydrocarbon materials (expected to be such high carbon polymers as pyrrone and polyphenylene). If desired, non-hydrocarbon refractory fibers could also be considered.

   This effort could be performed to evaluate thermal properties along with the generally desirable fire/fabric properties. Efforts could be performed in combination with fiber experts such that, not only thermal but other important items are considered and evaluated.

4) An analytical model has been developed which shows potential for prediction of fabric flammability for various fabrics exposed to various environments. It is suggested that this model be extended to include all the important chemical variables, and that testing be performed to define more exactly the quantities required in this analysis.

5) The fire environment defined by the mannikin testing can be used to evaluate the effect of enviroumental heating on various fabric. The actual test data can be used to define heat flux levels and time profiles for determination of the effects of various fire levels on individual fabric. These analytical results can then be directly related to fire pit results where many data have been obtained.

6) Tests should be run to quantify more completely the point of fabric breakage with level of temperature and strain. This test can be performed quite readily in the sample test facility used in this investigation to obtain fixed in position within the facility and temperature at which breakage occurs can be measured with various levels of tension and relaxation in the material.

7) The chemical composition of the materials used in the analysis can be changed to consider other potential fabric candidate compositions. TGA data along with chemical composition can be used to define the effects upon performance of material type.

8) Radiation properties for the fabrics of interest should be measured as a function of temperature to define these quantities more completely for the analytical model. In the investigation performed,

these quantities were measured only at room temperature and under a semi-charred state. The variations in proceeding from the virgin to the fully charred state should be known in order to define completely the fabric response.

9) A more detailed parametric study should be performed in which detailed fabric parameters are evaluated with the emphasis placed upon definition, fabrication, and test of alternate fabric designs. Parameters of interest would be weave, thickness, radiant properties, chemical composition, porosity, etc.

APPENDIX I

EXCERPTS FROM TRW FABRIC OPTICAL PROPERTY TEST REPORTS

I.1 MEASUREMENT METHOD FOR NOMEX AND PBI

I.1.1 Transmittance

Preliminary measurements indicated that the transmittance of both virgin samples (nomex and PBI) was primarily diffuse even out to wavelengths of 13 microns. Since standard integrating sphere coatings go black beyond about 2.5 microns, this convenient method of collecting and measuring the diffuse transmitted energy could not be applied at wavelengths greater than 2.5 microns. Measurements in the beyond 2.5 microns on the virgin samples were therefore made on a bidirectional basis; i.e., the sample was irradiated in the normal direction from one side while transmitted energy was measured one angle at a time on the other side. The resulting spatial distribution for each of several wavelengths was integrated arithmetically over the 2π steradian solid angle assuming geometric symmetry, to obtain the spectral transmittance (beyond 2.5 microns) distributions for virgin nomex and virgin PBI.

Since the charred samples were only slightly transparent beyond 2.5 microns, a simpler approximation - - still based on bidirectional measurements but without formal spatial integration - - was used.

The spectral transmittance distributions in the region of 0.5 to 2.5 microns were obtained from measurements made on a Beckman DK2A spectrophotometer with the sample placed in the beam at the integrating sphere entrance port. Energy reflected from the sample was thus kept out of the sphere, and only transmitted energy was integrated.

I.1.2 Reflectance

Spectral reflectance (ρ_λ) in the 0.5 to 2.5 micron wavelength region was determined for each of the samples by subtracting τ_λ as determined from the previously described spectral transmittance measurements from the quantity $\rho_\lambda + \tau_\lambda$ as determined from a second measurement in the Beckman DK2A integrating sphere. In the second measurement, the sample was placed in the beam as before but within the integrating sphere so that both the reflected and transmitted energy from the sample were integrated and detected.

Reflectance in the region beyond 2.5 microns was measured directly on the Gier Dunkle Model DB100 portable emissometer and was found to be quite low for all samples. As a consequence, the spectral reflectance beyond 2.5 microns for each sample was assumed to be uniform and equal to the total value measured on the emissometer.

I.2 MEASUREMENT METHOD FOR OTHER CANDIDATE FABRICS

Previous measurements of Nomex and PBI cloth samples have shown that fabrics may be diffuse transmitters in the wavelength region beyond 2.5 microns. Since conventional integrating sphere reflectometers only operate to about 2.5 microns, measurements in which the total diffuse transmittance is collected and measured must be made by other techniques. In the previously cited reference, bidirectional transmittance was measured at several angles and was integrated to obtain the diffuse value. In the work reported here, another method was used. Directional reflectance in the region 2.0 to 15 microns was measured in a paraboloid reflectometer (Ref. 72) with two different backings. The first set of measurements was made with a low reflectance (black paint) backing. The second set of data was taken with a high reflectance (gold) backing. Additionally, the reflectance of both the high and low reflectance backing materials was measured. All these data can be related in the following analytical relationship to define the reflectance, transmittance, and absorptance of partially transparent materials:

ρ_o = directional spectral reflectance measured with low reflectance backing

ρ_1 = directional spectral reflectance measured with high reflectance backing

R_o = directional spectral reflectance of low reflectance backing

R_1 = directional spectral reflectance of high reflectance backing

ρ = absolute directional spectral reflectance (equal to ρ_o when $R_o = 0$

τ = directional spectral transmittance

α = directional absorptance

For the partially transparent samples, the measured properties ρ_o and ρ_1 would be represented:

$$\rho_o = \rho + R_o\tau^2 + R_o^2\,\tau^2\rho + \ldots\ldots \quad (51)$$

$$\rho_1 = \rho + R_1\tau^2 + R_1^2\,\tau^2\rho + \ldots\ldots \quad (52)$$

Solving Equations (51) and (52) simultaneously:

$$\rho = \frac{R_1\rho_o - R_o\rho_1}{R_1 - R_o - R_1R_o\,(\rho_1 - \rho_o)} \tag{53}$$

and

$$\tau = \left[\frac{\rho_1 - \rho_o}{R_1 - R_o}\left[1 \pm (R_1 + R_o) + R_1R_o\rho^2\right]\right]^{1/2} \tag{54}$$

Since $\rho + \tau + \alpha = 1$

$$\alpha = 1 - \left[\frac{R_1\rho_o - R_o\rho_1}{R_1 - R_o - R_1R_o\,(\rho_1 - \rho_o)}\right] - \left[\frac{\rho_1 - \rho_o}{R_1 - R_o}\left[1 - (R_1 + R_o)\rho + R_1R_o\rho^2\right]\right]^{1/2} \tag{55}$$

These equations were solved at 42 separate wavelengths in the region between 2.5 and 15 microns using an on-line computer program.

Transmittance data in the region 0.55 to 2.5 microns was measured directly using the integrating sphere attachment for the Beckman DK2A spectroreflectometer.

Values of transmittance and absorptance to blackbody temperatures of 1800°F and 4500°F were computed from the plotted spectral data using 25-band overlays assuming Planckian distribution of the sources.

I.3 DATA

Spectral curves for the transmittance and the absorptance or reflection are shown in Figures 50 to 55 for each of the candidate fabrics in each of the two states considered, virgin and shrunken (charred).

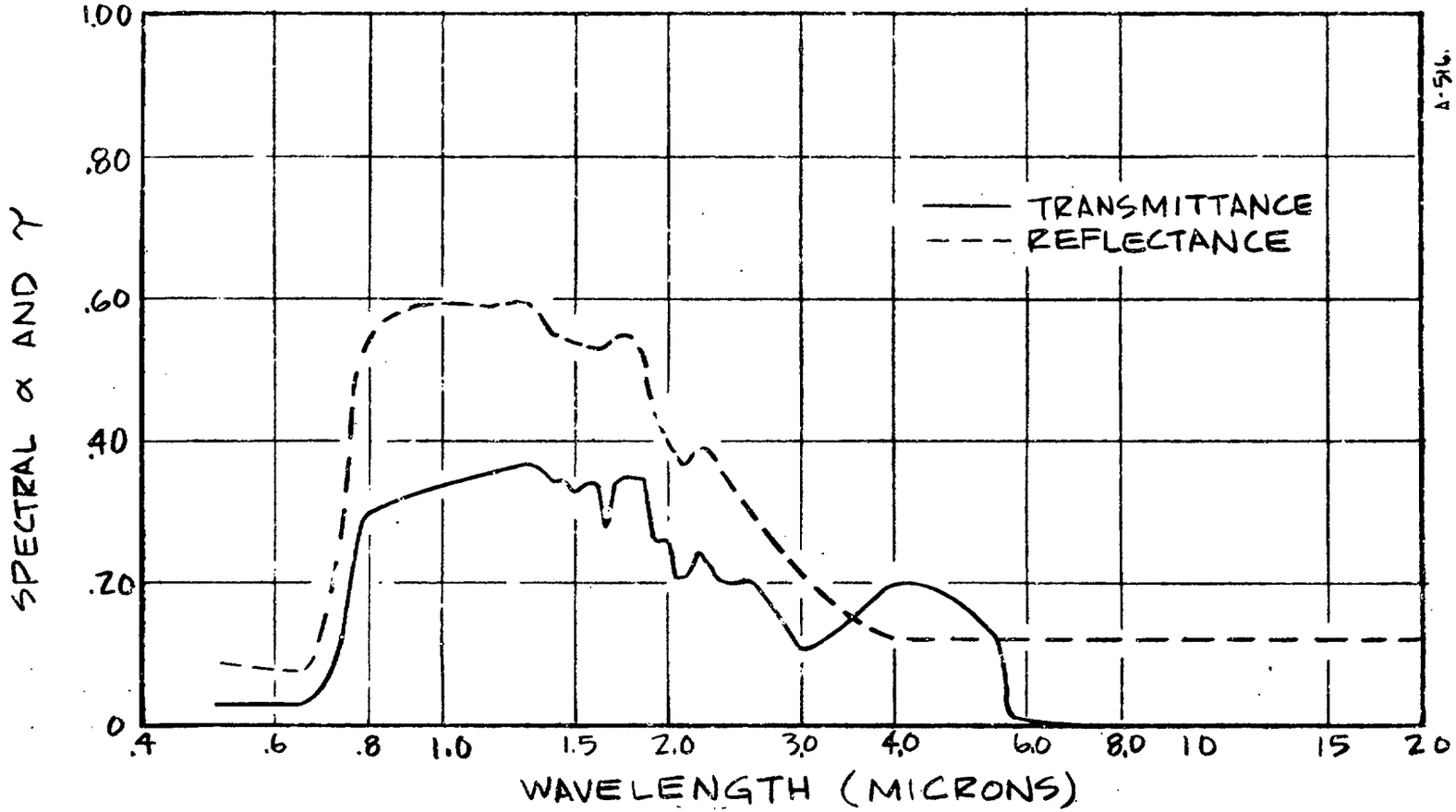

Figure 50. Spectral Transmittance and Reflectance of Virgin Nomex

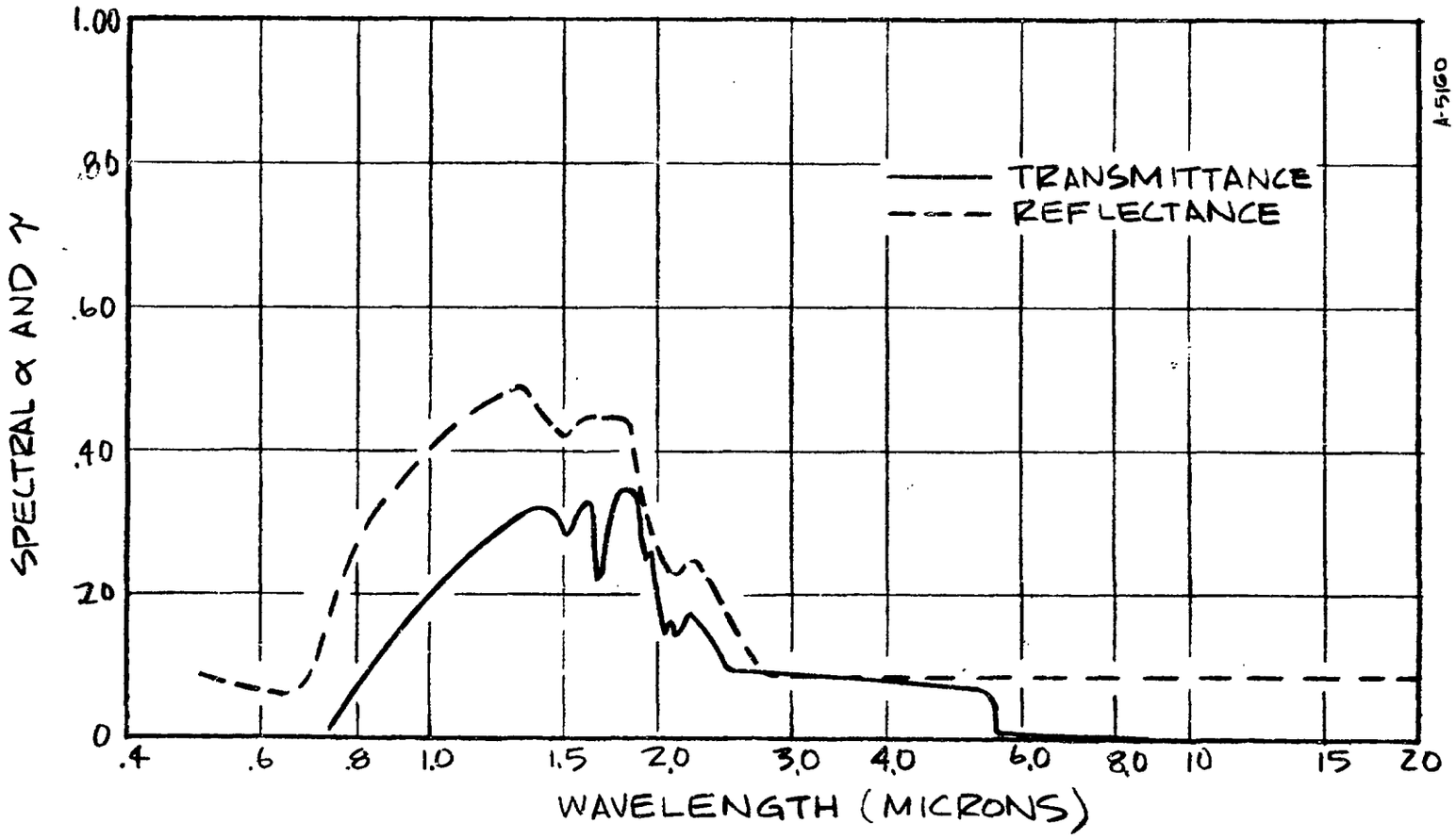

Figure 51. Spectral Transmittance and Reflectance of Charred Nomex

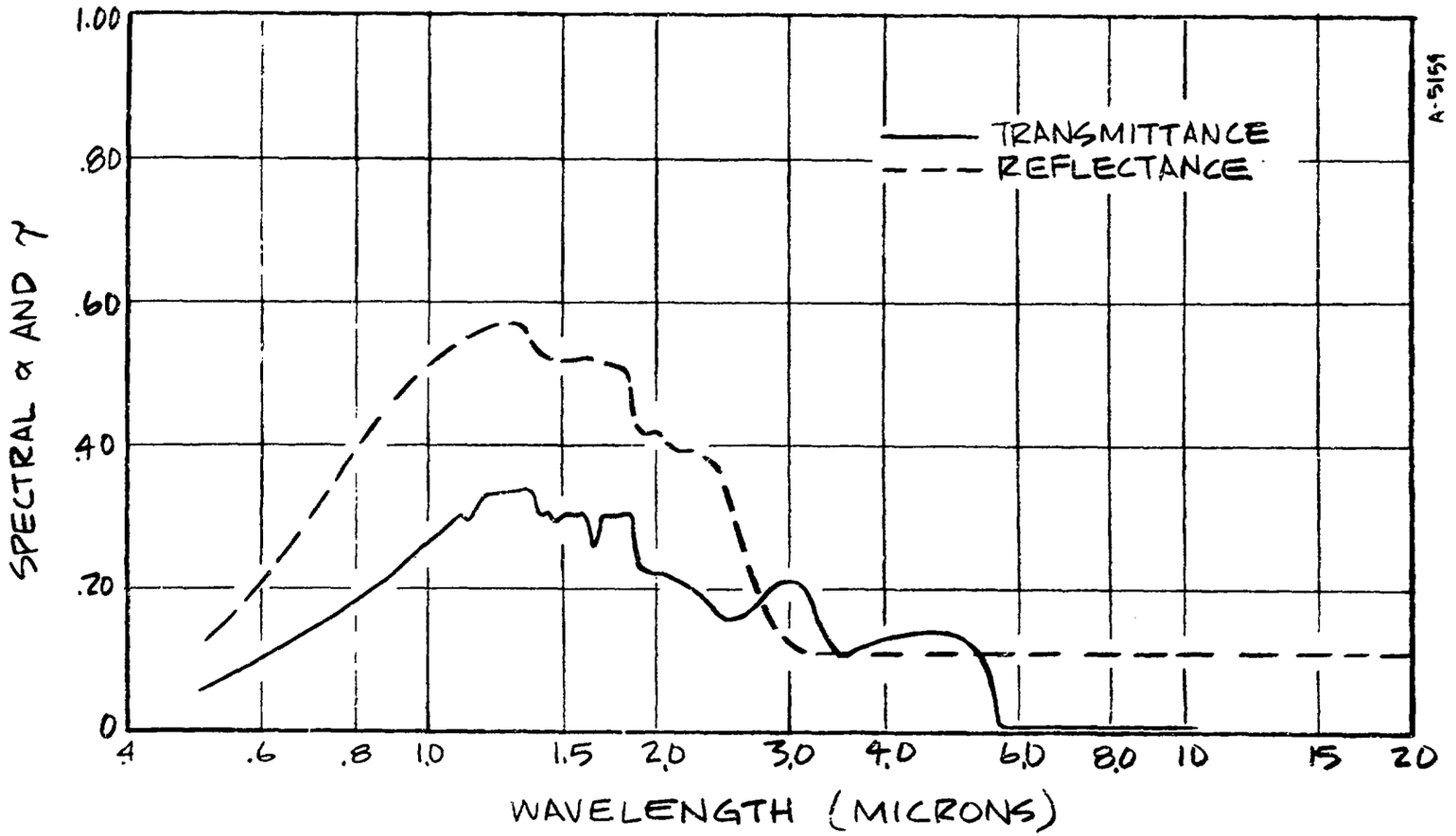

Figure 52. Spectral Transmittance and Reflectance of Virgin PBI

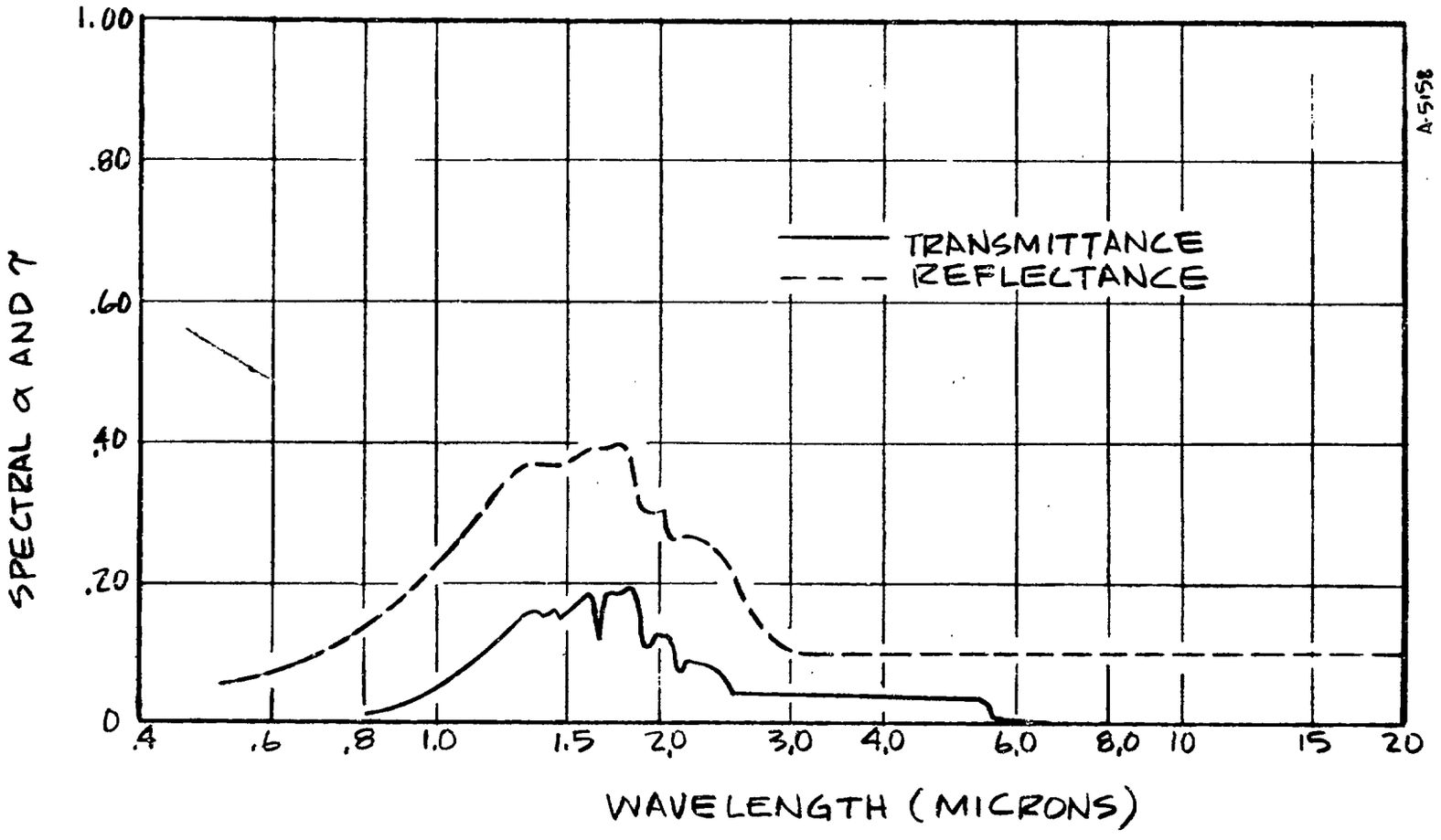

Figure 53. Spectral Transmittance and Reflectance of Charred PBI

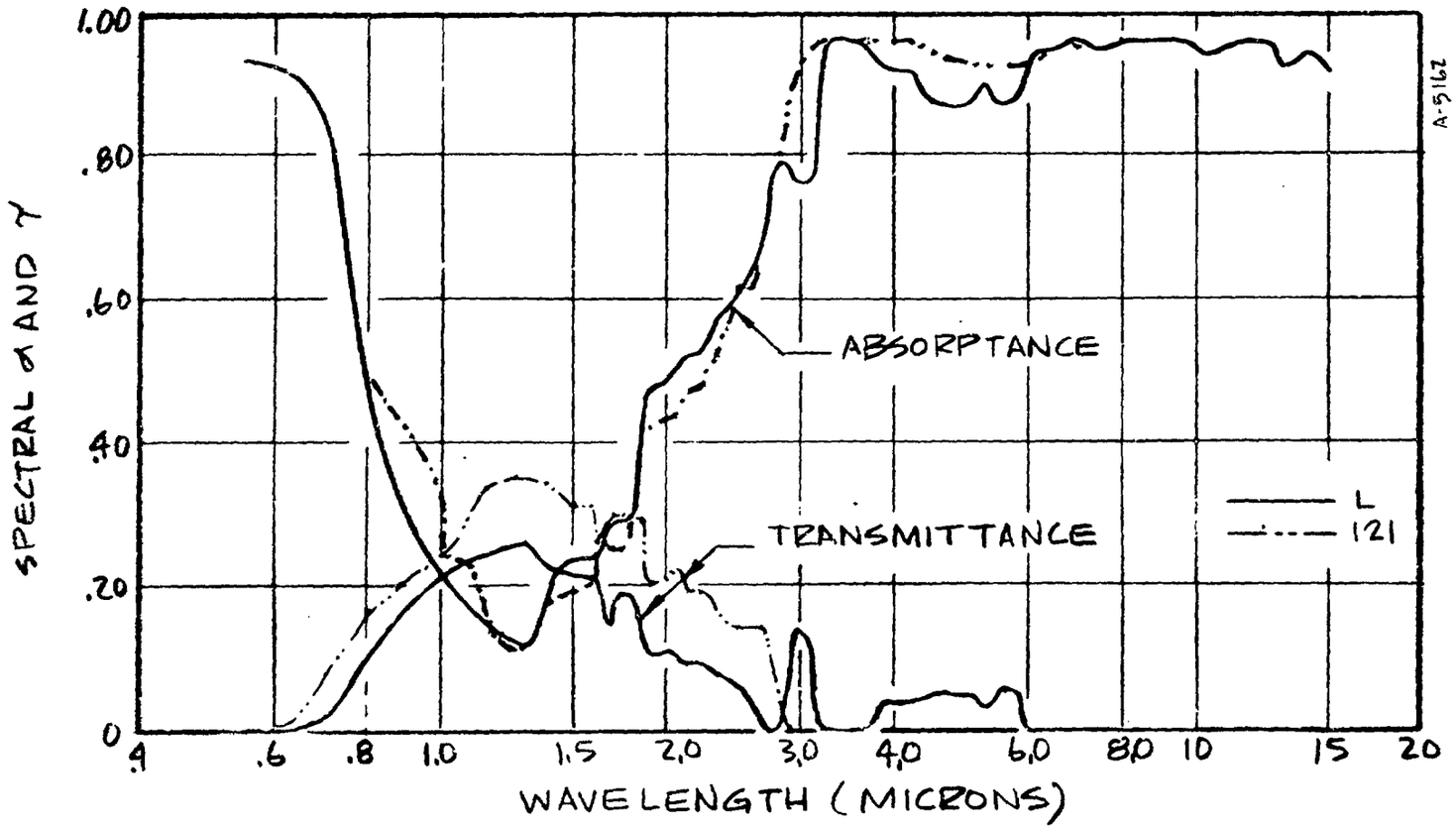

Figure 54. Absorptance and Transmittance of Virgin Stabilized PBI Fabrics (L and 121)

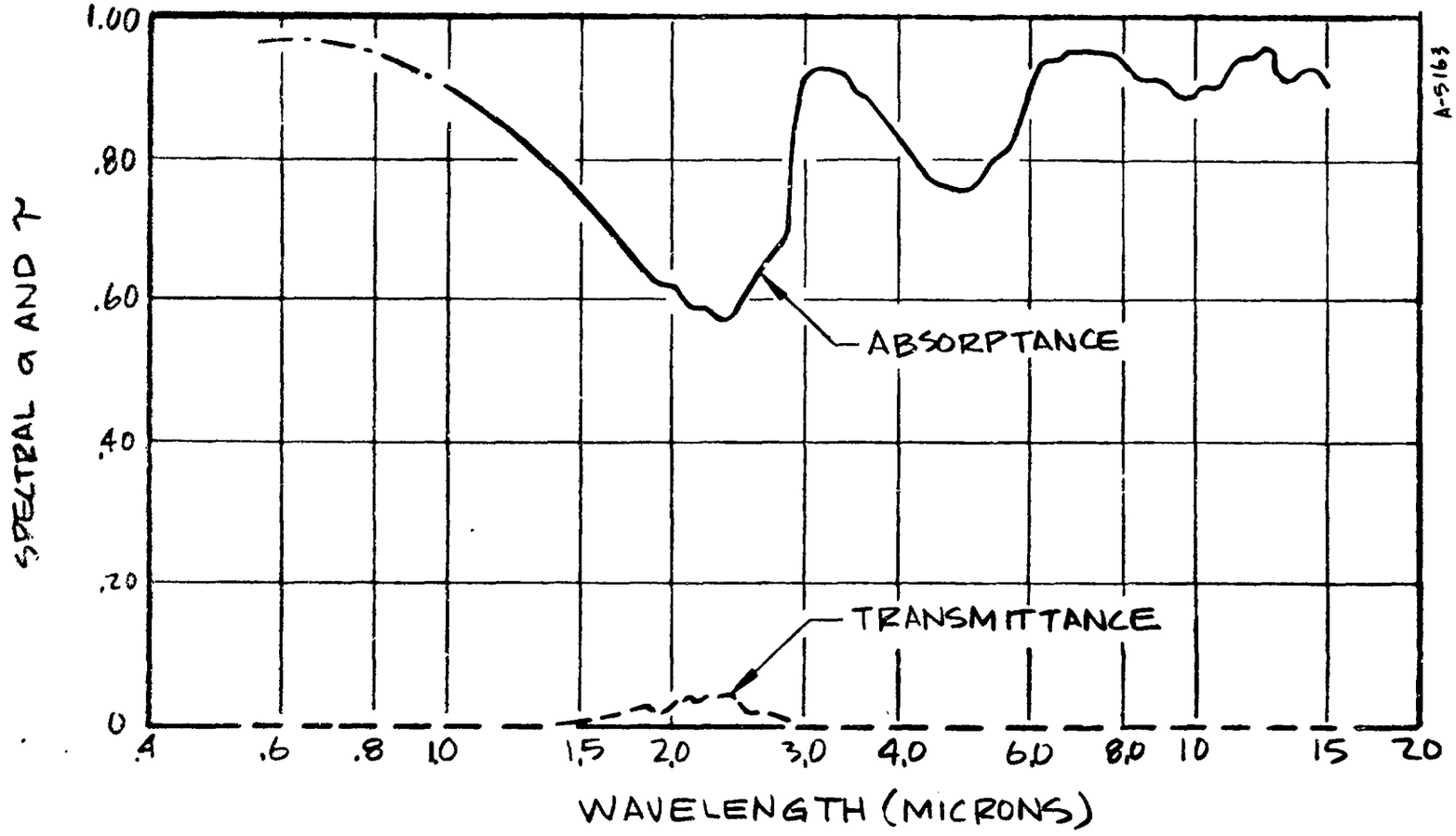

Figure 55. Absorptance and Transmittance of Charred Stabilized PBI Fabric L

APPENDIX II

TGA DATA

TABLE XXXVII

CMA DATA

Fabric	Dyed Nomex	Undyed PBI*	121**	122***
Wt. Fabric, oz/yd^2	4.1	4.3	4.3	4.3
Thickness, inches	0.0127	0.0143	0.0127	0.0137
% H_2O, Dry basis	5.0	12.0	14.0	5.2
% H_2O, Wet basis	4.76	10.71	12.3	4.94
ρ_o, lb/ft^3	25.782	22.374	24.7	24.863
E_1/R, °R	84391	9774.6	27755	56911
E_2/R, °R	69647	77451	33650	63881
E_3/R, °R	97514	58179	60357	62735
ρ_{o_1}, lb/ft^3	20.613	0.915	4.89	4.178
ρ_{o_2}	7.967	7.279	4.20	6.985
ρ_{o_3}	22.983	36.553	40.31	37.182
ρ_{r_1}	0.0	0.0	0.0	0.0
ρ_{r_2}	0.0	0.0	0.0	0.0
ρ_{r_3}	19.823	31.728	38.44	28.149
B_1, sec^{-1}	1.00×10^{29}	1.80×10^{9}	3.34×10^{11}	4.54×10^{12}
B_2	2.75×10^{28}	1.64×10^{21}	1.03×10^{11}	1.86×10^{19}
B_3	1.953×10^{28}	6.72×10^{18}	1.70×10^{28}	6.50×10^{28}
N_1	4.167	1.6064	6.0255	3.516
N_2	3.1690	1.3620	2.3114	1.078
N_3	2.7059	1.6269	3.5346	5.60
Γ	0.5	0.5	0.5	0.5

*It was necessary to combine Goldfarb's reaction 2 with 3, and 4 with 5.

**Goldfarb's reactions 4 and 5 were suppressed.

***Goldfarb's reaction 4 was suppressed.

TABLE XXXVIII

GOLDFARB'S REDUCED TGA DATA

Fabric	Dyed Nomex	Undyed PBI	121	122
F	0.615555	0.29095	0.358272	0.43392
E_1, cal/mole	93158.0	10279.01	30638.61	62823.5
E_2, cal/mole	76882.0	88363.91	37146.39	70517.952
E_3, cal/mole	107645.0	85497.54	66627.01	69251.98
E_4, cal/mole	--	104182.9	71740.99	79488.639
E_5, cal/mole	--	64223.09	96467.60	--
$Log_{10}A_1$	29.0	3.25431	11.523369	19.656855
$Log_{10}A_2$	20.4393	20.23019	11.011655	19.269536
$Log_{10}A_3$	23.8207	21.21431	20.018950	17.987295
$Log_{10}A_4$	--	24.46445	16.52098	17.592776
$Log_{10}A_5$	--	13.27577	20.662635	--
N_1	4.167	1.6064	6.0255	3.515581
N_2	3.1690	5.8249	2.3114	1.0782929
N_3	2.7059	1.3620	3.5346	5.5978247
N_4	--	3.0148	1.2969	2.5728015
N_5	--	1.6269	2.9025	--
P_1	0.649437	0.0702877	0.2756165	0.19363397
P_2	0.251007	0.257945	0.2372?2	0.32373027
P_3	0.099557	0.301164	0.1228477	0.41865331
P_4	--	0.081481	0.0944121	0.07998245
P_5	--	0.2891223	0.2699217	--

REFERENCES

1. Moyer, C. B., "Finite Difference Solution for the In-depth Response of Charring Materials Considering Surface Chemical and Energy Balances," NASA CR-1061, June 1968.

2. Aerotherm Corporation, Mountain View, California, "User's Manual, Aerotherm Charring Material Thermal Response and Ablation Program," Version 3, AFRPL-TR-70-92, April 1970.

3. JANAF Thermochemical Tables, 2nd Edition, The Dow Chemical Company, Midland, Michigan, 1970.

4. Moritz, A. R., and Henriques, F. C., "Studies of Thermal Injury II. The Relative Importance of Time and Surface Temperature in the Causation of Certaneous Burns," Am. J. Path., Vol. 23, 1947.

5. Mitchell, H. H., "A General Approach to the Problem of Estimating Personnel Damage on Atom Bombed Targets," Rand Report, RM-1149, October 1953.

6. Buettner, K., "Effects of Extreme Heat and Cold on Human Skin III. Numerical Analysis and Pilot Experiments on Renetrating Flash Radiation Effects," J. Appl. Physiology, Vol. 5, 1952.

7. Stolwijk, J. A. J., and Hardy, J. D., "Skin and Subcutaneous Temperature Changes during Exposure to Intense Thermal Radiation," in Thermal Problems in Aerospace Medicine ed by Hardy, AGAR Dograph III, October 1968.

8. Moritz, A. R., "Studies of Thermal Injury III. The Pathology and Pathogenes of Cutaneous Burns An Experimental Study," American J. of Pathology, Vol. 23, No. 6 November 1947.

9. Chato, J. C., "A Survey of Thermal Conductivity and Diffusivity Data on Biological Materials," ASME Paper 66-WA/HT-37.

10. Lipkin, M. and Hardy, J. D., "Measurement of Some Thermal Properties of Human Tissues," J. Appl. Physiol., Vol. 7, September 1954.

11. Shitzer, A., and Chato, J. C. "Analytical Solutions to the Problem of Transient Heat Transfer in Living Tissue," ASME Paper 71-WA/HT-36.

12. Shitzer, A., and Chato, J. C., "Steady-State Temperature Distribution in Living Tissue Modeled as Cylindrical Shells," ASME Paper 71-WA/HT-34.

13. Weaver, J. A., and Stoll, A. M., "Mathematical Model of Skin Exposed to Thermal Radiation," Aerospace Medicine, January 1969.

14. Buettner, K., "Effects of Extreme Heat and Cold on Human Skin I. Analysis of Temperature Changes Caused by Different Kinds of Heat Application," J. Appl Physiology, Vol. 3, No. 2, June 1951.

15. Mixter, G., "A Comparison Between Bone and Blackened Porcine Skin in Response to Pulses of High Intensity, Thermal Energy," UR-385, Univ. of Rochester, Atomic Energy Project, March 1955.

16. Hardy, J. D., "Method for the Rapid Measurement of Skin Temperature during Exposure to Intense Thermal Radiation," J. Appl. Physiol., Vol. 5, 1953.

17. Stoll, A. M., and Greene, L. C., "Relationship between Pain and Tissue Damage Due to Thermal Radiation," J. Appl. Physiol., Vol. 14, 1959.

18. Henriques, F. C., and Moritz, A. R., "Studies of Thermal Injury I. The Conductors of Heat to and through the Skin and the Temperatures Attained Therin," Am. J. Path., Vol. 23, 1947.

19. Hensel, H., "The Physiology of Thermoreception," Ergebn. Physiol., Vol. 47, 1952.

20. Hensel, H., "The Intracutaneous Variation of Temperature due to External Stimuli," and "Intracutaneous Temperature Sensation and Heat Transfer," ARch. f.d.ges. Physiol., Vol. 252, 1950.

21. Henriques, F. C., "Studies of Thermal Injury VIII. Automatic Recording Caloric Applicator and Skin-Tissue and Skin-Surface Thermocouples," Rev. Sci. Instr. Vol. 18, 1947.

22. Stoll, A. M., and Hardy, J. D., "Direct Experimental Comparison of Several Surface Temperature Measueing Devices," Rev. Sci. Instr., Vol. 20, 1949.

23. Spells, K. E., "The Thermal Conductivities of Some Biological Fluids," Phys. in Med. and Bio., Vol. 5 No. 2, 1960.

24. Hardy, J. D., Goodell, H., and Wolff, H. G., "The Influence of Skin Temperature upon the Pain Threshold as Evoked by Thermal Radiation," Science, Vol. 114, 1951.

25. Hardy, J. D., and Oppel, T. W., "Studies in Temperature Sensation. IV. The Stimulation of Cold Sensation by Radiation," J. Clin. Investigation, Vol. 17, 1938.

26. Davies, J. M., "The Effect of Intense Radiation on Animal Skin, A Comparison of Calculated and Observed Burns," Hdqs. Quartermaster Research and Engr. Command Report T-24, April 1951.

27. Vendrick, A. J. H., and Vos, J. J., "A Method for the Measurement of the Thermal Conductivity of Human Skin," J. Appl. Physiol., Vol. 11, 1957.

28. Boehm, R. F., and Tuft, D. B., "Engineering Radiation Heat Transfer Properties of Human Skin," ASME Paper 71-WA/HT-37.

29. Hardy, J. D., "The Radiation of Heat from the Human Body. I: An Instrument for Measuring the Radiation and Surface Temperature of the Skin," J. Clinical Invest., Vol. 13, 1934, pp. 593-604.

30. Hardy, J. D., "The Radiation of Heat from the Human Body. II. A Comparison of Some Methods of Measurement," J. Clinical Invest., Vol. 13, 1934, pp. 615-620.

31. Hardy, J. D., "The Radiation of Heat from the Human Body. III. The Human Skin as a Black-Body Radiator," J. Clinical Invest., Vol. 13, 1934, pp. 615-620.

32. Hardy, J. D. and Muschenheim, C., "The Radiation of Heat from the Human Body. IV: The Emission, Reflection, and Transmission of Infra-Red Radiation by the Human Skin," J. Clinical Invest., Vol. 13, 1934, pp. 817-831.

33. Hardy, J. D. and Muschenheim, C., "Radiation of Heat from the Human Body. V: The Transmission of Infra-Red Radiation through Skin," J. Clinical Invest. Vol. 15, 1935, pp. 1-9.

34. Hardy, J. D., "The Radiating Power of Human Skin in the Infra-Red," American J. Physiol. Vol. 127, 1939, pp. 454-462.

35. Hardy, J. D. and Muschenheim, C., "Heat Radiation through the Body," J. Clinical Invest., Vol. 15, 1936, pp. 1-7.

36. Hardy, J. D., Hammel, H. T., Murgatroyd, D., "Spectral Transmittance and Reflectance of Excised Human Skin," J. Appl. Phy., Vol. 9, 1956, pp. 257-254.

37. Hardy, J. D., "Infrared Reflectance of Human Skin," Abstract in Int. J. Biometeorology, Vol. 13, Suppl., 1969, pp. 23-24.

38. Derksen, W. L., Murtha, T. D., and Monahan, T. I. "Thermal Conductivity and Diathermancy of Human Skin for Sources of Intense Thermal Radiation Employed in Flash Burn Studies," J. Appl. Physiol. Vol. 11 No. 2, 1957.

39. Buettner, Konrad, "Effects of Extreme Heat and Cold on Human Skin. III: Numerical Analysis and Pilot Experiments on Penetrating Flash Radiation Effects," J. Appl. Phy., Vol. 5, 1942, pp. 207-220.

40. Elam, R., Goodwin, D. W., and Williams, K. L., "Optical Properties of the Human Epidermis," Nature, Vol. 198, No. 4884, June 1968, pp. 1001-1002.

41. Perkins, J. B., Pearse, H. E., and Kingsley, H. D., "The Relation of the Time and Intensity of Applied Thermal Energy to the Secerity of Burns," UR-283, Univ. of Rochester, Atomic Energy Project, December 1952.

42. Wight, A. and Robinson, D. M., "Estimation of the Severity of Porcine Burns," Report T-8, Quartermaster Research and Engineering Center, Natick, Mass., April 1956.

43. Knox, F. S., McCahan, G. R., Wachtd, T. L., Treventhan, W. P., Martin, A. S., Dubois, D. R., Keiser, G. M., "Engineering Test of Lightweight Underwear of the Winter Flight Clothing System: Thermal Protection," U. S. Army Aeromedical Research Laboratory Report No. 71-19, June 1971.

44. Davie, T. P., Hinshaw, J. R., and Pearse, H. E., "A Comparison of the Effects on Bare Porcine Skin of Radiant Energy Delivered in the Form of Square and Simulated Field Pulses," UR-418, Univ. of Rochester, Atomic Energy Project, December 1955.

45. Bales, H. W., Hinshaw, J. R., and Pearse, H. E., "A Comparison of the Effects of Radiant Thermal Energy on Bare Blackened and Whitened Pig Skin," UR-438, Univ. of Rochester, Atomic Energy Project, July 1956.

46. Goldsmith, A., and Takata, A. N., "Investigation of Means and Materials to Combat Thermal Radiation Burns," Report No. DO46, Armour Research Foundation of Ill. Inst. of Tech., January 1957.

47. Henriques, F. C., "Studies of Thermal Injury V. The Predictability and the Significance of Thermally Induced Rate Processes Leading to Irreversible Epidermal Injury," Arch. of Pathology, Vol. 43, 1947.

48. Bader, B. E., "Heat Transfer in Liquid Hydrocarbon Fuel Fires," SC-R-64-1366A, June 1965.

49. Enertech, Inc., "The Feasibility of Simulating JP-4 Fuel Fire Environments Under Reproducible Furnace Conditions," U.S. Army Aero Medical Research Lab., Fort Rucker, Alabama, January 1971.

50. Graves, K. W., "Fire Fighters Exposure Study," Cornell Aeronautical Lab. Inc., TR-AGFSRS-71-2, December 1970.

51. Burgess, D. S., Grumer, J., and Wolfhard, H. G., "Burning Rates of Liquid Fuels in Large and Small Open Trays," The Use of Models in Fire Research, Publ. 786, National Academy of Sciences-National Research Council, Washington D.C., W. G. Berl, Ed., 1961, pp.68-75.

52. Sparrow, E. M. and Cess, R. D., "Radiation Heat Transfer," Brooks/Cole Publishing Company, Belmont, California, 1966.

53. Morton, B. R., "Modeling Fire Plumes," Tenth Symposium (International) on Combustion, 1964, pp. 973-982.

54. JANAF Thermochemical Tables, The Dow Chemical Co., Midland, Michigan.

55. Dalzell, W. H. and Sarofim, A. F., "Optical Constants of Soot and their Application to Heat-Flux Calculations," J. Heat Transfer, Trans. ASME, February 1969, pp. 100-104.

56. Eckert, E. R. G. and Drake, R. M., Jr., Heat and Mass Transfer, McGraw-Hill Book Company, Inc., New York, 1959.

57. Engholm, G., Lis, S. J., and Bambeuck, R. A., "Instantaneous Local Temperatures of Aerodynamic Decelerators," Part II, WADD-TR-60-70, February 1961.

58. Freeston, W. D., Coskren R. J., Skelton, J. and Sebring, R. E., "Flammability and Heat Transfer Characteristics of PBI Fabric," AFML-TR-70-230, February 1971.

59. Stanton, Robert M. "Heat Transfer and Flammability of Fibrous Materials," AFML-TR-70-230, February 1971.

60. Morris, G. J., "Thermal Properties of Textile Materials," Journal of the Textile Inst., Vol. 44, No. 10, pp. 449-476, 1953.

61. Goldfarb, I. J., McGuchan, R., Meaks, A. C., "Kinetic Analysis of Thermogravimetry," AFML-TR-68-181, Part II, December 1968.

62. Moyer, C. B., Suchsland, K. E., Bartlett, E. P., "Fundamental Ablative Mechanisms of Reinforced Aromatic/Heterocyclic Resin Composites," (Draft) Aerotherm Corporation, Mountain View, California, Report 72-55, June 14, 1972.

63. Lee, H., Stoffey, D., and Novlile, K., New Linear Polymers, McGraw-Hill Book Company, Inc., San Francisco, 1967.

64. George, D. E., Dupont Co. (E. I. DuPont de Nemours & Co., Inc.), Wilmington, Delaware, Private Communication, July 23, 1971.

65. Perry, J.H., Chemical Engineers' Handbook, McGraw-Hill Book Co., New York, 1963 (Fourth Edition).

66. Stanton, R. M., "Heat Transfer and Flammability of Fibrous Materials," AFML-TR-70-238, February 1971.

67. Green, L., Jr., "Heat, Mass, and Momentum Transfer in Flow Through Porous Media," ASME Paper 57-HT-19, April 30, 1957.

68. Green, L., Jr., Duwex, P., "Fluid Flow Through Porous Metals," J. Applied Mechanics, March, 1951, pp. 35 - 45.

69. Hottel, H. C., et al, "Transient Heat and Moisture Transfer through Thermally Irradiated Cloth," Technical Report #8, Fuels Research Laboratory, MIT, Cambridge, Mass, December 1961.

70. Goldfarb, I. J., "Polymer Thermal Degradation Characteristics," to be published as an AFML TR.

71. Stanton, R. M., Schulman, S., "Evaluation of the Protective Characteristics of PBI and Nomex Coveralls in JP-4 Fuel Fires," AFML-TR-72, Arpil 1972.

72. Newman, B. E., Luedke, E. E. and Bevans, J. T., "High Temperature Reflectance Measurements with the Paraboloid Reflectometer," AIAA Paper 68-25, January 1968.